NATIONAL BUREAU OF STANDARDS REPORT

1123

Technical Report
on
High Temperature Thermodynamics

to

Office of Naval Research
Department of the Navy

U. S. DEPARTMENT OF COMMERCE
NATIONAL BUREAU OF STANDARDS

U. S. DEPARTMENT OF COMMERCE
Charles Sawyer, Secretary

NATIONAL BUREAU OF STANDARDS
E. U. Condon, Director

THE NATIONAL BUREAU OF STANDARDS

The scope of activities of the National Bureau of Standards is suggested in the following listing of the divisions and sections engaged in technical work. In general, each section is engaged in specialized research, development, and engineering in the field indicated by its title. A brief description of the activities, and of the resultant reports and publications, appears on the inside of the back cover of this report.

1. **ELECTRICITY.** Resistance Measurements. Inductance and Capacitance. Electrical Instruments. Magnetic Measurements. Electrochemistry.

2. **OPTICS AND METROLOGY.** Photometry and Colorimetry. Optical Instruments. Photographic Technology. Length. Gage.

3. **HEAT AND POWER.** Temperature Measurements. Thermodynamics. Cryogenics. Engines and Lubrication. Engine Fuels.

4. **ATOMIC AND RADIATION PHYSICS.** Spectroscopy. Radiometry. Mass Spectrometry. Physical Electronics. Electron Physics. Atomic Physics. Neutron Measurements. Nuclear Physics. Radioactivity. X-Rays. Betatron. Nucleonic Instrumentation. Radiological Equipment. Atomic Energy Commission Instruments Branch.

5. **CHEMISTRY.** Organic Coatings. Surface Chemistry. Organic Chemistry. Analytical Chemistry. Inorganic Chemistry. Electrodeposition. Gas Chemistry. Physical Chemistry. Thermochemistry. Spectrochemistry. Pure Substances.

6. **MECHANICS.** Sound. Mechanical Instruments. Aerodynamics. Engineering Mechanics. Hydraulics. Mass. Capacity, Density, and Fluid Meters.

7. **ORGANIC AND FIBROUS MATERIALS.** Rubber. Textiles. Paper. Leather. Testing and Specifications. Organic Plastics. Dental Research.

8. **METALLURGY.** Thermal Metallurgy. Chemical Metallurgy. Mechanical Metallurgy. Corrosion.

9. **MINERAL PRODUCTS.** Porcelain and Pottery. Glass. Refractories. Enameled Metals. Building Stone. Concreting Materials. Constitution and Microstructure. Chemistry of Mineral Products.

10. **BUILDING TECHNOLOGY.** Structural Engineering. Fire Protection. Heating and Air Conditioning. Exterior and Interior Coverings. Codes and Specifications.

11. **APPLIED MATHEMATICS.** Numerical Analysis. Computation. Statistical Engineering. Machine Development.

12. **ELECTRONICS.** Engineering Electronics. Electron Tubes. Electronic Computers. Electronic Instrumentation.

13. **ORDNANCE DEVELOPMENT.** Mechanical Research and Development. Electromechanical Fuzes. Technical Services. Missile Fuzing Research. Missile Fuzing Development. Projectile Fuzes. Ordnance Components. Ordnance Tests. Ordnance Research.

14. **RADIO PROPAGATION.** Upper Atmosphere Research. Ionospheric Research. Regular Propagation Services. Frequency Utilization Research. Tropospheric Propagation Research. High Frequency Standards. Microwave Standards.

15. **MISSILE DEVELOPMENT.** Missile Engineering. Missile Dynamics. Missile Intelligence. Missile Instrumentation. Technical Services. Combustion.

NBS PROJECT		NBS REPORT
0302-34-2605	August 20, 1951	1123

High Temperature Thermodynamics Technical Report

to

Office of Naval Research
Department of the Navy
Washington 25, D.C.

from

the Heat and Power Division
National Bureau of Standards

Contract NAonr-83-49
NR 016 415

WORK OF THE HEAT AND POWER DIVISION, NATIONAL BUREAU OF STANDARDS, IN HIGH TEMPERATURE THERMODYNAMICS

Foreword

In the present report are grouped together a number of summaries concerning the program of research in the general field of high temperature thermodynamics, currently under way in the Heat and Power Division of the National Bureau of Standards. This program has received substantial support from the Office of Naval Research, under Contract NAonr 83-49, as well as from other sponsoring agencies.

The main body of the report consists of brief statements of the aims and accomplishments of the staff engaged in high-temperature research. These comprise the following programs: Determination of gas temperatures by radiation methods; spectroscopic studies of flames; development of the noise thermometer; heat capacities at high temperatures; thermal conductivities at high temperatures; and work of the pyrometry laboratory. As appendices there are presented reports covering certain phases of the work in much greater technical detail, in the form both of progress reports and of reprints of published papers.

F. G. Brickwedde, Chief
Division of Heat and Power

CONTENTS

3-A. Heat Capacity of Sodium between 0° and 900°C.
D. C. Ginnings, T. B. Douglas and A. F. Ball . . . . . Reprint

3-B. Calorimetric Properties of Diphenyl Ether from 0° to 570°K.
G. T. Furukawa, D. C. Ginnings, R. E. McCoskey and R. A. NelsonReprint

3-C. Heat Capacity of Liquid Mercury between 0° and 450°C.
T. B. Douglas, A. F. Ball, and D. C. Ginnings. . . . . Reprint

1. Radiation Studies of High-Temperature Gases

R. D. Arnold and A. M. Bass

Radiation methods for the measurement of the temperature of hot gases are desirable in many applications. At the temperatures prevailing in freshly formed combustion products, or in explosions, materials of sufficiently high melting point or mechanical rigidity for use as thermocouples or resistance thermometers cannot be found. Even where they may be used, they are often undesirable because they introduce an interference with the process being studied. Moreover radiation methods may provide additional information that bears on the very important question whether the gas is in a state of thermodynamic equilibrium and at uniform temperature throughout its volume. If it is not in thermodynamic equilibrium, the concept of temperature breaks down, in that there is no single parameter T that governs the distribution of energy among the various states of the system, but it is still desirable and useful to speak of various "temperatures" associated with different modes of energy distribution. Spectroscopic studies provide direct evidence on this point, thus making it possible both to determine temperature or to demonstrate that equilibrium does not exist. They may also be so arranged as to show the variations in temperature (or in non-equilibrium energy distributions) at various portions of the gas in question, or at various times. All this may be achieved without disturbance of the gases, other than that required by providing observation windows or by introducing very small quantities of foreign atoms (e.g. sodium).

The ultimate aim of the present program is to study a large number of radiation methods of determining temperature, in a fundamental manner, so that we will not only be in a position to say which methods are best adapted for giving significant information for the more common problems that arise, but also to have the basic data that will permit application to other conditions and problems. The types of basic data required include a knowledge of the energy levels of the various molecules, free radicals, and atoms that occur in hot gases and flames; and of the rates at which energy is transferred among those energy levels. The energy may be transferred by radiation, in which case the studies will be of the intensities of spectral lines and their interpretation in terms of transition probabilities; or by collision, which may also be studied by spectral observations, following the intensity of lines of known transition probability as a function of time in a situation where a non-equilibrium state is brought to an equilibrium one by collision; or by chemical exchange, which may be similarly followed spectroscopically. An additional fundamental parameter, which is required in the interpretation of spectral intensities, and which also is connected with energy interchange in collisions, is the line width.

The long-range goals of this program are thus to acquire as much complete knowledge as possible of energy levels, transition probabilities, line widths, and rates of physical and chemical energy interchange. Its tools are spectroscopic, studying the emission and absorption of radiation from hot gases under equilibrium and controlled non-equilibrium conditions, in the ultraviolet, visible, and infrared regions. The

particular problems thus far under investigation fall into three groups. First, the study of the relative intensities of lines in the ultraviolet and visible spectra of H_2-O_2 and C_2H_2-O_2 flames, particularly in the spectra of OH, O_2, CH and C_2. This is summarized in greater detail in the following report by Dr. H. P. Broida. Here we will very briefly epitomize the results by pointing out that the availability of a photoelectric grating spectrometer, newly developed by the research department of the Leeds and Northrup Company and loaned to the National Bureau of Standards on a field trial basis, has permitted the obtaining of a large number of intensity determinations, from various well-defined regions in carefully controlled flames. From these there have been determined the effective rotational "temperatures" of OH radicals in their excited electronic state, as well as OH* vibrational "temperatures", the relative intensity of OH* and O_2*, all as a function of the position in the flame and of the fuel-oxygen ratio. Spectra have been obtained from which the studies may be broadened to include states of CH* and C_2*, but these have not yet been evaluated. In addition, for the relatively cool methane-air flames, it was possible to obtain the spectrum of OH in absorption and thereby to compute reversal "temperatures" and rotational "temperatures" for OH in its ground electronic-vibrational state. The latter are, for many conditions near the reaction front, considerably lower than the "temperatures" determined from the excited states, indicating that equilibrium does not exist, and from the gradual approach of the two "temperatures" an indication of the rate of approach to equilibrium could be obtained.

A second phase of the investigation concerns construction of apparatus for determining transition probabilities and line widths, needed for the final evaluation of the experiments on flames just outlined. For example, in order to know the absolute concentration of the OH radical, in its ground and excited states, one should be able to produce the radical in a state of thermal equilibrium and measure its concentration and absorption spectrum. Such measurements have been earlier reported over a limited temperature range; we have designed an absorption tube which it is hoped can be heated to 2000 degrees K, thus permitting a wider range of experimental conditions and a more accurate determination of equilibrium constants in the reaction $2H_2O \rightleftarrows H_2 + 2OH$, of the transition probabilities in the OH electronic spectrum, and of the dependence of OH line widths on pressure of foreign gases, etc. The design of the furnace, and the overcoming of some of the problems in obtaining optical windows that will be pressure-tight at elevated temperature, is described in an appendix by Dr. Arnold. With the furnace it is also hoped to investigate a number of other high-temperature absorption and emission spectra, both with the photoelectric spectrometer and in the infrared.

A third phase of the investigation concerns the analysis of infrared spectra of flames, and the development therefrom of methods of determining "temperatures". The infrared has the advantages that many more stable molecules possess spectra in that region, and that the excited states are of relatively low energy and hence are more readily brought into thermodynamic equilibrium. It is however difficult to obtain

spectra of sufficient intensity under high resolution. The recent development of photoconductive detectors, and their incorporation into grating spectrometers of high light-gathering power and good optical design, by Drs. E. K. Plyler and C. J. Humphreys of the Radiometry Section of the Bureau, and by Dr. Shirleigh Silverman of the Johns Hopkins Applied Physics Laboratory, has resulted in a very considerable improvement in the resolution of infrared flame spectra. We have worked with these investigators in the interpretation of their results on $CO-O_2$, H_2-O_2, and $C_2H_2-O_2$ flames, in the region from 1 to 2.8 μ, and are indebted to them for permission to cite the results in this report. Some of the results have been communicated at various meetings of the American Physical Society; the abstracts of the papers are given in an appendix, and a much more detailed presentation of various aspects of the work is given in another appendix.

The general results may be summarized here as follows. Between 1 and 2.8 μ there is infrared radiation from all three of the above-mentioned flames at nearly all wavelengths, showing in general an increase of intensity at longer wavelengths. There are various regions of strong emission in which rotational structure may be resolved more or less completely, and it has been possible to assign practically all of the emission to the molecules H_2O, CO_2, CO, OH, CN, and C_2. The spectra of the diatomic molecules are sufficiently well resolved so that they may be used to determine rotational "temperatures", and in the cases of CO and OH, vibrational "temperatures". The CO_2 emission in this region is too weak and cannot be resolved, and holds little promise of serving as a thermometer. The H_2O emission is extremely complex, but is sufficiently intense that high resolution can be obtained, leading to a partial interpretation, which is in process of being extended and shows promise of yielding both vibrational and rotational "temperatures". The "temperatures" obtained for CO, OH, C_2 and CN are in nearly all cases somewhat lower (by 200 to 500 degrees K) than are obtained from ultraviolet rotational temperatures, when corresponding regions of corresponding flames are studied. This is probably the result of two principal effects; first, the existence of temperature gradients across the line of observation; since the emitted intensity varies much more rapidly with temperature as one goes to shorter wavelengths, ultraviolet measurements will be weighted much more heavily towards the maximum temperature than will those in the infrared. The second cause is the much greater lifetime of excited states for infrared emission, due to the lower transition probabilities, and lower frequencies involved, which requires that emitting molecules in the infrared survive more collisions and hence more nearly approach equilibrium. The maximum emissivity in the infrared studies, from our relatively thin sources, is quite low, a further indication that the layers of relatively cool gas on the outer fringes of the flame are influential. The lower temperatures obtained in the infrared may also be indication that when non-equilibrium states are excited those of higher energy are more strongly out of equilibrium, a finding that seems to be of general application when

different sources in the ultraviolet have been compared. Non-equilibrium distribution of vibration-rotation states are evidenced, when observations are made near the inner cone, by the fact that rotational CO "temperatures" are as much as 500 to 1000 degrees K above vibrational "temperatures".

The results for the individual molecules observed are briefly as follows:

CO The vibration-rotation bands 2-0, 3-1, 4-2, and 5-3 have been observed between 4360 - 4000 cm^{-1}. Heads are formed at about J=50 and are prominent features of the spectrum of both $CO-O_2$ and $C_2H_2-O_2$ flames. The higher temperatures of the latter flames favor the higher vibrational levels. The rotational structure is well resolved, and may be followed out to J=46 in both the R and P branches of the 2-0 band. These measurements of higher rotational states than had previously been observed and the accuracy with which the vibrational heads could be measured, has resulted in improved molecular constants for this molecule. Rotational and vibrational temperatures may be obtained readily and with fair accuracy. In the outer regions of the flames these agree with each other, but are several hundred degrees below ultraviolet OH temperatures. Near the inner cone the rotational temperature exceeds the vibrational temperature.

OH The vibration-rotation bands 2-0, 3-1 and 4-2 have been observed in H_2-O_2 and $C_2H_2-O_2$ flames between 7180 to 5900 cm^{-1}. The region of the R branches, from 6600 to 7180 cm^{-1}, is badly overlapped by H_2O emission. The ratio of intensity of OH:H_2O is greatest when a near stoichiometric $C_2H_2-O_2$ flame is observed just above the inner cone. Under these conditions, all lines in the P branch of the 2-0 band from K6-19, in 3-1 from K3-15, and in 4-2 from K4-10 appear with intensity well above the H_2O background, with spin-doubling and Λ-doubling well resolved. Rotational and vibrational "temperatures" are in agreement at 2600 $\pm$ 200 degrees K. Under similar conditions measurements in the excited state (3064 A band) yield "temperatures" near 3000 degrees K. These observations were the first definite identification of rotation-vibration bands of a free radical in flame spectra.

The 3-0 and 4-1 bands have also been observed near 1μ, but since they are less than 2% as intense as the 2-0 sequence very wide slits were required, precluding well resolved spectra and quantitative temperature studies. The R branch of the 1-0 band, which must appear near 3900 cm^{-1}, is very much weaker than the H_2O ν_3 fundamental in that region and could not be identified; the spectra did not extend to the region of 2.9 - 3.1μ, where the P branches of 1-0 and 2-1 should be resolvable from the weaker H_2O emission.

C_2 This free radical has previously been observed through several electronic systems in the ultraviolet, visible and near photographic infrared. One of these, the Phillips System ($^1\Pi_u - {}^1\Sigma_g{}^+$) should extend into the region beyond 1μ, and has now been observed. The (0,0) band, centering at 8268.5 cm^{-1}, and the (1,0) band, at 9852.5 cm^{-1} are both

prominent features of the emission from the inner cone of fuel-rich oxy-acetylene flames. The rotational structure is clearly resolved even with the relatively wide slits required. Rotational "temperatures" of about 2600 degrees K are obtained. From the Swan bands ($^3\pi_g - {}^3\pi_u$), in the visible region, the corresponding region of the flame yields much higher "temperatures". A third band, (0,1) at 6441.0 cm^{-1}, has also been observed, but is weaker than the OH and H_2O emission in the same region.

CN. The "red" system of this radical ($^2\pi - {}^2\Sigma$), well known in the visible and photographic infrared, extends well beyond 1μ. The (0,0) band, at 9114.9 cm^{-1}, also has been observed in the inner cone of fuel-rich C_2H_2-O_2 flames, with about the same intensity as the C_2 bands. The more complicated band structure is poorly resolved, but the effective temperature connot be far from 2500 degrees K.

CO_2. At the effective temperatures prevailing in flames, the relatively low vibrational frequencies of this molecule ($\nu_2 = 667$ cm^{-1}) are so highly excited that a considerable overlapping of bands results, and no rotational structure can be resolved. Emission from a CO-O_2 flame in the region 5100-4700 cm^{-1} can be attributed to CO_2, but is relatively weak. A few characteristic features can be identified as the R-branch heads of the strongest expected bands. Preliminary results with prism spectrometers show sharply separated heads of the 001-000 band at 2397 cm^{-1} and the 011-010 band at 2385.5 cm^{-1}, the relative intensity of these two heads indicating vibrational temperatures near 2000 degrees K.

H_2O. Emission from this molecule extends throughout the near infrared. The regions 3900 - 4200 cm^{-1} (R branch of 001-000 and associated upper state bands 011-010, etc.), 4550 - 5900 cm^{-1} (011-000 and upper state bands), and 6500 - 7500 cm^{-1} (101-000, 021-000, and upper state bands) are particularly strong, and may be studied with slits narrow enough (0.2 cm^{-1}) to resolve much rotational structure. Most of the strongest lines may be arranged in series, which extend the known rotational assignments obtained from room-temperature absorption studies to higher levels. In particular, the strongest expected series $J_-J \leftrightarrow J + 1_-(J+1)$ has been followed out to $J = 22$ in the R branches of 001-000, 011-000, and 101-000, and in the P branches of the latter two bands. The intensities of resolved and analyzed lines, in the main bands and in their upper-state satellites, are consistent with rotational and vibrational "temperatures" of the order of 2500 degrees K for the outer cone of the H_2-O_2 flame. The measurement and analysis is being pursued.

Future Plans

The high-resolution studies make it possible to account for the frequencies of most of the observed radiation, and for the relative intensity of lines of a given molecule, in terms of an effective "temperature". It is in principle possible to use the absolute intensity of lines, or of unresolved bands, to calculate both temperatures and concentrations of the emitting molecules, if transition probabilities and line widths are known. Such data are available at room temperature for CO and CO_2,

with good accuracy, and for H_2O with fair accuracy. Using theoretical extrapolations to the indicated flame temperature, it appears that there is order-of-magnitude agreement with the observed emissivity, assuming equilibrium concentrations of the molecules. Near the inner cone, the CO concentration may exceed the equilibrium value. The inner-cone intensity of C_2 and CN, again assuming theoretical values for the transition probabilities, corresponds to concentrations of those radicals that are 10^4 in excess of equilibrium. It is desirable to refine and confirm measurements and calculations of this kind. We propose to determine the integrated absorption coefficients and emissivity of CO and H_2O as a function of temperature from room temperature up to the maximum that can be reached in the high-temperature furnace. The infrared measurements will be made with a Perkin-Elmer spectrometer, with glass, LiF, and rocksalt optics, that is now available. Quantitative studies of carefully controlled flames with this instrument are also in progress, and will be correlated with the high-dispersion results. It is also hoped to use the high-temperature furnace for the study of transition probabilities in the band systems of C_2 and CN.

Additional high-resolution spectra may also be obtained with a new spectrometer nearing final adjustment in the Radiometry Section, to cover the region from 2.8 - 5 μ. In this region it should be possible to study the P branch of the ν_3 fundamental and the R branch of the ν_2 fundamental of H_2O, the 1-0 and 2-1 bands of OH, and the CO fundamental, all of which should be useful as thermometers, and to explore the possibility of obtaining additional structural information and intensity distribution in reactant hydrocarbon molecules, such as CH_4, C_2H_4, and C_2H_2, and to search for other expected intermediates, such as CH_3 and CH_2.

The photoelectric spectrometer will be further used to study intensity distributions, emission and reversal temperatures, and concentrations in various portions of simple H_2-O_2 and hydrocarbon flames, with particular attention not only to the OH radical thus far studied but in addition to the CH and C_2 radicals. By coordinated experiments in both the ultraviolet and infrared it should be possible to cast further light on the relative concentrations of molecules in low and high excited states, and on the role of such species in the chemical- and physical-kinetic mechanisms of combustion.

2. Studies of Relative Intensities in UV and Visible Spectra from Flames*

H. P. Broida

The use of photoelectric detection coupled with high resolution spectroscopy has made it possible to study in detail the relative intensities of rotational lines of electronic vibration bands emitted from various portions of several flames. Initial investigations of rotational "temperatures" and relative intensities have been completed using the (0,0) band of the $^2\Sigma \leftrightarrow {}^2\pi$ electronic transition of OH. Vibrational and electronic temperatures of flames of one fuel have also been determined.

a) Methane-Air Flames. Rotational intensity distribution of OH in both emission and absorption have been measured. The ground state ($^2\pi$) was found to have an equilibrium concentration of OH radicals and to have a rotational temperature of 2000°K in both the inner and outer cones. The excited state ($^2\Sigma$) had an excessive concentration of radicals and the intensity distribution was not thermal. Two "temperatures" were found -- 1550°K for the low quantum numbers and 5200°K for the high. (Appendix 2-A).

b) Hydrogen-Oxygen Flames. Rotational, vibrational, and electronic distributions of OH have been measured for both the inner and outer cones in flames burning with mixtures from lean (H_2=O_2=1=1→H_2:O_2=1:1 by volume) to rich (6:1). Thermal equilibrium was found in the outer cones with temperatures from 125 to 450°C less than the calculated adiabatic temperatures. In the inner cones, rotational equilibrium was found but there was vibrational non-equilibrium as shown by an excess population of the $v'=2$ and $v'=3$ levels. (Appendix 2-B). Scanning through various portions of the flame has shown a maximum rotational temperature of 3000°K for all mixtures at the base of the inner cone. This temperature is near the calculated adiabatic temperatures. The temperature of the outer cone decreases about ½ of 1% per mm (5°C) above the tip of the inner cone. (Appendix 2-C).

c) Acetylene-Oxygen Flames. Rotational intensity distributions of OH have been measured in various portions of flames burning with mixtures from lean (C_2H_2=O_2=1:5→C_2H_2:O_2=1:5 by volume) to rich (4:5). Relative intensities of OH and CH have been measured. The rotational distribution of OH is apparently in equilibrium in both the inner and outer cones. However at the base of the inner cone of all mixtures, the measured temperature is 4250°K (in agreement with previous work of Gaydon and Wolfhard); this value is nearly 1000°C greater than the calculated adiabatic temperature. Near the tip of the cone, the temperature is of the order of 200°C less than the calculated temperature. In the outer cone, the temperature decreases about 1/4 of 1% (2½°C.) per mm above the tip of the inner cone. (Appendix 2-C). The sudden drop in intensity of CH past the tip of the inner cone indicates a radiative lifetime less than 10^{-7} seconds while the decrease in excessive OH rotational temperature indicates an OH radiative lifetime of the order of 10^{-6} seconds. Spectra of vibrational and electronic distributions of OH have been taken but are not yet analyzed. In addition, spectra of bands of C_2 and CH have been obtained over a range of acetylene to oxygen mixtures from 1:10 to 6:5. It is hoped to use these spectra to obtain rotational and vibrational temperatures.

*Supported in part by the Navy, Bureau of Aeronautics.

d) Methane-Oxygen and Propane-Oxygen Flames. Rotational intensities and distributions of OH have been determined as a function of position in stoichiometric mixtures of these flames. The same general trend as in hydrogen and acetylene flames in rotational temperatures is found in these flames. At the base of the inner cone, the methane flame is 3250°K, and at the tip, is 2800°K. The respective temperatures for the propane flame were 3350°K and 2850°K. (Appendix 2-C).

Future Plans.

A broad, continuing program has been planned for measuring the intensity distributions among the rotational and vibrational energy states of OH in various portions of several flames.

All possible branches of the various vibrational transitions of excited OH in an acetylene-oxygen flame are being measured to determine whether rotational equilibrium exists in each vibrational state. As a by-product will come the knowledge of the most usable branches for temperature measurements and a check will be made for the differences of the f_1 and f_2 levels reported by Gaydon and Wolfhard.

Because of the abnormal distribution observed in the methane-air flame (Appendix 2-A), the effects of diluents on flames with simpler constituents are being studied. Spectra from flames of stoichiometric mixtures of hydrogen and oxygen with diluents of argon, neon, and nitrogen are being obtained. It is hoped that this data will be of significance for the projected theoretical calculations of OH distributions to be made in cooperation with Hydrocarbon Research, Inc., and the ENIAC Computer of this Bureau. In addition if these calculations give hopeful results, a low pressure burner will be constructed with the aim of correlating observed distributions with the calculated ones.

In order to observe the inner cone without serious interference from the outer cone, a slot burner 5 cms by 0.0076 cms has been constructed. Preliminary experiments have shown an abnormal distribution of intensities with the maximum of the R_2 branch (0,0) of OH occurring at K=16.

Equipment is now being prepared for observing the rotational energy distributions and the concentrations of the ground state of OH in various flames by measuring the intensities of the absorption lines of the electronic transition. This data will be compared to that from excited OH and will determine under what flame conditions there is thermal equilibrium of OH. While principal emphasis will be placed upon studies of the OH radical, similar studies of the other radicals that emit in the visible and ultraviolet, i.e., CH, CN, C_2, O_2, NH, and of their relative intensities, will also be pursued.

3. Development Work on the Noise Thermometer
E. W. Hogue

The absolute noise thermometer was devised and developed by Garrison and Lawson of the University of Chicago Institute of Metals. (See Review of Scientific Instruments, Vol. 20, No. 11, 785-794.) In their results, an accuracy of 0.1% is claimed for temperature measurements near 1000°K.

The purpose of the noise thermometer project at the Bureau, supported by ONR, is to try to increase the accuracy of noise thermometer measurements; and to use the thermometer to provide independent determinations of temperatures in the region 1000°K to 1500°K for comparison with results obtained by other methods. For this development two thermometers constructed by Garrison and Lawson including one which had made successful measurements, were made available. The Bureau project began about October 1, 1950.

The first step was to re-assemble the thermometer which had been used by Garrison and Lawson, and make it operate dependably enough at least to duplicate the precision obtained by them. It was felt that in doing this much could be learned that would be of value in designing a more accurate thermometer.

Circuit diagrams were not complete so that several portions of the circuit had to be traced and detailed diagrams made. By the first of November the low-frequency amplifier and balancing system was in rough working order, but could only rarely be made to give a reasonable balance. This was traced to interference from a nearby television station, and efforts were started toward the procurement of a copper-screen room to house the thermometer. During November the high-frequency amplifier and balancing circuit were thoroughly checked and circuit diagrams were completed. The amplifier was made to function almost correctly at low gain despite the presence of low-level self-oscillation which could not be located with the limited equipment available. The amplifier would not function at all at high gain because of self-oscillation. By the end of November an order had been placed for the screen room.

Also about this time, procurement of materials from which to make the thermometer element was started. By the first of December it was realized that before much more progress could be made on the thermometer, the screen-room and additional equipment and work space were necessary. Delivery of the cage was hoped for sometime in January or February. During December a complete list of specifications for test equipment was made out, and arrangements were made to occupy room 111 West Building. Considerable time was devoted to laying out and procuring facilities and furniture for this room. These activities continued into January and February. Also during this time thought was being given to an improved circuit for averaging and making the noise balance in the thermometer. A circuit using an electronic feedback type integrator was built and tested. It proved unsatisfactory, but the method looks promising.

The screen room arrived toward the end of February, and had to be stored until room 111 West was made ready. The screen room was finally assembled in room 111 around April 1, and the thermometer was placed in it. It was found that the screening had eliminated all interference from television, but a good noise balance in the low frequency amplifier still could not be obtained. This was traced to two sources of distrubance. One of these proved, after considerable circuit checking, to be a faulty resistor. The second is an intense pulse-like distrubance probably resulting from a large gas discharge tube or mercury arc rectifier being operated from the same power line. An effort will be made to locate the source. When this disturbance was not present, a balance with both resistors at ambient chassis temperature, gave a resistance ratio of 1.0026. This balance was made without benefit of the auxiliary capacity-balance provided by the high-frequency amplifier section of the thermometer.

The test equipment needed for work on this amplifier had just arrived (May) so the next several weeks were mostly taken up with putting it into useful shape. A source of low-level oscillation was eliminated, and the amplifier was made much more stable. If it remains stable when connected to the preamplifier, the capacity balance it will provide should make the noise balance precision good enough for useful temperature measurements. The construction of the thermometer element is being carried out by Dr. R. J. Corruccini of the Pyrometry Laboratory.

4. Heat Capacities at High Temperatures
D. C. Ginnings and T. B. Douglas

The NBS program for the measurement of heat capacities at high temperatures emphasizes high accuracy up to 900°C (the limit of the present apparatus). The apparatus, which has been developed at this Bureau, is generally accepted as the most accurate in its field. Consequently, it has been used for establishment of certain standards of heat capacity in the high temperature range. As a result of investigation of aluminum oxide (synthetic sapphire), the Calorimetry Conference has recommended its use as a heat capacity standard up to 1770°K. Further measurements have been made on n-heptane and diphenyl ether as standards of heat capacity in the moderate temperature range where liquids are desired.

In addition to the establishment of heat capacity standards, very accurate measurements have been made on a number of materials which are useful as heat transfer media at high temperatures. Probably the most outstanding of these materials are sodium, potassium, and several of their alloys, which have been measured as high as 900°C. Mercury has also been investigated up to 450°C and a correlation of its thermodynamic properties has been made. It is expected that during the next year, several other materials will be investigated, including lithium, lead, lead-bismuth eutectic, and sodium hydroxide.

Recent Publications

Heat capacity of sodium between 0° and 900°C, the triple point and heat of fusion. J. Res. NBS 45, 23 (1950)
Also At. Energy Commission Document # 2639 (Appendix 3-A)

Calorimetric properties of Diphenyl Ether from 0° to 570°K
J. Res. NBS 46, 195 (1951) (Appendix 3-B)

Specific Heat of Beryllium between 0° and 900°
J. American Chemical Society 73, 1236 (1951)
Also At. Energy Commission Document # 2657

Heat capacity of liquid mercury between 0° and 450°C; calculation of certain thermodynamic properties of the saturated liquid and vapor.
J. Res. NBS 46, 334 (1951) (Appendix 3-C)

Heat Capacity of potassium and three potassium-sodium alloys between 0° and 800°C. Atomic Energy Commission Document # 1017
Also will be published in JACS or J. Res. NBS.

Publications Now Being Prepared

Calorimetric properties of aluminum oxide from 0° to 1173°K.
Calorimetric properties of n-heptane from 0° to 523°K.

5. Thermal Conductivities at High Temperatures
D. C. Ginnings and R. L. Nuttall

The thermal conductivity program includes measurements on both gases and liquids. The apparatus for gases, which probably will be completed by August, 1951, will be suitable for measurements up to 500°C and 100 atmospheres pressure. In spite of the increased difficulties in this range of higher temperatures and pressures, it is expected that the accuracy of the results will be comparable (1% or better) with the best of the results at ordinary temperatures and pressures. By obtaining such high accuracy in this range, it should be possible to extrapolate the thermal conductivity data to considerably higher temperatures and pressures where it is extrememly difficult to make direct measurements. During the next year, it is expected that thermal conductivity measurements will be made on a number of gases such as air, nitrogen, oxygen, carbon dioxide, and various mixtures, including the product gases from combustion in jet engines.

The program for the measurement of thermal conductivities of liquids has just recently been initiated and therefore, the apparatus will probably not be completed before about December, 1951. As in the case of gases, it is proposed to emphasize accuracy. It is hoped that accuracies approaching about 1% might be obtained for materials having high thermal conductivities, even though the temperature range will be extended up to nearly 1000°C for some of the materials. A number of design tests have been made, and it has been decided that measurements will be restricted at first to materials such as sodium, potassium, lithium, etc., having relatively high thermal conductivities. As part of this program, it is hoped to establish a good standard for liquid thermal conductivities in this temperature range. The primary need for accurate liquid thermal conductivity data at high temperatures is very similar to the need for heat capacity data. Both types of data are essential to problems involving heat transfer media at high temperatures.

6. Current Work of the Pyrometry Laboratory, Heat and Power Division
R. J. Corruccini

The following is a brief statement of lines of high-temperature work that have been active during fiscal year 1951. This work was unsponsored.

1. Resistance-thermometer development: Platinum resistance thermometers are widely used for temperature measurements of the highest accuracy up to 450°C. It is desired to extend the useful range of these instruments up to 1100°C. Measurement of temperatures on the platinum-resistance scale with an accuracy of 0.01 degree C up to 1100°C is desired. Maintenance of insulation resistance is the most critical feature in the design of these thermometers. Measurements have been made of the insulation resistance of thermometer components of porcelain, synthetic mica, alundum (impure aluminum oxide), and fused silica, both with d.c. and 60 cycle a.c. at 1100°C. Fused silica showed the highest resistivity. Also, its resistivity was independent of frequency, showing the absence of polarization. A design of fused silica supporting elements which achieves maximum insulation resistance has been tested and found satisfactory. Use of an unsupported monofilar coil of platinum wire has been tested and appears promising. This work is still in progress. If a satisfactory thermometer is developed, the temperature scale which it provides will be compared with the International Temperature Scale by means of direct comparison of resistance thermometers and standard platinum vs platinum-rhodium thermocouples.

2. Black-body radiation source: An experimental black-body radiator consisting of an inductively-heated graphite tube insulated by zirconia powder has been operated in air up to 2300°C. Oxidation of the graphite was less troublesome than would be predicted. However, in order to achieve higher temperatures, a neutral atmosphere will probably be used in the future. This blackbody will be used as a source of radiant energy of known intensity and spectral distribution for the calibration of spectrometers and radiation pyrometers. Its temperature will be measured in operation with an optical pyrometer.

Only preliminary work has been done on the following items. They are listed in order to show the fields in which interest exists.

3. Photoelectric pyrometer: Design studies show the feasibility of a photoelectric monochromatic pyrometer which would measure the temperature of a source by comparing its brightness with that of a standard tungsten lamp. The instrument would be a primary standard of temperature, depending for its calibration on a knowledge of known constants and of the angular openings of sector discs. It would retain most of the advantages of the optical pyrometer such as small field of view, small emissivity corrections, and operation according to an exact law (Planck's radiation formula), and in addition would be independent of the vagaries of the human eye and could be made fully automatic. Calculations indicate that a photomultiplier tube could be used as the sensitive element, though a lead sulfide cell might offer advantages.

4. Ribbon-filament tungsten lamps: A start has been made at studying the characteristics of lamps used as secondary standards of brightness temperature. It is intended to arrive at an improved design of lamp which would show minimum dependence on ambient temperature, polarity, orientation and other factors which affect the characteristics of present types of lamps.

5. High-temperature thermocouples: Furnaces are being built in which it will be possible to calibrate thermocouples for very high temperature service such as iridium vs iridium-rhodium. An optical pyrometer will be used as the primary standard of temperature. It is desired to attain temperatures of about 2000°C.

6. Tantalum-tube furnace: A furnace for general laboratory use consisting of a resistively-heated tantalum tube insulated by tantalum and molybdenum foil and operated in an inert atmosphere is being constructed. It should attain about 2500°C.

Appendix 1-A.

THEORETICAL STUDIES OF HIGH RESOLUTION INFRARED SPECTRA OF FLAMES

W. S. Benedict

I. Introduction

Considerable information has been obtained, by means of spectroscopic investigations in the visible and ultraviolet regions of the spectrum, concerning the combustion process. Various molecules and radicals have been identified in flames, in states of electronic excitation; and from the relative intensities of various lines of these spectra, the concentrations of these radicals in their various energy states have been determined. These may sometimes be interpreted in terms of an equilibrium distribution of states, to which a "temperature" may be assigned, or the deviations from equilibrium concentrations may be used to cast light on the mechanism of the combustion process. For a summary of earlier work in this field, the book "Spectrocopy and Combustion Theory", by A. G. Gaydon (London, 1948) is a standard reference; later work by Gaydon and colleagues, by R. C. Herman and G. Hornbeck (summarized in a paper delivered before the American Chemical Society meeting in Cleveland, April 1951), by G. H. Dieke and colleagues, and by others has further advanced our knowledge. Dr. H. P. Broida of this Division has also carried out recent investigations in the visible and ultraviolet regions of the spectrum, which are summarized elsewhere in this group of reports.

Corresponding investigations in the infra-red region of the spectrum have been few, principally because of the technical difficulties of studying relatively weak radiations with sufficient spectral resolution to obtain the relevant information. Low dispersion work in prism spectrometers has been carried out since the earliest days of infra-red spectroscopy; more recently E. K. Plyler and C. J. Humphreys of the Bureau[1] have made studies extending into the long-wave ranges; and Shirleigh Silverman of the Johns Hopkins University Applied Physics Laboratory has made a number of observations[2], including some at high scanning rates, and has discussed methods for using the results for temperature determinations. With the advent of sensitive infra-red detectors, the possibility of making high-resolution studies of flames in the infra-red now exists. Such observations of several simple flames (CO-O_2, H_2-O_2, C_2H_2-O_2) have now been made in the region 1 to 2.7 microns by both the above-named investigators. Drs. Plyler and Humphreys have used a 15000-line grating instrument; Dr. Silverman has used one with a 7200-line dispersing element, his spectrometer being evacuated to eliminate interference due to atmospheric absorption. The writer has collaborated in the theoretical interpretation of the results obtained with both instruments. The present report

attempts to summarize the theoretical position, in view of our previous knowledge of the spectra of the various molecules that may be encountered in such simple flames, and a few of the new results that have been obtained to date. Some of the new results have been presented before the American Physical Society; abstracts of these talks are collected in Appendix I-B. Further experimental and theoretical details will be published jointly elsewhere, and the writer wishes to thank Drs. Plyler, Humphreys, and Silverman for permission to quote their results in this report.

The experimental arrangement and results will be summarized briefly at this point. Since the principal objective of the work was identification of spectra, rather than the quantitative investigation of the intensities of emitted radiation flames, the burners used and the conditions of burning were not carefully controlled. The emission spectra of the various flames were obtained by burning premixed gases in a welding torch. The approximate relative proportions of the fuel and oxygen were metered with conventional flowmeters and the fuel-air ratio could be adjusted over relatively wide limits. In general, spectra were obtained by focusing various portions of the flame upon the entrance slit of the spectrometer. A mirror was placed back of the flame so that an image was formed inverted and superimposed on the flame. This resulted in very nearly doubling the intensity of the emission. The particular region of the flame that was focused upon the slit and the particular fuel-air ratio chosen were varied until maximum intensity of the emission in the desired spectral region or the emission of the desired identified molecule was obtained.

For the flames studied, namely, oxy-hydrogen, oxy-acetylene, and carbon monoxide-oxygen, some radiation was observed at practically all wavelengths between 1 and 2.7 microns, 2.7 microns was the long-range limit of observation with the 15,000-line spectrometer. This instrument gives very high resolution and very good response in the region between 1 and 2.2 microns, but at longer wavelengths the response decreases, both because of the decreasing sensitivity of the lead sulphide photo-conductive detector and because of the fact that the grating was being used at its extreme limit of angle. Moreover, between 2.5 and 2.7 μ the H_2O in the laboratory path and spectrometer greatly reduce the energy, there being nearly 100 percent absorption at many wavelengths[3].

The slit widths that were required to obtain spectra varied very greatly depending upon the particular type of flame being studied and upon the particular range under investigation. We will mention the effective slit widths and the approximate relative intensity of each molecule as it is discussed individually at a later point. Even under the conditions of most intense radiation, for example, in the emission of H_2O from oxy-hydrogen flames in the region of 2.5 microns, the emissivity of the radiation from a flame which had a depth of perhaps 1 cm in the tip of the outer cone was definitely well below unity as was proved by the fact that when the reflecting mirror was used the

observed intensity practically doubled. In this region it is possible to use slits with an effective resulting power as narrow as 0.2 cm^{-1}.

A brief description of the observed spectral features follows. It must be understood that we are here discussing average intensity, there being well resolved structure, with nearly zero intensity between the lines. Going to shorter wavelengths from the region of 2.5 μ the intensity of the H_2O emission gradually decreases. There is, however, strong emission between 2.5 and 2.3 microns, due both to the H_2O emission and in C_2H_2-O_2 and CO-O_2 flames, to the CO molecule. In all those flames slits of less than 0.4 cm^{-1} can be used out to 4360 cm^{-1} which is the high frequency limit of the CO emission. Beyond this point the intensity of emission from all flames drops rather sharply so that structure could not be observed except with slits as wide as 1 or 2 cm^{-1}. The intensity then gradually builds up again, reaching a maximum in the neighborhood of 2 μ (5000 cm^{-1}). The emission in this region between 4400 and 5000 cm^{-1} is due principally to the H_2O molecule and reaches a maximum emissivity of the order of perhaps 0.1 at 5000 cm^{-1}. Superimposed on the H_2O emission is emission due to the CO_2 molecule of somewhat weaker intensity except under conditions which strongly favor the production of CO_2 at the expense of H_2O, namely, in the emission from a well dried carbon monoxide-oxygen flame. Between 5000 and 5300 cm^{-1}, from 2 to 1.9 μ , the emission due to H_2O decreases in intensity as observed in the spectrometer, partly because of an intrinsic decrease in the emissivity and partly because of the atmospheric absorption due to H_2O, which, although not as strong as from 2.5 to 2.7 μ, greatly reduces the intensity received by the detector. Under conditions where the flame is burning with a very low oxygen-fuel ratio so that carbon particules are formed, resulting in a continuous background, it is clearly possible to see the effect of the absorption due to H_2O as contrasted with the regions where H_2O emission rises above the continuous background. This region of combined emission and absorption extends from approximately 5000 to 5400 cm^{-1}. The intensity gradually increases beyond this point and the absorption decreases, reaching a maximum around 5600 cm^{-1}, the maximum emissivity again being of the order of .1. Thereafter, the intensity decreases, reaching a minimum around 5900 cm^{-1}, and then starts increasing again as one goes to shorter wave lengths. In the region between 5900 and 6700 cm^{-1}, the emission is quite complex. Here in addition to the H_2O molecule, OH and C_2 spectra are observed. Depending upon the fuel-oxygen ratio and the particular region of the flame being observed, the relative intensity of these emitters can be varied. The maximum emissivity due to H_2O and OH in this region is reached around 6800 cm^{-1} and is only slightly less than that in the 5600 cm^{-1} region, being of the order of .08 or thereabouts. Between 7000 - 7400 cm^{-1} the atmospheric absorption again somewhat decreases the emission due to the flame. From 7400 - 7500 cm^{-1}, the H_2O emission again predominates and shows a rather sharp gathering together of the lines to form a head near 7500 cm^{-1}. Beyond this point, the intensity is very much decreased. With wide slits, additional emission may be observed all the way out to 10,000 wave numbers (1 μ) in all flames. However, the strongest emission is observed from the inner

cone of fuel-rich oxy-acetylene flames. This emission is attributed to the C_2 and CN molecules and reaches a maximum emissivity of the order of 0.01. There is also emission due to the H_2O molecule in this region, much weaker than that previously described, with a maximum emissivity of the same order (0.01) in the outer cone of oxy-hydrogen flames. With extremely wide slits, it is also possible to observe a very weak emission due to the OH molecule in the region between 9400 - 10,000 cm^{-1}.

In the subsequent sections of this report, we shall discuss the spectra of the molecules just named in greater detail. There are two principal problems in the interpretation of the spectra, first, the identification of the energy states responsible for the appearance of spectral lines, which is achieved when each line may be attributed to transitions between two energy levels, and all these levels correlated with a particular set of quantum numbers and molecular constants in a particular molecule. The second problem is the explanation of the intensity of each line in terms of the concentration of molecules in each such energy level. In general, absolute measurements of intensity are difficult experimentally, due to problems connected with the finite width both of the spectral lines and of the slits of the measuring instrument. The relative intensity of resolved lines can be much more easily measured and interpreted. The figures we have quoted in the previous paragraph concerning the emissivity of the lines are only semi-quantitative, and it would be extremely desirable to place them on a more quantitative basis. In the next section of this report we will summarize the general theoretically calculable facts concerning the equilibrium concentrations and intensities of the molecules that we have identified in the flame, as well as of other molecules which may be present. In following sections, we shall discuss the energy levels and absolute and relative transition probabilities in still greater detail.

2. Equilibrium Concentrations and Intensities.

One very important question in interpreting the mechanism of energy transfer in combustion is whether the concentrations of the molecules correspond to a state of equilibrium. The equilibrium among the various energy levels of a particular molecule, as a function of temperature, is one aspect of this problem, and second is the question whether the various molecules are themselves in a state of chemical equilibrium with each other at a particular temperature. From a knowledge of the heats of formation and entropies of the various possible reactants, intermediates, and products in flames, it is possible to calculate the equilibrium concentration of a large number of molecules under a large number of possible burning conditions. Because of the very wide variation in the chemical composition and burning conditions, it is impractical to cover all conditions in this report; much calculation of this kind has been carried out by S.R. Brinkley of the U.S. Bureau of Mines, by punched-card methods and should shortly be available. Further Hottel, Williams and Satterfield [4] present a number of charts from which equilibrium concentrations can be

obtained under a large number of conditions. In this section, we will present, for orientation purposes, the equilibrium concentrations that can be calculated for three simple types of flames, each at only one value of the fuel-air ratio, at one value of the total pressure, namely one atmosphere, and at three values of the temperature, namely 3000°K, 2600°K, and 2200°K. The results are summarized in Table 1.

It will be noted from Table 1 that the first mixture corresponds approximately to the products of carbon monoxide-oxygen flames at stoichiometric ratio. To this mixture we have considered the addition of a very small quantity of hydrogen, because it is difficult in practice to obtain carbon monoxide without the admixture of small quantities of hydrogen or water vapor as impurity, and in addition we have considered the addition of a very small amount of nitrogen because it is again impossible practically to exclude the nitrogen of the air from the burning mixture. The second mixture covered corresponds to a hydrocarbon-oxygen mixture, the hydrocarbon having the carbon-hydrogen ratio characteristic of ethane, and the fuel-oxygen ratio again being close to stoichiometric. Again a very small percentage of nitrogen has been added to simulate the actual appearance of this gas in the mixture. The third gas mixture considered is the oxy-hydrogen flame, again at stoichiometric ratio and again with very small quantities of carbon and of nitrogen added. For each such mixture, we tabulate the equilibrium concentration of a number of possible products of the reaction. The calculations were based principally upon the compilations of Hottel, Williams and Satterfield, which give the concentrations of the major constituents of these particular flames. The minor constituents were then calculated from various other sources for the equilibrium constants, mainly taken from the tables of free energy published by the National Bureau of Standards. For some of the free radicals considered, there are no reliable data concerning the free energies and heats of reaction. In this case, the results can be considered only of order of magnitude accuracy and are based upon estimates of the bond energy and the moments of inertia and vibrational frequencies.

The species considered in Table 1 include the main products of combustion, namely H_2O and CO_2, the products of partial combustion and unutilized reactants, namely CO, H_2, O_2 and N_2; the products of dissociation which are principally free diatomic radicals, such as OH, C_2, CN, NH, and the monatomic species O, H, and N; in addition, there are the polyatomic products of partial combustion, which may be present, CH_4, C_2H_2, CH_2O, HCN, and some hypothesized larger polyatomic radicals, namely HCO, CH_3, CH_2, and NH_2, which have never been identified with certainty by their spectra, except for NH_2, for which the evidence is quite convincing and for which the data concerning the equilibrium constants are completely speculative. For these polyatomic free radicals, the concentrations may be in error by 1 or 2 orders of magnitude; for the other substances, the calculated equilibrium concentrations are probably accurate within ±50% of the amount given for most of the species and are considerably more accurate for the well-known gases which are present in the largest concentrations.

A study of Table 1 shows that with the exception of OH the equilibrium concentration of the molecules which are not stable at room temperatures, namely the free radicals OH, CH, C_2, CN and NH is very small. The reason why these radicals may be observed in the visible and ultra-violet regions of the spectrum with relatively high intensity is the fact that in that region the emission is electronic in origin and has a very high transition probability as will be discussed directly, together with the possibility that these excited electronic states are formed in excess of the equilibrium concentration (chemiluminescence). In the infra-red region the spectra may be either electronic in origin, in which case the minor constituents may appear (and in fact C_2 and CN have appeared); or they may be due to vibration-rotation transitions without changes in the electronic quantum states. The transition probabilities for these are usually much smaller than for electronic transitions and therefore it has been possible only to observe those molecules which have the largest concentration as shown in Table 1.

Table 1 also reveals the relative change in concentration of the various free radicals and molecules that are to be expected with changing temperature. In general the concentration of free radicals decreases sharply as the temperature drops. The actual equilibrium temperature in the flame depends upon the adiabatic flame temperature, that is the temperature that would be attained if chemical equilibrium were reached due to complete combustion without the loss of any heat to the surroundings. The values of the adiabatic flame temperature for the various mixtures are included in Table 1. The actual temperature of the flame, assuming that equilibrium conditions prevail, a necessary condition for the concept of temperature to have meaning, will in general lie below that of the adiabatic flame temperature. The temperature may vary in the various regions of the flame depending on how far observations are made from the region where the reaction has taken place. It is to be expected that the actual equilibrium temperatures in the outer cone of flames may be from 100° to 200° below the calculated adiabatic flame temperatures and at greater distances from the luminous zone of the flame will fall towards room temperature. Table 1 shows how the free radical concentration drops in this intermediate region.

The second factor that determines the intensity of a spectral line or of the totality of spectral lines in an unresolved band, in addition to the equilibrium total concentration of the species which we have just discussed, depends upon the transition probability for the particular spectral line in question. In the following paragraphs, we shall discuss the available information concerning the transition probabilities in general and summarize briefly their relevance to the spectra of the region we are studying, namely from 1 to 2.7 microns. Each energy state of the molecule is characterized by various quantum numbers, namely the electronic quantum numbers (n), vibrational quantum numbers (v), and rotational quantum numbers (j). The intensity of a radiative transition between two states $E'_{n'v'j'}$ and $E''_{n''v''j''}$, having a frequency $\nu_{cm-1} = \frac{E'-E''}{hc}$ is dependent upon the frequency, the number of molecules in the upper state $N_{E'}$, and the transition probability. This transition probability may be expressed in a variety of of ways. Most fundamentally, it is given by the quantum mechanical expression

$$|R',''|^2 = \left|\int \psi'_{n'v'j'} \overrightarrow{ex} \psi''_{n''v''j''} \, d\tau\right|^2$$

where R is the dipole strength of the transition, ψ' and ψ'' are the wave functions of the two states, and ex is the electric dipole. $|R|^2$ may be separated into electronic, vibration, and rotation parts corresponding to the factoring of the wave function into those parts, and the dipole strength of each part may be computed separately from the properties of the wave functions. Thus, a familiar example is the rotational part of the transition probability for a $^1\Sigma - ^1\Sigma$ electronic transition in a linear molecule. This is given by $|R|^2_{J'J''} = CS_J$, where C is a constant depending on the magnitude of the dipole moment or its electronic-vibrational change, and

$$S_J = (J''+1)/(2J'' + 1) \qquad \text{for } J' = J'' + 1$$

$$S_J = J''/(2J'' + 1) \qquad \text{for } J' = J'' - 1$$

$$S_J = 0 \qquad \text{for other changes in J.}$$

For other types of transitions, and for non-linear molecules, more complicated expressions for S_J hold, but all are subject to the rotational sum rule that the sum of all the transitions from a given level J'' is unity. (At some times it is more convenient to omit the $2J'' + 1$ denominator in the expression for S_J, so that the sum is equal to $2J'' + 1$, the statistical weight of the state; however in our present discussion it is desirable to normalize to unity.) Similarly the $|R|^2_{v'v''}$ may be normalized to unity; for vibration-rotation transitions from the level $v = 0$, it is nearly unity for $\Delta v=1$, much lower for $\Delta v=2$, and still lower for higher values of Δv. The remaining factor in R^2, namely $|R^2_{n'n''}$ depends upon the distribution of electric charge in the two states, and must usually be determined from experiment, although order-of-magnitude calculations have been made for certain electronic transitions. It has the dimensions of $gm.cm^5.sec^{-2}$, or $(\text{electric charge} \times \text{length})^2$, and in what follows is expressed in units of $(\text{Debye})^2$ or 10^{-36} e.s.u.

Empirically, intensities are determined either in absorption or in emission. For thermal radiation, that is when the relative populations of upper and lower states are given by the Boltzmann distribution $N'/N'' = g'/g'' \, e^{-(E'-E'')/RT}$, the absorptivity α_ν and emissivity ϵ_ν, are equal according to Kirchoff's law. α_ν is defined as $(I/I_0)_\nu$, the fraction of incident radiation I_0 absorbed at the frequency ν; ϵ_ν is the ratio of emitted intensity to that emitted by a Planck black-body at temperature T and frequency ν. For line and band spectra, α is a rapidly varying function of ν. The variation across a single line depends upon the line width, a parameter which depends on such conditions of experiment as pressure, temperature, and composition, and which is difficult to determine by direct experiment under most conditions, since the line width is usually of the order of 0.1 cm^{-1} or less, whereas the effective slit width of all but the most highly dispersive spectrographs is much greater. Accordingly it is more meaningful to discuss the integrated intensity of lines or bands, defined by $\int \alpha_\nu d\nu$. This quantity has the dimensions of cm^{-1}, if frequency is expressed in those units; it is proportional to the path length and the amount of gas, and hence the

molecular parameter related to the transition probability is the integrated absorption coefficient $k_\nu d\nu = \frac{1}{p\ell}\int \alpha_\nu d\nu$, having dimensions cm^{-2} atm^{-1}. (Atmospheres refer to STP.) This quantity has been determined for a number of vibration-rotation bands, using pressures high enough to broaden the line width until the instrumental slit-width factor is eliminated. We may discuss it either for a single line, or for all the lines in a band or band system. The relation between the dipole strength and the integrated absorption coefficient is

$$|R^{',''}|^2 = \frac{3\,hc}{8\pi^3\nu N''}\int k_\nu d\nu$$

where N'' is the number of absorbing molecules per cm^3 in the initial state. If we are considering the integrated absorption coefficient of an entire band system, N'' refers to the total number of molecules of a given species, i.e., is related to Loschmidt's number. In that case, the numerical value of the proportionality factor becomes $0.08935\nu^{-1}$ $(Debye)^2/cm^{-2}$ atm^{-1}. For a single line, we must compute the fraction of molecules of that species in the initial state, by the usual quantum statistical methods, giving the result

$$\frac{N''}{N} = \frac{g\,e^{-E''/kT}}{\Sigma g\,e^{-E''/kT}} = ge^{-E''/kT}/Q\,,$$

Q being the sum of states.

Another way in which the transition probability is often expressed is in terms of the dimensionless f-value. This is given by the relation

$$f^{',''} = \frac{8\pi^2\mu c\nu}{3h\epsilon^2}\,|R^{',''}|^2$$

where μ and ϵ are the mass and charge of the electron. The numerical value of this factor is $4.7043\cdot10^{-7}\nu\,(Debye)^{-2}$. f-values are most commonly used in expressing probabilities of electronic transitions in atoms and molecules. For atoms, they are of the order of unity for resonance transitions. In some molecular transitions they approach unity, but they are generally of the order of 0.01.

The Einstein coefficients, especially the Einstein coefficient for emission, are also of interest in discussing radiative transition probabilities. The Einstein absorption coefficient,

$B^{',''} = \frac{8\pi^3}{3\,h^2c}\,|R|^2$, has the dimensions sec gm^{-1}, with the numerical value of the factor $= 6.2865\cdot10^{-7}$ sec gm^{-1} $(Debye)^{-2}$. The Einstein emission coefficient

$$A^{',''} = 8\pi hc\nu^3 B^{',''} = \frac{64\pi^4\nu^3}{3h}\,|R|^2\,,$$

has the dimensions of sec^{-1}, with the numerical value of the factor being $3.1373\nu^3$ sec^{-1} $(Debye)^{-2}$. The lifetime τ of an excited state is given by relation $\tau' = 1/\sum_{''} A^{',''}$. The ν^3 term in A/B results in the emitted intensity

Table 2a Conversion Table for Intensities and Transition Probabilities

To convert to ⟶ / multiply by entry ↓	$K_\nu d\nu$ $cm^{-2}atm^{-1}$	$[R]^2$ $(Debyes)^2$	f-value	B $sec\ gm^{-1}$	A sec^{-1}
$\int K_\nu d\nu$ $cm^{-2}atm^{-1}$	1	$.089359\nu^{-1}$	$4.2037 \cdot 10^{-8}$	$5.6175 \cdot 10^{6}\nu^{-1}$	$2.8035 \cdot 10^{-8}\nu^{2}$
$[R]^2$ $(Debyes)^2$	11.1908ν	1.	$4.7043 \cdot 10^{-7}\nu$	$6.2865 \cdot 10^{7}$	$3.1373 \cdot 10^{-7}\nu^{3}$
f-value	$2.3788 \cdot 10^{7}$	$2.1257 \cdot 10^{6}\nu^{-1}$	1	$1.3363 \cdot 10^{14}\nu^{-1}$	$0.66691\nu^{2}$
B $sec\ gm^{-1}$	$1.7801 \cdot 10^{-7}\nu$	$1.5907 \cdot 10^{-8}$	$7.4833 \cdot 10^{-15}\nu$	1	$4.9906 \cdot 10^{-15}\nu^{3}$
A sec^{-1}	$3.5670 \cdot 10^{7}\nu^{-2}$	$3.1874 \cdot 10^{6}\nu^{-3}$	$1.4995\nu^{-2}$	$2.0038 \cdot 10^{14}\nu^{-3}$	1

Table 2b Intensities and Lifetimes of Infrared Flame-Emitting Molecules

Molecule	T °K	Q_R	Q_v	$e^{-E_{el}/kT}$	Transition		ν	$\int K_\nu d\nu$ band	$\int K_\nu d\nu$ line 287°	$\int K_\nu d\nu$ line 2877°	f	τ' sec
CO	287.7	104.0	1.00001		v-r $^1\Sigma-{}^1\Sigma$	1-0	2143	259	12.3	2.3	$1.09\cdot10^{-5}$	.030
	2877.	1046.	1.521		v-r	2-0	4260	1.79	0.085	0.016	$7.5\cdot10^{-8}$	.015
OH	287.7	43.2/4	1.00000	10^{-7}	v-r $^2\pi-{}^2\pi$	1-0	3568	100		0.9	$4\cdot10^{-6}$	.03
	2877.	435.8/4	1.2063		v-r	2-0	6971	4		0.036	$1.7\cdot10^{-7}$	.015
					$^2\pi-{}^2\pi$	0-0	32600	$2.9\cdot10^4$		260.	$1.2\cdot10^{-3}$	$1.2\cdot10^{-6}$
CN $^2\Sigma$	2877.	2128/2	1.569	2.	$^2\pi-{}^2\Sigma$	0,0	9117	$5\cdot10^5$		3000.	.02	$9\cdot10^{-7}$
$^2\pi$	2877.	4732/4	1.705	.00105·4								
C_2 $^3\pi_u$	2877.	3720/6	1.809	6.								
$^1\Sigma^+_g$	2877.	553	1.676	.0706	$^1\pi u-{}^1\pi_g$	0,0	8268	$5\cdot10^5$		70.	.02	$1.1\cdot10^{-6}$
$^1\pi_u$	2877.	1258/2	1.834	.0013·2	$^3\pi_g-{}^3\pi_u$	0,0	19378	$7\cdot10^5$		600.	.029	$1.4\cdot10^{-7}$
$^3\pi_g$	2877.	3450/6	1.721	.00006·6								
CO_2	287.7	256.2	1.0768		v-r	010-000	667	187	5.1	.061	$7.9\cdot10^{-6}$	0.43
	2877.	2570.	36.9		v-r	001-000	2349	2700	74.	0.88	$1.14\cdot10^{-4}$	$2.25\cdot10^{-3}$
					v-r	101-000	3715	39	1.1	0.013	$1.6\cdot10^{-6}$	$2.1\cdot10^{-3}$
					v-r	201-000	4978	0.2	0.05	$6\cdot10^{-4}$	$8\cdot10^{-9}$	$2\cdot10^{-3}$
H_2O	287.7	167.3	1.00035		v-r	010-000	1595	300	10	0.50	$1.3\cdot10^{-5}$	.045
	2877.	5550.	2.6231			001-000	3755	180	6	0.30	$8\cdot10^{-6}$	.013
						011-000	5331	30	1.0	0.05	$1.3\cdot10^{-6}$	.0082
						101-000	7250	20	0.7	0.03	$8\cdot10^{-7}$	.010
						111-000	8807	0.6	0.02	0.001	$2.5\cdot10^{-8}$	.0073

being proportional to the (frequency)^4, since the absorbed intensity is proportional to the frequency.

The particular method of expressing the transition probability has differed with different investigators, because of the various interests of the researchers. The intensities of infrared vibration-rotation bands have usually been in terms of the integrated absorption coefficient $\int k_\nu \, d\nu$, or, when determined from the dispersion of the refractive index, in terms of the $|R|^2$ or an "effective charge". Electronic transition probabilities have generally been in terms of f-values. In discussing flame kinetics it is desirable to have the Einstein emission coefficients, which are simply related to the excited state lifetimes. Accordingly, we present in Table 2a, a conversion table for intensity calculations, which collects the numerical factors just quoted. In using the table, it must be recalled that ν is always the frequency in wave numbers, and that atmospheres refer to the gas at 273.16°K. If it is desired to use the wavelength, λ, in microns, the substitution $\nu = 10^4 \lambda^{-1}$ may be made.

In order to display the expected orders of magnitude of the intensity of emission from the various molecules of interest in the infrared, we collect various pertinent information in Table 2b. Table 2b lists at two temperatures, namely, 287.7°K and 2877°K, corresponding to room and flame conditions, for all the molecules whose spectra were observed in the course of this study, the following data: the state sum, Q, broken down into rotational and vibrational parts, as well as the fraction of molecules in some of the excited vibrational states of interest. Q_R is of importance since it is related to the number of rotational lines that will appear in any band, and Q_V likewise is related to the number of bands that appear in any sequence of constant Δv. Under transition in Table 2b are listed the most important transitions that have been found to contribute to the infrared emission from 1 to 2.7 microns as summarized in the preceding section, together with a few other important transitions outside this spectral region for the purposes of comparison and orientation. Next in Table 2 is listed the probability of this transition in several of the forms just discussed. Under $\int k_\nu d\nu$ are listed values, first for the entire band or band system, second for the most intense line in the band, at the two temperatures in question. The f-value and the lifetime of the upper state, derived from the Einstein A, relate to the entire band transition, and are essentially temperature independent.

The sources of the tabulated intensity data vary considerably in reliability, ranging from determinations of the integrated absorption coefficient that may be accurate to ±10%, to outright guesses based on analogy with similar molecules; these should however be within a factor of 10 of the true value. They are discussed in greater detail under the particular individual molecules in later sections.

There are two general conclusions that may be drawn from a study of Table 2b. First, if we are dealing with relatively thin burner flames, as we are in the experiments and studies reported at this time, the emissivity from thermally excited radiation will be well below unity.

The highest value of the integrated absorption coefficient for a single line of a rotation-vibration band at frequencies greater than 3900 cm^{-1} is approximately 0.3. This would apply to very strong line, such as $14_{-14} \longrightarrow 13_{-13}$ in ν_3 of H_2O at 3990 cm^{-1}. If the H_2O pressure, at STP is .07 atm, (corresponding to 75% H_2O at 1 atm. and 2877°K), the flame thickness 2 cm, and the line half-width $\delta_0 = 0.1$ cm^{-1}, the peak value of $P\ell\int k_\nu d\nu/\delta_0$ would be approximately 0.4. This value would lead to an emissivity and hence an emitted intensity very nearly proportional to $P\ell$, and suggests that self-absorption is not likely to occur in thin flames at these wavelengths. As was stated before, this also appears to be in accord with the approximate values of the experimental facts in the flames that we have studied.

It will be noted from a study of Table 2b that the intensities of the strongest lines in the electronic transitions are higher by 3 or 4 orders of magnitude than in the vibration-rotation bands. For C_2 and CN bands in our region, however, the thermal concentrations that were given in Table 1 for equilibrium conditions are so low that self-absorption will still not occur. However, it will be clear that if the OH concentrations approach 10%, as they do under equilibrium conditions as shown in Table 1, the OH electronic transition at 3064Å will show in its strongest lines integrated absorption coefficients very much higher than unity and will therefore very readily give rise to self-absorption and self-reversal effects in its stronger lines, as discussed by Dieke and Crosswhite [5] and by Broida [6].

The second conclusion of considerable importance to be drawn from Table 2b is that the lifetimes involved in vibration-rotation transitions in the infrared are of the order of 10^{-3} - 10^{-1} second, as contrasted with orders of 10^{-8} - 10^{-6} seconds for electronic transitions in the ultraviolet and visible, and 10^{-6} for the C_2 and CN transitions in the near infrared. This comes about principally from the ν^2 factor, in the relation between f and A, as well as from the much smaller amplitude of electronic oscillation involved in vibration-rotation transitions. Its consequence is of course that molecules that radiate vibration-rotation energy will have survived many collisions, and hence will have a very great chance of being in or near a state of thermodynamic equilibrium, as contrasted with the molecules that emit electronic energy.

The relatively high Q_v values to be noted in Table 2b at 2877°, especially for CO_2, which has one fundamental frequency as low as 667 cm^{-1}, indicate that transitions to levels above the ground state will be important in the vibration-rotation spectra of flames. Hence we will summarize here the general theoretical relations between the intensity of transitions $v' \leftrightarrow 0$, which predominate in room-temperature absorption, and those with $v'' > 0$. In the simplest theory that accounts for the relative intensity of fundamental and overtone bands [7], it appears that the vibrational transition probability $|R^{v+n,v}|^2$ is proportional to $(v+n)!/v!$. The proportionality factor for the fundamental involves the first derivative of the dipole moment with respect to internuclear distance ("effective charge"); that for the first overtone, n=2, involves the second derivative of the dipole moment ("electrical anharmonicity").

and the cubic terms in the intermolecular potential ("mechanical anharmonicity"); and successively higher values of n require correspondingly higher order terms in the electrical and/or mechanical anharmonicities. In more detailed theories [8, 9], it appears that the factorial expression $(v+n)!/v!$ applies only to that portion of the transition probability involving the electrical anharmonicity, wheras additional small correction terms must be applied to the mechanical-anharmonicity portion. For the first overtone, the latter part is proportional to 1, 3+28x, 6+112x, 10+280x, for $v = 0, 1, 2, 3$, where x is the anharmonicity constant. Since it is in general difficult to separate the electrical- and mechanical-anharmonicity portions, and since x is of the order of 0.01 for most diatomic molecules so that its neglect would not lead to gross errors, it seems proper to use the simple expression $(v+n)!/v!$ for the transition probability in most cases. It applies to diatomic molecules, and also separately to each non-degenerate mode of vibration in polyatomic molecules. This increase in transition probability with v'' has been taken into account in computing the lifetimes of the higher vibrational states in Table 2b; further examples of its influence will be discussed under the individual molecules.

3. CO

Of the molecules that are relatively abundant in flames (cf Table 1), CO has the simplest infrared spectrum, being a diatomic molecule with a $^1\Sigma$ ground state. Moreover, although its permanent dipole moment is low ($\sim$ 0.1 Debye), a relatively high effective charge is induced during vibration, so that in its vibration-rotation spectrum the fundamental and the first overtone are quite intense (cf Table 2b). The absolute intensity of these bands has been measured several times, most recently by Penner and Weber [10]. Their values of the integrated absorption coefficient, reported as 237 $cm^{-2}atm^{-1}$ and 1.64 $cm^{-2}atm^{-1}$ for the 1-0 and 2-0 transitions at 297°K, have been adopted for Table 2b. These should be accurate to ±10 percent.

In the course of recent absorption studies related to the present work, the first overtone has been observed under resolution high enough that the slit width was comparable to the line width; under these conditions it is possible to determine the integrated absorption coefficient of individual weak lines, yielding results that confirm the results of Penner and Weber. These measurements also cover the 3-0 band, yielding for the integrated band a value of 0.0093 cm^{-2} atm^{-1}.

The energy levels and molecular constants of the ground electronic state had been previously determined from various spectra. Most accurate were the data of the 4-0 band [11] in the photographic infrared. The 2-0 and 1-0 bands have been resolved [12], but a discrepancy exists, as pointed out by Rao [13] between these data and those of the 4-0 band, as well as from the same levels as observed in the ultraviolet Cameron system ($^3\Pi - {}^1\Sigma$) [14]. Farther in the ultraviolet, the fourth positive system ($^1\Pi - {}^1\Sigma$), which appears in discharges and in some flames, has given data [15] of less accuracy on levels up to $J = 21$. In none of the previous work did the observed rotational levels exceed $J = 22$.

In the course of the present work, new accurate measurements have been made of the 2-0, and 3-0 bands in absorption, and in emission the 2-0, 3-1, 4-2, and 5-3 bands have been discovered, and resolved out to $J = 46$. The new data yield improved values of the molecular constants, because they extend to higher energies, and are in essential agreement with the previous accurate data [11].

In the flame emission spectra, the lines of the 2-0 band extend to much higher J values than in absorption. A head is formed near $J = 50$ in the R branch, and is a prominent feature of the spectra. Additional heads due to the higher-state bands 3-1, 4-2 and 5-3 also appear. Figure 1 is a reproduction of the region from 4360-4180 cm^{-1} from an oxy-acetylene flame. Various fuel-oxygen ratios were used; the strongest lines were obtained when the ratio was about 2 C_2H_2: 1 O_2. A region of the flame about 1 inch above the inner cone was focussed on the slit. A mirror was placed back of the flame so that an image was formed inverted and superimposed on the flame. This resulted in

very nearly doubling the intensity of the CO lines. For the best runs, including that depicted in Figure 1, the effective slit width was 0.3 cm^{-1}. When comparison wavelengths were desired the mirror was used to focus the light of a rare-gas lamp through the flame and onto the slit.

Figure 2 shows the same spectral region for a CO-O_2 flame from a slit burner. The CO-oxygen flame spectra were obtained by burning premixed gases in the ratio of 5 CO to 1 of oxygen. Commercial grade CO containing approximately 1.5% of H_2 as principal impurity and ordinary tank O_2 were used in these experiments. Iron carbonyl was removed from the CO by passing the gas over a train of porcelain chips heated to 275°C. The gases were carefully metered through calibrated flow-meters, and burned from the end of a rectangular channel of 30 x 0.5 mm cross-section and 60 mm high. The 30 mm dimension of the burner is parallel to the optic axis of the instrument. To further increase the signal, a mirror was placed behind the flame, thus forming an image on the flame. The flames as described above with a total flow of 6 liters per minute burn with a stability such that the noise in the system is mainly electrical. Slits of 60 microns were used, which at this dispersion and frequency are equivalent to about 0.5 cm^{-1} for the vacuuum spectrometer. The region of the flame represented in Figure 2 was one inch high starting just above the inner cone.

As may be seen by comparing Figures 1 and 2, the 5-3 and 4-2 bands are much more prominent in the oxy-acetylene flames, due to the higher temperature. In both flames, the R-branches are well resolved, with little background noise. A further discussion of the relative intensities of the lines is given later. The emission lines of CO, corresponding to the P-branches of the bands, extend to longer wavelengths than illustrated. As mentioned in the introduction, emission lines due to H_2O are a complicating factor beyond 4200 cm^{-1}, particularly in the oxy-acetylene flames. These may be recognized by comparing the spectra taken under different conditions with oxy-hydrogen flame spectra; a few such lines are indicated by the symbol w in Figure 1. Between 4050-4000 cm^{-1} the H_2O emission lines are very strong compared to the lines of CO, even when relatively hydrogen-free CO is burned, and beyond 4000 cm^{-1} few if any CO lines can be recognized.

The frequencies of the band heads, measured in a manner to be described shortly, are listed in Table 3.1 and compared with the frequencies calculated from the molecular constants of Rao [13] and from the constants derived in the course of the present work (PBS). It will be noted that the new constants improve the fit considerably. It was originally hoped that the positions of individual lines as calculated from Rao's constants could be used as wavelength standards, but in view of the discrepancies noted in Table 3.1 and other inconsistencies in the relative positions of well resolved lines, it became desirable to make a very careful calibration of the spectrometers, using higher-order lines of atomic spectra as primary standards. By superposing spectra of Hg, Kr, and A, it was possible to obtain the positions of about 20 lines in both branches of the 2-0 absorption band with an accuracy of about 0.02 cm^{-1}, since these lines fall close to pairs of primary standard lines. A few emission lines in other bands also fell close to the standards, and are known with like accuracy.

For establishing a wavelength scale for the other lines, which fell between the atomic standard lines, recourse was made to the known regularities which the CO lines must follow. To a high accuracy the equation $\nu = \nu_0 + (B' + B'')m + (B' - B'')m^2 - 2(D' + D'')m^3 - 2(D' - D'')m^4$ (1) where $m = (J'' + 1)$ for the R branch and $m = -J''$ for the P branch, must represent the line positions. The lines near the atomic standards, which include a number in both branches from J = 17 to 27, as well as a few near the band center, were used to determine the constants of equation (1). This was done in the usual manner, by obtaining $\Delta_2 F''/J + \frac{1}{2}$ and $\Delta_2 F'/J + \frac{1}{2}$, and plotting against $J(J+1)$. For the state v = 0 our results, are in excellent agreement with the values, at lower J, derived from the measurements on the 4-0 band [11]. Our points, since they extend to higher J values, permit a more reliable determination of the slope of the lines which yield the constants D. Some points with $J(J+1) \sim 1600$ are also derived from emission lines in the P branch which fall close to atomic standards. The corresponding R-branch lines require a longer interpolation, and may be in error by ± 0.1 cm^{-1} but at J = 40 this introduces very little uncertainty in the determination of the constants.

Using the lines of the 2-0 band as standards, together with atomic comparison lines when they occur, it is now possible to obtain measurements of the other emission lines of CO, with an accuracy of ± 0.05 cm^{-1}, except where blended. Values, averaged from a number of measurements of both oxy-acetylene and CO-oxygen flames, are listed in Table 3.2. They are compared with values calculated from equations of the form (1) for each band. The constants used are derivable from those listed in Table 3.3. The observed lines in Table 3.2 that are underlined are those obtained directly from the atomic standards, and are presumably the most accurate. No "observed" values are given for a number of 2-0 lines that appear since the calculated values were used in establishing the wavelength scale.

The constants given in Table 3.3 are in essential agreement with earlier accurate data. The sum of our ν_0 for the 2-0 and 4-2 bands, 8414.44 cm^{-1}, may be compared with ν_0 for 4-0, 8414.46 cm^{-1} and the sum of the first four vibrational intervals for the Cameron bands, 8414.40 cm^{-1}. The vibrational constants we obtain differ from those of Rao principally in $\omega_e y_e$, which is very sensitive to small changes in the data; it may be noted that our constants give good agreement with the levels up to v = 21 determined (with less accuracy) from observations of the fourth positive system [15]. The rotational constants we obtain are also in good agreement with the other accurate results, which however extend only to $J \leq 20$. Our value of D_e, 5.95×10^{-6} cm^{-1}, is probably accurate to $\pm 3\%$; it agrees within this limit with the theoretically calculated value, $4B_e^3/\omega_e^2 = 6.12 \times 10^{-6}$ cm^{-1}. There is no observable regular trend in D with vibrational state; we have therefore arbitrarily taken $\beta = 0$; the theoretically calculated value is -1.8×10^{-9} cm^{-1}. It may be noted that although the changes in the constants y_e, D, α, β, and γ that we propose are relatively minor, so far as any effect on the lines of $J \leq 20$ is concerned, they are needed to account for the position

of the band heads (Table 3.1).

Table 3.1 Band Heads in the CO Emission Spectrum

Band	νobs, cm^{-1}	νcalc, PBS	νcalc, Rao
2-0	4360.01	4360.02	4359.46
3-1	4305.20	4305.29	4304.85
4-2	4250.80	4250.86	4250.09
5-3	4196.54	4196.49	4195.78

As discussed in Section 2, the relative intensity of the emission lines may be used to test whether the various upper-state energy levels are in thermodynamic equilibrium, and to determine the "temperature" corresponding to the modulus of Boltzmann distribution of states in various modes. For the rotational modes the transition probabilities are proportional to $(J'+J''+1)$. For the closely spaced lines of the R branches the instrumental sensitivity and the factor ν^4 are nearly constant within each band; hence if we plot the height of each unblended line, from J = 13 to 34, as $\ln I/(2J+1)$, vs. the energy E' of the upper state, we should obtain straight lines of slope 1/kT if there is thermal equilibrium. This has been done in Figure 3 for the spectrum of the CO-O_2 flame previously illustrated (Figure 2). This has also been done for a number of other spectra. The accuracy of measurement, limited by flame stability, resolving power, etc., is about $\pm 5\%$. In Figure 3 it is seen that each of the vibrational states v = 2, 3 and 4 are sensibly in rotational equilibrium with about the same "temperature" of 2800°K. Similar straight lines for the rotational distribution have been obtained from other flames studied, with temperatures ranging from as low as 1900°K for the outer fringes of the outer cone of CO-O_2 flames to as high as 3600°K for the inner cone of the C_2H_2-O_2 flame.

A "vibrational temperature" may also be obtained from the relative intensity of the heads or of corresponding resolved lines in the various bands. This requires a knowledge of the relative vibrational transition probabilities, which cannot be precisely calculated, as discussed earlier. Since for CO, x = .00612, there is an uncertainty of some 10% in the transition probabilities. This is the same order as the experimental uncertainty in the determination of vibrational temperature, for fewer points are available to determine a slope, and the instrumental sensitivity may vary over the wider frequency range involved. In Figure 3 we also present the results of a determination of vibrational temperature, plotting the logarithm of the intensity of the R 19 line of the three bands, divided by the Herman [9] transition probabilities x ν^4, against ϵ^0. Again a fairly good straight line is obtained, but with a lower effective temperature, 2360°K, for the vibrational mode than the 2800°K that was found for rotation. This would indicate that complete thermal equilibrium has not been established. This finding is not unexpected since the observations were made in a region of the flame just above the reaction zone, where conditions definitely are not in equilibrium. In the outer cone of similar flames the vibrational temperatures are nearly identical with the rotational temperatures. In the oxy-acetylene flames the same general finding

Band	2-0				3-1				4-2				5-3			
J"	R(J)		P(J)		R(J)		P(J)		R(J)		P(J)		R(J)		P(J)	
	obs	calc	obs	calc	obs	calc	obs	calc	obs	calc	obs	calc	obs	calc	obs	calc
0	a	4263.84														
1	a	4267.54	a	4256.22												
2	a	4271.18	a	4252.30												
3	a	4274.74	a	4248.32												
4	a	4278.23	4244.24	4244.26	4225.08	4225.17										
5	a	4281.66	4240.14	4240.14	4228.55	4228.56	4187.39	4188.42								
6	a	4285.01	a	4235.95	(4231.75)	4231.87	4183.20	4183.27								
7	a	4288.29	a	4231.68	4235.04	4235.11	4179.09	4179.04	4182.05	4182.05						
8	a	4291.50	a	4227.35	4238.29	4238.29	(4174.68)	4174.71	(4185.28)	4185.20	4122.27	4122.18				
9	a	4294.63	a	4222.95	4241.43	4241.39	(4170.03)	4170.39	4188.27	4188.25	(4117.89)	4117.89				
10	a	4297.70	a	4218.48	4244.44	4244.42	4165.90	4165.94	4191.34	4191.25	4113.50	4113.50				
11	a	4300.69	a	4213.94	4247.32	4247.39	4161.53	4161.44	4194.13	4194.18	(4108.97)	4109.03				
12	a	4303.62	a	4209.32	4250.38	4250.28	4156.91	4156.85	4197.03	4197.04	4104.41	4104.48	4113.95	4143.95	(4052.04)	4052.28
13	4306.47	4306.47	a	4204.66	4253.13	4253.09	4152.13	4152.22	(4199.92)	4199.82	4099.83	4099.89	4146.69	4146.69		4047.71
14	4309.27	4309.24	a	4199.92	4255.84	4255.83	4147.45	4147.52	4202.53	4202.52	4095.21	4095.22	4149.38	4149.35		4043.07
15	4312.02	4311.95	4195.13	4195.10	4258.53	4258.51	4142.74	4142.74	(4204.9)	4205.17	(4090.6)	4090.48	(4151.8)	4151.94		4038.36
16	4314.59	4314.59	4190.25	4190.23	4261.05	4261.11	(4137.72)	4137.90	4207.79	4207.74	(4085.76)	4085.68	(4154.18)	4154.48		4033.58
17	4317.15	4317.15	4185.26	4185.28	4263.60	4263.63	(4132.90)	4132.98	4210.28	4210.23	4080.69	4080.80	(4156.91)	4156.94		4028.74
18	4319.63	4319.63	4180.27	4180.26	4266.10	4266.09	4128.01	4128.01	4212.59	4212.65	4075.87	4075.87	(4159.53)	4159.32	4023.82	4023.84
19	4322.04	4322.05	4175.15	4175.18	4268.51	4268.47	4122.91	4122.96	4215.03	4215.00	4070.72	4170.83	(4161.53)	4161.63		
20	4324.38	4324.39	4170.06	4170.03	4270.80	4270.77	4117.89	4117.84	4217.30	4217.26	(4065.71)	4065.76	4163.86	4163.88		
21	4326.69	4326.66	4164.86	4164.81	4273.07	4273.01	4112.65	4112.66	4219.45	4219.46	4060.47	4060.61	(4165.90)	4166.05		
22	4328.84	4328.86	4159.52	4159.53	4275.27	4275.16	4107.39	4107.41	4221.60	4221.58	(4055.04)	4055.41	4168.00	4168.13		
23	4330.98	4330.98	4154.18	4154.18	4277.33	4277.26	4102.05	4102.10	4223.61	4223.65	4049.85	4050.16	(4170.03)	4170.16		
24	4333.00	4333.03	4148.78	4148.76	4279.34	4279.27	(4096.80)	4096.72	4225.65	4225.63	(4044.85)	4044.80	4171.99	4172.10		
25	4334.99	4335.00	4143.25	4143.27	(4281.37)	4281.21	(4091.06)	4091.26	(4227.35)	4227.54	(4039.24)	4039.37	4173.88	4173.99		
26	4336.90	4336.90	4137.74	4137.72	4283.21	4283.09	4085.76	4085.75	4229.37	4229.38	4033.86	4033.89	(4175.4)	4175.70		
27	4338.69	4338.73	4132.09	4132.10	(4285.10)	4284.89	(4080.15)	4080.16	4231.11	4231.15	(4028.22)	4028.34	4177.64	4177.53		
28	4340.43	4340.49	4126.34	4126.42	4286.74	4286.59	4074.43	4074.52	4232.78	4232.81	4022.63	4022.73	(4179.09)	4179.16		
29	4342.17	4342.17	4120.75	4120.67	(4288.29)	4288.23	4068.75	4068.80	4234.32	4234.41	(4016.9)	4017.04	(4181.08)	4180.73		
30	4343.76	4343.77	4114.87	4141.85	4290.00	4289.81	4062.87	4063.03	(4235.95)	4235.95	4011.14	4011.30	(4182.12)	4182.23		
31	4345.28	4345.30	4109.05	4108.97	(4291.50)	4291.31	4057.00	4057.18	4237.49	4237.41	(4005.6)	4005.49	4183.82	4183.65		
32	4346.69	4346.76	4102.16	4103.02	4292.91	4292.73	4051.22	4051.27	4238.85	4238.81	3999.6	3999.61	(4185.28)	4184.97		
33	4348.08	4348.14	(4096.82)	4097.01	4294.23	4294.08	4045.19	4045.29	(4240.14)	4240.13	3993.8	3994.0	4186.35	4186.32		
34	4349.40	4349.44	4091.06	4090.95	4295.39	4295.35	4039.24	4039.24	4241.35	4241.36			4187.49	4187.51		
35	4350.67	4350.67	4084.88	4084.79	4296.56	4296.55	(4033.36)	4033.14	4242.44	4242.51			(4188.27)	4188.64		
36	4351.86	4351.83	4078.53	4078.58	(4297.70)	4297.57	(4026.95)	4026.97	4243.58	4243.59			4189.70	4189.68		
37	4352.92	4352.91	4072.35	4072.30	4298.72	4298.72	4020.86	4020.73	(4244.54)	4244.60			4190.71	4190.65		
38	4353.93	4353.91	(4065.71)	4065.96	4299.70	4299.68	(4014.7)	4014.42	4245.61	4245.55			4191.57	4191.57		
39	4354.86	4354.84	4059.56	4059.56	(4300.69)	4300.58	4008.10	4008.05	4246.38	4246.41			4192.45	4192.39		
40	4355.75	4355.70	4053.11	4053.09	4301.36	4301.39	4000.41	4001.62	(4247.26)	4247.19						
41	4356.54	4356.47	4046.51	4046.56	4302.14	4302.12	3994.8	3995.12	4248.00	4247.89						
42	4357.28	4353.17	(4040.18)	4039.96					4248.61	4248.54						
43	4357.90	4357.80	4033.30	4033.30					4249.16	4249.10						
44	4358.42	4358.34	(4026.72)	4026.58												
45	4358.99	4358.82	4019.72	4019.79												
46		4359.21	4012.80	4012.93												
50-52	4360.01	4360.02			4305.20	4305.39			4250.80	4250.86			4196.54	4196.49		

Note a: Line observed (in absorption or emission). Wavelength not reported since calculated value was used to establish the wavelength scale. See text.

Table 3.2

occurs: in the inner cone $T_r > T_v$; the farther from the reaction zone, the more nearly does $T_r = T_v$.

The uncertainty in the vibrational transition probabilities does not affect the above conclusions. Somewhat better linearity of the plots was found when the x term was included, which might be taken to indicate that the mechanical anharmonicity term predominates in the expression for the first overtone intensity. It may be noted that in one of the alternative derivations of these constants [10] P'_e, the electrical anharmonicity, is nearly zero.

It should also be noted that the CO "temperatures" obtained in these preliminary studies in general fall several hundred degrees lower than "temperatures" that would result from the rotational energy distribution of the OH radical in the 3064Å band, when observed from the corresponding regions of corresponding flames. This is presumably a consequence of the much greater lifetimes involved in the infrared emission.

Since the absolute transition probabilities of the overtone bands have been determined, it is possible to calculate the expected emission intensity corresponding to thermal equilibrium at the indicated rotational or vibrational "temperatures". This leads to emissivities of the order of 0.01 for the strongest lines whereas the observed emissivity in the flames, which has not been determined quantitatively, appears to be of the same order or perhaps a little higher (~0.05). Further work is needed in this respect, to determine if deviations from thermal equilibrium exist between the upper and lower states involved, and if the emitted intensity may be used to determine the CO concentration and distribution in flames. However there is little doubt that, if a spectrograph of high resolution is available, study of the CO overtone bands is a simple and direct method of determining energy distributions.

Table 3.3 Vibrational and Rotational Constants for CO

$$E_v, J = G_v + B_v J(J+1) - D_v J^2(J+1)^2$$

$$G_v = 2169.81(v+\tfrac{1}{2}) - 13.284\ (v+\tfrac{1}{2})^2 + 0.010\ (v+\tfrac{1}{2})^3$$

$$B_v = 1.93130 - 0.017543\ (v+\tfrac{1}{2}) + 4.5\cdot 10^{-6}(v+\tfrac{1}{2})^2$$

$$D_v = 5.95\cdot 10^{-6} + 0(v+\tfrac{1}{2})$$

4. OH

The equilibrium abundance of this molecule in flames (cf. Table 1) approaches 10%, so that it may be considered under those conditions as a molecule of equal stability with any other rather than a labile free radical. Its ultraviolet spectrum ($^2\Sigma - {}^2\pi$) is a very intense feature in a wide variety of flames. One might expect to observe its vibration rotation spectrum, if the intensity of the fundamental and first overtone are of the same order of magnitude as they are for other diatomic molecules, expecially the hydrides, HBr, HCl and HF. This possibility has been long recognized; it was pointed out by Gaydon, and Dieke and Crosswhite, in their comprehensive study of the energy levels and ultraviolet band system [16], have listed the frequencies of the strongest expected lines in the 2-0, 1-0, 2-1, and pure rotation (0-0) bands. Experimentally, Plyler and Humphreys [1] detected some coincidences between these calculated frequencies and some peaks in the oxy-acetylene emission as observed with a prism spectrometer near 3.3μ , but their resolution was insufficient to make a positive identification, since H_2O will also emit strongly in the same region.

The spectrum of the first - overtone sequence is a very characteristic feature of the emission of H_2-O_2 and C_2H_2-O_2 flames in the region of 1.6μ when observed under high resolution. There is much overlapping of the spectrum of OH with that of H_2O between 6700 - 7189 cm^{-1} and some overlapping between 6400-6700 cm^{-1}, but between 5900-6400 cm^{-1} the OH-lines may be observed with only a weak background due to H_2O. A reproduction of a typical spectrum between 5800-6800 cm^{-1} is shown in Figure 4. The source was an oxy-acetylene flame of near-stoichiometric ratio observed in the region just above the tip of the inner cone. The effective slit width was 0.5 cm^{-1}. Three series of lines, each grouped in clusters of four, are observed; these are identified as the P branches of the 2-0, 3-1, and 4-2 bands. The number above each cluster of 4 is the K value of the lower state. The splitting of each K-value into four lines is due to the $^2\pi$ character of the electronic state. The interaction of the electronic spin and angular momentum with the rotational angular momentum of the molecule splits each level into 4, and the selection rules permit the appearance of 4 strong lines, as observed. (There are also "satellite" lines, too weak to be identified.) The groups of 4 consist of pairs (spin-doublets) whose separation decreases with increasing K, each of which is a close pair (Λ-doublets) whose separation increases with increasing K. The Λ-doublets are clearly resolved for $K > 7$, corresponding to a calculated separation of greater than 0.9 cm^{-1}. This clear resolution of the fine-structure, as well as the close agreement of the line positions with those calculated from the tables of Dieke and Crosswhite, is positive proof that the lines are due to OH.

The intensity of the OH spectrum relative to that of H_2O varies with the region of the flame. In the inner cone, it is still high, but the total OH intensity is not so great as in the region just above that point. Higher in the flame, the OH/H_2O ratio decreases. In oxy-hydrogen flames the same spectra can be observed, and with somewhat greater total

intensity, but the H_2O/OH ratio is greater, so that the conditions are not so favorable for observing the OH.

Wavelengths of the OH lines were checked by basing a dispersion curve for the spectrometer upon second-order lines of Kr and Ne. The results, which should be good to ± 0.3 cm^{-1}, are not accurate enough to constitute an improvement upon the frequencies derived from the ultraviolet bands, but confirm them nicely. The lines we have observed in the P branches of the 2-0, 3-1 and 4-2 bands are given in Table 4.1, together with approximate values of their intensity, as averaged from several records taken under conditions similar to that of Figure 4. The observed intensity refers to the average of the two components of the Λ-doublets, which theoretically have equal intensity. When these are unresolved or partially resolved, the observed peak intensity must be correspondingly reduced. We have also been able to identify some of the lines in the R branches of 3-1 and 2-0, forming heads near 6845 cm^{-1} and 7189 cm^{-1} respectively, but because of the serious overlapping with H_2O we shall not tabulate them; the frequencies may be readily obtained from the energy-level table [16]. Identification of Q-branch lines is rather dubious, since they are relatively weak; the position of Q1 of 3-1 is indicated in Figure 4 but the peak at that point may be principally due to H_2O.

As mentioned previously, the present measurements are not of sufficient accuracy to improve the determination of the energy levels and molecular constants of the $v = 0$, 1, 2, and 3 states beyond the values previously reported. The $v = 4$ state had however not been previously reported. Very recently Hornbeck and Herman [17] have observed the 4-0 band, and higher members of the $\Delta v = 4$ sequence, in the photographic infrared. Our measurements yield energy levels of the $v = 4$ state that are in good agreement with theirs. Since however their results are more extensive, and should be more accurate, we will present at this time only the following approximate values for the inertial constant and vibrational interval of this new level: $B_4 = 15.733$ cm^{-1}, $\Delta G_{7/2} = 3077.5$ cm^{-1}.

The second-overtone sequence, 3-0 and 4-1, should also appear in flame spectra, since these bands lie in a region of relatively weak H_2O emission (R-heads at 10356 cm^{-1} and 9856 cm^{-1} respectively; P 10 at 9660 cm^{-1} and 9252 cm^{-1} respectively). They have been observed, but in order to do so it was necessary to open the slits so wide (to 2-3 cm^{-1}) that the Λ-doublets could not be resolved. Even under these conditions the lines were quite weak; it is estimated that the intensity ratio of corresponding lines in the bands 3-0 and 3-1, which have equal upper-state populations, is about 50:1. Observed features include the spin doublets in the P-branch lines of both 3-0 and 4-1 from $Q = 5$ to 10, and the R-branch heads.

The 1-0 band has not been observed in the present studies with the 15,000 line grating spectrometer. The instrument might reveal a few of the lines of the R-branch, whose frequencies are tabulated (16), in portions of the region 3850-3950 cm^{-1} where absorption by atmospheric H_2O is not complete. No such lines could however be identified, the emission due to higher levels in the H_2O molecules (see section 8 of this report) being stronger. A preliminary search of the region 3100-3500 cm^{-1} with a new grating instrument using slits about 2 cm^{-1} wide has however shown lines which definitely appear to be the P-branch doublets of the 1-0 band, with intensities greater than the H_2O background emission in that region. Further observations will be pursued. For the present one can only say that the 1-0 band has been observed, and that its intensity relative to the overtone (2-0) is somewhat lower than the relative intensity of the corresponding bands of H_2O (001-000 and 101-000).

The integrated absorption intensities that have been entered in Table 2b for 1-0 and 2-0 of OH are estimated, based on the observed comparative intensities of H_2O, CO, and OH vibration-rotation bands, the known intensities of the former, and the calculated equilibrium concentrations of the three molecules. The resulting OH intensities cannot be expected to be accurate by a factor of better than 2 or 3, but are seen to be of the correct order of magnitude for bands of diatomic hydrides.

From the relative intensity of the well resolved lines of the P branches in the 2-0 sequence, it is possible to determine a vibration-rotation "temperature" of the OH ground state, by a procedure exactly analogous to that described for CO. For this purpose we need the rotational transition probabilities for a $^2\pi - {}^2\pi$ transition, in which both upper and lower states are intermediate between Hund's case a and case b. The formulas for this do not appear to have been previously worked out in detail, but may readily be calculated from the basic theory of Hill and Van Vleck [18]. The results are presented in Table 4.2, where for completeness we include the unobserved satellite branches, as well as the strong P_1, P_2, R_1 and R_2 branches. Two alternative notations, those of Mulliken [19] and Dieke and Crosswhite [16] are given. The line strengths apply strictly to only the 0-0 band, being calculated for the case where the parameter $Y = A/B$ is the same in the upper and lower state, and has the numberical value -7.54, characteristic for $v = 0$. Since $Y = -7.88$, -8.21, -8.57 and -8.96 for $v = 1$, 2, 3, and 4, its variation should not lead to errors of more than 0.01 in the strengths.

In Figure 5 the logarithm of the observed intensity, divided by $\nu^4 x$ the rotational transition probability, is plotted against the initial energy. Lines of the 2-0, 3-1 and 4-2 bands are included, the intensities of the latter two being further divided by the relative vibrational transition probabilities, 3 and 6. A single straight line falls fairly well through all points, indicating that equilibrium has been attained between the rotational and vibrational modes. The slope of the

Table 4.1 Observed P Branch Lines in Overtone Bands of OH

K	Band f	2 - 0 ν	2 - 0 Int.	3 - 1 ν	3 - 1 Int.	4 - 2 ν	4 - 2 Int.
	2,2'	6818.8	bl	6494.4	14		
4	1,1'	6803.3	bl	479.8	14	6159.24	bl
	2,2'	769.2	33	447.36	20	128.25	4
5	1,1'	756.6	44	434.74	26	115.70	5
	2,2'	717.5	47	397.3	24	(079.5)	bl
6	1	707.5	42	387.22	28	068.95	5.6
	1'	706.9		286.44			
	2,2'	663.6	45	345.0	20	028.81	6.6
7	1	655.45	49	336.65	22	020.39	7.1
	1'	654.43		335.52		6019.32	
	2	607.66	50	290.60	bl	5975.89	5.0
	2'	607.10		290.15			
8	1	600.54	53	283.46	24	968.39	4.5
	1'	599.69		282.44		967.51	
	2	549.28	45	233.81	20	920.8	4.5
	2'	548.55		233.11		920.1	
9	1	543.24	47	227.74	21.5	(914.5)	4.5
	1'	542.19		226.63		(913.5)	
	2	488.73	46.5	174.67	17	863.2	5.6?
	2'	487.82		174.09		862.6	
10	1	483.38	52	169.45	19.5	858.2	6 ?
	1'	482.32		168.35		856.8	
	2	425.74	34.5	113.53	14.5		
	2'	424.77		112.58			
11	1	421.21	41	108.99	15.3		
	1'	419.86		107.51			
	2	360.54	31	050.10	10		
	2'	359.69		049.34			
12	1	356.73	33	046.14	12.5		
	1'	355.41		6044.65			
	2	293.54	26	5984.78	10.5		
	2'	292.24		983.63			
13	1	290.17	29	981.19	10.4		
	1'	288.31		979.56			

Table 4.1 (Continued)

Band K	f	2 - 0 ν	Int.	3 - 1 ν	Int.
	2	224.27	18	917.06	
	2'	222.92		915.87	7.6
14	1	221.95	21.5	914.03	
	1'	219.34		912.3	9.0
	2	152.17	16	847.4	6.3
	2'	151.39		846.0	bl
15	1	150.12	18	844.61	bl
	1'	148.16		842.72	6.3
	2	079.51	15		
	2'	078.06			
16	1	076.98	13		
	1'	074.99			
	2	004.28	8.5		
	2'	002.52	bl		
17	1	6002.10			
	1'	5999.76	8.0		
	2	926.95	8.0		
	2'	925.2	bl		
18	1				
	1'	922.78	8.0		
	2	848.19	6.0		
	2'	846.2	bl		
19	1				
	1'	843.80	bl		

Table 4.2 Rotational Line Strengths for OH
(Intermediate $^2\Pi - {}^2\Pi$, $Y' = Y'' = -7.548$)

	Branches						
D + C	$P_1(K)$	$P_2(K)$	$Q_1(K)$	$Q_2(K)$	$R_{21}(K)$	$Q_{21}(K)$	$S_{21}(K)$
	$R_1(K-1)$	$R_2(K-1)$			$P_{12}(K+1)$	$Q_{12}(K)$	$O_{12}(K+2)$
Mull.	$P_1(K)$	$P_2(K)$	$Q_1(K)$	$Q_2(K)$	$^RQ_{21}(K)$	$^QP_{21}(K)$	$^SR_{21}(K)$
	$R_1(K-1)$	$R_2(K-1)$			$^PQ_{12}(K+1)$	$^QR_{12}(K)$	$^OP_{12}(K+2)$
K''							
1	0	0	2.305	0.667	0.031	0.040	0.005
2	1.623	1.293	1.402	0.300	0.045	0.037	0.006
3	2.899	2.339	0.983	0.223	0.049	0.303	0.008
4	4.040	3.370	0.735	0.188	0.052	0.027	0.007
5	5.14	4.37	0.57	0.17	0.05	0.02	0.006
6	6.21	5.38	0.46	0.16	0.05	0.02	0.005
7	7.26	6.39	0.37	0.15	0.05	0.01	-
8	8.30	7.39	0.33	0.15	0.05	0.01	-
9	9.32	8.40	0.29	0.14	0.04	0.01	-
10	10.34	9.41	0.26	0.14	0.04	0.005	-
11	11.36	10.42	0.24	0.12	0.04	-	-
12	12.37	11.42	0.22	0.11	0.04	-	-
13	13.38	12.43	0.20	0.10	0.03	-	-
14	14.39	13.43	0.18	0.10	-.03	-	-
15	15.40	14.43	0.16	0.10	0.03	-	-
16	16.41	15.44	0.15	0.10	0.03	-	-
17	17.42	16.44	0.14	0.10	0.03	-	-
18	18.42	17.44	0.13	0.09	0.02	-	-
19	19.43	18.44	0.12	0.09	0.02	-	-
20	20.43	19.44	0.11	0.09	0.02	-	-

line corresponds to 2600 ± 100°K. This is in fairly good agreement with the "CO rotational temperature" observed for the same region of the oxy-acetylene flame, but is 300 - 500° below the temperatures obtained from studies of the $^2\Sigma - ^2\pi$ electronic transition of similar flames. Again the most likely explanation is that the longer lifetime of excited states for infrared radiation lead to a "temperature" corresponding to a closer approach to true thermodynamic equilibrium. The facts that we are here observing a situation in which the emissivity is low, so that molecules from the full thickness of the flame are contributing to the observed intensity, and that at these long wavelengths the relatively cool outer fringes of the flame will make a significant contribution to the total intensity, undoubtedly also play a part in the lower "temperatures".

5. C_2

Several electronic band systems have been observed for this molecule in flames. The ground state is $^3\pi_u$; the Swan bands in the visible spectrum are a transition from a $^3\pi_g$ to the ground state. Two low-lying singlet states are also known; the transition between them; $^1\pi_u - {}^1\Sigma_g^+$, was discovered by Phillips, [25] who located the (2,0), (3,1), (3,0), (4,1) and (5,2) bands in a discharge. The same bands, lying between 7700-9000 Å, were found by Hornbeck and Herman [26] in the photographic infrared in the oxy-acetylene flame. Since the constants of both electronic states are accurately known ($^1\Sigma_g^+$ is the lower level of the Mulliken bands, and $^1\pi_u$ the lower level of the Deslandres-D'Azumbuja bands), it is possible to calculate with good accuracy the positions of the lines of the (1,0), (0,0), and (0,1) bands, which should be the strongest bands of the system under conditions of thermal excitation. The f-value of the system has not been measured or calculated, but it should be of the same order as the Swan bands, and the other band systems involving similar electron-transfer spectra [27], namely ~.02.

We have now observed (1,0) and (0,0) bands, which are the most intense features of the emission from the inner cone of the fuel-rich oxy-acetylene flame in the region of the spectrum where they occur. The (1,0) band has its head at 9865.7 cm^{-1} (10107A), and may be followed to beyond Q40, at 9491.5 cm^{-1}. The rotational structure is relatively open, there being only the three branches characteristic of a $^1\pi_u - {}^1\Sigma_g^+$ transition; a strong Q branch, and P and R branches that are weaker by a factor of 2. Moreover, because of the zero spin of the C^{12} nucleus, only even values of J, for the lower state, appear. The spacing of the Q branch lines at the maximum, near J = 24, is 22 cm^{-1}, which permits clear resolution of all three branches, even with the relatively wide slits of ~1.5 cm^{-1} required. The (1,0) band, in our tracings, is overlapped by a strong violet-shaded band head at 10330 Å. Since the second-order visible radiation was not completely removed by filters this is clearly the (0,0) Swan band, strongest band in that system, in the second order. It is of interest that the ratio of intensity of the Swan/Phillips systems showed no significant variations with conditions of excitation.

The (0,0) Phillips band extends from the head at 8282.9 cm^{-1} (12070A) to beyond Q40, at 7936 cm^{-1}. A reproduction is given in Figure 7. The wavelengths of the lines in this band have not been measured to an accuracy of better than 0.5 cm^{-1}; within that limit the agreement with the values calculated from the constants given in Herzberg's compilation [24] is perfect. The equations for the band lines are:

(1,0) band: R and P branches: $\nu = 9852.55 + 3.40224m - 0.22024m^2 - 2.8 \cdot 10^{-5} m^3$

Q branch $9852.55 - 0.22004m - 0.22004m^2$

(0,0) band, R and P branches: $\nu = 8268.50 + 3.41964m - .20304m^2 - 2.8 \cdot 10^{-5} m^3$

Q branch $8268.50 - 0.20284m - .20284m^2$

(0,1) band, R and P branch: $\nu = 6441.03+3.40132m-.18474m^2-2.8.10^{-5}m^3$

Q branch: $6441.02-0.18454m-.18454m^2$

where m is related to the J value of the lower state, which takes only even values, as follows: Q and P, m=-J; R, m=J+1.

The (0,1) band falls in the region of strong emission due to OH and moderately strong emission due to H_2O. A number of the stronger lines of the Q branch, from J"=10 to 30, may be identified by comparing tracings of the inner- and outer-cone radiation in this region; the inner cone favors C_2, the outer, H_2O. Considerable overlapping occurs, however, and, under the most favorable conditions, its intensity does not exceed 30% of that of the OH lines in the region.

The (0,0) band is quite free from overlapping under the conditions where it appears strongly (there is weak H_2O emission in the region of the head, decreasing towards longer wavelengths, due to the high-J and upper-state lines in the P branch of the (111-000) sequences: see section 8. Hence the relative intensities of the resolved Q, P and R lines may be used to determine a C_2 rotational "temperature". The rotational transition probabilities for $^1\pi-{}^1\Sigma$ are well known (Herzberg, p. 208):

$$S_J = \frac{2J+1}{4} \quad \text{(Q branch, } J'=J''\text{)}$$

$$S_J = \frac{J+2}{1} \quad \text{(R branch, } J'=J''+1\text{)}$$

$$S_J = \frac{(J-1)}{4} \quad \text{(P branch, } J'=J''-1\text{)}$$

Plotting $\log I/S_J \cdot \nu^4$ against E' a fairly good straight line is obtained, whose slope corresponds to a temperature of 2600 ± 200°K. We may also apply the iso-intensity method to this band: the point at which the intensities of neighboring lines in the P and R branches are very nearly equal is at P=18, R=34; at higher J the P branch is stronger, at lower J the R branch is stronger, for the close pairs. We have

$$36\ e^{-B'\cdot 35\cdot 36/kT} = 17\ e^{-B'\cdot 18\cdot 17/kT}, \text{ or}$$

$$T = (1260-306) \times 1.6084 \times 1.4387/\ln(36/17) = 2880°K.$$

While these "temperature" determinations on C_2 are relatively rough, due to the necessity of using wide slits and the presence of a considerable background and noise level, it is certain that the rotational distribution yields a temperature of the same order as that given by CO and OH, for the outer cones, and indicated by CN, as well as what is calculated for over-all thermal equilibrium in the reaction products. This is in marked contrast to findings in similar flames when the Swan bands of C_2 are observed[28] where "temperatures" in excess of 4000°K are indicated. This would appear to mean that the triplet states, involved in the Swan transition, are formed in the chemical reaction with

excess rotational energy which they are not able to equilibrate through collisions in their radiative lifetime of $\sim 10^{-7}$ sec whereas the singlet states involved in the Phillips transition are formed either by chemical reaction with no excess rotational energy, or by collisions efficient enough to bring their rotational mode in equilibrium with the rest of the flame in their lifetime of $\sim 10^{-6}$ sec.

The intensity (emissivity) of the strongest lines of the (0,0) and (1,0) bands is of the same order as that of CN (0,0), i.e., perhaps 0.03. Since most of the radiation coming from the 0 level is in (0,0) [(0,1) is less intense by a factor of 5 or thereabouts], we can, as with CN, estimate the concentration of excited C_2 ($^1\Pi$), if an f-value of 0.02 is assumed for the system. Because of the more open rotational structure, the result is about one order less than CN, i.e., about 10^{-7} cm atm for the excited state. The position of the singlet system relative to the ground state is not precisely known; Herzberg estimates 5300 cm^{-1} for the $^1\Sigma_g^+$. This would place the total C_2 concentration at about 10^{-4} atm, again very much in excess of the calculated equilibrium values, indicating a chemiluminescent rather than a thermal origin for this species.

6. CN

This radical has two intense electronic band systems, each with an f-value in the neighborhood of 0.02. The violet system ($^2\Sigma^+$-$^2\Sigma^+$) is a characteristic feature of carbon-rich flames burning in air; the red system ($^2\pi_i$-$^2\Sigma^+$) has also been observed in such sources, but less prominently, in the red and near infra-red. The origin of this system has recently been found [20,21] to lie farther in the infra-red than was earlier believed. The (0,0) band, which extends from 9195.6 cm^{-1} to beyond 8500 cm^{-1}, has its origin at 9117.3 ± 0.1 cm^{-1}. This band was photographed with high resolution by Kiess, [21] using a carbon arc in air as the source, and was observed with a low-resolution infra-red spectrometer by Herzberg and Phillips [20] from a discharge through benzene vapor.

We have observed this band as a very prominent feature of the radiation from the inner cone of a fuel-rich oxy-acetylene flame. In the outer cone it may be very weakly present, but is masked by water-vapor emission in the same region. A reproduction of one of our tracings is shown in Figure 6. The slit width was about 1.5 cm^{-1}. Under these conditions the complex rotational structure, consisting of 6 strong branches and two weak satellite branches, is not fully resolved. A number of the lines, especially in the strong Q branches, stand out clearly. The positions of the lines of the 6 main branches and of the R_{21} branch are indicated.

We have not measured the wavelengths on our tracings, since more accurate results may be expected either from a measurement of Dr. Kiess' plates, or of tracings taken with the present instrument using a carbon-arc source and narrower slits. The line positions can however be predicted quite closely, since other bands of this system, including the (2,0) and the (1,0) band, have been well resolved. The wavelengths of most of the lines of (2,0) appear in the Fraunhofer solar spectrum, as tabulated by Babcock and Mrs. Moore Sitterley [22]; and (1,0) has been measured by Parker [23]. Although they have not previously been so identified, many lines of the (0,0) band also appear in the solar spectrum, when not obscured by telluric water-vapor. Using these when possible, and the positions of the heads given by Kiess, the differences of corresponding lines (1,0)-(0,0) can be found. When these are plotted against $(K+1)^2$ for the R branch, K^2 for the Q branch, and $(K-1)^2$ for the P branch, the differences fall on straight lines. This permits prediction of the remaining lines. The results are given in Table 6.1. In this table wavenumbers of two-decimal accuracy are those of lines observed by Babcock and Moore; the others are calculated. From this analysis we derive the value of ν_{00} = 9117.3 cm^{-1} and $\Delta G\ 1/2$ = 1787.8 cm^{-1}. These are respectively 2.7 cm^{-1} greater and 0.9 cm^{-1} less than the values recommended by Herzberg [24] from an extrapolation of the higher-frequency bands. More precise measurements of the bands should yield definitive values for these constants.

The R_2 head and some of the stronger Q branch lines of the (1,1) band, whose origin is calculated to be 8862.7 cm^{-1}, may also be

recognized on our tracings. The structure beyond 8700 cm^{-1} is increasingly dominated by this band, as well as by the H_2O emission.

In view of the imperfect resolution, it does not seem feasible to use this band for a determination of the rotational temperature. The height of the identifying lines in the P, Q and R branches have however been drawn very approximately proportional to the calculated relative intensity at 2500°K, and it will be noted that there is rough agreement with observation. Hence one may conclude that there is no large deviation from thermal equilibrium involved in the excitation of the various rotational levels within this band.

Other members of this system are to be expected farther in the infrared. The (0,1) band, origin at 7074.9 cm^{-1}, was observed under low dispersion by Herzberg and Phillips, and has been obtained with good resolution by Humphreys with a carbon-arc source. It falls in the region of strong emission due to both H_2O and OH, and hence we have been unable to identify it with certainty on our tracings, although it appears to be present. Its intensity seems however not to equal that of the (0,0) band. The (0,2) band, with origin at 5059.0 cm^{-1}, cannot be identified. Interference from H_2O and CO_2 is only partly responsible; the intensity appears to be at least 10 times less than (0,0). The Condon parabola is such that the transition probability might be expected to be about equal to (0,0), but the ν^4 factor on the intensity undoubtedly is the principal reason for its non-appearance. The (1,3) band falls in an even more favorable position, but likewise could not be identified; its transition probability should be somewhat greater than (0,2), but not sufficiently so to give it equal intensity, if the excitation is thermal.

The order of magnitude of the $CN\ ^2\pi$ concentration may be very roughly estimated. If we accept the estimate of Herzberg and Phillips[20], the integrated intensity of the entire red system corresponds to an f-value of .02. Assuming T = 2876°, the vibrational population places 59% of the molecules in the 0 level. The non-appearance of (0,2) and the doubtful appearance of (0,1) would mean that the f value of (0,0) is at least 50% of the total radiation from that level, or $\sim$.02 X .5 X .6 = .006. The intensity of the strongest lines of (0,0) in the inner cone is comparable to that of the strong OH lines, which we have previously estimated to be of the order of 0.05; the average emissivity over the band width of 300 cm^{-1}, is $\sim$ .01. Accordingly $N_{CN^*} = 0.01 \times 300/5.10^6 = 6.10^{-7}$ cm atm. For the inner-cone depth of 0.5 cm, this gives a concentration of CN* of $1.2 \cdot 10^{-6}$ atm; if in thermal equilibrium with the ground state, the total concentration of CN is 9117 1/2 $\cdot 10^{-6} \cdot e^{9117/k \cdot 2876} = 1.2 \cdot 10^{-4}$ atm. This is 10^5 times greater than the estimated concentration at thermal equilibrium (Table 1). If these very rough results are confirmed by more quantitative measurements of the emissivity, it means that the CN* is formed in some of the chemical reactions in the inner cone, and that the radiation is chemiluminescent in origin. Temperature measurements using these bands would then have little meaning, except to demonstrate whether the radical survives through enough collisions to attain thermal equilibrium within its rotational modes. This appears to be the case.

Table 6.1 Frequencies in 0,0 Band of CN ($^2\pi - {}^2\Sigma$)

K	R_2	Q_2	P_2	R_1	Q_1	P_1	R_{21}
0	9144.0						
1	145.9	9140.9		9098.1	9090.5		
2	147.4	139.4	9132.7	102.4	091.3	9082.3	9154.1
3	148.6	136.8	127.0	106.2	091.2	078.9	159.2
4	149.5	134.1	120.9	109.2	091.7	075.9	164.0
5	150.0	131.0	114.6	111.8	090.7	072.2	168.5
6	150.19	127.6	107.9	114.0	089.46	067.6	172.1
7	50.1	124.0	100.8	115.9	088.2	062.7	175.9
8	49.8	120.3	093.5	117.2	086.2	057.3	179.5
9	149.20	115.9	085.9	118.1	083.5	051.7	182.7
10	147.94	111.71	078.0	118.48	080.40	045.4	185.6
11	146.	106.43	069.7	118.48	077.48	038.8	188.1
12	145.1	101.29	061.0	118.0	073.5	031.6	190.1
13	143.23	095.7	052.2	117.0	069.2	024.1	192.0
14	141.0	090.09	043.0	115.70	064.73	015.9	193.3
15	(138.16)	083.94	033.6	114.43	059.77	007.4	194.3
16	(134.88)	077.46	023.4	112.21	054.5	999.0	194.9
17	(131.68)	070.81	012.9	109.97	048.57	989.5	195.4
18	127.97	(064.07)	002.6	107.2	042.3	980.0	195.6
19	(123.96)	056.2	991.9	104.10	035.7	970.2	195.4
20	(119.67)	048.57	980.45	100.6	028.8	959.8	
21	114.97	040.5	969.17	096.4	021.45	049.3	
22	109.97	032.09	957.9	091.9	013.60	938.4	
23	104.55	023.3	945.4	087.17	9005.56	926.8	
24	098.9	014.2	932.9	082.0	8996.0	914.9	
25	092.8	004.8	920.01	076.40	988.0	902.59	
26	086.3	994.91	906.9	070.40	978.7	889.8	
27	079.54	984.8	893.3	064.07	969.17	876.7	
28	072.35	994.2	879.4	057.62	959.1	863.33	
29	064.73	963.47	865.1	050.2	948.6	849.81	
30	057.12	952.2	850.4	042.7	927.8	(835.25)	
31	048.57	940.7	835.05	034.8	926.7	820.8	
32	040.2	928.7	819.8	026.63	915.2	805.8	
33	031.2	916.33	804.1	017.95	903.21	790.6	
34	021.9	903.8	788.1	9008.0	890.90	774.0	
35	012.3	890.90	771.9	8999.8	878.2	759.0	
36	002.3	877.6	755.4	990.1	885.2	742.7	
37	991.9	863.80	738.3	979.8	851.6	725.9	
38	981.0	849.81	720.9	969.3	838.1	703.7	
39	969.5	835.5		958.0	883.8		
40	958.7	820.8		947.30	899.4		
41		805.7			794.6		
42		790.2			779.4		
43		774.3			763.7		
44		757.98			747.6		
45		741.38			731.2		

7. CO_2

We next consider this linear triatomic molecule, which is of course the principal product of combustion of all carbonaceous matter, and whose infrared radiation has long been recognized in flames. Its room-temperature absorption spectrum has been extensively investigated, both with paths available in the laboratory, and by studying the absorption of the CO_2 in the terrestrial atmosphere, with the sun as the source. A large number of bands have been observed, many with high resolution, and the spectrum, including the finer details, is quite well understood. Because of the low value of the doubly degenerate deformation frequency ($\nu_2 = 667.3\ cm^{-1}$), and the fact that the symmetrical stretching frequency ($\nu_1 = 1342.1\ cm^{-1}$) is very nearly equal to $2\nu_2$, resulting in strong Fermi resonances among all pairs of levels with $\Delta v_1 = -2\Delta v_2$, the absorption spectrum in the region 3700-10000 cm^{-1} is already quite complicated at room temperature, and will become increasingly so at rising temperature. As pointed out in Section 2, at 2877°K the vibrational Q = 36.9; hence for each band in a sequence ending on the (000) level, there will be very many bands going to higher levels with appreciable intensity. This tendency will be further augmented by the fact that the vibrational transition probabilities increase with increasing v_1, just as for the diatomic molecule.

Molecular constants for CO_2 have been presented in various places [29,30,31]. We have recalculated them from a consideration of all data on hand up to January 1950 (including some unpublished results kindly communicated by Dr. Herzberg): the results are listed in Table 7.1. They differ only very slightly from the previous correlations. Since that time additional data have been added [32,33] whose inclusion would lead to further slight revisions of the constants, but these do not appear justified for the present purpose, which is to calculate the positions and relative intensities of the strongest CO_2 bands in flames.

Table 7.1 Molecular Constants for CO_2

$$E_{vJ} - E_0 = G_v + B_{v_1v_2v_3} J(J+1) - D J^2(J+1)^2$$

$$G_v = 1342.9\, v_1 + 667.3\, v_2 + 2349.4\, v_3 - 3.06\, v_1^2 - 0.67\, v_2^2 + 1.17\ell^2 - 12.5\, v_3^2 + 3.20\, v_1v_2 - 20.50\, v_1v_3 - 11.75\, v_2v_3$$

$$\text{Resonance } (v_1+1,\ v_2^{\ell},\ v_3 \mid v_1, v_2-2^{\ell},\ v_3) = 51.69(1-.039\, v_3)\left\{(v_2^2-\ell^2)(v_1+1)\right\}^{1/2}$$

$$B_{v_1v_2v_3} = 0.39038 - .00116\, v_1 + .00072\, v_2 - .00307\, v_3$$

$$D = 1.8 \cdot 10^{-7}, \text{ independent of } v_i$$

The intensities of the active fundamentals ν_2 and ν_3, and of the combination bands near 3700 cm^{-1} ($\begin{matrix}02l\\101\end{matrix}$ - 000) have been accurately determined by the method of pressure broadening [34,35]; the results have been incorporated in Table 2b. An approximate value for the band at 4978 cm^{-1}, which is the strongest member of the triplet {041, 121, 201 - 000}, is also given in Table 2b; this was derived from the published high-resolution atmospheric spectrum obtained at Mt. Wilson Observatory [36], assuming the normal CO_2 atmospheric content, and should not be in error by a factor of more than 2. By comparing the 4260 cm^{-1} region of CO with the 3700 cm^{-1} region of CO_2, as given in Table 2b, it will be noted that the former is weaker in band intensity by a factor of over 20, but that the strongest-line intensity, at 2877°K, is about the same, for equal abundance of the two molecules. The CO_2 bands in the 4900 cm^{-1} region are weaker than the 3700 cm^{-1} bands by a factor of nearly 200. It will further be noted from the atmospheric spectra [36] that the bands at shorter wavelengths, namely the 6200 cm^{-1} group, are weaker by another factor of 50 or more, and hence will not be expected to appear in burner flames.

In order to calculate the intensity of upper-state transitions relative to those ending on the ground state, the following assumptions have been made. (1) If Fermi resonance did not occur, the intensity of higher-order combination bands, e.g., 021-000, would be negligible compared to that of a lower-order band, e.g., 101-000. (2) The effect of Fermi resonance is to distribute the intensity of the lowest-order combination band a among the resonating states in proportion to the squares of the fraction of unperturbed wavefunction of a in the perturbed wavefunctions. (These two assumptions are borne out by the detailed measurements and calculations on the 3612-3715 pair [35]). (3) In any sequence with $\Delta v_1 = n_1, \Delta v_3 = n_3$ the unperturbed transition probabilities are proportional to $(v''_1+n_1)!(v''_3+n_3)!/v''_1!v''_3!$. This last assumption is the appropriate generalization to the polyatomic molecule of the rule for diatomic vibrational probabilities, and is subject to the same approximation, namely, the neglect of anharmonic wavefunctions.

From the molecular constants given it is possible to calculate both the origins of the various bands in a sequence, and the position of the head which will be formed at high J in the R branch. For linear CO_2, head formation follows the same laws as in a diatomic molecule: namely $\nu_{head} - \nu_0 = (B'+B'')^2/4(B''-B') - (D'+D'')(B'+B'')^3/4(B''-B')^3 = (0.7808 - \alpha)^2/4\alpha - 4.2\cdot10^{-8}/\alpha^3$. In calculating $\nu_{head} - \nu_0$ for CO_2, Table 7.2, which gives this quantity, as well as J_{head}, as a function of $\alpha = B''-B'$, should be of use. Since at a temperature of 2877°K the intensity maximum occurs at J = 62, and lines up to J = 140 are still quite strong, R-heads should be a prominent feature of all bands with $\alpha \geq .00270$.

It should further be noted that when $l>0$, the α will be slightly different for the two components of the double band ("l-type doubling"). The constants for this effect are known only in a few cases, it has been taken into account in an approximate manner. The splitting of the heads due to this effect should rarely exceed 5 cm^{-1}.

Table 7.2 Head Formation in CO_2 Bands

$B''-B'$, $cm^{-1} \cdot 10^5$	150	200	250	300	350	400	450	500	550	600	650	700	750	800
J_{head}	260	195	152	130	112	98	86	78	70	65	60	56	52	49
$\nu_{head} - \nu_0$ cm^{-1}	88.2	72.5	58.3	48.8	42.5	37.3	33.3	30.1	27.4	25.2	23.3	21.6	20.2	18.9

Taking into account the facts just cited, we have calculated the contributions of various bands to the CO_2 emission in the regions of 3700 and 4900 cm^{-1}; the results, for the stronger bands at T = 2500°K, are given in Tables 7.3 and 7.4. When the ν_0 is given with the figure after the decimal points, both upper and lower states involved have been observed, and the entries should be reliable to ±1 cm^{-1}; otherwise to ±5 cm^{-1}. The upper states are not listed, since they all are members of resonance groups, but they can readily be deduced. Both Tables 7.3 and 7.4 are far from complete; the point to be made from a study of the tables is that there will be a tremendous overlapping of bands of roughly similar intensity, so that it is hopeless to expect to resolve any individual rotational lines at these temperatures. The most that might be expected is that some of the more prominent heads could be recognized.

The very large number of bands of comparable intensity has however one advantageous result: the spacing of individual lines becomes of the same order or less than the line width, so that the spectrum is more nearly that of a true continuum than of a discrete source. Hence such temperature-measuring techniques as the two-path method, using broad-band filters or monochromators of low resolving power, are more likely to give correct results in regions where the emission is principally due to CO_2, than when the other molecules discussed in this report are the emitters.

In the experimental studies thus far, the 3700 cm^{-1} region has not been observed with sufficient resolution to locate any of the heads predicted in Table 7.3. The strong absorption and emission due to H_2O make this region difficult to study, even with the vacuum spectrometer. There are however indications of a sharp rise in intensity near 3770 cm^{-1}, in accordance with the large number of predicted heads in that region.

In the 4700-5000 cm^{-1} region the H_2O absorption does not interfere, but emission due to this molecule is very intense, so that even with relatively hydrogen-free CO, the principal recognizable structural features in the $CO-O_2$ flame are due to H_2O. By comparison of $CO-O_2$, $C_2H_2-O_2$, and H_2-O_2 spectra, it is possible to distinguish a weak general emission in the $CO-O_2$ flame, between 4500-5100 cm^{-1}, that is, due to CO_2. Slits of $\gtrsim 1$ cm^{-1} are required to produce it with sufficient intensity.

Table 7.3 Calculated CO_2 Bands in 3700-cm^{-1} Region

v_1''	v_2''	ℓ''	v_3''	ν_0, cm^{-1}	$\bar{S}$, cm^{-1}-10^5	ν_{head}	$I_{2500°K}$
0	0	0	0	3612.9	277	3667	43
0	0	0	0	3714.6	309	3764	57
0	1	1	0	3581	274 ± 18	3634 ± 3	57
0	1	1	0	3724	312 ± 14	3771 ± 2	79
1	0	0	0	3465.7	209	3536	22
0	2	2	0	3551	273 ± 1	3604	37
0	2	0	0	3568.5	239	3630	17
1	0	0	0	3589.9	369	3631	31
0	2	0	0	3692.7	399	3730	25
0	2	2	0	3725	313 ± 1	3772	55
1	0	0	0	3711.6	262	3767	25
0	2	0	0	3814.4	300	3863	20
1	1	1	0	3398.4	214 ± 21	3467 ± 7	30
0	3	3	0	3538	283	3590	25
0	3	1	0	3542.3	247 ± 16	3601 ± 4	24
1	1	1	0	3566.2	346	3609	42
0	3	1	0	3710.1	378 ± 9	3750 ± 1	33
1	1	1	0	3716	270 ± 4	3770 ± 1	34
0	3	3	0	3738	303	3786	37
0	3	1	0	3859	302 ± 1	3907	27
0	0	0	1	3565	274	3616	22
0	0	0	1	3670	312	3717	29
0	1	1	1	3530	271 ± 18	3584 ± 3	29
0	1	1	1	3677	315 ± 14	3724 ± 2	41

etc., etc.

Table 7.4 Calculated CO_2 Bands in 4900 - cm^{-1} Region

v_1''	v_2''	ℓ''	v_3''	ν_0, cm^{-1}	α, $cm^{-1} \cdot 10^3$	ν_{head}	$I_{2500°K}$
0	0	0	0	4854.0	210	4924	18
0	0	0	0	4978.2	370	5019	60
0	0	0	0	5099.1	267	5154	22
0	1	1	0	4807.6	217 ± 34	4866	26
0	1	1	0	4965.4	348 ± 9	5008 ± 1	70
0	1	1	0	5125	272 ± 19	5178 ± 4	40
1	0	0	0	4687.6	137	-	14
0	2	2	0	4757	221 ± 5	4823 ± 2	19
0	2	0	0	4790.4	167	-	11
1	0	0	0	4840.0	357	4882	38
0	2	0	0	4942.8	387	4981	31
1	0	0	0	4959.9	371	5000	42
0	2	2	0	4980	351 ± 3	5022	46
0	2	0	0	5062.7	401	5100	34
1	0	0	0	5114.6	211	-	21
0	2	2	0	5147	265 ± 5	5202 ± 1	28
0	2	0	0	5217.4	241	5278	17
0	0	0	1	4785	193	-	9
0	0	0	1	4911	364	4952	30
0	0	0	1	5029	290	5079	12

etc., etc.

Table 7.5 Observed CO_2 Peaks in 4900-cm^{-1} Region

Int	Character	ν_{obs}	ν_{calc}
10	R-Head	5019	5019
7	R-Head	5012	5009
12	R-Head (+H_2O)	5007	5007
5	Broad line	4987	?
10	Head ?	4971	4981 ?
8	Line ?	4966	?
10	Line ?	4962	?
18	R-Head (+H_2O)	4952	4952
15	R-Head	4925	4924
12	Line ?	4911	?
8	Line ?	4907	?
25	Broad line ?(+H_2O)	4904	?
10	Head ?	4898	?
10	Line	4894	?
12	Head ?	4891	4882 ?
15	Broad Line ?	4865	4866
20	Broad line ?	4858	?
8	Sharp Line	4851	?
15	Head ?	4838	4825 ?
8	Wide head	4804	?
10	Sharp line	4782	?

The CO_2 emission is strongest from 4700-5050 cm^{-1}, reaching maxima near 4858 and 4903. Most of the peaks have the appearance of lines rather than R-heads, and may arise from fortuitous overlapping of a number of individual lines. The most prominent have been measured, and are listed in Table 7.5. There are numerous agreements with the strongest predicted heads in Table 7.4; it must be recalled that many higher-level bands of comparable intensity have been omitted from Table 7.4. The agreement is suggestive, but it is apparent that the heads are not sufficiently distinct to permit any check on the molecular constants, or to make it possible to determine a "CO_2 vibrational temperature" from the relative intensity of the peaks in this region.

In the region of the ν_3 fundamental, the number of bands is less, because resonance among the lower-lying levels is not so extensive. This region has not yet been studied with a grating instrument, but a prism spectrometer, using a LiF prism and a sensitive detecting system that permitted slits as narrow as $\sim$2.2 cm^{-1}, has clearly revealed the strongest predicted heads, of the 001-000 band at 2397 cm^{-1}, of 011-010 at 2385 cm^{-1}, and of an incomplete group near 2374 cm^{-1}. Even here however, it is likely that problems of overlap, atmospheric- and self-absorption would render difficult any determinations of vibrational temperature.

8. H_2O (In collaboration with A. M. Bass)

By far the largest amount of the resolved emission between 3700 - 10,000 cm^{-1}, from flames of all hydrogenous materials, is due to H_2O. The absorption spectrum of this molecule, which has the vibrational spectrum of a non-linear triatomic molecule, and the rotational structure of a quite asymmetric rotator with three relatively low moments of inertia, has been extensively studied, until it is perhaps the best understood molecule of its class. The most recent work has been that of the present writer [37], who has revised and extended the earlier analyses of the vibration-rotation spectrum [38,39,40,41]. This spectrum has been observed both in the laboratory and in the earth's atmosphere, with the sun as a source, and extends from the far infra-red to well in the visible. The emission spectrum has not previously been studied under high resolution, but it has long been recognized that the strong emission from flames in the regions of 2.8 μ, 1.9 μ, and 1.4 μ is due to this source, and Gaydon [42] has attributed, undoubtedly correctly, some of the weaker emission in the red and photographic infrared to the higher overtone- and combination bands.

Because of its three quite different and quite low moments of inertia, the rotational structure of each vibrational band is complicated, and extends over a very wide spectral range. Lines in the pure rotation spectrum have been identified up to 1019 cm^{-1}, where they overlap, in the atmospheric absorption, lines of the ν_2 fundamental vibration. In this strong vibration-rotation band, with origin at 1594.6 cm^{-1}, some 600 lines have been identified, extending from 898 cm^{-1} to beyond 2250 cm^{-1}. Lines of the other two fundamentals, ν_1 with origin at 3657.0 cm^{-1}, and the very much stronger ν_3 with origin at 3755.8 cm^{-1}, are intermingled: over 600 lines have been identified from 3300 - 4350 cm^{-1}. For the higher overtone and combination bands there is even more overlapping of the lines from different vibrational transitions, and the spectrum can better be characterized as a "many-line" spectrum than as a banded spectrum.

At the high temperatures of flames, the number of rotational lines, and the extent of the bands, will be further increased, and the appearance of "upper-state" transitions is an additional complication. Nevertheless the principal features of the extensive emission spectrum, which is sufficiently intense that slits narrow enough to resolve many individual lines can be employed, can be recognized. The present section will summarize briefly the results of the room-temperature absorption studied, and point out some of the more obvious features of the emission spectrum. A more detailed analysis of the emission is in progress.

There are two types of bands, those in which the change of dipole moment is parallel to the symmetry axis of the molecule, which is the axis of intermediate moment of inertia B; and those in which the change is perpendicular to the symmetry axis, along the axis of least moment of inertia A. The former type includes the pure rotation band and the

two symmetrical fundamentals, ν_1 the symmetrical stretching vibration, and ν_2 the bending vibration, together with all overtones and combination bands in which the quantum number of ν_3 changes by an even integer; the latter type includes the ν_3 fundamental, the asymmetrical stretching vibration and all its odd overtones and combinations. It is an empirical fact that with the exception of the ν_2 fundamental, all the strong vibration-rotation bands are of the latter type, here called perpendicular or type A bands. In the solar spectrum, which provides a path of water vapor equivalent to about 5000 cm. atm., some 40 vibrational states have been identified. These are listed in Table 8.1, which gives the three vibrational quantum numbers of the state, the energy of its rotationless level G_v, the three effective rotational constants A_v, B_v, and C_v, the asymmetry parameter $k = 2B-(A_v+C_v)/A_v-C_v$, the moments of inertia ($I_x=27.9934\cdot 10^{-40}/X$), and the approximate intensity of the transition from the ground level, in $\int k_\nu d\nu$ and $(\text{Debyes})^2$. The source and significance of these constants will be discussed presently.

For the vibrational energy G_v, a formula has been developed, which fits the 40 levels with an average deviation of less than 1 cm^{-1}. The formula contains 23 constants, including terms up to the cubic in the three quantum numbers, as well as terms which take into account the existence of perturbations between levels of like symmetry that differ by 1 or 2 units in the quantum numbers. Table 8.2 gives the constants and the results of the calculation; G_v' is the calculated energy to the first approximation, ignoring the resonance perturbations; G_v'' takes into account the perturbation of levels with $\Delta v_1 = -\Delta v_3 = 2$; G_v''' is the finally calculated G_v, taking into account the perturbation of levels with $2\Delta v_1 = -\Delta v_2 = 2$.

The values G_v in Table 8.1 are those of the rotationless level 0 of each vibrational state. Built upon this are the rotation-vibration levels, each characterized by the two quantum numbers $J\tau$, or in the alternative notation of KHC [43], the three quantum numbers $J_{K_{-1}K_1}$, with $\tau = K_{-1}-K_1$. As explained in reference [43], the numerical values of the energy levels can be calculated, to first approximation, in terms of the three rotational constants (and, to a higher approximation, in terms of centrifugal stretching constants) and the asymmetry parameter which is a function of these. Table 8.1 shows that there is a wide variation in these constants from one vibrational state to another; k, which is -0.4377 in the ground state, varies from -0.2849 to -0.6620 in observed levels, and the rotational constant A increases by nearly 100% from its lowest value, in some of the levels of high v_2. An empirical formula that gives the rotational constants as functions of the vibrational quantum numbers is given in Table 8.3, and the resulting calculated constants are compared with the observed ones in Table 8.4. When resonance occurs among the levels with $v_1 = v_3 \pm 2$, this has been taken into account in the calculation (cf [40]).

A very large number of vibration-rotational levels have been identified in the absorption spectrum. Those for the lower vibrational states, up to (011), are listed in Table 8.5. It will be noted

Table 8.1 Vibration-Rotation Absorption Bands of H_2O

V_1	V_2	V_3	G_v	A	B	C	k	I_A	I_B	I_C	Δ	Intensity $\int K_\nu d\nu$	Intensity $(D)^2$
			cm^{-1}	cm^{-1}	cm^{-1}	cm^{-1}		10^{40} gm cm^{-2}				$cm^{-2}atm^{-1}$	10^{-36} esu
0	0	0	0.00	27.877	14.512	9.285	-.4377	1.0038	1.9283	3.0138	.0817		3.46
0	1	0	1594.59	31.12	14.66	9.152	-.4985	0.8992	1.9088	3.0576	.2496	300.	$1.7\cdot10^{-2}$
0	2	0	3151.53	35.47	14.83	9.01	-.5714	0.7887	1.8869	3.1089	.436	1.	$3\cdot10^{-5}$
1	0	0	3657.05	27.13	14.29	9.105	-.4247	1.0315	1.9583	3.0734	.0836	8.	$2\cdot10^{-4}$
0	0	1	3755.79	26.636	14.40	9.156	-.4000	1.0506	1.9433	3.0563	.0624	180.	$4.5\cdot10^{-3}$
0	3	0	4666.62	42.03	14.95	8.88	-.6338	0.6658	1.872	3.151	.614	.008	$1.6\cdot10^{-7}$
1	1	0	5235.0	30.28	14.44	8.99	-.4880	0.924	1.938	3.113	.251	1.	$2\cdot10^{-5}$
0	1	1	5331.19	29.54	14.59	9.00	-.4557	0.947	1.918	3.109	.244	30.	$5.3\cdot10^{-4}$
1	2	0	6775.00	34.35	14.63	8.81	-.5442	0.815	1.913	3.176	.449	.03	$4\cdot10^{-7}$
0	2	1	6871.34	33.29	14.75	8.87	-.5184	0.841	1.897	3.155	.417	1.4	$1.9\cdot10^{-5}$
2	0	0	7201.40	26.38	14.13	8.99	-.4089	1.061	1.981	3.113	.071	2.0	$2.6\cdot10^{-5}$
1	0	1	7249.77	25.93	14.19	8.94	-.3771	1.079	1.972	3.130	.079	20.	$2.6\cdot10^{-4}$
0	0	2	7445.16	25.53	14.19	9.03	-.3745	1.096	1.972	3.099	.031	0.15	$1.9\cdot10^{-6}$
1	3	0	8273.94	40.57	14.73	8.68	-.6212	0.690	1.900	3.224	.634	.005	$6\cdot10^{-8}$
0	3	1	8373.70	38.64	14.91	8.75	-.5878	0.724	1.877	3.198	.597	.02	$2.3\cdot10^{-7}$
2	1	0	8761.56	28.92	14.38	8.78	-.4439	0.968	1.946	3.187	.273	.01	$1\cdot10^{-7}$
1	1	1	8806.95	28.68	14.42	8.77	-.4324	0.976	1.941	3.191	.274	.6	$6\cdot10^{-6}$
0	1	2	9000.10	28.15	14.47	8.87	-.4243	0.994	1.934	3.155	.227	.02	$2\cdot10^{-7}$
0	4	1	9833.54	46.8	15.04	8.58	-.6620	0.598	1.861	3.262	.803	.002	$2\cdot10^{-8}$
2	2	0	10284.									<.001	$<10^{-8}$
1	2	1	10328.70	32.33	14.56	8.69	-.5034	0.866	1.922	3.220	.432	.06	$5\cdot10^{-7}$
3	0	0	10599.66	25.47	13.95	8.75	-.3849	1.099	2.006	3.198	.093	.015	$1.4\cdot10^{-7}$
2	0	1	10613.26	25.20	13.94	8.83	-.3757	1.110	2.007	3.169	.051	.3	$2.7\cdot10^{-6}$
1	0	2	10868.81	25.25	14.03	8.79	-.3633	1.083	1.994	3.184	.107	.01	$1\cdot10^{-7}$
0	0	3	11032.37	24.53	14.20	8.87	-.3193	1.141	1.971	3.155	.043	.05	$4\cdot10^{-7}$
1	3	1	11813.17	37.52	14.71	8.56	-.5753	0.746	1.902	3.269	.621	.003	$2.5\cdot10^{-8}$
3	1	0	12139.79	28.2	14.2	8.57	-.426	0.992	1.971	3.265	.303	.0015	$1\cdot10^{-8}$
2	1	1	12151.22	28.11	14.16	8.69	-.4367	0.996	1.976	3.220	.248	.15	$1.2\cdot10^{-6}$
1	1	2	12407.61	28.0	14.20	8.62	-.4241	0.999	1.971	3.246	.276	.002	$1.5\cdot10^{-8}$
0	1	3	12564.87	26.88	14.43	8.75	-.3734	1.041	1.939	3.198	.218	.02	$1.5\cdot10^{-7}$
2	2	1	13652.65	31.25	14.31	8.53	-.4912	0.896	1.955	3.304	.453	.015	$1\cdot10^{-7}$
2	0	2	13828.3									<.0005	$<3\cdot10^{-9}$
3	0	1	13830.93	24.72	13.71	8.62	-.3677	1.132	2.041	3.246	.073	.08	$5\cdot10^{-7}$
4	0	0	14221.20	24.74	13.70	8.61	-.3689	1.131	2.043	3.250	.076	.002	$1.3\cdot10^{-8}$
1	0	3	14318.77	24.12	13.75	8.61	-.3372	1.160	2.035	3.250	.055	.02	$1.3\cdot10^{-7}$

Table 8.1 (Continued)

V_1	V_2	V_3	G_v	A	B	C	κ	I_A	I_B	I_C	Δ	Intensity $\int K_\nu d\nu$		(D)
			cm^{-1}	cm^{-1}	cm^{-1}	cm^{-1}		10^{40} gm cm^{-2}				$cm^{-2}atm^{-1}$		10^{-36} e
3	1	1	15347.89	27.23	13.95	8.52	-.4196	1.028	2.006	3.284	.251	.005	3	$\cdot 10^{-8}$
1	1	3	15832.47									.0005	3	$\cdot 10^{-9}$
3	2	1	16821.59	29.52	14.00	8.35	-.4662	0.948	1.999	3.351	.404	.005	3	$\cdot 10^{-8}$
3	0	2	16898.38									.001	6	$\cdot 10^{-9}$
4	0	1	16898.79	24.85	13.61	8.50	-.3749	1.126	2.056	3.292	.110	.01	6	$\cdot 10^{-8}$
2	0	3	17495.46	23.75	13.85	8.34	-.2849	1.178	2.020	3.355	.157	.002	1	$\cdot 10^{-8}$
4	1	1	18394.43									.0005	3	$\cdot 10^{-9}$

Table 8.2 Vibrational Levels of H_2O

V_1	V_2	V_3	G_v' calc	G_v'' calc	G_v^{III}	$G_{v_{obs}}$	Δ(obs-calc)
0	0	0	0.00		0.00	0.00	--
0	1	0	1594.59		1594.59	1594.59	--
0	2	0	3151.71		3151.31	3151.53	+0.22
1	0	0	3656.65		3657.05	3657.05	--
0	0	1	3755.79		3755.79	3755.79	--
0	3	0	4667.57		4666.51	4666.62	+0.11
1	1	0	5233.90		5234.96	5235.0	+0.04
0	1	1	5331.06		5331.06	5331.19	+0.13
0	4	0	6138.40		6136.52		
1	2	0	6774.09		6775.09	6775.00	+0.09
2	0	0	7228.62	7200.87	7201.75	7201.40	-0.35
0	0	2	7417.12	7444.90	7444.90	7445.16	+0.26
0	2	1	6872.10		6871.57	6871.34	-0.23
1	0	1	7249.24		7249.77	7249.77	.00
0	5	0	7560.41		7557.61		
1	3	0	8273.42		8273.89	8273.94	+0.05
2	1	0	8787.58	8759.04	8961.37	8761.56	+0.19
0	1	2	8981.73	9000.28	9000.28	9000.10	-0.18
0	3	1	8375.11		8373.72	8373.70	-0.02
1	1	1	8805.41		8806.80	8806.95	+0.15
0	6	0	8929.82		8926.07		
1	4	0	9728.14		9727.71		
2	2	0	10309.90	10281.26	10283.68	(10284)	
0	2	2	10495.35	10524.00	10523.41		
3	0	0	10717.20	10598.17	10600.07	15099.66	-0.41
1	0	2	10749.40	10868.44	10869.03	10868.81	-0.22
0	4	1	9836.32		9833.90	9833.54	-0.36
1	2	1	10327.75		10328.76	10328.70	-0.06
2	0	1	10659.04	10611.96	10613.37	10613.26	-0.11
0	0	3	10985.48	11032.55	11032.55	11032.37	-0.18
1	5	0	11134.46		11128.14		
2	3	0	11791.77	11763.67	11762.15		
0	3	2	11984.16	12012.15	12010.72		
3	1	0	12256.95	12134.46	12139.26	12139.79	+0.53
1	1	2	12283.15	12405.64	12407.17	12407.61	+0.44

Table 8.2 (Cont.) Vibrational Levels of H_2O

V_1	V_2	V_3	G_v' calc	G_v'' calc	G_v'''	$G_{v_{obs}}$	Δ(obs-calc)
0	5	1	11251.97		11248.42		
1	3	1	11812.48		11812.46	11813.17	+0.71
2	1	1	12195.17	12147.27	12150.84	12151.22	+0.38
0	1	3	12518.09	12566.00	12566.00	12564.87	-1.13
2	4	0	13219.23	13192.26	13192.75		
0	4	2	13424.22	13451.19	13448.58		
3	2	0	13760.46	13637.13	13643.82		
1	2	2	13786.30	13909.64	13916.58		
4	0	0	14121.06	14220.30	14221.68	14221.20	-0.41
2	0	2	14000.37	13824.69	13820.36	13828.3	+7.9
0	0	4	14458.94	14535.38	14535.38		
1	4	1	13255.83		13252.80		
2	2	1	13697.89	13649.79	13650.57	13652.65	+2.08
0	2	3	14022.93	14071.02	14070.21		
3	0	1	13987.11	13827.65	13829.90	13830.93	+1.03
1	0	3	14158.45	14317.91	14318.72	14318.77	+0.05
1	5	1	14653.99		14645.44		
2	3	1	15163.42	15115.79	15116.36		
0	3	3	15496.20	15543.83	15541.76		
3	1	1	15502.26	15340.00	15347.96	15347.89	-0.07
1	1	3	15668.45	15830.71	15832.78	15832.47	-0.31
3	4	0	16643.01	16525.98	16531.03		
1	4	2	16686.31	16803.34	16752.99		
4	2	0	17115.08	17216.49	17219.20		
2	2	2	16988.41	16809.50	16846.82		
0	2	4	17462.27	17539.77	17538.81		
5	0	0	17441.75	17453.84	17458.07		
3	0	2	17169.36	16886.33	16903.12	16898.38	-4.74
1	0	4	17475.70	17746.44	17747.40		
2	4	1	16588.02	16541.38	16589.74		
0	4	3	16934.18	16980.82	16977.25		
3	2	1	16984.38	16821.18	16822.10	16821.59	-0.51
1	2	3	17151.07	17314.23	17315.61		
4	0	1	17232.19	16887.58	16899.34	16898.79	-0.55
2	0	3	17251.76	17493.69	17495.92	17495.46	-0.46
0	0	5	17839.65	17942.33	17942.33		

Table 8.2 (Cont.) Vibrational Levels of H_2O

v_1	v_2	v_3	G_v' calc	G_v'' calc	G_v'''	G_v obs	Δ (obs-calc)
2	5	1	17957.79	17912.72	19709.67		
0	5	3	18122.96	18168.03	18164.68		
3	3	1	18431.58	18268.09	18263.83		
1	3	3	18600.73	18764.21	18762.17		
4	1	1	18723.75	18373.65	18394.71	18394.43	-0.28
2	1	3	18737.35	18983.29	18988.68		
0	1	5	19324.25	19328.41	19328.41		

$$G'_v = 3698.99\,v_1 + 1612.07v_2 + 3803.02v_3 - 42.393v_1^2 - 16.847v_2^2 - 47.283v_3^2 - 17.078v_1v_2 - 164.952v_1v_3 - 20.265v_2v_3 + .053v_1^3 - 0.63v_2^3 + 4.053v_3^3 - 0.47v_1^2v_2 + 0.676v_1^2v_3 + 1.617v_2^2v_3 + 0.205v_1v_2^2 + 1.076v_1v_3^2 - 1.76v_1v_2v_3 - 0.67v_2v_3^2$$

G_v'' from G_v', resonance $(v_1v_2, v_3+2 \mid v_1+2, v_2v_3)$ $= \{6009(v_1+2)(v_1+1)(v_3+2)(v_3+1)(1+.0103v_2-.0246\,v_3)\}^{\frac{1}{2}}/2$

G_v''' from G_v'', resonance $(v_1, v_2+2 \mid v_1+1, v_2)$ $= \{200(v_1+1)(v_2+2)(v_2+1)\}^{\frac{1}{2}}/2$

Table 8.3 Rotation Vibration Interaction Constants for H_2O

General Formula: $\log_{10} X = \log_{10} X_0 + \sum_{i=1}^{3} \alpha_i^X v_i + \sum_{i,j} \alpha_{ij}^X v_i v_j + \sum_{ijk} \alpha_{ijk}^X v_i v_j v_k$

0	X=A	X=B	X=C	$\pi \cdot X$	
I_e^X	1.0224	1.9180	2.9404		10^{-40} gm·cm^2
X_e	27.370	14.590	9.517		cm^{-1}
X_0	27.877	14.512	9.285		cm^{-1}
$\log_{10} X_0$	1.4453	1.1618	0.9678	3.5749	
α					
1	-.0119	-.00633	-.00915	-.02738	
2	.04665	.0042	-.0067	.04415	
3	-.0199	-.00233	-.00595	-.02818	
11	.0001	0	-.0001	0	
12	.0002	-.0002	-.0001	-.0001	
13	.0002	0	-.0002	0	
22	-.0001	0	0	-.0001	
23	-.0024	-.0002	-.0001	-.0027	
33	.0001	0	-.0001	0	
111	0	-.000067	0	-.000067	
112	.0002	.0002	0	.0004	
113	0	-.0002	0	-.0002	
122	-.0003	0	0	-.0003	
123	.0004	.0004	0	.0008	
133	0	-.0002	0	-.0002	
222	.0014	0	0	.0014	
223	-.0009	0	0	-.0009	
233	.0002	.0002	0	.0004	
333	0	-.000067	0	-.000067	

Table 8.4 Observed and Calculated Rotational Constants of H_2O

	V_2 →	0		1		2		3		4	
	$V_1 V_3$	obs.	calc.	obs.	calc.	obs.	calc.	obs.	calc.	obs.	calc.
	0 0	27.877	27.877	31.12	31.13	35.47	35.43	42.03	41.90		52.47
	1 0	27.13	27.13	30.28	30.31	34.35	34.45	40.57	40.63		50.69
	0 1	26.636	26.64	29.54	29.54	33.29	33.24	38.64	38.70	46.8	47.52
	1 1	25.93	25.94	28.68	28.79	32.33	32.39	37.52	37.65		
A_1 cm^{-1}	2 0 } 11	26.38	26.31	28.92	29.39						
	0 2 }	25.53	25.58	28.15	28.21						
	3 0 } 11	25.47	25.33	28.2	28.17						
	1 2 }	25.25	25.21	28.0	28.04						
	2 1	25.20	25.16	28.11	27.96	31.25	31.39				
	0 3	24.53	24.45	26.88	26.83		29.70				
	3 1 } 11	24.72	24.33	27.23	27.02	29.52	29.29				
	1 3 }	24.12	24.03		26.54		28.59				
	0 0	14.512	14.512	14.66	14.66	14.83	14.80	14.95	14.94		
	1 0	14.29	14.30	14.44	14.45	14.63	14.61	14.73	14.76		
	0 1	14.40	14.43	14.59	14.59	14.75	14.47	14.91	14.90	15.04	15.06
	1 1	14.19	14.21	14.42	14.39	14.56	14.57	14.71	14.75		
	2 0 } 11	14.13	14.11	14.38	14.29						
	0 2 }	14.19	14.31	14.47	14.49						
B_1 cm^{-1}	3 0 } 11	13.95	13.95	14.2	14.16						
	1 2 }	14.03	13.98	14.20	14.20						
	2 1 } 11	13.94	13.99	14.16	14.21	14.31	14.42				
	0 3 }	14.20	14.19	14.43	14.41		14.63				
	3 1 } 11	13.71	13.76	13.95	14.03	14.00	14.29				
	1 3 }	13.75	13.86								

Table 8.4 (Continued)

	V_2	0		1		2		3		4	
	V_1V_3	obs.	calc.	obs.	calc.	obs.	calc.	obs.	calc.	obs.	calc.
	0 0	9.285	9.285	9.152	9.143	9.01	9.003	8.88	8.865		
	1 0	9.105	9.088	8.99	8.948	8.81	8.808	8.68	8.672		
	0 1	9.156	9.156	9.00	9.014	8.87	8.874	8.75	8.736	8.58	8.600
	1 1	8.94	8.959	8.77	8.817	8.69	8.679	8.56	8.541		
C_1 cm^{-1}	2 0 } ^{11}	8.99	8.908	8.78	8.766						
	0 2 }	9.03	9.010	8.87	8.870						
	3 0 } ^{11}	8.75	8.754	8.57	8.616						
	1 2 }	8.79	8.770	8.62	8.630						
	2 1 } ^{11}	8.83	8.777	8.69	8.636	8.53	8.498				
	0 3 }	8.87	8.877	8.75	8.736		8.596				
	3 1 } ^{11}	8.62	8.607	8.52	8.468	8.35	8.330				
	1 3 }	8.61	8.651		8.510		8.372				

Table 8.5 Some Energy Levels of H_2O

J_t	$v_1v_2v_3$ 000	010	020	100	001	030	110	011
0	0.00	1594.59	3151.53	3657.05	3755.79	4666.62	5335.0	5331.19
1_{-1}	23.79	1618.41	3175.4	3680.36	3779.36	4690.47	5258.35	5354.78
1_0	37.13	1634.94	3196.2	3693.26	3791.52	4717.41	5274.16	5369.76
1_1	42.37	1640.48	3202.0	3698.44	3796.75	4723.51	5279.64	5375.41
2_{-2}	70.06	1664.93	3222.06	3725.87	3824.94	4737.17	5304.06	5400.68
2_{-1}	79.48	1677.07	3237.77	3734.88	3833.36	4758.94	5315.54	5411.42
2_0	95.17	1693.62	3255.26	3750.55	3849.13	4777.19	5332.05	5428.16
2_1	134.91	1742.51	3316.0	3788.58	3885.58	4855.23	5378.72	5472.29
2_2	136.15	1743.64	3317.0	3789.84	3887.14	4856.16	5380.01	5473.62
3_{-3}	136.77	1731.92	3289.27	3791.35	3890.80	4804.91	5369.67	5466.58
3_{-2}	142.27	1739.63	3300.1	3796.51	3895.43	4820.68	5376.97	5473.13
3_{-1}	173.36	1772.30	3334.55	3827.41	3926.75	4856.85	5409.59	5506.32
3_0	206.28	1813.87	3387.8	3858.82	3956.60	4926.82	5449.0	5544.22
3_1	212.16	1819.16	3392.90	3864.57	3962.83	4931.32	5454.58	5549.67
3_2	285.25	1907.60	3500.4	3934.98	4030.02	5065.21	5539.31	5629.97
3_3	285.40	1907.71	3500.5	3935.17	4030.27	5065.38	5538.82	5630.13
4_{-4}	222.04	1817.35	3375.3	3875.02	3974.54	4891.80	5453.67	5550.65
4_{-3}	224.83	182.163	3381.9	3877.60	3977.27	4902.10	5457.43	5552.98
4_{-2}	275.48	1875.42	3438.6	3927.63	4027.69	4961.54	5510.87	5608.29
4_{-1}	300.38	1907.94	3482.0	3951.21	4049.94	5021.33	5541.83	5639.69
4_0	315.73	1923.04	3495.85	3966.47	4066.16	5033.68	5557.85	5652.98
4_1	382.49	2004.89	3597.80	4030.71	4125.19	5162.57	5635.02	5726.27
4_2	383.86	2006.12	3598.8	4031.75	4126.62	5162.97	5633.37	5727.51
4_3	488.16	2129.60	3746.8	4135.16	4224.87	5344.8	5756.5	5842.02
4_4	488.17	2129.60	3746.8	4134.69	4224.88	5344.8	5756.5	5842.02
5_{-5}	325.36	1920.70	3479.1	3976.23	4076.06	4996.17	5554.84	5652.10
5_{-4}	326.59	1922.80	3482.5	3977.35	4076.86	5002.58	5556.5	5653.55
5_{-3}	399.45	2000.80	3565.5	4049.61	4149.98	5089.96	5634.16	5731.93
5_{-2}	416.12	2024.24	3598.6	4064.84	4165.45	5138.13	5653.08	5749.70
5_{-1}	446.50	2053.87	3627.0	4095.66	4195.80	5164.00	5686.13	5783.36
5_0	504.00	2126.44	3719.2	4150.35	4244.35	5284.56	5754.8	5846.47
5_1	508.79	2130.52	3722.55	4154.00	4248.10	5287.16	5761.05	5851.26
5_2	610.12	2251.67	3868.3	4257.75	4345.39			5963.03
5_3	610.34	2251.83	3868.5	4256.46	4345.57	5467.2	5877.3	5963.16
$5_{4,5}$	742.10	2406.24	4052.8	4381.73	4468.55	5678.9		6106.26

Table 8.5 (Continued)

J_t	000	010	020	100	001	030	110	011
6-6	446.71	2041.73	3600.4	4095.15	4195.49	5117.83		5771.09
6-5	447.24	2042.73	3602.0	4095.84	4195.96	5121.53	5674.39	5771.68
6-4	542.87	2146.39	3713.1	4189.70	4290.72			5874.72
6-3	552.92	2161.31	3736.2	4199.30	4296.39	5276.47	5790.55	5885.70
6-2	602.67	2211.23	3784.3	4249.53	4350.74			5939.32
6-1	648.97	2271.60	3864.8	4293.16	4387.18	5432.93	5897.82	5990.15
60	661.54	2282.56	3873.55	4308.05	4408.00		5914.17	6002.31
61	756.76	2398.39	4015.1	4394.48	4490.06		6022.54	6108.51
62	757.70	2399.27	4015.8	4402.14	4491.35			6109.33
63	888.67	2552.95	4197.4	4526.4	4613.72			6251.73
64	888.71	2552.98	4197.4	4526.4	4613.72			6251.77
65,6	1045.15	2734.24	4411.0		4759.80			6420.17
7-7	586.28	2180.68	3738.6	4232.25	4332.79	5256.53	5809.32	5907.70
7-6	586.43	2181.27	3739.5		4332.92	5258.86	5809.75	5907.91
7-5	704.20	2309.89	3879.05	4347.82	4448.95	5409.60	5936.7	6035.08
7-4	709.50	2318.48	3894.5		4452.46			6041.11
7-3	782.41	2392.38	3967.4	4426.50	4527.97		6019.51	6118.75
7-2	816.65	2440.06	4038.7		4553.18			6156.56
7-1	842.36	2462.87	4053.0	4492.14	4586.70			6179.78
70	927.76	2569.66	4187.8	4563.95	4658.90		6193.28	6277.87
71	931.23	2572.11	4190.8	4572.35	4663.21			6281.20
72	1059.68	2724.15		4695.85	4782.77			6421.44
73	1059.89	2724.30		4695.87	4782.90			6421.58
74,5	1216.39	2905.43			4929.03			6590.10
76,7	1394.85	3110.02			5096.24			6779.26
8-8	744.09	2337.61	3894.4	4387.1	4488.21	5412.92	5963.46	6061.98
8-7	744.14	2337.84	3894.8		4488.21	5414.11	5963.46	6061.98
8-6	882.97	2490.42	4063.9	4524.2	4624.33			6212.07
8-5	885.64	2495.25	4071.6		4625.85			6215.15
8-4	983.09	2595.9			4725.11			6318.73
8-3	1006.14	2630.28	4224.8		4741.08			6344.56
8-2	1050.20	2670.75			4792.38			6394.27
8-1	1122.78	2764.75	4383.9	4756.45	4851.46			6471.22
80	1131.88	2771.67		4770.25	4861.97			6479.95
81	1255.19	2919.76			4976.10			6615.32
82	1255.98	2920.26			4977.06			6616.07
83,4	1411.59	3101.28			5122.40			6784.02
85,6	1590.60	3306.58			5289.9			6975.17
87,8	1789.09	3531.05						7176.7

Table 8.5 (Continued)

	000	010	020	100	001	030	100	011
9-9	920.20	2512.37	4068.8	4459.8	4661.55	5586.74	6134.79	6234.07
9-8	920.22	2512.50			4661.55	5587.35		6234.07
9-7	1079.16	2688.26	4266.7		4817.22			6406.20
9-6	1080.51	2690.73			4818.06			6407.60
9-5	1202.04	2818.40			4939.83			6537.13
9-4	1216.37	2841.57			4948.94			6553.37
9-3	1283.02	2904.82			5022.30			6624.67
9-2	1341.03	2983.43			5067.18			6687.75
9-1	1360.56	2999.45			5089.95			6706.19
90	1475.14	3139.65		5108.35	5193.49			6833.27
91	1477.46	3141.55			5196.63			6835.48
92	1631.44	3321.0			5339.70			7001.8
93	1631.58	3321.10			5339.8			7002.0
94,5	1810.76	3526.77			5507.5			
96,7	2009.99	3752.58			5694.4			
98,9	2225.56	3994.39						
10-10	1114.59	2705.20	4260.7	4750.5	4852.88			6423.82
10-9	1114.59	2705.23			4852.88			6423.82
10-8	1293.22	2903.38			5027.49			6617.35
10-7	1293.80	2904.68			5027.90			6618.11
10-6	1438.19	3058.60			5171.38			6772.07
10-5	1446.23	3072.95			5176.10			6781.4
10-4	1538.31	3162.53			5273.67			6878.66
10-3	1581.53	3224.80			5304.90			6926.26
10-2	1616.49	3253.91			5355.45			6959.66
10-1	1719.36	3383.65		5335.44	5435.03			
10 0	1724.80	3387.67			5442.27			7080.58
10 1	1875.24	3565.00						
10 2	1875.72	3565.3			5582.1			
10 3,4	2054.55	3770.95						
10 5,6	2254.55	3997.80						
10 7,8	2471.59	4241.0						
10 9,10	2702.09							

Table 8.5 (Continued)

	000	010	020	001	011
11-11,-10	1327.25	2916.09	4470.1	5062.22	6631.42
11-9	1525.02	3135.9		5255.6	6846.07
11-8	1525.31	3136.66		5256.7	6846.42
11-7	1690.85	3315.0		5417.87	7022.87
11-6	1695.24	3323.55		5421.43	7028.50
11-5	1813.47	3441.22		5445.0	
11-4	1843.32	3487.59		5563.58	7185.97
11-3	1899.21	3532.9			
11-2	1986.08	3650.84		5700.1	7340.12
11-1	1999.34	3660.20			7352.05
110	2143.01	3832.7		5845.88	7509.0
11_1	2144.46	3833.86		5847.52	
11_2	2322.20	4038.62			
11_3	2322.25	4038.70			
$11_{4,5}$	2522.46	4266.05			
$11_{6,7}$	2740.73				
$11_{8,9}$	2973.07				
$11_{10,11}$	3216.6				
12-12,-11	1558.07	3144.77		5289.14	6856.48
12-10	1774.75	3386.27		5501.52	7092.4
12-9	1774.88	3386.53		5501.55	7092.4
12-8	1960.38			5683.38	7289.9
12-7	1962.60	3592.71		5685.0	7292.7
12-6	2106.7			5830.4	7444.05
12-5	2124.84	3771.13		5842.2	
12-4	2205.95			5930.0	7550.61
12-3	2275.65	3940.56			
12-2	2300.94			6013.69	
12-1	2434.14	4123.73			
120	2437.84				
12_1	2613.26	4329.83			
12_2	2613.49	4330.0			
$12_{3,4}$	2813.94	4557.87			
$12_{5,6}$	3033.17				
$12_{7,8}$	3267.2				
$12_{9,10}$	3514.3				
$12_{11,12}$	3767.1				

Table 8.5 (Continued)

	000	010	001	011
$13_{-13,-12}$	1806.94	3391.46	5534.33	7099.27
13_{-11}	2042.5	3654.28	5764.42	7355.4
13_{-10}	2042.5		5764.42	7355.4
13_{-9}	2247.0	3877.9	5964.9	
13_{-8}	2248.24		5965.6	
13_{-7}	2415.95			
13_{-6}	2425.2		6241.7	
13_{-5}	2534.14			
13_{-4}	2586.5			
13_{-3}	2629.54			
13_{-2}	2748.4			
13_{-1}	2756.61	4443.0		
13_{0}	2927.38			
13_{1}	2928.45			
$13_{2,3}$	3128.25			
$13_{4,5}$	3348.2			
$13_{6,7}$	3584.0			
$13_{8,9}$	3831.4			
$13_{10,11}$	4087.9			
$13_{12,13}$	4351.3			
$14_{-14,-13}$	2073.81	3655.74	5797.16	7359.68
$14_{-12,-11}$	2328.2	3940.1	6045.4	7637.0
14_{-10}	2551.0		6262.2	
14_{-9}	2551.5			
14_{-8}	2740.5			
14_{-7}	2745.5			
14_{-6}	2883.5			
14_{-5}	2919.5			
14_{-4}	2983.6			
14_{-3}	3085.0			
14_{-2}	3101.65			
14_{-1}	3264.2			
14_{0}	3266.36			
14_{1}	3465.18			
14_{2}	3465.4			
$14_{3,4}$	3685.6			
$14_{5,6}$	3923.5			
$14_{7,8}$	4172.9			
$14_{9,10}$	4431.9			
$14_{11,12}$	4697.4			
$14_{13,14}$	4969.0			

Table 8.5 (Continued)

	000	101	001	011
15-15,-14	2358.58	3937.87	6077.4	7636.8
15-13,-12	2631.6			
15-11	2872.56			
15-10	2872.9			
15-9	3081.2			
15-8	3084.2			
15-7	3252			
15-6	3277			
15-5	3365			
15-4	3446			
15-3	3473.0			
15-2	3624			
15-1	3628.7			
15 0	3825.5			
15 1	3826.1			
15 2,3	4045.8			
15 4,5	4285			
15 6,7	4537			
15 8,9	4798			
15 10,11	5066			
15 12,13	5340			
15 14,15	5619			
16-16,-15	2661.2	4237.5	6375.5	7931.9
16-14,-13	2953			
16-12,-11	3211.5			
16-10	3437.7			
16-9	3439.7			
16-8	3639.9			
16-7	3657.1			
16-6	3768			
16-5	3830			
16-4	3865			
16-3	4010			
16-2	4020			
17-17,-16	2981.5	4554.6	6691.0	8244.1
17-15,-14	3291			
17-13,-12	3567.5			
17-11	3811.5			
17-10	3812.6			
17-9	4047.1			
17-8	4057.3			

Table 8.5 (Continued)

	000	001	011
18-18,-17	3319.4	7023.7	8573.4
18-16,-15	3648		
18-14,-13	3940.8		
18-12,-11	4202		
19-19,-18	3674.7	7373.7	8920.1
19-17,-16	4022		
19-16,-15	4331		
20-20,-19	4048	7740.7	9283.5
20-18,-17	4412		
21-21,-20	4438		
22-22	4846		

that the largest number of rotational levels have been found in the ground state, because the dipole strength of the pure-rotation transition is much greater than it is for rotation-vibration transitions; the number of identified levels in the latter transitions is roughly parallel to the strengths listed in Table 8.1.

The numerical values of the vibrational intensities in Table 8.1 were obtained by the following procedure. The rotational part of the transition probability has been tabulated for certain values of the asymmetry parameter, by Cross, Hainer and King [44]. In the absorption spectra obtained with the highest resolving power, most of the lines have been identified by the procedure discussed in detail in reference [3]; in some cases there is overlapping of lines, but by a careful scrutiny of all the data it is possible to pick out in each band a number of lines that fulfill the following criteria. (a) They have an observed maximum absorption of 10 - 25%, that is, strong enough so that fairly accurate measurement can be made of the percentage of peak absorption, yet weak enough that one is still in the range where the peak absorption is nearly proportional to the true line strength, if the line width and instrumental slit width are of the same order of magnitude; (b) they are unblended lines; (c) they fall in different branches (P, Q, and R) yet have a common lower level. From such lines it is possible to check whether the theoretically calculated rotational line strengths are in accord with observation: this is in general the case, but there are a number of bands in which anomalies occur, in that the lines of one branch are stronger than theoretical, while those of the complementary branch are weaker. These anomalies are however generally less important at low J, and can be compensated for by inclusion of a sufficient variety of lines. For lines that are satisfactory by the above criteria, $\int \alpha_\nu d\nu$ can be measured with fair accuracy. The amount of water vapor in the absorbing path, in the laboratory absorption measurements, is known to perhaps ± 25%, from the optics of the spectrometer and the prevailing absolute humidity; hence $\int K_\nu d\nu$ of the line can be computed. The ratio of the observed $\int K_\nu d\nu$ for a line to the product of the rotational line strength and the Boltzmann factor of the lower level is next determined; the average value of this quantity, for a large number of suitable lines in the band, multiplied by Q, is the $\int K_\nu d\nu$ for the band, as given in Tables 8.1 and 2b. The value of this quantity, for the stronger bands that appear in the laboratory absorption spectra with good intensity, and which are also the most important bands in flame emission, should be accurate to within ±40%; for the weaker bands, the extension of the above procedure yields values that are less accurate, since the quantity of water vapor in the atmosphere is more uncertain, but these should not be in error by a factor of more than 3.

The analysis of nearly all the observed lines (some 5000 in all) in the observed absorption spectrum [3, 22, 36, 37, 39, 46] has been satisfactorily accomplished, in that all the predicted rotational lines of strong and medium intensity, in the 40 observed bands, have been found with the theoretically correct relative intensity, at positions that correspond to reasonable values of the energy levels of the upper and lower states.

In the emission spectrum, the analysis is complicated by two factors. 1) Vibrational transitions to levels other than the ground state will have appreciable intensity. 2) Strong rotational transitions will involve levels of higher energy than have been observed in absorption, and of such high J (>12), that their calculation is laborious, both because convenient tables [43] are not available, and because the centrifugal-stretching corrections to the energy are very large.

The vibrational transitions can be readily calculated, both as regards position and intensity. The position is obtained from the levels of Table 8.2. The intensity, relative to the ground-state transition, is obtained from the relations previously discussed for CO_2, taking into account the effects of resonance. Table 8.6 lists the expected bands whose intensity at 2877°K, exceeds 10% of the strongest ground-state intensity, for the sequences in the regions of 1.9 μ and 1.4 μ. The strongest members of the 021-000 sequence are also listed, with intensity taken relative to 101-000. Numerous weaker bands will also appear. (In Table 8.6, as well as Table 8.7 which follows, the ν^4 factor is omitted from the intensity.) It is clear from Table 8.6 that a few of the upper-state bands should appear with appreciable intensity as long-wave satellites of the principal bands, but that their contribution is not nearly so overwhelming as in CO_2.

The intensities of the rotational lines can be calculated at any desired temperature to a fair degree of approximation. This involves an extrapolation to $J > 12$ of the line-strength tables [44], which can be done readily in view of the regularities displayed in those tables, and by checking the results against the sum rules. It also involves making approximate estimates of all the ground-state energy levels up to 6000 cm^{-1}; those that have not been observed from the spectra may be calculated with an accuracy of perhaps 1% by extrapolating the series regularities that the known levels and their various combinations obey. The resulting calculated relative intensities of the lines in the R branch of a type A band are given in Table 8.7. In calculating Table 8.7 it is of course assumed that no anomalies occur, due either to vibrational-rotational interactions or to K being different in the upper and lower states. If we further assume equal rotational energies in the two states, the table also applies to the R(J+1) branch in emission, or to P (J) in emission, if allowance is made for the changed structural weights. The entries in Table 8.7 are given only to 1 or 2 significant figures because of the uncertainties in the calculation, but should serve to show the expected number and relative intensities of strong lines if at flame temperatures. A boundary line has been drawn to enclose lines having 10% or more of the intensity of the strongest line: these might reasonably be observed in well resolved emission spectra, such as we have obtained. Similar lines have been drawn to enclose the field of lines of 10% intensity or greater at 1438° and 287°K, temperatures at which corresponding calculations have also been made. The number of strong lines is seen to increase appreciably with increasing temperature, but not to a degree precluding the resolution and identification of a number of features.

Table 8.6 Calculated Band Origins and Relative Intensities, 2876°, H_2O

v_1'	v_2'	v_3'	v_1''	v_2''	v_3''	ν_o	T_v	I_{2876}
0	1	1	0	0	0	5331.2	100	100
0	2	1	0	1	0	5277.0	200	90
0	3	1	0	2	0	5221.8	300	62
0	4	1	0	3	0	5166.9	400	39
0	5	1	0	4	0	5112	500	23
0	6	1	0	5	0	5067	600	12
1	1	1	1	0	0	5149.9	100	16
0	1	2	0	0	1	5244.3	178	28
0	2	2	0	1	1	5192	355	25
0	3	2	0	2	1		531	16
1	2	1	1	1	0	5093.7	200	15
1	0	1	0	0	0	7249.8	100	100
1	1	1	0	1	0	7212.3	100	45
1	2	1	0	2	0	7177.2	100	21
2	0	1	1	0	0	6956.2	177	28
2	1	1	1	1	0	6916.2	177	12
1	0	2	0	0	1	7113.0	112	17
3	0	0	0	0	1	6843.9	88	14
0	2	1	0	0	0	6871.3	7	7
0	3	1	0	1	0	6779.1	21	9
0	4	1	0	2	0	6682.0	42	9
0	5	1	0	3	0	6581.8	70	7

Table 8.7 Relative Intensities of Type A R-Branch Absorption Lines of H_2O at 2877°K

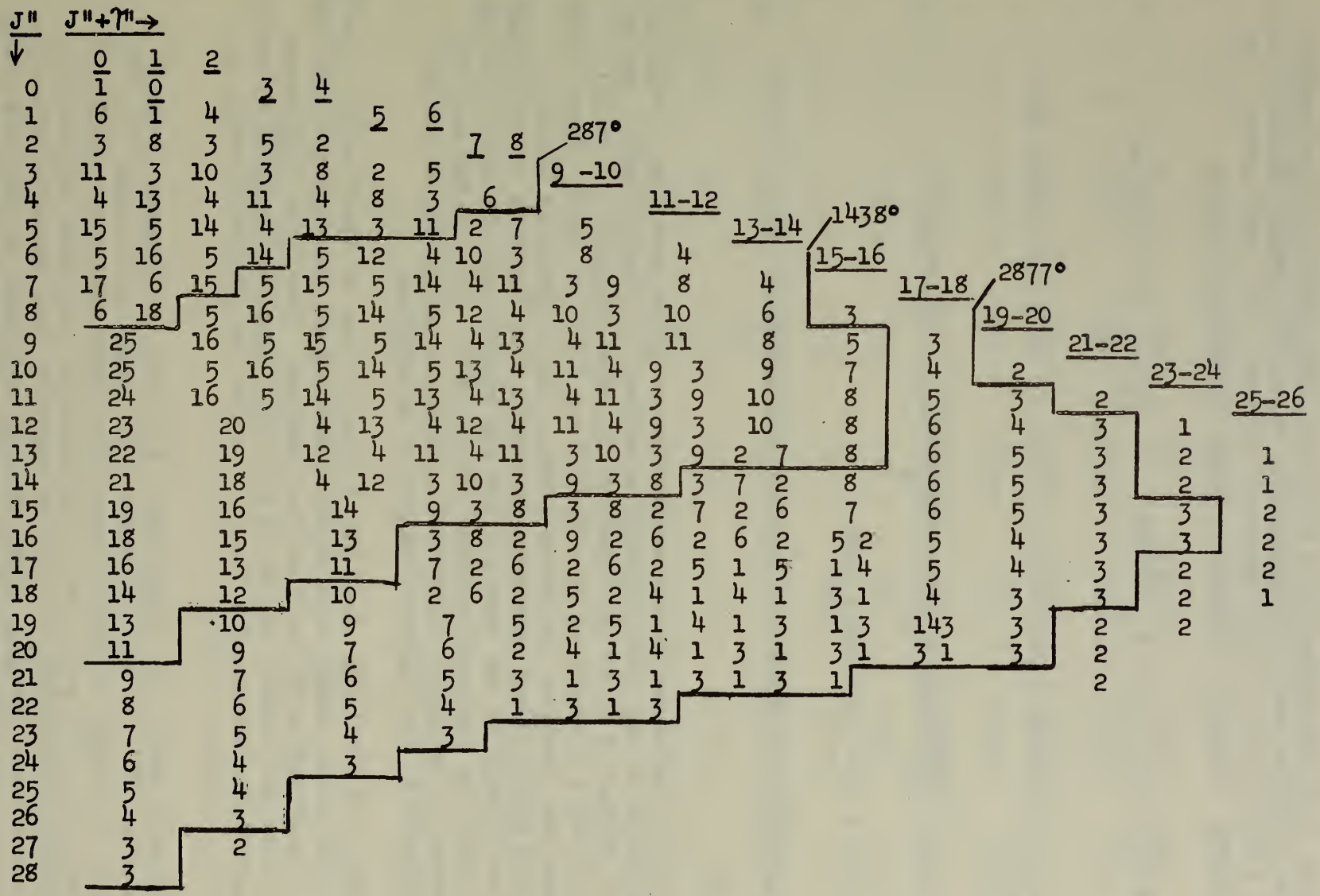

An additional help in the analysis is the fact that the strongest lines of the R and P branches, which it will be noted from Table 8.7 are those with low values of $(J + \tau)$, are the ones whose frequencies show the simplest series regularities, being most nearly characteristic of the limiting case of the symmetric rotator. For such levels, the rigid energy levels are given to a good approximation by

$$E = \frac{A+B}{2} J(J+1) + \left(C - \frac{A+B}{2}\right)K^2, \qquad (K = J,\ J-1,\ J-2,\ \text{etc.}) \qquad (8.1)$$

so that the R-branch lines with $J + \tau = 0,1$, or $K = J$, would have frequencies

$$\nu = \nu_0 + \frac{A''+B''}{2} - C'' + \left[2C'' + \frac{A'-A''+B'-B''}{2}\right]J + (C'-C'')J^2, \qquad (8.2)$$

those with $J + \tau = 2,3$, would have

$$\nu = \nu_0 + 4\left(\frac{A''+B''}{2} - C''\right) - \left(\frac{A'+B'}{2} - C'\right) + \left[4C'' - 2C' + \frac{3(A'-A''+B'-B'')}{2}\right]J + (C'-C'')J^2 \qquad (8.3)$$

etc.

In the observed emission spectra, these series have been recognized, as extensions of the known absorption series, in several bands. As an example, Table 8.8 lists the lines of the main series $(J + \tau = 0,1)$ for the P and R branches of the 011-000 and 101-000 bands. These lines are among the strongest in the spectrum. The differences R(J+1) - P(J-1) are also listed; these are combination differences of the ground state, and should be the same for the two bands; this is seen to be the case, within the measured accuracy of ± 0.5 cm^{-1}. Also listed are the differences in the 010-000 absorption band, in which the series have been followed to the highest J values in absorption.

Table 8.9 similarly lists the R-branch lines of the 001-000, 011-000, and 101-000 bands, along with those calculated by the pure rotation band from the combination differences just derived. The first differences of the lines are listed, and it is seen that there is parallelism between the second differences and $\Delta C = C'' - C'$ for the particular band, as required by equation (8.2).

The main series, as listed here, are seen to converge in the R branch, since $C'' > C'$ for all bands. The series with higher $(J + \tau)$ lie either to higher or lower frequencies, depending principally upon the sign of $A' - A''$, with some irregularities. In bands with $\Delta v_2 = 0$, e.g. 001-000 and 101-000, $A' - A''$ is negative, and the main series provides most of the strongest lines at high frequency; in 101 this effect is so marked that a characteristic band head is formed, near 7496 cm^{-1}. Similar heads appear in the photographic bands [42]. When $\Delta v_2 > 0$, however, $A' - A''$ is positive, and numerous strong lines of the $(J+\tau) =$

Table 8.8 Combination Differences in H_2O Main Series

J'	I^R_{2876}	011-000			101-000			Δ(010)
		R(J+1)	P(J-1)	Δ	R(J+1)	P(J-1)	Δ	
10	24.2	5503.5	5096.6	406.9	7405.1	6998.1	407.0	406.9
11	23.4	5516.6	5073.3	443.3	7416.0	6972.7	443.3	443.3
12	22.3	5529.1	5049.3	479.8	7426.2	6946.5	479.8	479.7
13	20.9	5541.1	5025.5	515.6	7435.9	6920.0	515.9	515.8
14	19.4	5552.4	5000.0	552.4	7444.7	6892.8	551.9	552.1
15	17.6	5563.0	4975.7	587.3	7452.4	6865.5	586.9	587.4
16	16.0	5573.3	4950.5	622.8	7460.0	6837.1	622.9	623.0
17	14.3	5582.9	4924.7	658.2	7466.1	6808.2	657.9	
18	12.6	5592.0	4898.5	693.5	7471.9	6778.7	693.2	
19	10.8	5600.7	4872.2	728.5	7477.4	6748.8	728.6	
20	9.4	5608.8	4845.3	763.5	7481.9	6717.7	764.2	

Table 8.9 R-Branch Series in Several Bands

Band -	000		001		011		101	
$\Delta C \rightarrow$	0		0.13		0.26		0.35	
J=14	266.9	$\Delta\nu$	3990.2	$\Delta\nu$	5552.4	$\Delta\nu$	7444.7	$\Delta\nu$
		17.9		13.4		10.6		7.7
15	284.8		4003.6		5563.0		7452.4	
		17.8		13.3		10.3		7.6
16	302.6		4016.9		5573.3		7460.0	
		17.7		12.9		9.6		6.1
17	320.3		4029.8		5582.9		7466.1	
		17.6		12.4		9.1		5.8
18	337.9		4042.2		5592.0		7471.9	
		17.7		12.1		8.7		5.5
19	355.6		4054.3		5600.7		7477.4	
		17.6		11.7		8.1		4.5
20	373.2		4066.0		5608.8		7481.9	

(2,3), (4,5), 6, 7, etc. series fall at higher frequencies. Hence the short-wave end of the 011-000 band shows no head.

In the observed spectra, it has been thus far possible to measure and identify a number of lines, but the analysis is not complete, and will be discussed only in outline. In the region 3800-4200 cm^{-1} identified lines include those found in absorption, with an extension of the $R_{0,1}$ branch (see Table 4 of reference 3) by 1 or 2 units of J. The analysis will doubtless be capable of extension to higher J, since many well resolved intense lines are unassigned from 4000-4200 cm^{-1}, when measurements of corresponding resolution are available in the region of the $P_{0,1}$ branch, from 3200-3500 cm^{-1}. Additional lines, especially between 3800-4000 cm^{-1}, agree well with the predicted $R_{0,1}$ lines of (011-010) and (021-020) that can be calculated from Table 8.5 and its extension. There is some overlapping of lines, and measurements with the vacuum spectrometer are desirable since the atmospheric absorption is so intense, so that accurate measurement of temperature is not yet possible. The relative intensity of the upper-state bands is however consistent with a vibrational temperature in the neighborhood of 2500°K.

The (011-000) region, extending from 4500-5900 cm^{-1}, has been carefully measured, with more than 600 of the stronger lines resolved. Again the absorption analysis can be confirmed and extended by one or two J's, with the (J+1) = (0,1), and (2,3) series further extended to J = 20, in both the R and P branches, as given in Table 8.8. A reproduction of the region in the R branch from 5510-5680 cm^{-1} is shown in Figure 8, with various of the lines identified. The flame was near-stoichiometric H_2-O_2, observed near the top of the outer cone, with slits of 0.3 cm^{-1}. The height of the leading lines in the series at the top of Figure 8 is proportional to the 2877°K intensity. There is a reasonable parallelism between the calculated intensities and those of the identified lines, with the latter showing a somewhat greater decrease in intensity with increasing J, corresponding to an effective rotational temperature in the neighborhood of 2400°K. The more complete analysis of this band should result in the identification of a number of resolved lines that will be suitable for rotational temperature determinations, inasmuch as neighboring lines in different series have widely different initial energy levels. Figure 9 shows the portion of the P branch of the same band, from 4910-5050 cm^{-1}, with identification of some of the series in (011-000), and in addition in the upper-state bands. Again the effective rotation-vibration temperatures appear to be definitely lower than 2877°K.

In the 6300-7500 cm^{-1} region, the wavelengths have not been completely measured, but as was shown in Table 8.8, the main series, as well as some of the subsidiary series have been identified, in 101-000, and also in 111-010. Further work in this region is in progress. In the 8000-9200 cm^{-1} region, the H_2O emission is much weaker, so that much wider slits ($\sim$1.0-1.5 cm^{-1}) were required, with very little well resolved structure resulting.

The relative intensities of the H_2O emission regions are consistent with the values of the integrated absorption coefficients listed in Tables 2b and 8.1, and, if the observed emissivity of the strongest lines (e.g. 13_{-12}-14_{-13}), is 0.1-0.2, as rough measurements indicate, the absolute intensity in these regions is also consistent with the H_2O radiation being that of a gas in thermodynamic equilibrium near 2500°K. There is no evidence for abnormal excitations in either the rotational or vibrational energy levels, nor for a chemiluminescent origin for the radiation.

9. Discussion and Conclusions

The observed infrared radiation from the outer cone of flames from 3700-10000 cm^{-1} has all been ascribed to the vibration-rotation spectra of the four most abundant molecules with such allowed spectra, namely, CO, OH, CO_2 and H_2O; in the inner cone the electronically excited CN and C_2 radicals also contribute. Search has been made for spectra from the other molecules and radicals listed in Table 1, but with negative results. In the inner cone of oxy-acetylene flames, electronic bands of CH are very intense. The P branch of the 2-0, and especially the 3-1 band of the vibration-rotation spectrum falls in the region of 4500 cm^{-1}, where other emission is relatively weak. The positions of the lines, which because of the $^2\pi$ character of the state will split into close groups of 4, can be predicted with good accuracy; they have not been observed, even with very wide slits, and it can be stated with assurance that they are less than 1% as strong as the overtone bands of CO or OH. If as is reasonable the effective charge for vibration of CH is of the same order as in OH, the concentration of non-electronically excited CH in the inner cone is therefore less than 10^{-3}. But since a much lower concentration of excited radicals suffices to produce the electronic bands, and since the equilibrium concentration is very much lower still, the non-appearance of vibration-rotation CH was to have been expected. Even in the region of the fundamental it will still be extremely unlikely that it could be found.

Analogous reasoning holds for such molecules as C_2H_2, HCN, CH_4, H_2CO, etc., whose spectra are known; the additional fact that all will have a very high vibrational Q, greater than that for CO_2, makes their non-appearance in the overtone region to be expected, and their appearance as fundamentals very dubious, unless they are present in very high concentrations at relatively low temperatures, such as might be the case if a very large excess of CH_4 or C_2H_2 were burned. Equally unlikely are the possibilities of detecting the radicals with unknown spectra, such as CH_3, CH_2, or HCO, although it is again conceivable that they might appear in the region of the C-H fundamental ($\sim 3.5\mu$) under the same conditions that produce the emission spectra of CH_4 or H_2CO.

The general finding of these studies, with regard to the intensity and energy distribution of the various emitters, is also in accordance with the discussion in Section 2. In every case where a "temperature" could be measured from resolved spectra, the results were from 2400-2800°K, whereas visible and ultraviolet spectra from the same regions of comparable flames would be > 3000°K. The principal reason for the difference, as has repeatedly been mentioned, must be the greater life-times for radiation in the infrared, so that the lower-lying excited states that are responsible for infrared emission show a much closer approach to complete thermodynamic equilibrium than when states with higher amounts of electronic excitation are studied.

We might summarize the usefulness of resolved infrared spectra as thermometers as follows. CO rotational - excellent; no further studies needed. CO vibrational - very good; comfirmation of the relative

vibrational transition probabilities desirable. OH rotational - very good; OH vibrational - good, determination of absolute and relative vibrational transition probabilities desirable. C_2 rotational - quite good. CN rotational - poor, unless stronger sources and better resolution are developed. CO_2 rotational and vibrational - very poor, inherent in the nature of the spectra at high temperatures. H_2O rotational and vibrational - fair, with promise of being very good when further analysis has been done on the spectra.

It is hoped to continue these studies, with extension to longer wavelengths, and to make more quantitative determinations of the emitted intensities and of the high-temperature transition probabilities, to cast further light upon the concentrations of the molecules in different regions of the flames and upon the problems of equilibrium and non-equilibrium states.

Appendix 1A References

[1] E. K. Plyler and C. J. Humphreys, J. Research NBS 40, 449 (1948).

[2] S. Silverman, "Third Symposium on Combustion Flame and Explosion Phenomena". p. 498 (Williams and Wilkins, Baltimore, Md., 1949).

[3] W. S. Benedict and E. K. Plyler, J. Research NBS 46, 246 (1951).

[4] H. C. Hottel, G. C. Williams and C. N. Satterfield, "Thermodynamic Charts for Combustion Processes" (Wiley and Sons, New York, 1949).

[5] G. H. Dieke and H. M. Crosswhite, Progress Reports for Contract NOrd 8036 (1948-1951).

[6] H. P. Broida, Appendices 2A, 2B, 2C to this report.

[7] B. L. Crawford, Jr. and H. L. Dinsmore, J. Chem. Phys. 18, 983 (1950).

[8] K. Scholz, Z. Physik 78, 751 (1932).

[9] R. C. Herman, private communication.

[10] S. S. Penner and D. Weber, J. Chem. Phys. 19 807, 817 (1951).

[11] G. Herzberg and K. N. Rao, J. Chem. Phys. 17, 1099 (1949).

[12] R. T. Lagemann, A. H. Nielsen and F. P. Dickey, Phys. Rev. 72, 284 (1947).

[13] K. N. Rao, J. Chem. Phys. 18, 213 (1950).

[14] K. N. Rao, Ap. J. 110, 304 (1949).

[15] D. M. Read, Phys. Rev. 46, 571 (1934).

[16] G. H. Dieke and H. M. Crosswhite, Bumblebee Report #87 Johns Hopkins University, 1948.

[17] G. A. Hornbeck and R. C. Herman, paper presented at Symposium on Combustion Chemistry of the Division of Petroleum Chemistry, American Chemical Society (1951).

[18] E. L. Hill and J. H. Van Vleck, Phys. Rev. 32, 250 (1928).

[19] R. S. Mulliken, Rev. Mod. Phys. 3, 89 (1931).

[20] G. Herzberg and J. G. Phillips, Ap. J. 108, 163 (1948).

[21] C. C. Kiess, Ap. J. 109, 551 (1949).

[22] H. D. Babcock and C. E. Moore, Carnegie Inst. of Washington, Publ. #579 (1947).

[23] A. E. Parker, Phys. Rev. 41, 274 (1932).

[24] G. Herzberg, "Molecular Spectra and Molecular Structure I: Diatomic Molecules"(D. Van Nostrand, New York, 1950).

[25] J. G. Phillips, Ap. J. 107, 389 (1948).

[26] G. A. Hornbeck and R. C. Herman, 19, 512 (1951).

[27] G. Stephenson, Proc. Phys. Soc. A64, 99 (1951).

[28] A. G. Gaydon and H. G. Wolfhard, Proc.Roy. Soc. A201, 570 (1950).

[29] D. M. Dennison, Rev. Mod. Phys. 12, 175 (1940).

[30] G. Herzberg, "Infrared and Raman Spectra of Polyatomic Molecules" (D. Van Nostrand, New York, 1945).

[31] L. Goldberg, O. C. Mohler, R. R. McMath, and A. K. Pierce, Phys. Rev. 76, 1848 (1949).

[32] J. H. Shaw, Ohio State University Reports on RF Project 381, 1950-51, and private communication.

[33] J. Taylor, private communication.

[34] A. M. Thorndike, A. J. Wells, and E. B. Wilson, Jr., J. Chem. Phys. 15, 157 (1947).

[35] D. F. Eggers, Jr. and B. L. Crawford, Jr., Symposium on Molecular Structure and Spectroscopy Paper C2 (Ohio State University, Columbus, Ohio, 1951).

[36] O. C. Mohler, A. K. Pierce, R. R. McMath and L. Goldberg "Photometric Atlas of the Near Infra-Red Solar Spectrum λ8465 to λ 25,242" (University of Michigan Press, Ann Arbor, 1950).

[37] W. S. Benedict, Phys. Rev. 74, 702, 703, 1246 (1948), and unpublished data.

[38] R. Mecke, Z. Physik 81, 373 (1933).

[39] H. M. Randall, D. M. Dennison, N. Ginsburg, and L. R. Weber, Phys. Rev. 52, 160 (1937).

[40] B. T. Darling and D. M. Dennison, Phys. Rev. 57, 128 (1940).

[41] H. H. Nielsen, Phys. Rev. 62, 422 (1942).

[42] A. G. Gaydon, Proc. Roy. Soc. A181, 197 (1942).

[43] G. W. King, R. M. Hainer, and P. C. Cross, J. Chem. Phys. 11, 27 (1943).

[44] P. C. Cross, R. M. Hainer, and G. W. King, J. Chem. Phys. 12, 210 (1944).

[45] A. Adel, Phys. Rev. 71, 806 (1947).

[46] R. C. Nelson, "The Absorption of Water Vapor in the Regions 1.33 to 1.48 and 1.77 to 1.98 Microns", Summary Report #4 on Contract NObs 28373 (Northwestern University, 1949).

List of Figures

CO EMISSION
5-3
4-2
3-1
2-0
DEFLECTION
4360cm⁻¹
4340
4320
4300
4280
4260
4240
4220
4200
4180
R
P
W

Figure 1

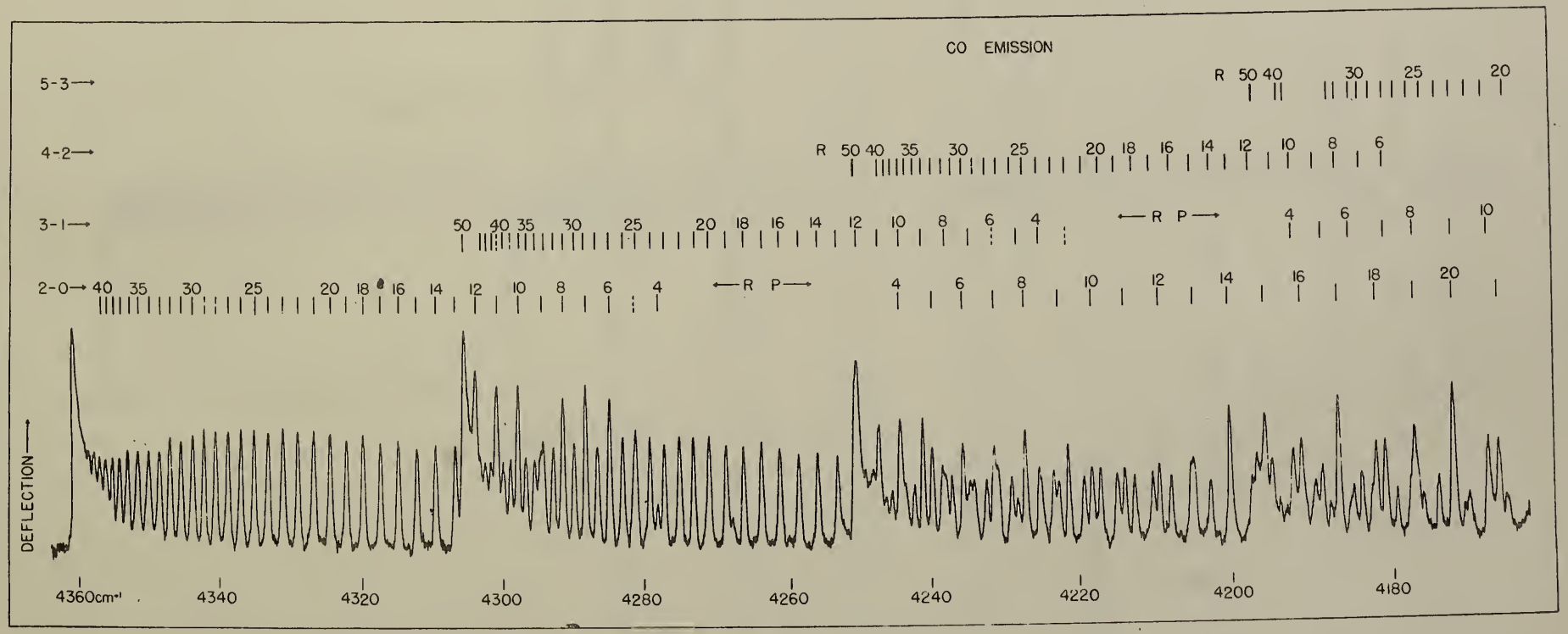
CO EMISSION
5-3→
R 50 40 30 25 20
4-2→
R 50 40 35 30 25 20 18 16 14 12 10 8 6
3-1→
50 40 35 30 25 20 18 16 14 12 10 8 6 4 ←R P→ 4 6 8 10
2-0→ 40 35 30 25 20 18 16 14 12 10 8 6 4 ←R P→ 4 6 8 10 12 14 16 18 20
DEFLECTION
4360cm⁻¹
4340
4320
4300
4280
4260
4240
4220
4200
4180

Figure 2

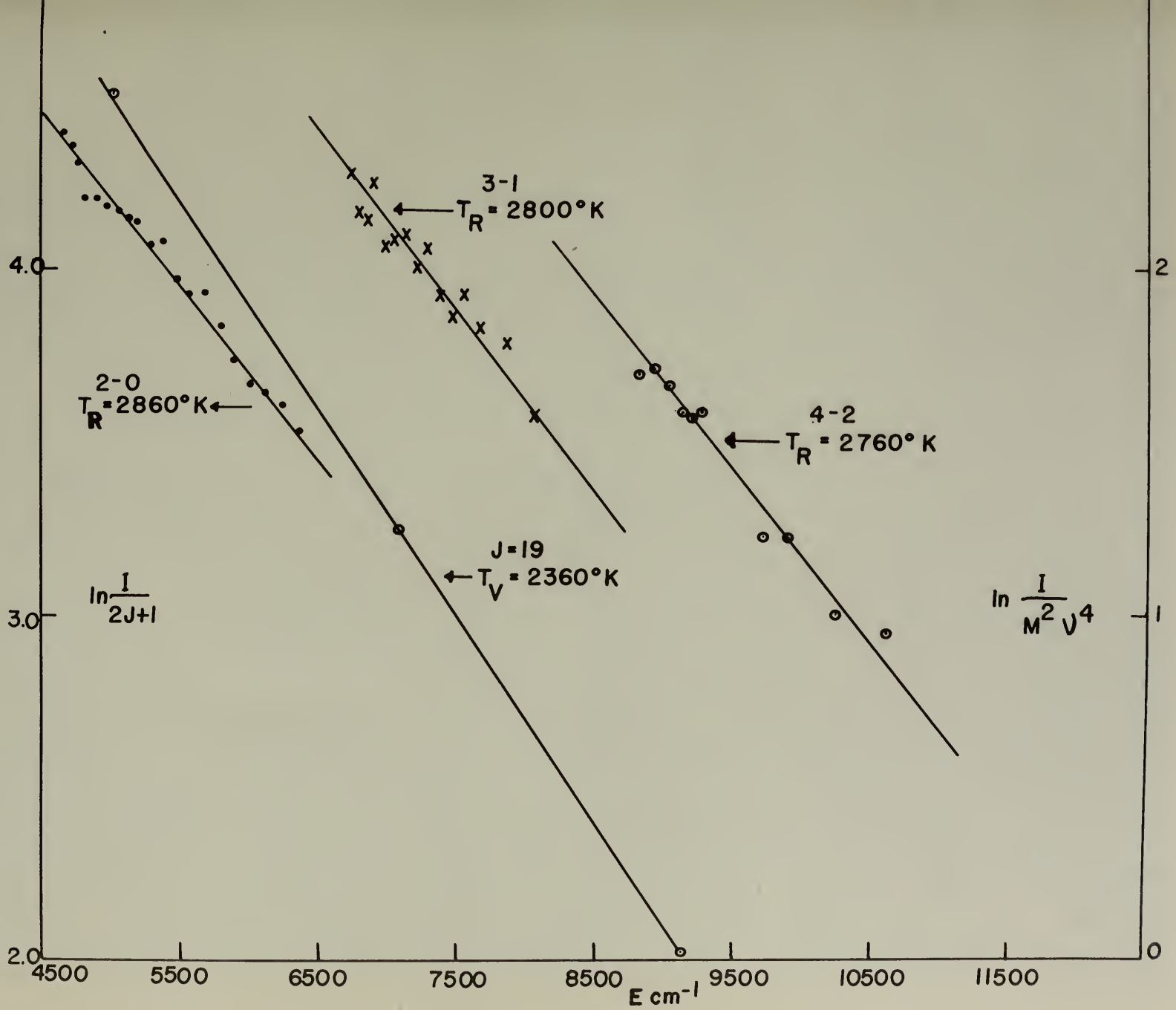
3-1
T_R = 2800°K
2-0
T_R = 2860°K
4-2
T_R = 2760° K
J = 19
T_V = 2360°K
$\ln \frac{I}{2J+1}$
$\ln \frac{I}{M^2 V^4}$
4.0
3.0
2.0
2
1
0
4500
5500
6500
7500
8500
9500
10500
11500
E cm^{-1}

Figure 3

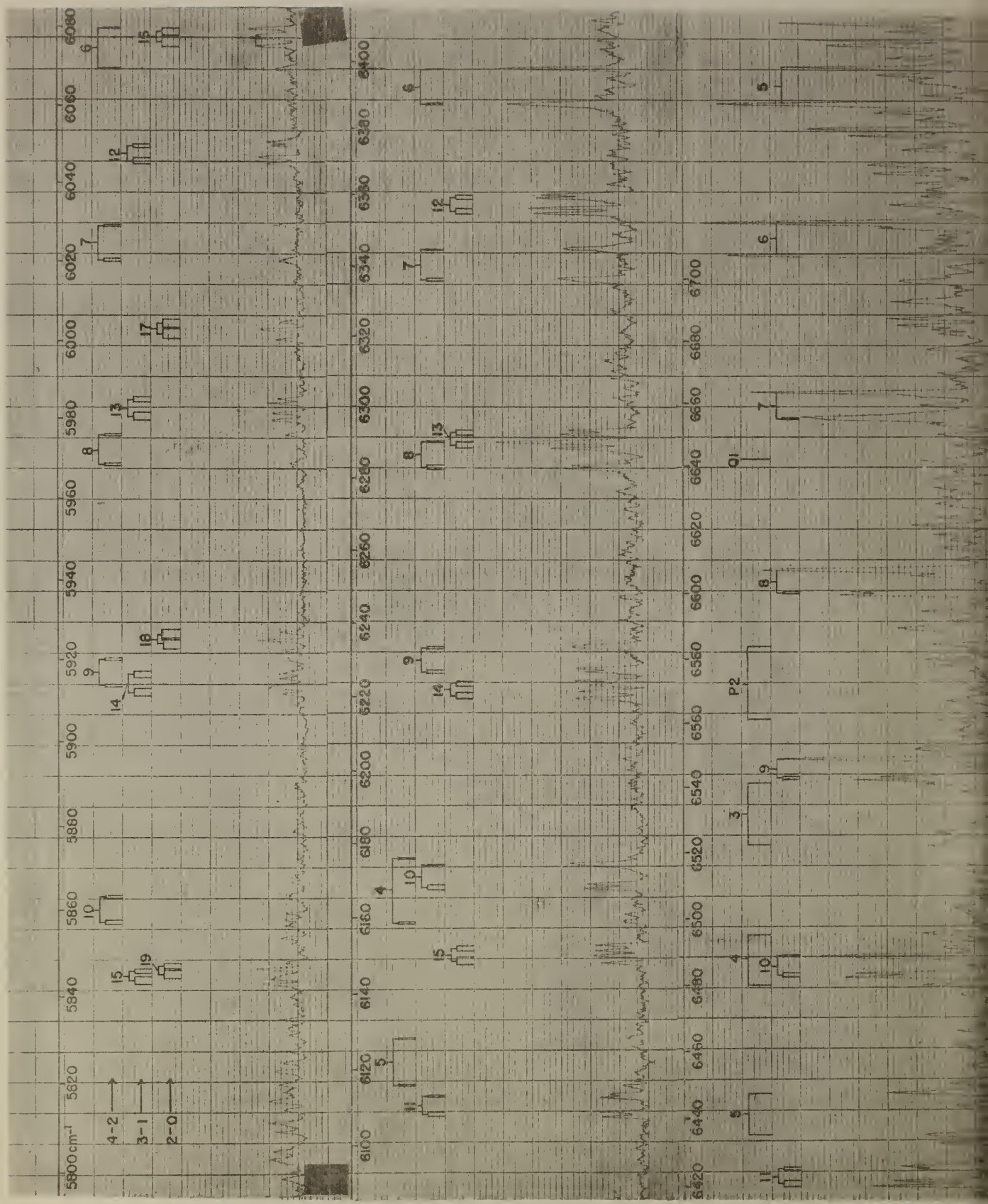
5800cm⁻¹
5820
5840
5860
5880
5900
5920
5940
5960
5980
6000
6020
6040
6060
6080
6100
6120
6140
6160
6180
6200
6220
6240
6260
6280
6300
6320
6340
6360
6380
6400
6420
6440
6460
6480
6500
6520
6540
6560
6580
6600
6620
6640
6660
6680
6700
4-2
3-1
2-0
P2
Q1

Figure 4

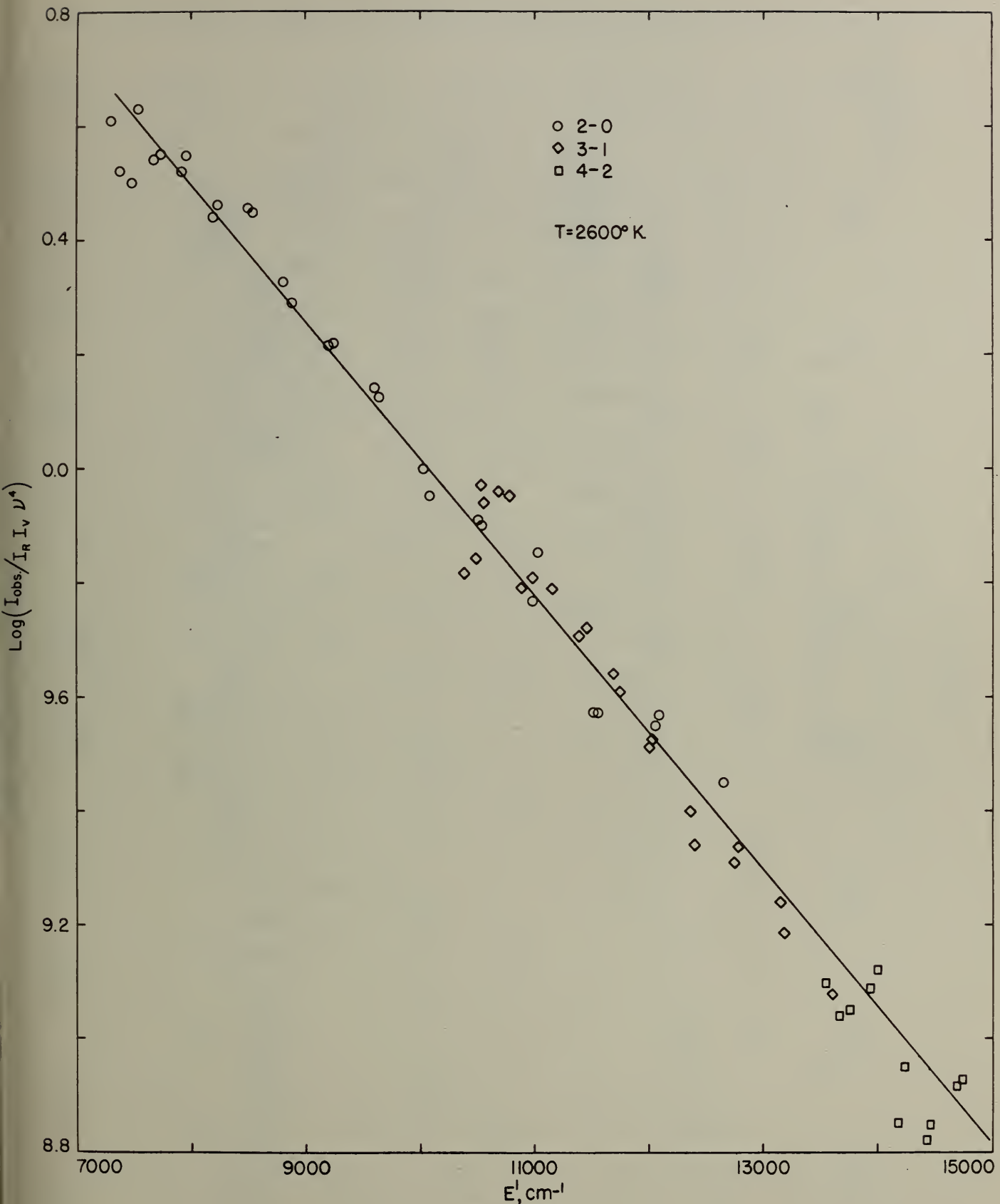
0.8
0.4
0.0
9.6
9.2
8.8
7000
9000
11000
13000
15000
E', cm-1
Log(Iobs./IR Iv ν4)
o 2-0
◇ 3-1
□ 4-2
T=2600° K.

Figure 5

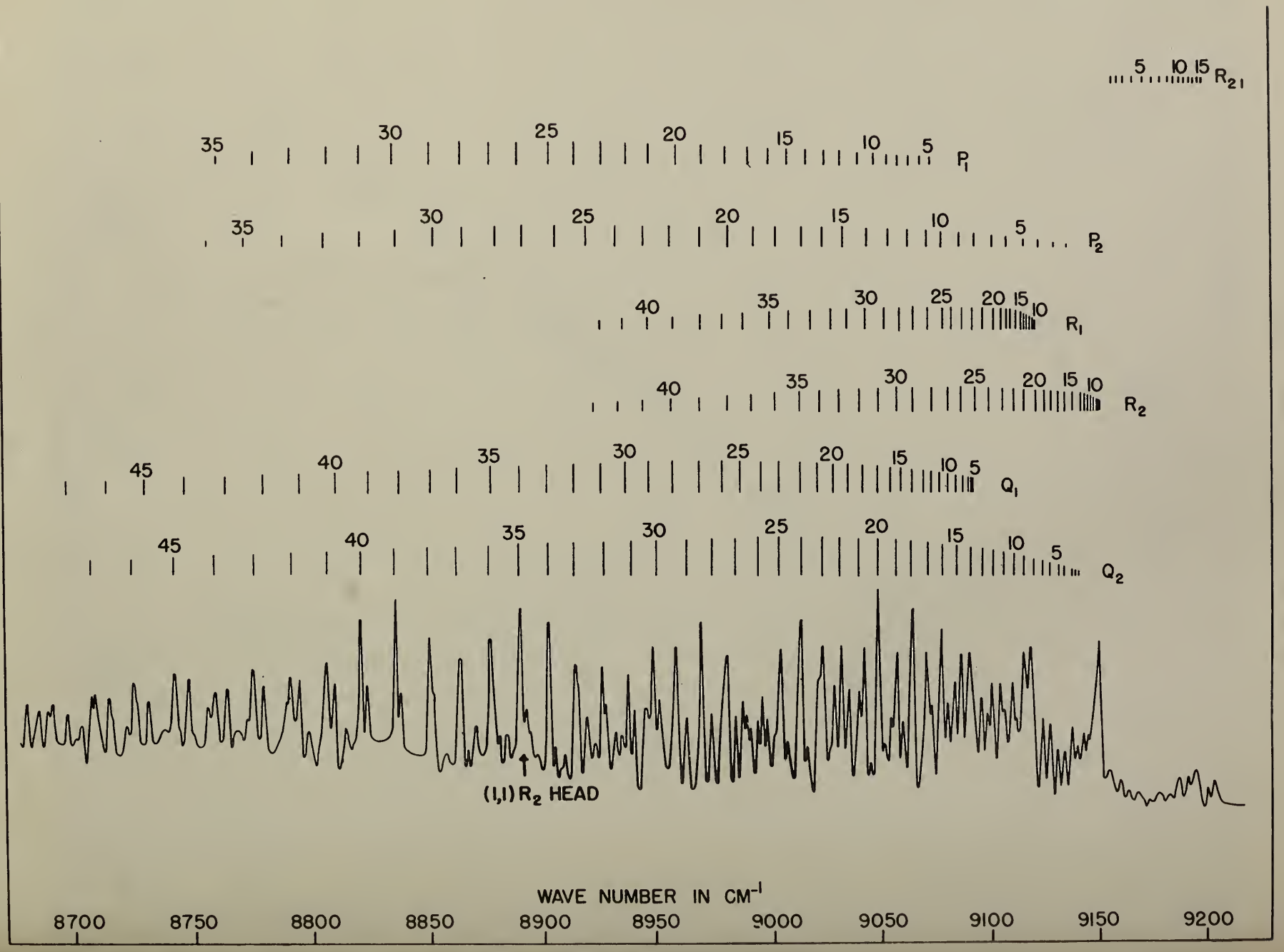
5 10 15 R21
35 30 25 20 15 10 5 P1
35 30 25 20 15 10 5 P2
40 35 30 25 20 15 10 R1
40 35 30 25 20 15 10 R2
45 40 35 30 25 20 15 10 5 Q1
45 40 35 30 25 20 15 10 5 Q2
(1,1) R2 HEAD
WAVE NUMBER IN CM-1
8700 8750 8800 8850 8900 8950 9000 9050 9100 9150 9200
RED CN (2Π → 2Σ+)(0,0)

Figure 6

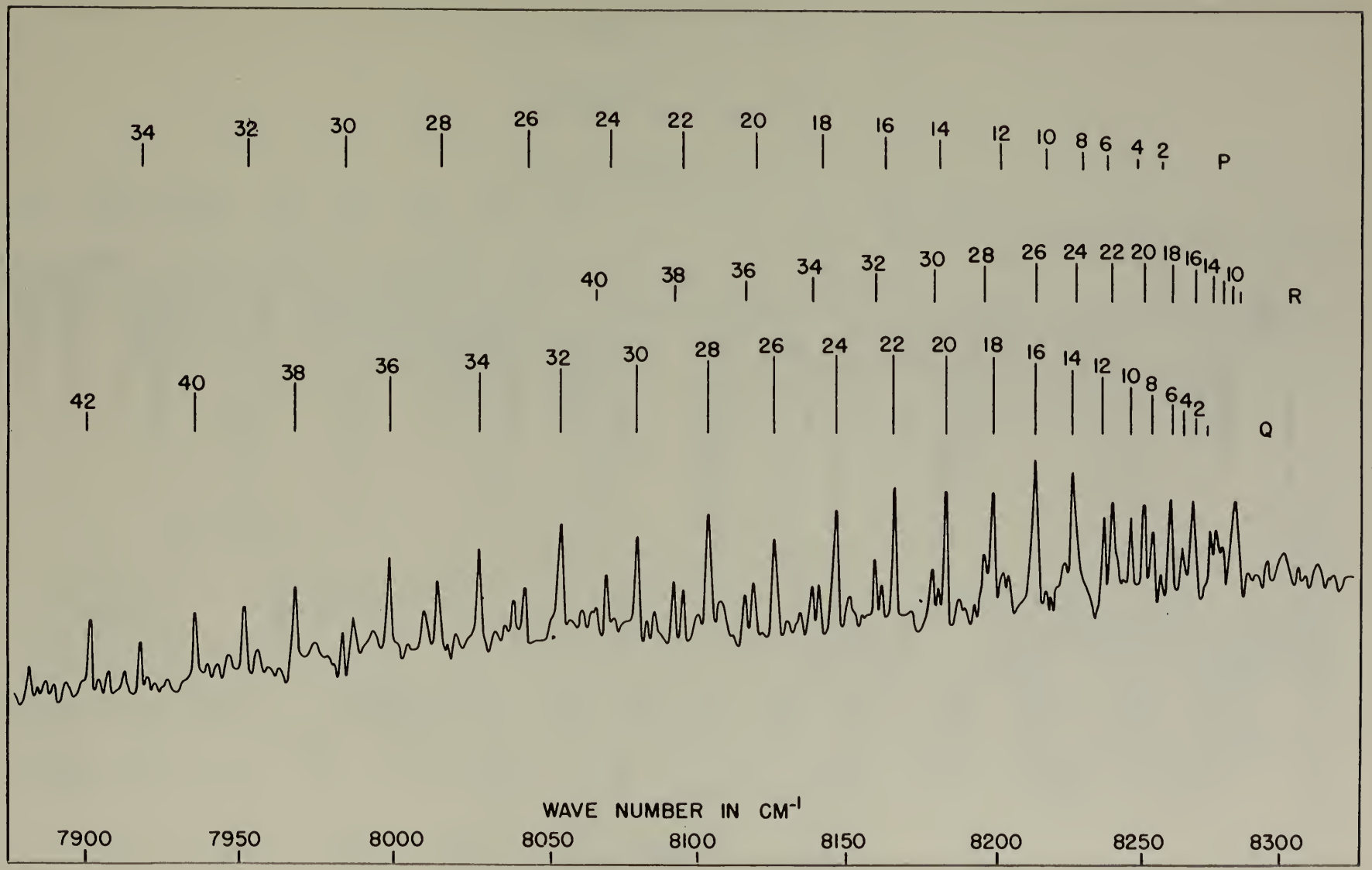

C_2 PHILLIPS SYSTEM ($^1\Pi_u \rightarrow {}^1\Sigma_g^+$) (0,0)

Figure 7

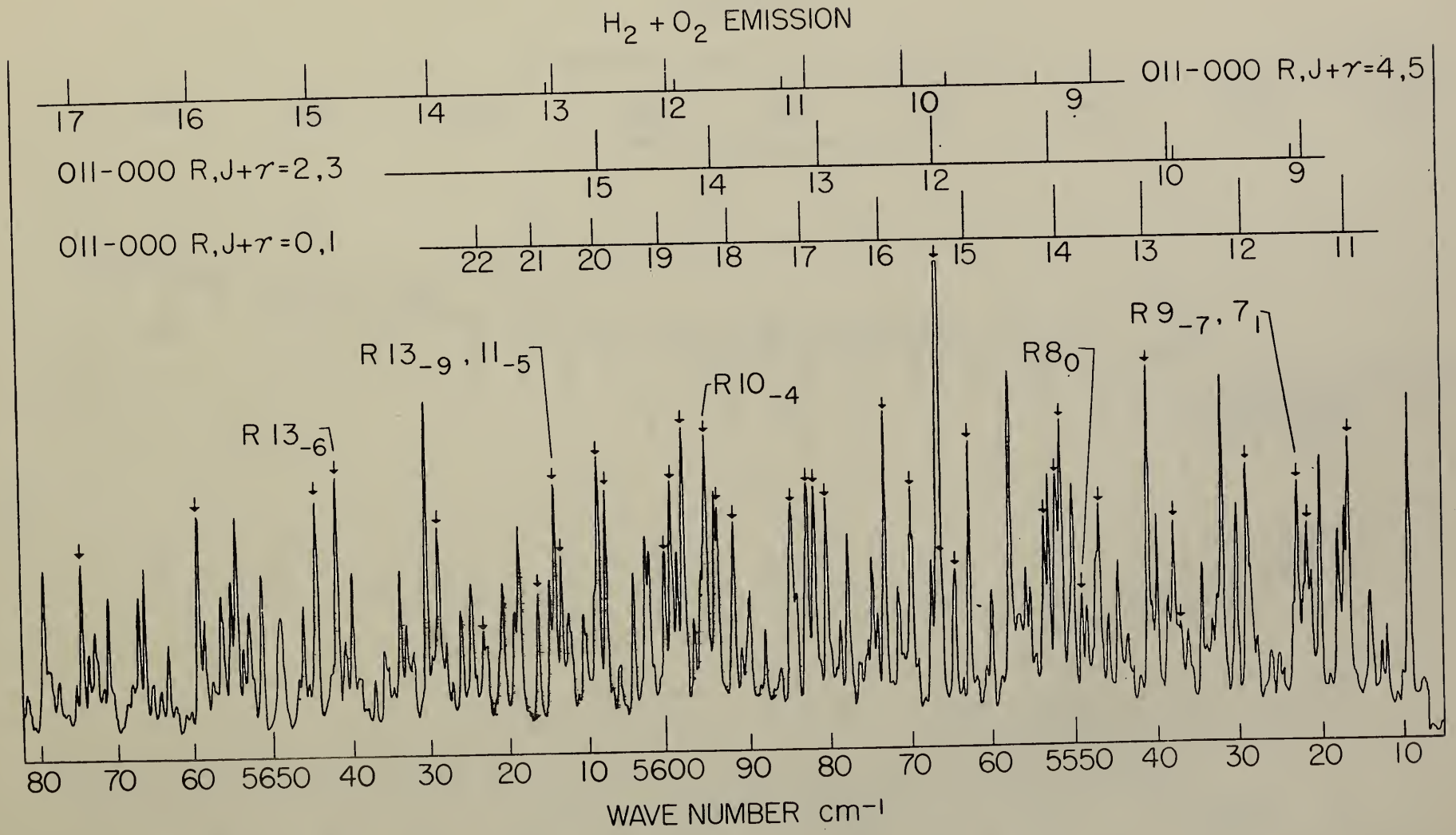
$H_2 + O_2$ EMISSION
011-000 R,J+τ=4,5
011-000 R,J+τ=2,3
011-000 R,J+τ=0,1
R 13$_{-6}$
R 13$_{-9}$, 11$_{-5}$
R 10$_{-4}$
R8$_0$
R 9$_{-7}$, 7$_1$
WAVE NUMBER cm^{-1}

Figure 8

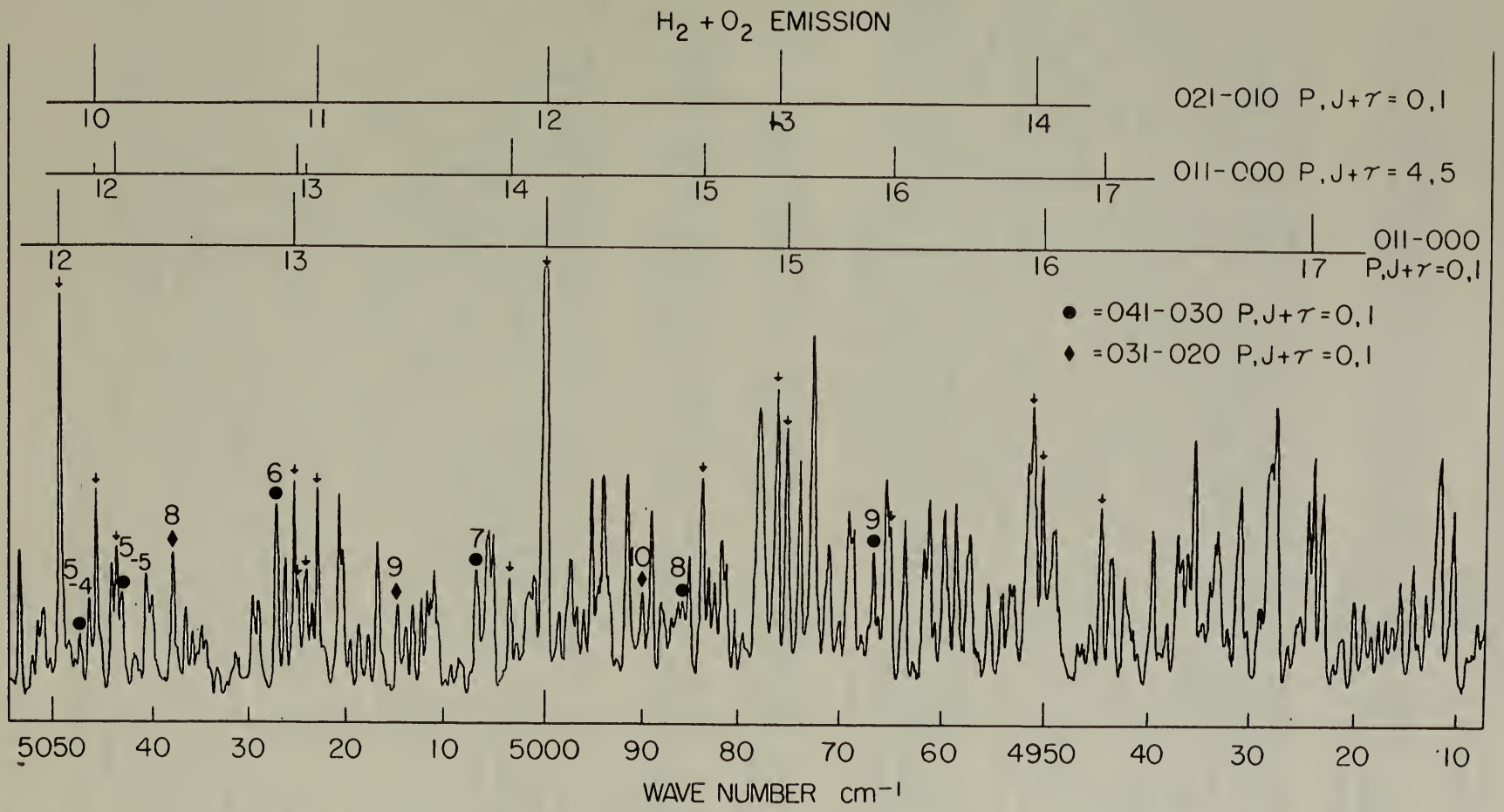
$H_2 + O_2$ EMISSION
021-010 P, J+τ = 0,1
011-000 P, J+τ = 4,5
011-000 P, J+τ = 0,1
● = 041-030 P, J+τ = 0,1
♦ = 031-020 P, J+τ = 0,1
WAVE NUMBER cm⁻¹

Figure 9

Appendix 1-B.

I. Copy of Abstract of Paper at the American Physical Society Meeting, New York, February 1-3, 1951.

1. Paper No. N-2, "Vibration-Rotation Bands of CO in Flame Spectra.*", by S. Silverman, The Johns Hopkins University, and W.S. Benedict, National Bureau of Standards.

"The emission of carbon monoxide-oxygen flames has been studied with a 7200-line vacuum grating spectrometer. Between 2.3μ and 2.6μ the vibration-rotation bands of CO appear as a well-developed spectrum, with only slight interferences from other bands (CO_2?) at the long-wavelength end. The 2-0, 3-1, 4-2, and 5-3 bands all appear, and extend to J values above 50. Heads are formed in the R branches at J~30, and are a prominent feature of the spectrum. The positions of the lines of higher v' and J show slight deviations from those calculated according to the constants of Herzberg and Rao[1]. From the observed relative intensities and theoretical transition probabilities, rotational and vibrational "temperatures" may be calculated. These are both about 2000 degrees K ±10 percent. This is much lower than the calculated flame temperature (~3000°K) or the observed "temperature" of 2900 degrees K derived from the rotational distribution of levels in the OH radical at 3064A."

*Supported by U. S. Navy, ONR and Bureau of Ordnance.
[1]G. Herzberg and K.N. Rao, J. Chem. Phys. 17, 1099 (1949).

2. Paper No. W-3, "Vibration-Rotation Lines of OH in Flame Spectra.*", by W.S. Benedict, E.K. Plyler, and C. J. Humphreys, National Bureau of Standards.

"The emission from oxy-acetylene and oxy-hydrogen flames has been recorded in the spectral region 1.1μ-2.5μ with a 15,000-line grating spectrometer and PbS detector. Under favorable conditions, slits as narrow as 0.025 mm could be used, affording good resolution of the complex structure, which is principally due to vibration-rotation bands of H_2O. In the region of 1.6μ, which in the oxy-acetylene flame is relatively free from H_2O emission, numerous vibration-rotation lines of OH have been identified. These include all lines from P(5) to P(19) in the 2-0 band, from P(4) to P(15) in the 3-1 band, and from P(4) to P(10) in the 4-2 band. The spin doublets, and at high K the Λ-doublets are resolved. From the observed relative intensities and theoretical transition probabilities, it is possible to calculate effective rotational and vibrational "temperatures." Preliminary results yield 2600° ±200°K by both methods, for the oxy-acetylene flame, at a position in the outer cone where measurements using the ultraviolet band at 3064A normally yield "temperatures" around 3000°K."

*Supported in part by ONR.

II. Copy of Abstract of Paper at the American Physical Society Meetings, Washington, D. C., April 26-28, 1951.

1. Paper No. Z-3, Bulletin of the American Physical Society, 26, Page 54 (1951), "Bands of C_2 and CN in Infrared Flame Spectra.", by W. S. Benedict and Earle K. Plyler, National Bureau of Standards.

"In the inner cone of the oxy-acetylene flame, as observed under high resolution using a 15,000-line grating spectrometer and lead sulfide cell, several bands appear between 1μ and 1.6μ. These have been identified as the (1,0), (0,0), and (0,1) bands of the Phillips system of C_2 ($^3\Pi_u - {}^1\Sigma_g^+$), with origins at 9852, 8268, and 6441 cm^{-1}, and the (0,0) and (1,1) bands of the red system of CN ($^2\Pi - {}^2\Sigma$), with origins at 9117 and 8862 cm^{-1}. The rotational structure of the C_2 bands shows an intensity distribution characteristic of thermal equilibrium with an effective temperature near 2400 degrees K."

III. Copy of Abstract of Paper at the Symposium on Molecular Structure and Spectroscopy, Ohio State University, Columbus, Ohio, June 11-15, 1951, under the joint sponsorship of the University and the American Physical Society.

1. Paper No. H-3, "Emission and Absorption Spectrum of CO in the Region of 2.3μ", by S. Silverman, E.K. Plyler, and W. S. Benedict, National Bureau of Standards, Washington, D. C.

"New measurements have been made in the CO spectrum in the region of the overtone band, both in emission and in absorption, using the 15,000-line grating spectrograph at the National Bureau of Standards and the 7200-line vacuum-grating spectrograph at the Applied Physics Laboratory. In absorption, the 2-0 band of $C^{12}O^{16}$ has been measured between R-30 and P-29, and 27 lines of $C^{13}O^{16}$ and 8 lines of $C^{12}O^{18}$ have also been measured. In emission from oxyacetylene and CO-oxygen flames, the 2-0, 3-1, 4-2, and 5-3 bands, which form heads in the R branch near J=50, have been identified. The 2-0 band shows resolved lines out to J=46 in both the R and P branches.

"The wavelengths were determined by superposing emission lines in higher orders of Kr, A, Xe, and Hg discharges. In this way a number of lines, which fall close to one or another of the standard lines, could be measured with high accuracy. The remaining lines could be measured by interpolation between these secondary standards. The measurements are believed accurate to better than $\pm$0.02 cm^{-1}.

"The measurements show small but definite discrepancies from

the values calculated according to the constants of Herzberg and Rao (J. Chem. Phys. 17, 1099 (1949)) and Rao (J. Chem. Phys. 18, 213 (1950)). The lines of $J \leq 25$, in the 2-0 branch, are consistently 0.08 cm^{-1} lower than the predicted values; at higher J the R-branch lines fall above and the P-branch lines fall below their values. A comparison of provisional constants derived from our measurements with their values is given in Table 1.

TABLE 1

Constant	ω_e	$x_e\omega_e$	$y_e\omega_e$	B_e	α_e	D_e	β_e
Value, cm^{-1} according to SPB	2169.81	13.284	0.0110	1.93130	0.017523	$5.96 \cdot 10^{-6}$	$0.0 \cdot 10^{-6}$
Value, cm^{-1} according to H & R	2170.21	13.461	0.0308	1.93139	0.017485	$6.43 \cdot 10^{-6}$	$0.04 \cdot 10^{-6}$

"The observed isotope shift of the 2-0 band origin, for C^{12}-C^{13}, is 93.258 $\pm$0.01 cm^{-1}. Using our molecular constants, and the atomic masses C^{12}=12.00382 and C^{13}=13.00751, the calculated shift is 93.241 cm^{-1}. For O^{16}-O^{18} the observed shift is 101.01 $\pm$0.05 cm^{-1}, and the calculated shift, with O^{18}= 18.0049, 101.025 cm^{-1}.

"The emission spectra permit the determination of vibrational and rotational "temperatures" with an accuracy of $\pm$5 percent. Agreement between the two modes is observed in the outer cone of the CO-oxygen flame, but in the region just above the reaction zone the rotational "temperatures" are several hundred degrees higher."

2. Paper No. H-4, "Emission of H_2O in the Region 1.7-2.2μ", by A. M. Bass, W. S. Benedict, and E. K. Plyler, National Bureau of Standards, Washington, D. C.

"The emission of oxyhydrogen and oxyacetylene flames has been studied under high resolution with a 15,000-line grating spectrometer and lead sulfide cell. Slits as narrow as 0.2 cm^{-1} could be employed. The water-vapor band, which in room-temperature absorption extends from about 1.80-1.96μ, is broadened in emission

from 1.7-2.2μ (5900-4550 cm^{-1}). Over 600 strong lines have been measured in this region, and a number of weaker, partially resolved lines appear reproducibly. The analysis of the rotational structures is progressing. Many lines of the (011-000) band agree with those found in laboratory and atmospheric absorption,[1] when allowance is made for the greatly increased effective temperature, and many additional lines from higher energy levels may be identified. The principal series $J \leftrightarrow (J+1)$ may be followed out to $J' = 22$ in both the P and R branches. Corresponding lines in the upper-state bands (021-010) and (031-020) have also been identified with somewhat lower intensity, and a few lines may be assigned to the (041-030), (111-100), and (012-001) bands."

---

[1] R.C. Nelson and W. S. Benedict, Phys. Rev. 74, 703 (1948)

Appendix 1-C

Tube Furnace for Spectroscopic Observation of Hot Gases in Thermal Equilibrium

R. D. Arnold

The desired end product of the constructional phase of this work is a column of gas of known pressure, original (room temperature) composition, and temperature (up to 2000°K). It must be possible to project a light beam through the column and the gas temperature should be nearly uniform along the entire optical path through the gas being observed.

Use of fused quartz for a container or windows is precluded by the maximum temperature goal and the necessity for having the window in the hot zone for temperature uniformity along the optical path. Artificial white sapphire is a satisfactory material; m.p. 2030°C, ultraviolet transmission greater than 70% at 3000A, infrared transmission 90% at 4μ. Single-crystal windows of 7/8" diameter and 1/8" thickness have been purchased. The optic axis of the crystal is along the axis of the window to avoid birefringence and to insure uniform thermal expansion in the window plane.

High-purity Alundum (about 99% alumina) is to be used as a container. This material can be operated up to about 1900°C. Tubes of a lower purity Alundum (less impermeable) were found by gas leakage tests to be adequately impermeable up to 1500°K. The greatest problem is that of effecting a sufficiently gas-tight seal between the window and the tube. Requirements for tightness may be reduced by mounting the windows not on the container tube but on sight tubes probing into the container and by pumping on the sight tubes. This design also means that the window will always be pressed into its seat by gas pressure. It has been found by experiment on $\frac{1}{2}$" diameter sample windows that a satisfactory seal is obtained by electro-plating platinum on the edge of the window and placing it into a close-fitting seat ground in the Alundum sight tube. At room temperature the seal is quite poor but the window expands slightly more rapidly than the tube and in the range 1000-1500°C it is possible to maintain a pressure ratio of greater than 5,000 across the window by pumping continuously with a 0.5 liter/sec. forepump with air at atmospheric pressure on the outside of the tube. Although some minor improvements may yet be made it is felt that the performance of the design described above justifies accepting it in proceeding with the remainder of the furnace design, certain details of which are contingent upon the form of the window.

Inlet and outlet conduits for the test gas will be the annular space between the sight tubes and the container tube. This will permit the conduit seals to be outside of the furnace and therefore cold. A molybdenum resistance winding will be wound on the container tube and the annular space between this tube and a larger concentric tube will be filled with an atmosphere protective to the winding. Next will come a thickness of insu-

lating material and then an outer winding of platinum-rhodium alloy in several separately controlled segments to aid in obtaining temperature uniformity along the tube. Outside of this winding will be still more insulating material.

Construction of the furnace will proceed as parts, which are on order, are received.

Appendix 2-A.

ROTATIONAL TEMPERATURES OF OH IN METHANE-AIR FLAMES*

Herbert P. Broida
National Bureau of Standards

Abstract

ROTATIONAL TEMPERATURES OF OH IN METHANE-AIR FLAMES

Rotational line intensity distributions in emission and absorption of the 0↔0 band of the $^2\Sigma \leftrightarrow {}^2\Pi$ transition of OH have been measured in methane-air flames. The number of electronically excited OH radicals in the inner cone greatly exceeds the equilibrium concentration, and the intensity distribution of the high quantum numbers gives a temperature of 5200°K. However, OH radicals in the ground state were in thermal equilibrium at 2000°K. A break in the intensity distribution indicates a two stage combustion reaction. It is suggested that the excessive amount of excited OH is due to its formation in intermediate reaction steps. Line reversal temperatures using Na, Hg, and OH have been measured in the same flame for purposes of comparison. Also the rotational temperature of excited OH in a methane-oxygen flame was measured.

1. INTRODUCTION

Current expansion in the use of power units driven by hot gases has stimulated in physicists and chemists a renewed interest in flame phenomena. One of the major obstacles to a complete understanding of the operation of gas turbines, jet engines and rockets is the lack of an adequate theory of flame propagation. Furthermore, limitations of conventional immersion type pyrometric devices and radiation pyrometers have hindered the development and practical use of such propulsion units. Because of the promise appearing in research methods involving optical spectroscopic analysis of burning regions, many laboratories have undertaken programs of spectroscopic studies of flames. Such studies have contributed greatly to the present knowledge of intermediate particles within the flame zone, and also have led to various methods for determining temperatures in burning gases. Although quantitative measurements of intensities in both emission and absorption are necessary to an understanding of the relative importance of excited and unexcited intermediate particles of the chemical reactions within the flame zone, only a small number of absorption studies have been made because of the many experimental difficulties inherent in such work.

Since neither thermal nor chemical equilibrium exists in a flame region, there is not a flame temperature because, in a strict thermodynamic sense, temperature applies only to an equilibrium state. However, less precise use of the word temperature has become commonly accepted in order to simplify discussions concerning the measurement of

*This work was done under the sponsorship of the Navy Bureau of Aeronautics.

radiation intensities from hot gases. The temperature of a flame generally depends upon the technique of measurement and therefore it is common practice to use a modifying adjective or phrase descriptive of the method by which the number associated with the temperature was obtained. For example "OH rotational temperature" refers to the temperature obtained from the distribution of intensity among the various rotational states of an OH band. This paper reports investigations of the rotational energy distribution of the $0 \leftrightarrow 0$ band of the $^2\Sigma \leftrightarrow {}^2\Pi$ transition (between 3064 and 3133 Angstrom units) of the hydroxyl radical in absorption and emission in flames at atmospheric pressure of methane pre-mixed with air and oxygen.

The OH radical was selected for initial studies of radiation from flames for the following reasons:

1. It occurs strongly in most hydro-carbon flames;

2. It is an important intermediate in reaction chains;

3. There is evidence [1] that in some flames, the OH produced is chemiluminescent;

4. Its electronic transition is in a convenient region to observe spectroscopically;

5. Its spectrum [2] is well known;

6. Experimental "f numbers" [3] have been measured; and

7. The rotational distribution is in a relatively narrow wavelength interval, but the lines are separated sufficiently for temperature determinations.

The band specified above, which is degraded to the red and which has a head at 3064 Angstrom units is not only the most intense band of the OH electronic transition but also is very prominent in the ultraviolet spectra of hydrocarbon flames. For temperature measurements, the R_2 branch is the most usable of the 12 branches since it has many lines which do not overlap in a small region (22 A.U.). A spectrograph of fairly high dispersion is required both to separate these lines and to measure absorption coefficients.

A search of the literature has revealed no information on rotational intensity distributions in absorption by OH in a flame. Failure to apply this technique to combustion studies is probably the result of the difficulties of bringing together the appropriate apparatus. One major problem is the need of an intense source of continuum that is steady with time, and has no superimposed emission or absorption lines. Another outstanding need is a sensitive detecting instrument of high resolution. Since no continuum source of the intensity and uniformity required for studies with oxygen flames was available, it was necessary to cool the flame with nitrogen (i.e. by using air), so that a tungsten lamp could be used. A direct reading monochromator with high resolution capable of detecting absorption of 1 percent with relative ease served as the needed detector.

In addition to the determination of the OH rotational temperatures in emission and absorption, three separate line reversal temperatures have been measured by comparing the emission from added sodium, from added mercury and from rotational lines of OH with a calibrated tungsten strip lamp. Analysis of the data indicates that thermal equilibrium exists in the outer cone and that, in the inner cone, there is a two stage reaction in which OH is formed in an excited electronic state.

2. METHOD AND EXPERIMENTAL RESULTS

2.1 Apparatus

Figure 1 is a photograph of the flame used in these studies. A homogeneous mixture of dried air and methane (99.6% purity) flowing upward through 1 meter of steel tube 38 mm in diameter, is burned above an accelerating nozzle having a throat diameter of 12.7 mm. A more complete description of the apparatus for controlling the flame has been given elsewhere [4]. This flame differs from the conventional Bunsen flame burning above a tube in that the gas emerges from the nozzle with a uniform velocity rather than with a parabolic velocity distribution. A more nearly conical burning zone results from this uniform velocity pattern. It is of interest to note that the visible region begins about 0.6 mm above the nozzle and has a diameter greater than the throat of the nozzle by about 2.5 mm. Both emission and absorption measurements were made along the side of the inner cone where the intensity is greatest, and near the base where the effects of the surrounding outer cone are least. Measurements on the outer cone were made about one cm above the tip of the inner cone.

The portion of the flame to be studied was focused by a quartz lens having a magnification of two, upon the entrance slit (8 mm high) of a direct reading monochromator [5]*. The desired spectral region is scanned by rotating the grating. Radiation is detected by a 1P28 photomultiplier tube behind the exit slit, and intensity is recorded directly as a function of wavelength. Although this monochromator has a resolving power of 55,000, the full resolution could not be used because the weak intensity of this flame (due to the cooling by the nitrogen in the air) made it necessary to use relatively wide slits (0.015 mm). For absorption spectra, radiation from a tungsten strip lamp was focused by either a spherical mirror or a quartz lens on the region of the flame being studied. A quartz lens focused both the flame and the image of the lamp on the slit of the monochromator.

2.2 Rotational Distribution of OH

If there is thermal equilibrium in a flame, the intensity distribution of an emission or absorption band of a molecular species can be used to determine temperature [6]. For a fixed electronic and vibrational transition of the molecule, the intensity $I_{K \rightarrow L}$ of an emitted line depends only upon the number of molecules, N_K, in the Kth rotational level of the excited state and upon the transition probability, A_{KL}. Thus

$$I_{K \rightarrow L} = \text{constant} \times A_{KL} \times N_K \qquad (1)$$

*This instrument was constructed by the research division of Leeds and Northrup Company and was loaned to the Combustion Section at the National Bureau of Standards on a field trial basis.

Although the constant term is linear with frequency, the change in frequency over a small frequency range is negligible and need not be considered. The equilibrium number of molecules in an excited state with an energy E_K is determined by the Maxwell-Boltzman distribution and is given by

$$N_K = N_0(2K + 1) \exp(-E_K/kT) = N_0 \, g \exp(-E_g/kT) \quad (2)$$

where k is the Boltzman constant, T is the absolute temperature, and N_0 is the total number of molecules. Eqs 1 and 2 can be combined and written in an experimentally useful form as

$$\log_{10}(I_{K\rightarrow L}/g_K A_{KL}) = \text{constant} - (E_K/kT) \log_{10} e \quad (3)$$

Thus a plot of $\log_{10}(I_{K\rightarrow L}/g_K A_{KL})$ as a function of E_K can be made from the known transition probabilities and measured intensities. This is a straight line, the slope of which is proportional to 1/T. When experimental errors have been eliminated, a lack of linearity of this plot may be an indication of non-equilibrium. Eq 3 for absorption differs from that in emission only in that the transition depends upon the number of molecules N_L in the energy level E_L in the unexcited or ground state. There is also a difference in the constant term but this is unimportant for temperature measurement over a narrow wavelength interval.

Figure 2 is a 10 Angstrom region of the OH spectrum, in both emission and absorption, from the inner cone of a stoichiometric methane-air flame. The lower curve shows the intensities of emitted radiation and the upper curve shows the absorption of the continuum by the flame. The resolved lines of the three branches in this region are marked; the satellite lines of the Q_1 branch are not shown. It will be noticed that transitions from the higher rotational levels are not observable in absorption even though transitions from the lower levels are of an intensity comparable to that of emission. This relative weakness of lines from the higher rotational levels is a clear indication that in the ground state, the OH is at a much lower rotational temperature than the excited state.

A quantitative measure of this difference can be obtained from the logarithmic plot suggested by eq 3. Figure 3 shows the results of intensity measurements of the R_2 branch of OH emitted from the inner cone of a stoichiometric mixture of methane and air. The observed points lie on two distinct straight lines; one line corresponds to the intensities from the lower rotational states and the other line of completely different slope corresponds to the intensities from the higher states. From the slopes of the two lines "temperatures" of 2350°K and 5200°K are found for the lower and higher states, respectively. Repeated measurements show a precision in each of these "temperatures" of approximately ± 5 percent. The line marked 1550°K will be discussed later.

An analysis of possible experimental errors that might have caused a break in the logarithmic plot indicated that the break was real and is characteristic of the flame itself. No error was introduced by the small

amount of emitted continuum, since intensities were measured directly as heights above this continuous background. Although there was only small self absorption (of the order of 5 percent) by the weak methane air flame, a correction factor for this type of error was easily obtained from the absorption measurements of the continuum from the strip lamp. Such corrections did not change the characteristics of lines and did not affect the slopes by as much as the experimental error. Although there was some overlapping of lines, a weak line only 0.2 A.U. removed from a line 6 times as strong was still resolved, and a sufficient number of lines were resolved and measured so that the lack of resolving power was of no consequence. Circles in figure 3 represent lines completely resolved and the squares represent lines that either are not completely resolved or which have weak superimposed lines. The straight lines are drawn to best fit the circles.

Another manner of illustrating the non-equilibrium is by using the iso-intensity method developed by Dieke and Crosswhite [2]. This method has the advantage that for lines of equal intensity, the effect by self-absorption will cancel out in the first approximation. Shuler [7] has shown for lines of equal intensity and small difference in wavelength that

$$A_{K'}/A_K = \exp\left[(E_{K'} - E_K)/kT\right]. \qquad (4)$$

A plot of $E_{K'} - E_K$ vs log $(A_{K'}/A_K)$ will be a straight line going through the origin for an equilibrium rotational distribution. Figure 4 shows such a plot for the emission from the methane-air inner cone. Since a straight line cannot be drawn through the experimental points and the origin, a non-equilibrium is indicated.

The persistence of a non-equilibrium distribution as indicated by figures 3 and 4 can be interpreted as showing that the large number of collisions which the OH radical undergoes during its lifetime are not sufficient to bring about rotational equilibrium. Since the radiative lifetime of electronically excited OH is of the order of 10^{-6} second [8] and the time between collisions at atmospheric pressure is of the order of 10^{-10} second (10^{10} collisions per second), the observed non-equilibrium rotational temperature would mean that 10,000 collisions per lifetime of the excited OH are not very effective for bringing about thermal equilibrium. Such a lag in the equipartition of rotational energy with other forms of energy is consistent with the observation of Oldenberg [9] that OH radicals show an abnormal rotational intensity distribution in electric discharges through water vapor.

Breaks in logarithmic curves similar to figure 3 have been observed in flames with other gases, particularly by Gaydon and Wolfhard [1], but the cause is unexplained when experimental errors have been eliminated. Continuous temperature gradients in the flame would not be expected to cause such an abrupt change in the intensity distribution but Dr. Henry Crosswhite (by private communication) of the Johns Hopkins University has suggested that such a distribution would be expected from two

distinct temperature regions. Assuming that there are two temperature regions, it is possible to separate the effect of the intensity of the "cold" region from that of the "hot". When the straight line for the higher rotational states of figure 3 is extrapolated to the lower states, and these extrapolated intensities are subtracted from the measured values, the intensity of the "cold" region alone (lower curve on the left side of figure 3) is found to correspond to a temperature of 1500°K.

It might be expected that this "cold" region would be associated with the cooler outer cone, but the intensity of emitted radiation in the outer cone was of the order of 1/25 of that in the inner cone. Consequently its effect on the distribution would not be observed. This extremely low intensity of emission made it impossible to obtain a meaningful intensity distribution in the outer cone since even the intensity from the inner cone was so weak that thermal noise from the first surface of the photomultiplier tube was troublesome. The entire measured radiation must come from the inner cone, since the radiation from the outer cone alone was too weak to be observed on the background of the more intense emission from the inner cone. Consequently, it seems reasonable to assume that the two temperature regions are evidence of a two-stage combustion process occuring within the narrow region of the inner cone. A two-stage reaction is known to occur in compression-ignition engines [10] and under some conditions a "pre-flame" reaction appears to be completed before the final burning occurs. In flames of ether mixed with air, Powling [11] has separated the "cool flame" from the ordinary "hot" flame. Although there is no evidence from low temperature reaction studies [8] of methane-air mixtures that a two stage process exists, it is known that acetylene is formed in a methane flame. The formation of these larger molecules might lead to conditions under which a two stage reaction could take place. Another possibility which exists for the formation of a two temperature region, and which would account for the experimental facts, is the existence of two different intermediate reactions giving rise to excited OH with separate rotational distributions. Until more experimental evidence is available, it is not possible to consider and eliminate all reasonable possibilities for the two temperatures.

For the purpose of discussion, let the reaction producing excited OH with a rotational distribution corresponding to 1550°K be called reaction a and that producing radicals with a rotational distribution corresponding to 5200°K be called reaction b. The relative numbers of radicals formed in these two reactions can be calculated from the experimental results if it is assumed that the only loss of excited OH is by radiation to the ground state. Following the approximation of Herzberg [6] which is sufficiently good at the high temperatures found in this flame, it is possible to find the total number of radicals, N, from the rotational state sum, Q_r, and the number of radicals, N_K in some particular level, K.

$$N = \frac{N_K Q_r}{2K+1} \exp(E_K/kT) = \frac{K(K+1)N_K}{(2K+1)E_K} kT \exp(E_K/kT) \qquad (5)$$

According to eq 1, N_K is proportional to I_K/A_{KL} and therefore the intersection in figure 3 of the curves for the two reactions gives the energy, E_3, at which the reactions form the same number of radicals. E_3 is the rotational contribution to the energy, whereas figure 3 shows the total energy. The ratio of the number of OH radicals formed in reaction a to the number formed in reaction b is

$$N_a/N_b = (T_a/T_b) \exp E_3/k(1/T_a - 1/T_b) \qquad (6)$$

$$= (1550/5200) \exp [(163/.695)(1/1550 - 1/5200)] = 0.3$$

Thus for every OH radical formed by reaction a, three are formed by reaction b.

Absorption measurements in the inner and outer cone of the same stoichiometric flame gave a rotational temperature of 2000 ± 100°K in both cone, as shown by the representative results in figure 5. The uncertainty of ± 100°K is estimated from data of over 30 measurements of the inner and outer cones. Since the same temperatures were observed in the inner and outer cones, the rotational states of unexcited OH are probably in thermal equilibrium in both regions.

In addition to giving the temperature of the ground state, absorption measurements can be used to determine the concentration of the absorbing molecules. Following the approximation given by Gaydon[8] for the integrated absorption coefficient, the number of OH radicals per cubic centimeter, in the Lth state N_L, is given in terms of the observable quantities as:

$$N_L \approx \left(\frac{\mu c^2}{2e^2 f}\right)\left(\frac{I_{abs}/I_o}{\Delta X}\,\Delta\nu\right) \qquad (7)$$

μ and e are respectively the mass and charge of an electron; c is the speed of light; I_{abs}/I_o is the fraction of light absorbed at the center of a spectral line of half width $\Delta\nu$ by an absorbing region of thickness ΔX; and f is the "f-number" of the absorbed line. Neglecting the change of temperature within the hot gases and using the edge of the visible cone as the extent of the absorbing region, ΔX of the outer cone was approximately 2 cms. For the R_2 (3) line, the measured values of $\Delta\nu$ and I_{abs}/I_o were of the order of 0.8 cm^{-1} and 0.06, respectively. Using the

corrected "f-number", 4.6×10^{-4}, of Oldenberg and Dwyer [3] for this line, N_2 is found to be 0.9×10^{14} OH radicals per cm^3. The total number of OH radicals per cm^3 in the ground state as calculated from eq 5 is 8×10^{14}. This value is in reasonable agreement with that of 2×10^{15} given in the tables calculated from thermodynamic data by Hottel, Williams and Satterfield [12] for the equilirbrium concentration at 2000°K.

It is difficult to estimate with any certainty the accuracy of the calculated concentration, because of the numerous possible sources of error. In addition to the errors inherent in the assumptions used in deriving eqs 5 and 7, the largest uncertainties are: in lack of knowledge of the temperature and its distribution in the hot region; in the measurements of the half-width of the spectral line; and in the fraction of radiation absorbed at the center of the line. The effect of the latter appears to be neglibible, because it was found that the monochromator slit could be increased to more than double its optimum width for maximum resolution before the overlapping of radiation from adjacent wavelengths reduced the absorption noticeably. The resultant of all these errors is not likely to cause the measured concentration to be in error by more than a factor of five.

It is difficult to determine quantitatively the difference in concentrations of OH in the inner and outer cones because the inner cone cannot be observed except through a region ofthe outer cone. However, the relative absorption intensity in the two regions indicate that the concentration of OH in the inner cone is greater by a factor of at least 2.5. This value was estimated from measurements which show that intensities of absorption lines in the inner cone were 25 percent greater than those in the outer cone. The thickness of the outer cone surrounding the inner cone was about 1/2 that of the outer cone above the tip of the inner cone. At atmospheric pressure the visible region of the inner is about 0.2 mm thick.

It will be noticed that the experimental value for the first absorption lines in the inner cone (lower curve of figure 5) do not lie on the straight line through the other points, but are somewhat higher. Although the separation of these points from the straight line is only slightly greater than the experimental error, the effect was found only for the inner cone and never for the outer cone alone. These facts show that there are more OH radicals in the first (and possibly other lower levels) than is to be expected from a Maxwellian distribution of the radicals among the energy states. An average of six measurements showed an excessive absorption of the first state of about 30 percent. This extra population of the first state in the inner cone may be due to the superposition of two temperature regions, as has been postulated for the excited state. Also it is possible that this extra population may come about as a result of the type of phenomena that would be expected from from Golden's [13] quantum mechanical theory of reaction rates.

Measurements made with methane-air mixtures varying from 0.75 to 1.25 of stoichiometric fuel gave results similar to those made on stoichiometric mixtures, and need not be presented here.

2.3. Line Reversal Temperatures

The line reversal method [14] of measuring gas temperature is probably used more widely than any other spectroscopic means because of the relative simplicity of the apparatus and of interpreting the measured quantities. Essentially the method consists of comparing the intensity of monochromatic radiation emitted by the hot gases with the intensity of light of the same wavelength emitted by a continuum source at a known temperature. This method gives the excitation temperature of the atoms or molecules whose radiation is being observed. For gases in equilibrium, this temperature is equal to the thermodynamic temperature. Although various reversal temperatures of methane-air flames were determined, the procedure for making such measurements is so well known that the method need not be described in detail.

A large number of careful determinations of temperature were made using a flame totally colored with sodium (5890, 5896 A.U.). These showed that the measured temperature depended upon the region of the flame that was observed. The maximum temperature was found about 3 mm above the tip of the inner cone. Care was taken with the optical alignment and apertures of the lenses so that no errors from these sources would enter. For a stoichiometric mixture of methane and air, this measured maximum temperature was 2075 ± 10°K. The uncertainty of 10°K is the accidental error in the measured temperature of a given flame, and does not include the unknown systematic errors of the method of measurement. Determinations made through the inner cone yielded temperatures about 35°C less than the maximum. This is probably due to a lack of thermal equilibrium between the newly formed sodium atoms and the hot gases. The measured temperature is some 125°C lower than that calculated from specific heat data. This difference is probably due to the cooling of the gases by the surrounding atmosphere.

By a mercury line reversal method (at 2537 A.U.) the temperature in the inner cone was observed to be 2500°K. This value may include an error by as much as 10 percent because of the uncertainty in the value of the reflectivity at this wavelength of the concave aluminum mirror used to focus the image of the strip lamp on the flame. Because of the large amount of cold mercury within the inner cone, it was expected that the measured temperature might be much lower than the theoretical flame temperature. However the high measured value is another indication of excess energy in some energy states within the reaction zone. The non-equilibrium amount of emitted mercury radiation might be caused by collisions of the second kind between mercury atoms and highly excited molecules. It is also possible that the mercury may actually enter into the chemical reactions.

Using an OH line, the reversal temperature was found to be 2300°K, a high value that might be expected from the excessive radiation already mentioned. There was also a measurable difference in temperature depending upon the OH rotational level observed, the temperature being higher

for higher energy levels. For example, the temperature determined from the R_2 (9) transition was 20° higher than that determined from the Q_1 (6) line. This difference is not significant as a temperature but emphasizes the lack of meaning of the measured value when thermal equilibrium has not been attained.

2.4 Methane-Oxygen

As a check upon the emission from methane-air flames, measurements were made of the rotational distribution of the OH band in a stoichiometric methane-oxygen flame burning above an acetylene torch having a port diameter of 1.6 mm. Although there is a small amount of self-absorption of the intense lines of the R_2 branch, the iso-intensity method [2] shows that the temperatures of the inner and outer cone were respectively 3000°K and 2700°K. The temperature in the outer cone is in good agreement with the rotation temperature of approximately 2600°K measured by Shuler [7] in a similar flame. The lower temperature of the outer cone probably is a result of the cooling by the surrounding atmosphere. No indication of abnormal distribution was found in this flame. Absorption measurements were not made on the flame of methane and oxygen because no appropriate light source with a brightness temperature greater than 3000°K was available.

Gaydon and Wolfhard [8] report that rotational temperatures of OH at low and high energy levels are 2800°K and 7500°K, respectively, in flames of methane and oxygen at low pressure. The values reported here for flames at atmospheric pressure agree well with the low energy value but no evidence of abnormal intensity at higher levels was noticed, even though the R_2 branch was measured to the 27th line.

The various temperatures of the stoichiometric mixtures are summarized in table 1. All the measured temperatures are affected by the averaging over the cooler regions surrounding the hotter core of the flame.

3. DISCUSSION AND CONCLUSIONS

In methane-air flames, the emission of OH is stronger in the inner cone than in the outer cone. This phenomenon and the abnormally high rotational temperature of the higher energy state may be due to chemiluminescence. Gaydon and Wolfhard [1] have suggested that OH may be formed in the electronically excited state as a result of the strongly exothermic reaction.

$$CH + O_2 \rightarrow OH' + CO. \qquad (8)$$

Although this suggestion is reasonable, a mechanism to account for a distribution of energy states that will lead to the straight lines shown in figure 3 is difficult to conceive. Perhaps this distribution can be explained by eq 8 and calculations of the type that Golden and Peiser [13] used to predict an abnormal rotational distribution of HBr produced by the reaction between atomic bromine and molecular hydrogen at 500°C. The HBr is predicted to have a temperature below that of the ambient temperature, whereas in methane-air flames the abnormal temperature is greater than the equilibrium value. This might be due to the formation of OH in an exothermic reaction. In the hotter methane-oxygen flame at atmospheric pressure the intensity of emission from OH in thermal equilibrium is probably sufficiently high to mask the weaker chemiluminescence.. This does not rule out the possibility of detecting such abnormal distribution at low pressures, where the number of OH radicals produced thermally is much smaller.

Although absorption measurements show thermal equilibrium so far as the rotational energy of the ground state of OH is concerned, the non-equilibrium number of unexcited radicals in the inner cone indicates that OH is not in chemical equilibrium within the burning zone. This increased amount of unexcited OH in the inner cone might be caused by the transition of radicals from the excessive number in the excited state. The radicals in the ground state may reach thermal equilibrium by collisions before being consumed in chemical reactions. The excessive absorption of the first rotational level in the inner cone again can be considered as evidence of a two stage combustion or it might come about from the lack of time to reach thermal equilibrium.

The available experimental evidence does not permit a firm choice among the various possible explanations that can be advanced for the observed abnormal conditions. However, one consistent and plausible explanation of the experimental facts is as follows. Electronically excited OH may be formed in two steps, occuring simultaneously within the flame. Both reactions may form OH with a Boltzmann distribution of rotational energy in the excited state. One reaction may form OH with a rotational distribution equivalent to 5200°K, while the other reaction may form OH with a rotational distribution in the neighborhood of 1550°K. The excited OH may radiate before reacting with other particles in the flame zone and before the excess rotational energy is distributed among the other modes of energy by collision. In the ground state, OH reacts with the other molecules and except for the lowest rotational states, assumes an equilibrium rotational energy distribution.

Until both the intermediate reaction steps and the energy distribution of products from these steps are known, it will be difficult to interpret fully the complicated conditions within a flame region. However, attmpts to interpret spectra of flames may prove to be an important step in the development of tenable theories of flame propagation. Experimental studies using fuels that are simpler than methane may yield data which are less involved, and thus lead to more rapid progress. Such studies with hydrogen are now in progress at the National Bureau of Standards.

4. REFERENCES

1. A. G. Gaydon and H. G. Wolfhard, Third Symposium on Combustion Flame and Explosion Phenomena, 504-508, Williams and Wilkins (1949).

2. G. H. Dieke and H. M. Crosswhite, The Ultra-Violet bands of OH, Bumblebee Series, Report No. 87 (Bu Ord., USN) (1948).

3. O. Oldenberg and F. F. Ricke, J. Chem. Phys. 6, 439, 779 (1938).

   O. Oldenberg and R. J. Dwyer, J. Chem. Phys. 12, 351 (1944).

4. F. R. Caldwell, H. P. Broida, J. J. Dover, and E. F. Fiock, Symposium on Combustion Chemistry, Cleveland (April 12, 1951).

5. W. Fastie, J. Opt. Soc, Am. 40, 800(A) (1950).

6. G. Herzberg, Molecular Spectra and Molecular Structure I, 204, 124, D. Van Nostrand (2nd edition, 1950).

7. K. E. Shuler, J. Chem. Phys. 11, 1466 (1950).

8. A. G. Gaydon, Spectroscopy and Combustion Theory, 138-141, Chapman and Hall (2nd edition, 1948).

9. O. Oldenberg, Phys. Rev. 46, 210 (1934).

10. J. Levedahl and F. H. Ward, J. Res. NBS 46, 301 (1951).

11. J. Powling, Fuel 28, 25 (1949).

12. H. C. Hottel, G. C. Williams, and C. N. Satterfield, Thermodynamic Charts for Combustion Processes, Wiley and Sons (1949).

13. S. Golden, The Quantum Mechanics of Chemical Kinetics of Homogeneous Gas Phase Reactions, I. General Considerations, J. Chem. Phys. 17, 630 (1949).

14. For example, see E. Griffith and J. H. Awberry, Proc. Roy. Soc. 123A, 401 (1929).

Table I

Temperatures in Methane-Air Flames

	Temperatures °K	
	Inner Cone	Outer Cone
OH Rotational Distribution		
Emission		
Low quantum numbers	1550	
High quantum numbers	5200	
Absorption	2000	2000
Reversal		
Na (5890,5896)	2040	2075
Hg (2537)	2600	
OH (3089)	2400	
Calculated (Methane-Air) [12]		2200 (max.)
Calculated (Methane-Oxygen) [12]		3050 (max.)

FIGURE LEGEND

1. Flame of stoichiometric mixture of methane and air burning above a 1/2 inch nozzle.

2. Absorption and emission spectra of OH from a stoichiometric methane-air flame. Upper curve is absorption. The resolved branches are marked.

3. A plot of log (I_K/A_{KL}) vs E_K for the R_2 branch of the (0 - 0) band of OH $(^2\Sigma, ^2\Pi)$ in the inner cone of a stoichiometric methane-air flame.

4. A plot of $E_{K'} - E_K$ vs $\ln(A_{K'}/A_K)$ for the R_2 branch of the (0 - 0) band of OH in the inner cone of a stoichiometric mixture.

5. Plots of log (I_L/A_{KL}) vs E_L for the R_2 branch in absorption of the (0-0) band of OH $(^2\Sigma \leftarrow ^2\Pi)$ in the inner and outer cones of a stoichiometric methane-air flame.

Figure 1

ABSORPTION AND EMISSION OF OH

METHANE-AIR FLAME STOICHIOMETRIC MIXTURE

1 A.U./MIN. SCANNING RATE

NATIONAL BUREAU OF STANDARDS 1-30-51

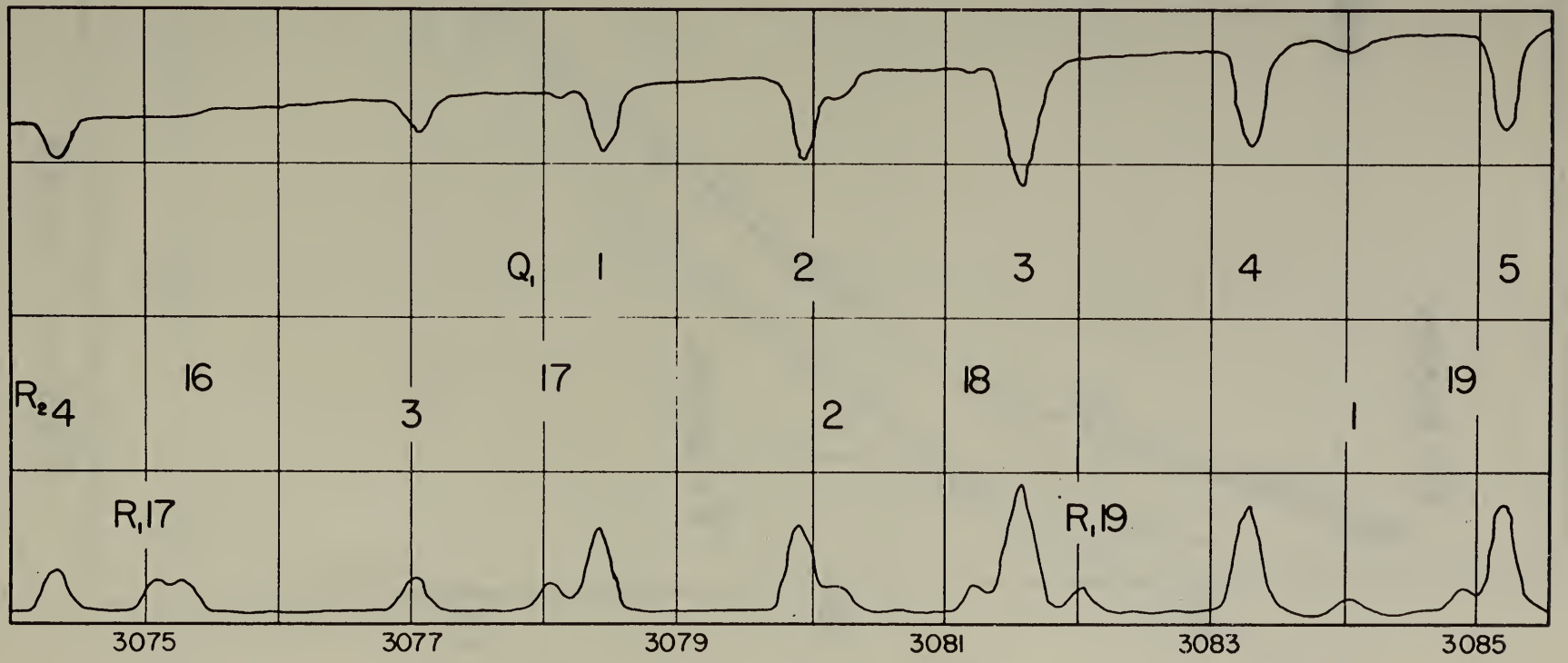

Figure 2

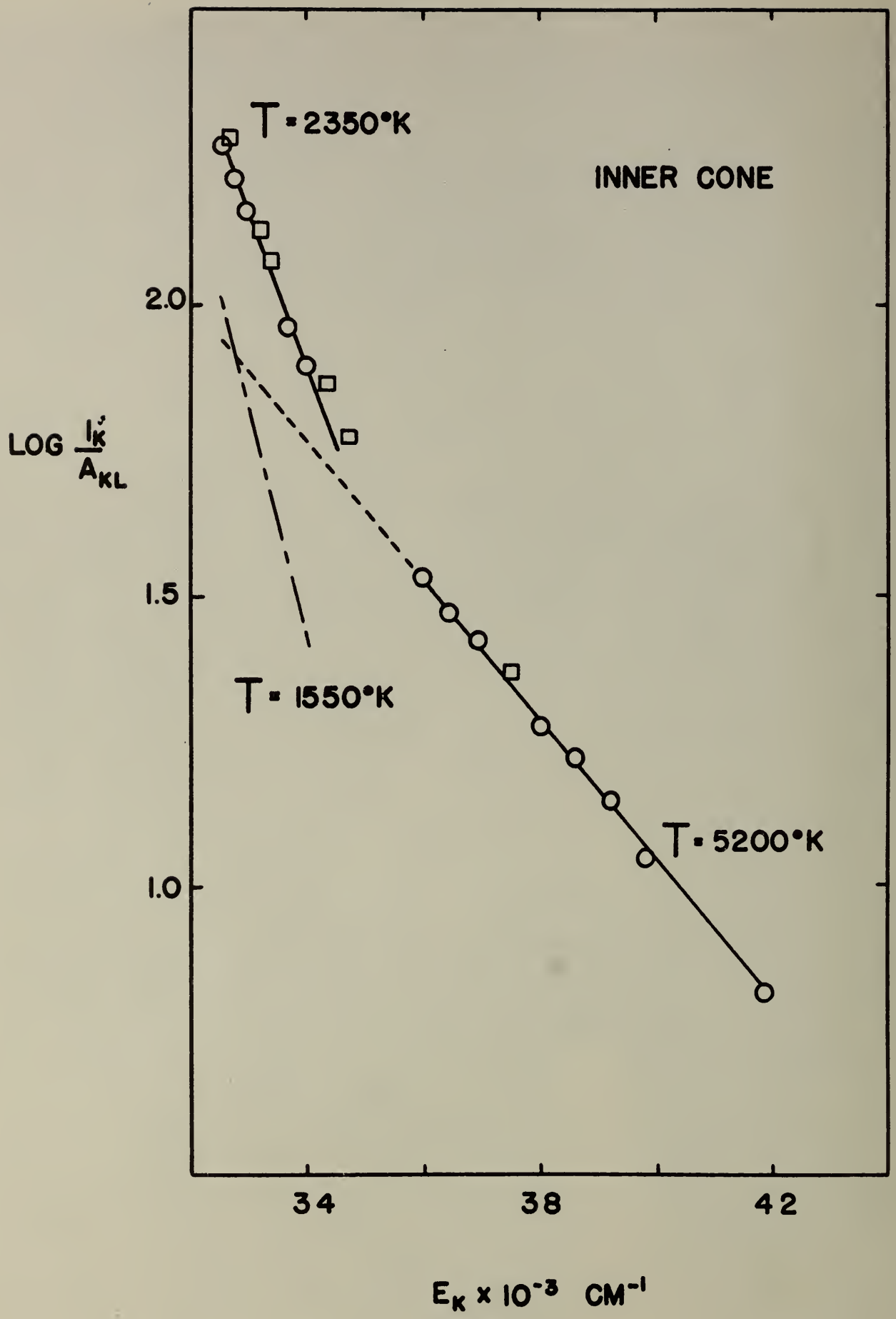
T = 2350°K
INNER CONE
2.0
LOG $\frac{I'_K}{A_{KL}}$
1.5
T = 1550°K
T = 5200°K
1.0
34
38
42
$E_K \times 10^{-3}$ CM^{-1}

Figure 3

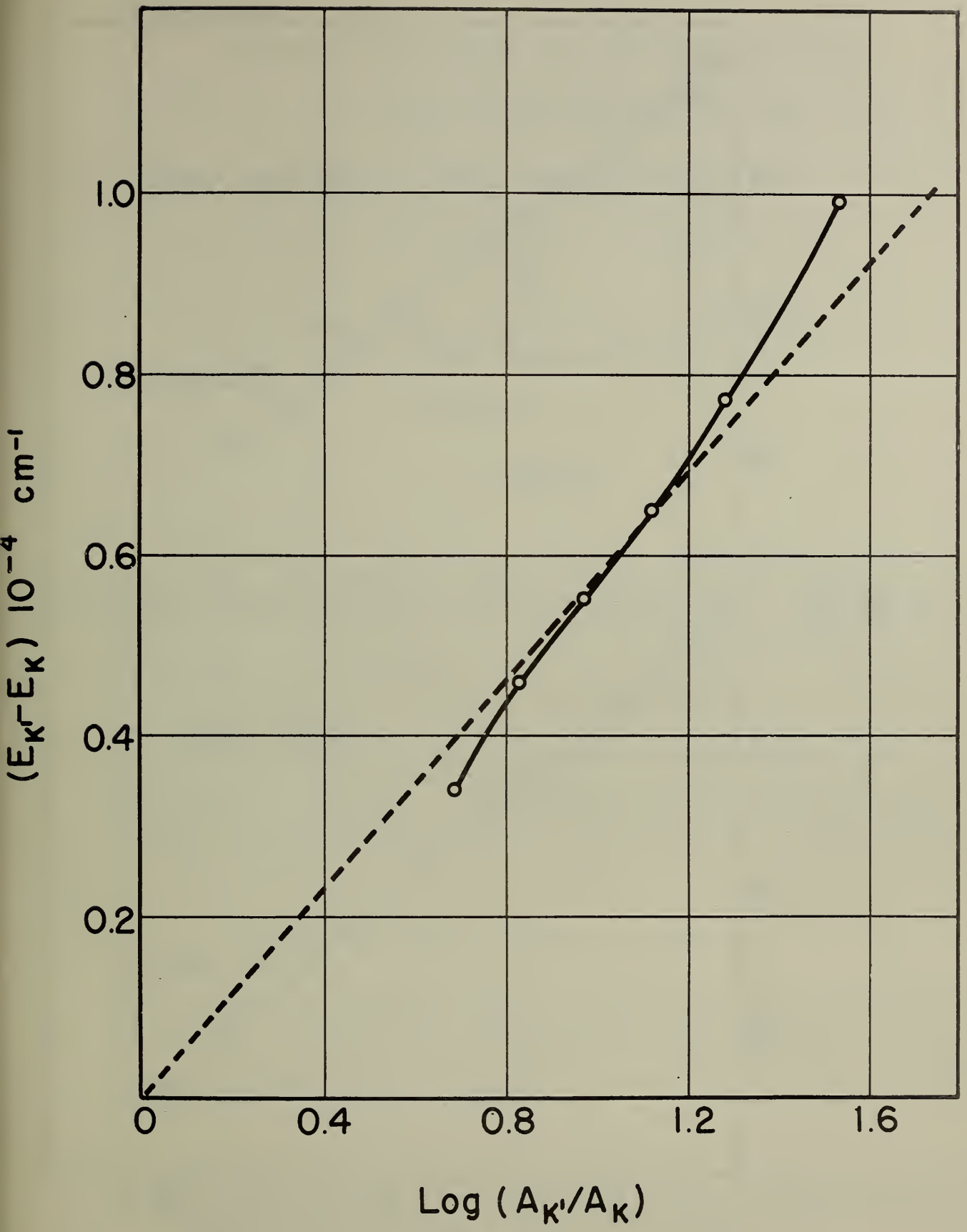

Figure 4

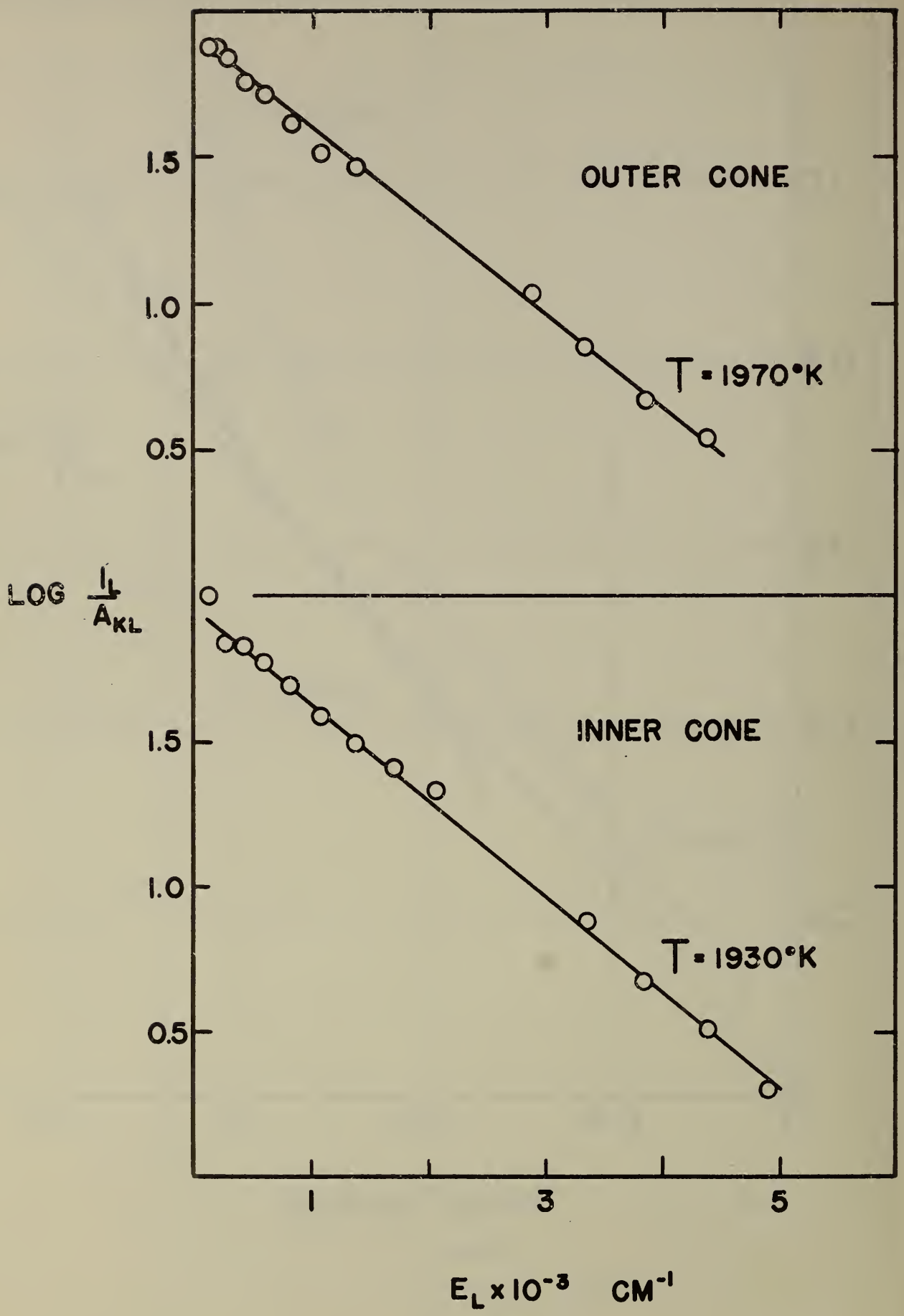
OUTER CONE
T = 1970°K
INNER CONE
T = 1930°K
LOG $\frac{I_L}{A_{KL}}$
1.5
1.0
0.5
1
3
5
$E_L \times 10^{-3}$ CM^{-1}

Figure 5

Appendix 2-B.

KINETICS OF OH RADICALS FROM FLAME EMISSION SPECTRA

IV. A STUDY OF THE HYDROGEN-OXYGEN FLAME

H. P. Broida and K. E. Shuler

National Bureau of Standards,* Washington, D. C.

and

Applied Physics Laboratory,** the Johns Hopkins University
Silver Spring, Maryland

(Received)

ABSTRACT

The inner and outer cones of hydrogen-oxygen flames burning with lean (1:1), stoichiometric (2:1) and rich (4:1, 6:1) mixtures at atmospheric pressure have been studied spectroscopically with the object of gaining some information as to the elementary processes occurring in this flame. The rotational vibrational and electronic distribution of OH ($^2\Sigma^+$) has been determined for both the inner and outer cone of each fuel mixture. A thermal equilibrium distribution of the internal degrees of freedom was found for OH ($^2\Sigma^+$) in the outer cones for all fuel ratios: in the inner cones there was a vibrational nonequilibrium distribution indicated by an excess population of the levels $v' = 2$ and 3. It is suggested that this nonequilibrium is due to a preassociation reaction involving H and O atoms in excess of their thermal concentrations which may be written schematically as

$$H(^2S) + O(^3P) \longrightarrow OH(^2\Sigma^-) \longrightarrow OH(^2\Sigma^+).$$

This assumes, in agreement with the suggestion of Gaydon and Wolfhard, that the $^2\Sigma^+$ state of OH is weakly predissociated between the levels $v' = 2$ and 3 by a $^2\Sigma^-$ state. The possible significance of this excess atomic concentration for the active particle diffusion theory of flame propagation is indicated briefly.

* This work was done under sponsorship of the Navy Bureau of Aeronautics.
** The work described in this paper was supported by the Bureau of Ordnance, U. S. Navy under Contract NOrd-7386.

A. INTRODUCTION

In the preceding papers of this series[1], (hereafter referred to as I, II and III), the determination of the rotational and vibrational distribution of OH ($^2\Sigma^+$) and of the relative concentration of OH ($^2\Sigma^+$) and $O_2(^3\Sigma_u^-)$ from spectroscopic studies on flames has been discussed in some detail. It is the purpose of this paper to apply the methods and calculations of I, II and III to a spectroscopic study of the hydrogen-oxygen flame to see whether it is possible to gain some information as to the elementary reactions in this flame from the energy distribution of the electronically excited OH ($^2\Sigma^+$). This study has been carried out under a wide variety of experimental conditions, i.e., for both the inner and outer cones of hydrogen-oxygen flames burning lean, stoichiometric, and rich at atmospheric pressure.

The hydrogen-oxygen flame was chosen for two reasons. In the first place, this system has only two atomic constituents, O and H, so that the elucidation of the elementary processes should prove to be simpler than for a hydrocarbon flame where one has an additional atomic component and thus is faced with a much greater variety of possible reactions. Secondly, previous spectroscopic work on the hydrogen-oxygen flame has indicated that there are abnormal, i.e., non-thermal, intensity distributions of OH ($^2\Sigma^+$)[2,3] so that a further and more detailed study of this system promised to give valuable information relevant to the elementary processes occurring in this flame.

B. EXPERIMENTAL

The hydrogen-oxygen fuel ratios used in this investigation were 1:1 (lean), 2:1 (stoichiometric) and 4:1 and 6:1 (rich): the measurements thus cover a rather wide range of burning conditions. The total flow rate was adjusted to 200 cm^3/sec at NTP for all fuel ratios in order to eliminate any possible effect of variable flow rates on the geometry and kinetic behavior of the flame. The apparatus is the same as that described in appendix 2-C.

C. ANALYSIS OF DATA

The wave length regions analyzed were:

1) 3060 - 3090 Å

2) 3275 - 3285 Å

3) 3420 - 3435 Å

1. Region (1) contains the (0,0) band of OH ($^2\Sigma \rightarrow {}^2\Pi$) from R_21 to R_220.[4] This band was used to determine the rotational temperature of OH by the modified iso-intensity method outlined in Section IV of II. The main advantage of this method is that it gets around the difficulties

caused by self-absorption by utilizing only lines of equal intensity. Doubt has recently been expressed regarding the applicability of the iso-intensity method when the emitting and absorbing layers of gas are at different temperatures.[5] While the question raised by Dieke and Crosswhite is of importance in case the iso-intensity method shows an apparent non-equilibrium distribution, it does not appear to seriously affect the validity of the method when a rotational equilibrium distribution is indicated as is the case in our investigation. If the modified iso-intensity method [1] shows a rotational equilibrium distribution, this could have been brought about in only two ways: either there is actually a rotational equilibrium distribution in the flame, or the variable self-absorption brought about by the temperature gradient in a flame where the radicals are in a rotational non-equilibrium distribution is of such a nature that it gives rise to an apparent equilibrium distribution. Since we have found a rotational equilibrium distribution for 18 different combinations of fuel ratios and flame positions, each determination being made on 7 pairs of rotational lines, it is evident that this latter possibility of concelling errors need not be seriously considered. One may say in general that if the modified iso-intensity method[1] shows a rotational equilibrium distribution, the possibility that this is due to cancelling errors is extremely slight and an actual rotational equilibrium distribution in the flame is most strongly indicated. An example of the type of plot obtained in the analysis for rotational equilibrium is shown in the next section.

2. Region (2) covers part of the overlap region of the (0,0), (1,1), (2,2) and (3,3) bands of the $^2\Sigma^+ \longrightarrow {}^2\Pi$ system of OH. The lines studied were P_1 26 (0,0), P_2 26 (0,0), Q_1 27 (1,1), P_1 21 (1,1), Q_2 19(2,2), P_1 14 (2,2), Q_2 5 (3,3), Q_1 8 (3,3), and Q_2 7 (3,3). These lines are weak enough not to be seriously affected by self-absorption, are free of blends and satellites and could easily be resolved by our spectrograph. By choosing such a small wave length interval ($\sim$10Å) one can carry out the analysis without the necessity of standardizing the phototube for change of response with wave length.

The determination of the vibrational energy distribution of OH in the levels $v' = 0$ to 3 was based essentially on the method outlined in Sections II and V of II. The intensity $I_{k,v}$ of a rotational line K with upper vibrational state $v' = v$ is given for the case of a rotational-vibrational equilibrium distribution by

$$I_{K,v} = C A_r A_v e^{-Er/kTr} e^{-Ev/kTv} h\nu_{K,v} \qquad (1)$$

where C is a numerical factor which contains the electronic transition probability, A_r and A_v are the rotational vibrational transition probabilities, E_r is the rotational energy which also contains the rotation-vibration interaction term, E_v is the vibrational energy, and T_r and T_v are the rotational and vibrational temperatures respectively. Equation

(1) can be transformed into

$$L \cong \log I_{K,v} - \log A_r = \log A_v + .4343\, E_r/kT_r \cong -4343\, E_v/kT_v + C' \quad (2)$$

where the $h\nu_{K,v}$ of Eq. (1) has been taken into C' since $\nu_{K,v} \approx$ constant over the small wavelength region investigated. In this equation, all the terms except T_v are known. $I_{K,v}$ is obtained from the monochromator tracing, E_r, E_v, A_r and A_v have been calculated and tabulated [1,4] and the rotational temperature T_r is obtained independently by the modified iso-intensity method. By plotting the left hand side of Eq. (2) against E_v one can then obtain some information in regard to the vibrational energy distribution. If this plot gives a straight line, then one is dealing with a vibrational equilibrium (Boltzmann) distribution and the vibrational temperature T_v can be obtained from the slope. When $T_v = T_r$ one has an equilibrium-equipartition distribution in the rotational vibrational energy levels; when $T_v = T_r$, and both T_v and T_r are well defined through the appropriate straight line relationships, one has vibrational and rotational equilibrium but a non-equipartition of energies. If the plot of L vs E_v does not lead to a straight line relationship, one is dealing with a vibrational non-equilibrium distribution and a vibrational "temperature" is of course not defined. Examples of these different types of distributions are shown in section D.

3. Region (3) covers part of the overlap region of the (0,1) band of OH ($^2\Sigma^+ \rightarrow {}^2\Pi$) and of the (0,14) band of O_2 ($^3\Sigma^-_u \rightarrow {}^3\Sigma^-_g$). This region was used to determine the relative concentration of OH ($^2\Sigma^+$) to O_2 ($^3\Sigma^-_u$) as described in detail in III. The principle of this method is to compare the experimental intensity ratio of OH [R1 10; (0,1)] ($^2\Sigma^+$) and O_2 [P (31) + R (35); (0,14)] ($^3\Sigma^-_u$) with the calculated equilibrium intensity ratio using T_r as the equilibrium temperature. Possible deviations from a thermal distribution will then be indicated by the non-equality of the experimental and calculated intensity ratios. It would of course be possible to calculate an electronic "temperature" form the experimental intensity ratios using Eq. (15) of III and then compare this T_{el} with the rotational and vibrational temperatures T_r and T_v. This procedure, however, is not as sensitive to the trend of the data as comparing the calculated and experimental intensity ratios. The temperature enters Eq. (15) both explicitly in the exponential factor and implicitly in the term N_{OH}/N_{O_2} and experience has shown that a rather large variation of the experimental I_{OH}/I_{O_2} will have only a small effect on the "temperatures" calculated from Eq. (15).

D. EXPERIMENTAL RESULTS

The overall results of this study are presented in Table 1. A rotational equilibrium distribution of OH ($^2\Sigma^+$) was found for all fuel ratios in both the inner and outer cone. Figure 1 which can serve as a representative example of the type of relationship obtained, shows the analysis for the inner cone of the stoichiometric ($H_2/O_2 = 2/1$)

hydrogen-oxygen flame. The plots for the other fuel mixtures in both the inner and outer cone are very similar and are therefore not reproduced here. In all cases, the good straight line relationship between log $A_{K'}/A_K$ and $E_{K'}-E_K$ and the 0,0 intercept are indicative of a rotational equilibrium distribution.[1]

The rotational temperatures T_r determined from the slopes of the lines are in fair agreement with the calculated adiabatic flame temperatures. In the inner cone, T_{rot} follows the trend of $T_{adiab.}$ but is generally somewhat lower possibly reflecting the heat loss by radiation which is of course not taken into account in adiabatic flame temperature calculations. The rotational temperature in the outer cone is less than that for the inner cone corresponding to the cooling undergone by the hot gases as they move away from the reaction zone. It may be noted incidentally that while there is a difference of about 300° K between T_{rot} for the inner and outer cones for both the lean (1/1) and stoichiometric (2/1) fuel mixture, there is only a much smaller amount of cooling ($\sim$70°K) for the hydrogen rich (4/1) mixture. While this may be due partly to the changed geometry of the flame (so that one is not really observing comparable regions of the outer cone), one contributing reason for this apparent anomaly may well be the burning of excess hydrogen with the oxygen from the surrounding air.

A vibrational equilibrium distribution of OH($^2\Sigma^+$) was found in the outer cone for all fuel mixtures. An example of the graph obtained from Eq. (2) is shown in Fig. 2 which refers to the outer cone of the lean (1/1) hydrogen-oxygen flame. The rather good straight line which can be drawn through the experimental points indicates the vibrational equilibrium. The graphs of L vs E_v for the outer cones of the other fuel ratios are very similar and are therefore not shown here. The vibrational temperatures T_v which may be obtained from the slopes of the lines are in good agreement with the corresponding rotational temperatures in the outer cones, the discrepancy of about 100°K being attributable largely to the various approximations introduced in the calculation of the vibrational matrix elements.[1]

The analysis for the vibrational distribution of OH ($^2\Sigma^+$) in the inner cones indicates a distinct non-equilibrium distribution for all the fuel ratios examined. This is pointed up in Figs. 3 to 5 which clearly show that no straight line, indicative of an equilibrium distribution, can be drawn through the experimental points. The curvature is particularly pronounced for the lean and rich mixtures, while the plot for the stoichiometric one approaches more closely to that of a straight line. An analysis of these curves carried out by determining the vibrational "temperatures" from straight line segments drawn between $v' = 0$ and 1, $v' = 1$ and 2 and $v' = 2$ and 3 shows that the vibrational levels $v' = 2$ and 3 are over populated as compared to a Boltzmann distribution with $T_{equil} = T_r$. This is particularly true of the level $v' = 3$. The values obtained for the vibrational "temperatures" in the above manner are listed

in Table 1; the figures there quoted indicate that the deviation from the vibrational equilibrium distribution is most pronounced for the non-stoichiometric fuel mixtures.

The experimental values for the relative intensities of excited OH to $O_2(^3\Sigma_u^-)$ are in good agreement with the calculated equilibrium intensity ratios for both the inner and outer cones as shown in Table 1. The agreement is comparable with that noted in III, and an equilibrium distribution of excited OH to O_2 in the hydrogen-oxygen flame is strongly indicated. Owing to the various approximations in the theoretical treatment and to the somewhat uncertain experimental data (f values, heat of formation of OH) entering into the calculation of the equilibrium intensity ratios not too much significance should be attached to the differences between $I_{OH^*}/I_{O_2^*}$ calculated and experimental in any one column. In particular, attempts to draw any conclusion as to the finer details of the $OH(^2\Sigma^+)/O_2(^3\Sigma_u^-)$ distribution in the various fuel mixtures in both inner and outer cones would not seem to be warranted by the accuracy of the data or by that of the calculations.

The reproducibility of the data is very good. Several runs were made on some of the fuel mixtures, for both inner and outer cone, by different personnel and at different times. All these runs gave concordant results as to the equilibrium or non-equilibrium distributions and temperatures ($\pm 3\%$). Furthermore, the data reported here for T_{rot} of the inner cones and the $OH(^2\Sigma^+)/O_2(^3\Sigma_u^-)$ distribution for the various fuel ratios are in good agreement with those obtained previously (III) on a Jarrell-Ash spectrograph with the conventional photographic technique.

E. INTERPRETATION OF DATA

The finding of rotational vibrational and electronic equilibrium in the outer cone of all these flames is not very surprising since one is dealing here mostly with the hot gases streaming away from the reaction zone. In flames burning at atmospheric pressure there will probably have been a sufficient number of equilibrizing collisions by the time the radiating species reaches the outer cone for a Boltzmann distribution among the various energy levels to be established even if these species should have been formed in a non-equilibrium distribution in the inner cone reaction zone. The equality of T_{vibr} and T_{rot} in the outer cones indicates that the vibrational transition probabilities calculated in I are essentially correct, a conclusion which is in accord with the results reported previously from a study of the outer cone of an oxy-methane flame (II). In the inner cone one finds a rotational temperature in good agreement with the adiabatic flame temperature and Na line reversal temperatures[6]; there is furthermore electronic equilibrium as revealed by the thermal distribution of $OH(^2\Sigma^+)$ to $O_2(^3\Sigma_u^-)$. Considering all these facts one would be inclined to conclude that the radiation due to $OH(^2\Sigma^+)$ in the hydrogen-oxygen flame is of a purely thermal nature were it not for the observed non-equilibrium distribution among the vibrational levels.

A vibrational non-equilibrium distribution of $OH(^2\Sigma^+)$ in hydrogen-oxygen flames has been reported previously, both for low pressure [2,3] and atmospheric pressure [7] burning. In particular, Gaydon and Wolfhard noted a selective excitation to the $v' = 2$ and 3 levels of $OH(^2\Sigma^+)$ in a hydrogen-air flame at atmospheric pressure; our results are in agreement with this. It was attempted at first [2,3] to explain these observed non-equilibrium distributions as being due to some specific chemical reactions which excited the OH radicals preferientially to the $v' = 2$ and 3 levels of $OH(^2\Sigma^+)$. The recent work of Gaydon and Wolfhard [7], however, has shown that a much more likely explanation for the anomalous vibrational distribution of $OH(^2\Sigma^+)$ is that the $^2\Sigma^+$ state of OH is weakly predissociated [8] by the $^2\Sigma^-$ state of OH between $v' = 2$ and 3 in the manner shown in Fig. 10. The evidence for such a predissociation has been set forth fully by Gaydon and Wolfhard, and since we are in substantial agreement with their views there is no need to repeat their discussion here.

The preferential excitation to the $v' = 2$ and 3 in the inner cones of the H_2-O_2 flames of various fuel ratios may now be attributed to an inverse predissociation (pre-association) involving ground state $O(^3P)$ and/or $H(^2S)$ atoms in excess of their thermal equilibrium concentration. This process may be formulated schematically as [7]

$$O(^3P) + H(^2S) \longrightarrow OH(^2\Sigma^-) \longrightarrow OH(^2\Sigma^+) \quad . \qquad (3)$$

Reaction (3) points up again the importance of intersecting potential curves in the formation of electronically excited species.[9] Since the Franck-Condon principle must be obeyed in predissociations, the $OH(^2\Sigma^+)$ formed in reaction (3) will be predominantly in the vibrational levels near which the intersection of the potential curves occurs. Since the excess population is in the levels $v' = 2$ and 3 it must be assumed, as also suggested by Gaydon and Wolfhard, that the intersection of the $^2\Sigma^-$ and $^2\Sigma^+$ curves occurs in that region as shown in Fig. 6.[10]

If this interaction between the $^2\Sigma^+$ and $^2\Sigma^-$ states of OH really takes place it should affect the calculated vibrational transition probabilities of the levels $v' = 2$ and 3 and might throw some doubt on the results of the vibrational distributions reported here. The perturbation of the two states is, however, so weak that it should not affect the calculated values of the vibrational matrix elements to any large extent.[11] This may be seen from the fact that in the outer cone, where equilibrium might be presumed to exist, a vibrational and rotational equilibrium distribution with $T_{vibr} = T_{rot}$ is always found for the hydrogen-oxygen flame.

Regardless of the detailed path of the inverse predissociation reaction leading eventually to $OH(^2\Sigma^+)$ one of the prerequisites for the observed non-equilibrium distribution in the vibrational levels is that the atoms entering into the reaction are present in excess of their thermal equilibrium concentration.[12] Such an abnormally high concentration of atoms

(and radicals) in the reaction zone of flames may readily be expected.[13] In flames, the absence of any walls on which atoms can be removed facilitates the build-up of these atoms, formed in chain propagating and chain branching steps, to a much higher steady state concentration than corresponds to equilibrium. The main removal processes must be gas phase reactions and diffusion out of the reaction zone.

The gas phase recombination and removal processes of atoms involve most probably three body collisions and the effectiveness of these processes will thus depend upon the ability of the third body to carry away some of the energy of reaction. The most efficient third body in the hydrogen-oxygen flame is undoubtedly H_2O whose efficiency in the removal of excess energy is well known from sound dispersion studies.[14] This property of H_2O would then explain the less pronounced vibrational non-equilibrium distribution in the stoichiometric fuel mixture; there is a larger concentration of H_2O in the stoichiometric flame which will serve to reduce the excess concentration of atoms via 3 body collisions. As the combustion intermediates, such as H and O atoms, move out of the reaction zone toward the outer cone they will continuously undergo e collisions leading to recombination and to formation of OH and H_2O so that by the time the surviving atoms have reached the outer cone they will be in a thermal equilibrium concentration and give rise to a Boltzmann distribution of $OH(^2\Sigma^+)$ in its vibrational energy levels.[15]

The thesis of this paper that there is a concentration of atoms in excess of their equilibrium thermal value in the reaction zone of the hydrogen-oxygen flame would seem to have an interesting bearing on the active particle diffusion theory of flame propagation advanced by Lewis and von Elbe [16] and by Tanford and Pease.[17] This excess atomic concentration in the reaction zone increases the concentration gradient along which the atoms will diffuse into the unburned gas and may thus facilitate the propagation of the flame. It may be of interest to follow up this point in more detail.

REFERENCES

1. (I) K. E. Shuler, J. Chem. Phys. 18, 1221, (1950).
(II) ibid., 18, 1466, (1950).
(III) ibid, 19, 888, (1951).

2. V. Kondratjew and M. Ziskin, Acta Physichochim. U.R.S.S. 7, 65 (1937)

3. A. G. Gaydon and H. G. Wolfhard, Re. Inst. Frac., Petrole et Ann. Combustibles liquides IV, No. 8, 405 (1949).

4. The spectroscopic notation of this paper corresponds to that of the report of G. H. Dieke and H. M. Crosswhite, The Ultraviolet Bands of OH, Bumblebee Series Report No. 87, 1948, The Johns Hopkins University. This report also contains the wavelengths of the various transitions and the rotational transition probabilities used in the present study.

5. G. H. Dieke and H. M. Crosswhite, Quarter Report NOrd-8036, JHB-3, Problem A, January 1 - March 31, 1951.

6. H. H. Lurie and G. W. Sherman, Ind. Eng. Chem. 25, 404 (1933)

7. A. G. Gaydon and H G. Wolfhard, Proc. Roy. Soc. (to be published). One of us (K.E.S.) is greatly indebted to Prof. Gaydon for furnishing him with a manuscript of this paper prior to publication.

8. This predissociation is weakly allowed by the breakdown of the $K = 0$ selection rule owing to the coupling of $\underset{\sim}{S}$ with the internuclear axis. For details see ref. 7.

9. K. J. Laidler and K. E. Shuler, Chem. Rev. 48, 153 (1951).

10. As indicated above, reaction (3) is only schematic. The detailed process probably involves the reactions $H + O_2$ and $O + H_2$, the predissociation then being due to intersecting HO_2 (or H_2O) surfaces. This will be discussed in more detail in a subsequent communication.

11. The matrix elements for the levels $v' = 2$ and 3 should have been calculated from

$$\int [a\,\psi'(^2\Sigma^+) + b\,\psi'(^2\Sigma^-)]\; q\; \psi[(2\pi)]\; d\tau$$

where q is the appropriate component of the dipole moment. The coefficient b, however, must be very small since the interaction of the $^2\Sigma^+$ and $^2\Sigma^-$ states is due to only a very small spin - internuclear axis coupling term in the Hamiltonian of the perturbation matrix.

12. In the case of complete thermal equilibrium, a preassociation can not lead to a non-equilibrium distribution since it will, by the principle of detailed balancing, be exactly balanced by the predissociation reaction.

13. K. J. Laidler and K. E. Shuler, paper delivered at the A. C. S. Symposium on Combustion Chemistry, Cleveland, April 9-12, 1951, Ind. Eng. Chem. (to be published).

14. A. Eucken and R. Becker, Z. phys. Chem. 20B, 467 (1933); 27B, 219 (1934)
I. M. Metter, Phys. Z. Sowjet. 12, 232 (1937)

15. The rotational and electronic energy distributions determined as outlined in section C of this paper are not affected by the predissociation and preassociation discussed above since the relevant data for their analysis were obtained from the $v' = 0$ level of $OH(^2\Sigma^+)$ which for the low K values ($K \leq 20$) used in this work, is too far removed from the region of intersection of the potential curves to be affected by it. (c. f. reference 8).

16. B. Lewis and G. von Elbe, J. Chem. Phys. 2, 537 (1934)

17. C. Tanford and R. N. Pease, J. Chem. Phys. 15, 431, 861 (1947)

TABLE I

Temperatures and Energy Distributions of OH ($^2\Sigma^+$) in the Hydrogen-Oxygen Flame

	H_2/O_2 = 1/1 (Lean) $T_{adiab.}$ = 2920°K (a)		H_2/O_2 = 2/1 (Stoichio.) $T_{adiab.}$ = 3100°K		H_2/O_2 = 4.1 (Rich) $T_{adiab.}$ = 2850°K		H_2/O_2 = 6/1 (Rich) $T_{adiab.}$ = 2450°K
	Inner Cone	Outer Cone	Inner Cone	Outer Cone	Inner Cone	Outer Cone	Inner Cone
T_{rot} (°K)	2830°K	2530°K	2875°K	2650°K	2800°K	2730°K	2670°K
T_{vibr}(°K)	Non-equilibrium	2440	Non-equilibrium	2550	Non-equilibrium	2640	Non-equilibrium
$v' = 0-1$	2600		2400		2600		2600
$v' = 1-2$	3300		2800		3200		3000
$v' = 2-3$	5000		3400		4000		5000
$I_{OH^*}/I_{O_{2^*}}$ (calc.)	0.5	0.5	2.6	2.5	53	80	120
$I_{OH^*}/I_{O_{2^*}}$ (exp.)	0.9	1.4	2.5	3.9	~30	(b) $>10^2$	(b) $>10^2$

(a) The adiabatic flame temperatures have been calculated from the tables of H. C. Hottel, G. C. Williams and C. N. Satterfield, "Thermodynamic Charts for Combustion Processes". (John Wiley and Sons, Inc., New York, 1949.)

(b) No O_2 ($^3\Sigma\bar{u} \rightarrow {}^3\Sigma\bar{g}$) Schumann-Runge bands could be detected under these burning conditions. This makes $I_{O_{2^*}}$ less than ~0.1 on our recorder scale.

LEGENDS FOR FIGURES

Fig. 1 A plot of $E_{K'}-E_K$ vs log $(A_{K'}/A_K)$ for the R_2 branch of the (0,0) band of $OH(^2\Sigma^+ \rightarrow {}^2\Pi)$ in the inner cone of a stoichiometric H_2-O_2 flame. The rotational temperature, T_r, is determined from the slope of the graph.

Fig. 2 A plot of L vs E_v for the outer cone of a lean (1/1) H_2-O_2 flame for several lines in the vibrational levels $v' = 0, 1, 2$ and 3 of the $OH(^2\Sigma^+ \rightarrow {}^2\Pi)$ transition. The vibrational temperature, T_v, is determined from the slope of the graph.

Fig. 3 A plot of L vs E_v for the $OH(^2\Sigma^+ \rightarrow {}^2\Pi)$ transition in the inner cone of a lean (1/1) H_2-O_2 flame. The curvature of the line connecting the experimental points indicates the vibrational non-equilibrium distribution of OH ($^2\Sigma^+$).

Fig. 4 A plot of L vs E_v for the $OH(^2\Sigma^+ \rightarrow {}^2\Pi)$ transition in the inner cone of a stoichiometric (2/1) H_2-O_2 flame. The curvature of the line connecting the experimental points indicates the vibrational non-equilibrium distribution of $OH(^2\Sigma^+)$.

Fig. 5 A plot of L vs E_v for the $OH(^2\Sigma^+ \rightarrow {}^2\Pi)$ transition in the inner cone of a rich (4/1) H_2O_2 flame. The curvature of the line connecting the experimental points indicates the vibrational non-equilibrium distribution of OH ($^2\Sigma^+$).

Fig. 6 The predissociation of $OH(^2\Sigma^+)$ and $OH(^2\Sigma^-)$. The potential curves of $OH(^2\Sigma^+)$ and $OH(^2\Pi)$ were drawn using the data of reference 6. The dotted potential curve for $OH(^2\Sigma^-)$ is schematic (after Gaydon and Wolfhard, ref. 10).

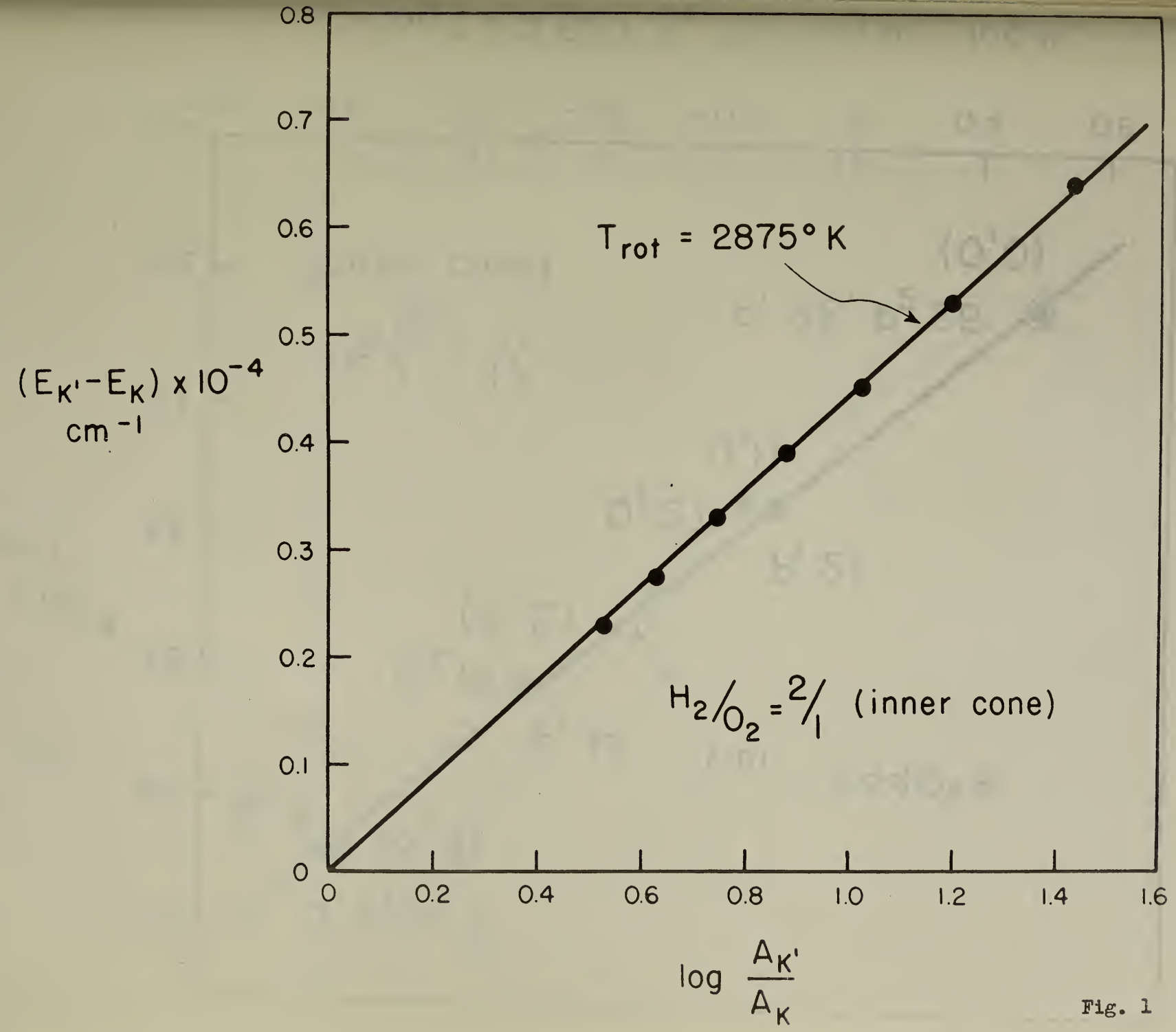
0.8
0.7
0.6
0.5
0.4
0.3
0.2
0.1
0
$(E_{K'}-E_K) \times 10^{-4}$
cm^{-1}
T_{rot} = 2875° K
$H_2/O_2 = 2/1$ (inner cone)
0
0.2
0.4
0.6
0.8
1.0
1.2
1.4
1.6
$\log \frac{A_{K'}}{A_K}$

Fig. 1

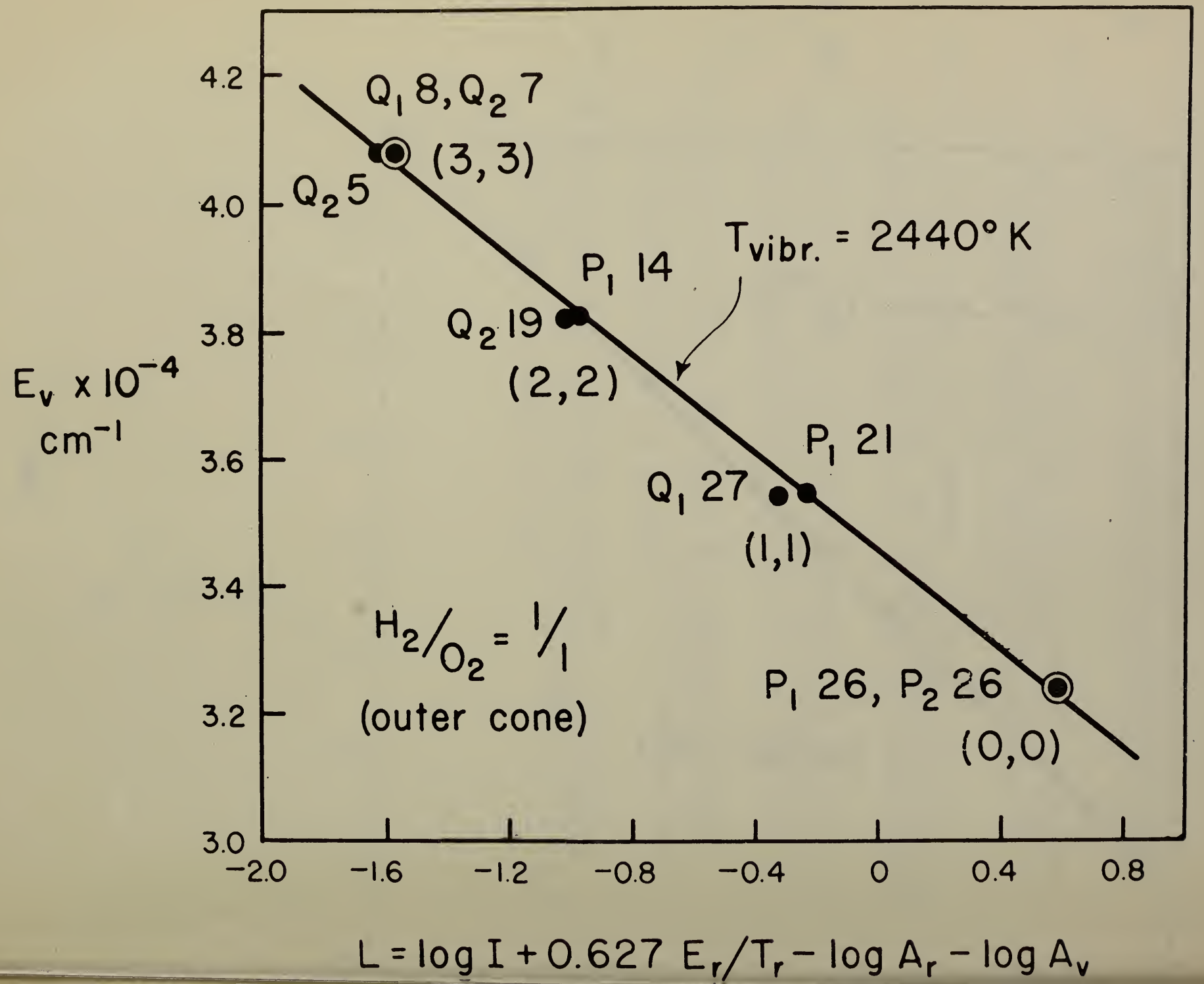
4.2
4.0
3.8
3.6
3.4
3.2
3.0
$E_v \times 10^{-4}$ cm^{-1}
Q_1 8, Q_2 7
(3,3)
Q_2 5
$T_{vibr.}$ = 2440° K
P_1 14
Q_2 19
(2,2)
P_1 21
Q_1 27
(1,1)
H_2/O_2 = 1/1
(outer cone)
P_1 26, P_2 26
(0,0)
−2.0
−1.6
−1.2
−0.8
−0.4
0
0.4
0.8
$L = \log I + 0.627\ E_r/T_r - \log A_r - \log A_v$

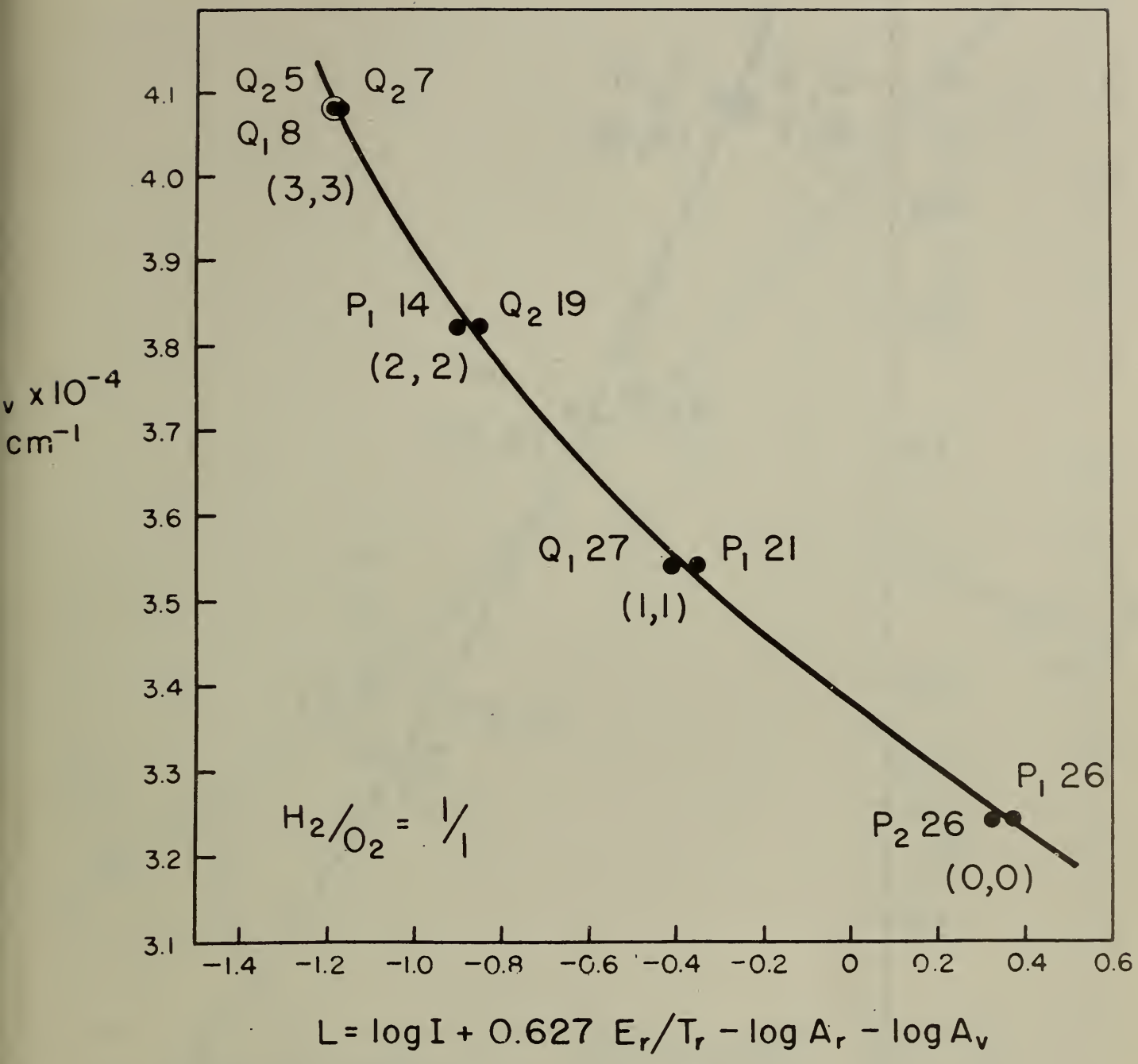
Q2 5
Q2 7
Q1 8
(3,3)
P1 14
Q2 19
(2,2)
Q1 27
P1 21
(1,1)
P1 26
P2 26
(0,0)
H2/O2 = 1/1
4.1
4.0
3.9
3.8
3.7
3.6
3.5
3.4
3.3
3.2
3.1
ν x 10-4
cm-1
-1.4
-1.2
-1.0
-0.8
-0.6
-0.4
-0.2
0
0.2
0.4
0.6
L = log I + 0.627 Er/Tr − log Ar − log Av

Fig. 3

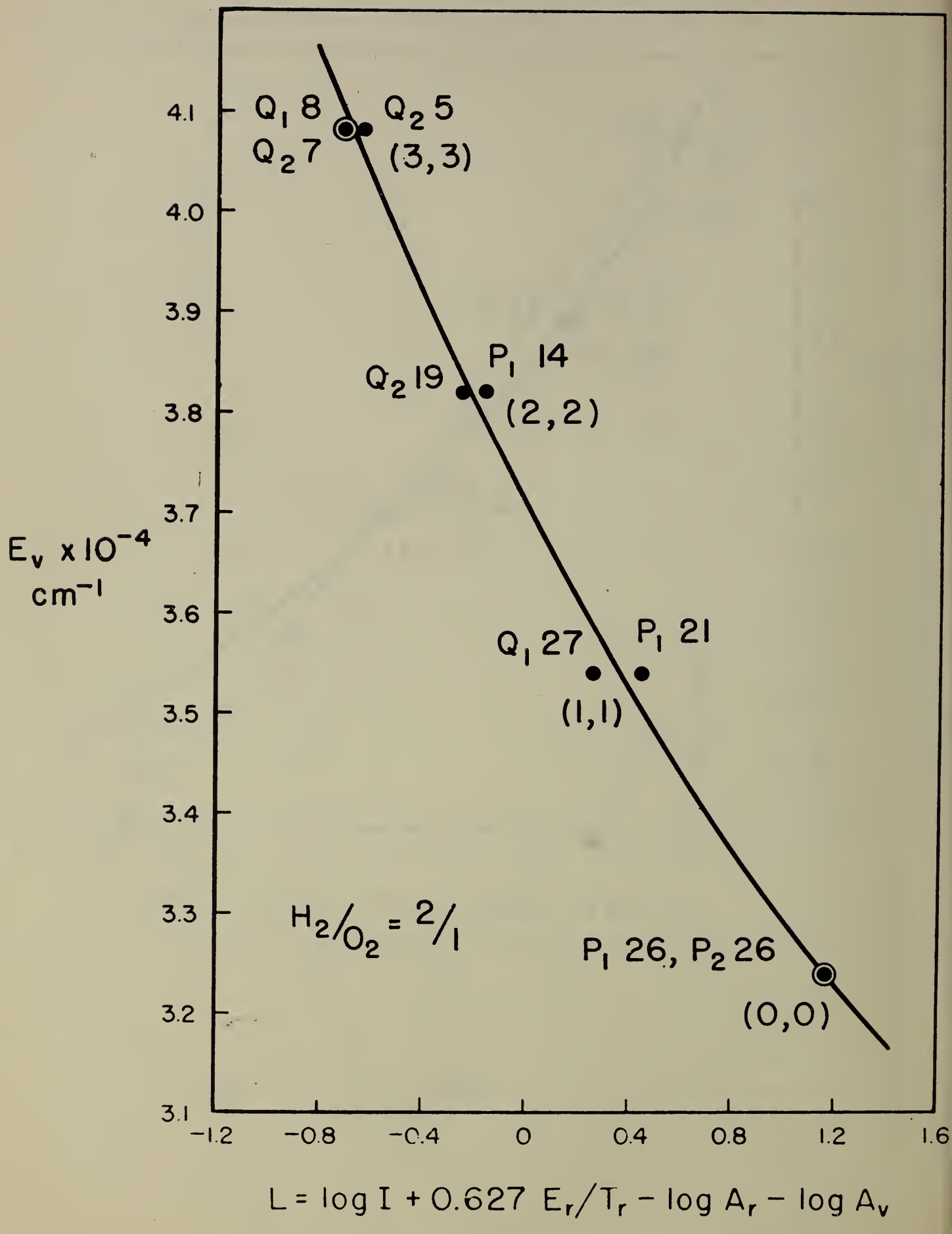
Q_1 8
Q_2 5
Q_2 7
(3,3)
Q_2 19
P_1 14
(2,2)
Q_1 27
P_1 21
(1,1)
$H_2/O_2 = 2/1$
P_1 26, P_2 26
(0,0)
$E_v \times 10^{-4}$ cm^{-1}
4.1
4.0
3.9
3.8
3.7
3.6
3.5
3.4
3.3
3.2
3.1
−1.2
−0.8
−0.4
0
0.4
0.8
1.2
1.6
$L = \log I + 0.627\ E_r/T_r - \log A_r - \log A_v$

Fig. 4

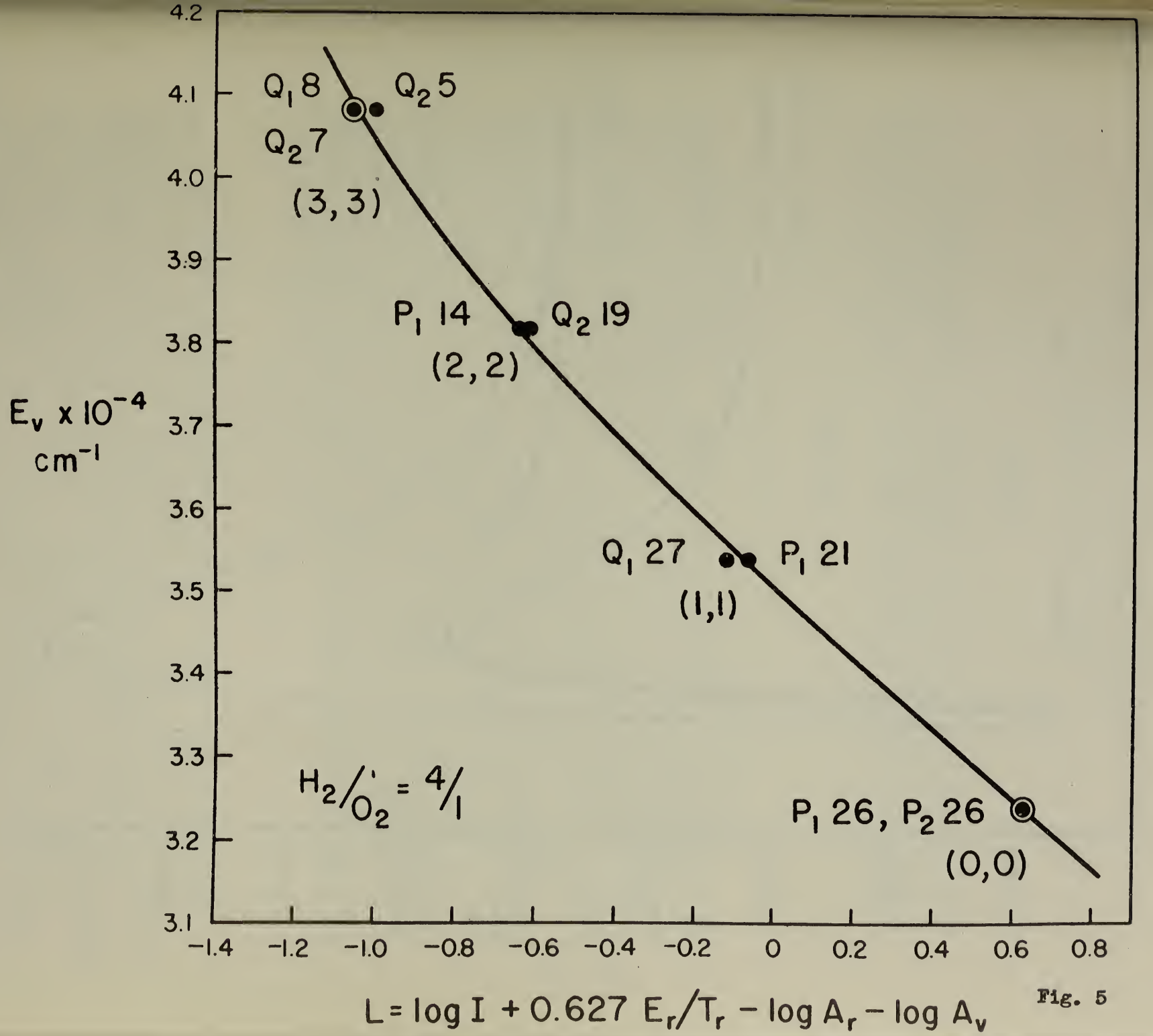
4.2
4.1
4.0
3.9
3.8
3.7
3.6
3.5
3.4
3.3
3.2
3.1
$E_v \times 10^{-4}$
cm^{-1}
Q_1 8
Q_2 5
Q_2 7
(3,3)
P_1 14
Q_2 19
(2,2)
Q_1 27
P_1 21
(1,1)
$H_2/O_2 = 4/1$
P_1 26, P_2 26
(0,0)
−1.4
−1.2
−1.0
−0.8
−0.6
−0.4
−0.2
0
0.2
0.4
0.6
0.8
$L = \log I + 0.627\, E_r/T_r - \log A_r - \log A_v$

Fig. 5

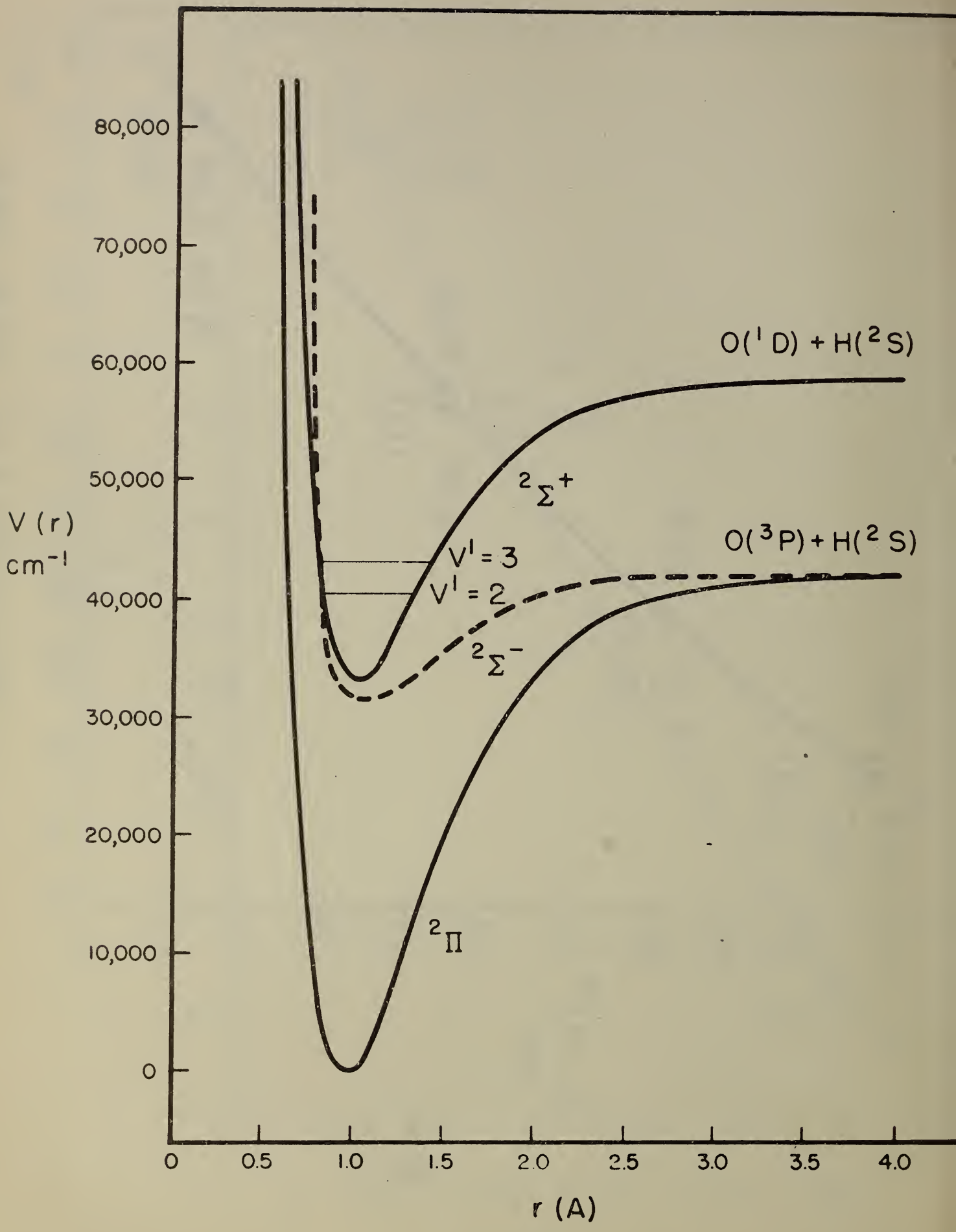
80,000
70,000
60,000
50,000
40,000
30,000
20,000
10,000
0
V (r)
cm⁻¹
O(¹D) + H(²S)
O(³P) + H(²S)
²Σ⁺
²Σ⁻
²Π
V' = 3
V' = 2
0
0.5
1.0
1.5
2.0
2.5
3.0
3.5
4.0
r (A)

Fig. 6

Appendix 2-C.

Rotational Temperatures of OH in Flames

H. P. Broida and G. T. Lalos
National Bureau of Standards

1. SUMMARY

Emission spectra of the $^2\Sigma - ^2\Pi$ electronic transition of OH have been recorded from flames of hydrogen, of acetylene, of propane and of methane with oxygen at various fuel to oxygen ratios and at various positions in the flame. Rotational temperatures of the excited radical in the ground vibrational state have been measured from the records.

2. APPARATUS

2.1 Experimental Set-up

The arrangement for these experiments is illustrated in the photograph of figure 1. Radiation from the flame, F, is focused on the slit, S, of the direct-reading monochromator, M, by a quartz lens, L, of 3 inch focal length and 2.25 inch diameter. Vertical and horizontal positioning of the flame is possible with the rack and pinion devices, D. Initial focusing is made visually, and the final adjustments are made with the aid of the photoelectric responser; the maximum intensity being used as a criterion for correct positioning. After traversing the dispersing system, the light falls upon the cathode of a 1P28 photomultiplier tube, T. A continuous variation of the dynode voltages from 45 to 129 volts can be made with the power supply, P. The current from the anode of the phototube is fed into the d.c. amplifier, A, with a range from 1×10^{-11} to 4×10^{-6} amperes and a response time of 3 seconds to within 1 percent of the final reading. The zero reading of the amplifier is stable to better than 1 percent of full scale reading. Electrical output from the amplifier goes into the pen recorder, R, with a response time of approximately 2 seconds for full scale travel. Linear intensity is recorded along the horizontal axis of the chart and wave-length along the vertical axis.

2.2 Burner and Gas Flow

An ordinary acetylene burner of 1.5 mm diameter was adapted for the burner, F, by straightening the tube to make it more convenient for positioning. With the rack and pinion, D, it is possible to set the location of the burner to within 0.2 mm both vertically and horizontally. Tank gases were used and controlled at 5 lb/in^2 gauge pressure by regulators on the tanks. Gas purities were specified by the manufacturer as follows: oxygen, 99.7 percent; hydrogen, 99.8 percent; acetylene, 98 percent; methane, 99.6 percent; and propane, 98 percent. Needle valves controlled the flow. Calibrated flowmeters, C, of the floating ball type were used for flow measurement to an accuracy of the order of 5 to 10 percent.

2.3 Monochromator

The spectral dispersing system, M, is an experimental, high resolution grating monochromator (1) which was constructed by the Research Division of Leeds and Northrup Company and loaned to the Heat and Power Division at the National Bureau of Standards on a field trial arrangement. This equipment is a special adaptation for laboratory use of a more general instrument designed for industrial metallographic analysis. It includes the optical and mechanical parts, the housing of the monochromator, and the appropriate electronics for the photoelectric detection and recording of light intensities.

A schematic diagram of the light path is shown in figure 2. Light from a selected portion of the flame, F, is focused by the quartz lens, L, on the entrance slit, S_1, of the monochromator. The light passes through the slit to part of the 8 inch diameter concave spherical mirror, K, at the focal distance (30 inches) from the slit and is reflected in a parallel beam to the grating, G. G is a flat reflection grating, 3 x 3 inches, ruled with 30,480 lines per inch on aluminum coated glass. It is blazed for strong second order diffraction in the region of 3000 A.U. The intensity of the first Rowland ghost is less than 1/200 of the parent line in the second order. The diffracted beam is refocussed by another portion of the mirror, K, to the exit slit, S_2, and then to the photomultiplier tube, T. The aperture of the system is F:10. The slit widths are continuously variable from about 0.001 to 0.150 mm. However, below 0.01 mm, the width is not reproducible and the sides of the slit do not remain parallel. Use of diaphragms make it possible to use range of slit heights from 0.3 mm to the maximum of 6 mm. Thus, it is possible to observe a section of the flame only 0.01 mm wide by 0.3 mm high.

A motor drive rotates the grating for scanning the spectrum at 1.18 and 5.9 A. U. per minute in the second order. There is also a rapid drive for changing wavelength regions and a provision for manual operation of the scanning. The grating is so mounted that it is possible to scan continuously from 1800 to 3550 A.U. in the second order and 3575 to 7100 A.U. in the first order. The entire monochromator, exclusive of the electronics, is contained in a rugged tubular housing of cast iron and a dust cover having dimensions of only 34 by 14 by 12 inches. This conveniently small size and the ruggedness have aided the usefulness of the equipment.

2.4 Reproducibility and Resolution

Figure 3A shows the stability of the flame over a one minute interval. This tracing was obtained by setting the grating of the monochromator such that the peak of a line emitted by the flame was focused on the slit. The small fluctuations of intensity are probably caused by the random emission from the photoelectric surface. Figure 3B records the intensity of the same line taken repeatedly first in the direction of increasing wavelength and then in the opposite direction. The reproducibility in

(1) W. G. Fastie, J. Opt. Soc. Am. 40, 800(A) (1950).

intensities shown in figure 3B is characteristic of the reproducibility obtained over much longer times.

Although this equipment is still in the process of development, it has been possible to separate lines in the second order of 0.054 A.U. in the OH spectrum at 3100 A.U. This indicates a resolving power, $\lambda/\Delta\lambda$ of the order of 55,000, which is about 30 percent of the theoretical value.

As an example of the usefulness of the monochromator for studies of flames Figure 4 shows a 9 A.U. region of the (0,0) band of OH which includes low and high K transitions of the R_2 branch. The resolution is distinct and the noise level is low, so that a quantitative comparison of relative intensities is not difficult. It is a tremendous advantage in making intensity measurements to use photoelectric detection rather than photographic techniques. There are none of the difficulties of processing and calibrating plates or of making densitometer tracings. In addition, continuous background is not a source of error with the direct reading monochromator since intensities are measured directly as heights above the background. Of course for very weak sources or for instantaneous surveys over a wide wavelength range, photographic exposures must be made.

2.5 Spectral Response of the Monochromator

The relative spectral response curve of the monochromator with a 1P28 photomultiplier is given by figure 5. This calibration was obtained by measuring the intensity of a tungsten filament lamp at a brightness temperature of 2455°K at 6650 A.U. and by using the known intensity distribution as given by the Wien black body radiation formula. Corrections have been made for variations with wavelength of the emissivity of tungsten and of the transmission of the optical parts inserted into the light path. The break in the curve is caused by the overlapping of the first and second orders. For most of the results reported here, the change in response of the monochromator is less than one-half percent and has negligible effect on the directly measured intensities. Since the R_2 branch doubles back on itself, most intensity comparisons of the (0,0) transition (near 3100 A.U.) were made with lines that are separated by less than 10 A.U.

3. EFFECTS OF EXPERIMENTAL OPERATING CONDITIONS ON MEASURED TEMPERATURES

Several operating parameters which might affect measured intensity distributions were varied separately to make certain that the measured values were independent of the apparatus. Table 1 lists the parameters and the range over which they were varied. Although the intensities measured by the photomultiplier varied by more than a factor of 250, no determinable effect was found on measured temperature to within less than 5 percent.

Table 1

Parameter	Range
Gas Flow	14 to 200 cm^3/sec. (NTP)
Burner Diameter	1/2 to 1 1/2 mm.
Scanning Rate	1 and 5 A.U./min.
Slit Width	0.008 to 0.020 mm.
Slit Height	0.3 to 6.0 mm.

Most measurements were taken at a flow rate of 200 cm^3/sec with the flame burning above the 1.5 mm diameter nozzle by scanning at 5 A.U. per minute with the slit 0.10 mm wide. Slit heights of 1 and 6 mm were used. Intensities were taken as the average of determinations from two spectra, one taken while scanning toward decreasing wavelengths and the other while scanning toward increasing wavelengths.

The rotational temperatures of OH were determined from the intensity distribution of the R_2 branch of the (0,0) vibrational transition. Figure 6 shows an 8 A.U. reproduction of a portion of this band from the inner cone of a hydrogen-oxygen flame.

4. METHODS OF OBTAINING TEMPERATURES FROM THE MEASURED INTENSITIES

For rotational equilibrium, the intensity of a transition from a rotational level, K, with an energy, E_k, is given by

$$I_k = CA_k e^{-(E_k/kT)} \qquad (1)$$

where A_k includes the transition probability of the particular transition, the frequency factor, and the statistical weight; k is the Boltzman constant; T is the rotational temperature; and C is a constant for a particular electronic and vibrational transition. Usually temperatures are measured from the slopes of plots of log (I_k/A_k) vs E_k. However, for intense sources this is not satisfactory because the self-absorption can cause serious error. To show this, data for the R_2 branch obtained from the base of the inner cone of a stoichiometric mixture of acetylene and oxygen are used for this logarithmic plot in figure 7. The points do not form a single straight line but can be represented by two lines of different slope. "Temperatures" obtained from these slopes differ by 2790°K. However, in this case, the break in the curve is due entirely to self-absorption of the stronger lines and the measured "temperature" is not an indication of the temperature in the flame. If a longer flame path is observed, there is more absorption and the difference in the slopes is increased.

The iso-intensity method, developed by Dieke and Crosswhite (2) is not affected by absorption within the flame providing that the temperature is uniform. Therefore this method makes it possible to obtain temperatures under conditions which make the log plot of figure 7 inapplicable. It follows from Equation (1) that for lines, X and X', of equal intensity,

$$A_{X'}/A_X = e^{(E_{X'} - E_X)/kT} \qquad (2)$$

and

$$T = \frac{E_{X'} - E_X}{k \log (A_{X'}/A_X)} \qquad (3)$$

Using values of energy levels, transition frequencies, and transition probabilities of the various lines of the R2 branch calculated and tabulated in reference 1, an expanded graph of temperatures of interest in oxygen flames is given by figure 8. In practice all that is necessary is to match the intensity of a low X line (1, 2, 3, 4 or 5) with the intensity of X' line and to read the temperature from the graph. An indication of equilibrium or non-equilibrium is obtained by comparing temperatures obtained with two or more such pairs.

For more precise results, a longer procedure was used. First the intensities of well-resolved lines were plotted against the K value and a smooth curve drawn through the experimental points. Figure 9 is this type of plot using the same data as used for figure 7. Iso-lines for the first 5 K values were found and the corresponding temperatures taken from figure 8. These temperatures are marked on the graph; the total spread in numbers seen are less than 3 percent. This is a good indication of a Maxwell-Boltzman distribution of the excited OH radicals.

An extension of this iso-intensity method, developed by Shuler (3) is a more elegant method and perhaps a better indication that the distribution is that of an equilibrium. Equation (2) is used and figure 10 shows a plot of $E_{X'} - E_X$ vs $\log (A_{X'}/A_X)$ for the iso-intensity pairs. Values of $E_{X'}$ and $A_{X'}$ were obtained by linear interpolation from the adjacent integral X' values. From the slope, a rotational temperature of 3330° is found. This is in excellent agreement with the values obtained from figure 9.

The temperature can also be found from the line of maximum intensity. Differentiation of equation (1) shows that the K value corresponding to maximum intensity is given by (4).

---

(2) G. H. Dieke and H. M. Crosswhite, "The Ultra-violet Bands of OH", Bumblebee Series Report No. 87 (Nov. 1948) unclassified.

(3) K. E. Shuler, "Kinetics of OH Radicals from Flame Emission Spectra II" J. Chem. Phys. 18, 1466-70 (Nov. 1950).

(4) G. Herzberg, "Spectra of Diatomic Molecules", p. 125, 2nd Edition, Van Nostrand (1950).

$$K_{max} = \sqrt{kT/2Bhc} \qquad (4)$$

where $K = J + 1/2$ for the R_2 branch, $B = 16.98$ (2) for the $^2\Sigma$ state of OH, h is Planck's constant, and c is the velocity of light. The line of maximum intensity is difficult to locate with much certainty because the maximum occurs near the head of the R_2 branch where there is considerable overlapping of lines. The maximum intensity in figure 9 is between $K = 7$ and $K = 8$. These two values of K correspond to temperatures between 2600 and 3400°K.

The procedure adopted for measuring the temperatures reported here has been to find three iso-intensity pairs from each of two spectra obtained under the same conditions, to read the corresponding temperatures from figure 6, and to make an arithmetical average of the six values. The spread in these values was sometimes as small as 1 percent and never exceeded 10 percent. Measured temperatures were generally self-consistent and reproducible to better than 5 percent. Spot checks of this were made by using the long Shuler method on each type of flame in both inner and outer cones. No indication of non-equilibrium was found.

5. RESULTS

Emission spectra have been obtained from various portions of flames of hydrogen, of acetylene, of methane, and of propane burning with oxygen. Temperatures have been measured as described in section 4; but as yet there has not been time for more than a preliminary interpretation of these results.

Except for the investigation of instrumental effects mentioned in section 3, the monochromator slit has been set at a width of 0.01 mm and a height of 1.0 mm. Flames were scanned vertically and horizontally in 1 mm steps in the inner cone and somewhat longer steps in the outer cone. During the vertical scanning of the inner cone, an attempt was made to view the intense trace of the cone by setting the flame so that there was maximum response.

Figures 11 through 17 show OH rotational temperatures and relative intensities of the observed lines as a function of position. Intensities of line $R_2 3$ are used for the relative intensity plots of OH with the maximum intensity taken as 100. The peak intensities of the Q head of the $^2\Sigma \rightarrow {}^2\pi(0,0)$ transition of CH at 3143 A.U. are used for the CH plots. Additional fuel to oxygen mixtures from 0.5 to 2.0 times the fuel requred for stoichiometric were burned; but since there was relatively little difference in the trends observed, no graphs have been included.

From the vertical scans, it is seen that the temperature in the outer cone drops very slowly above the tip of the inner cone, amounting to less than 100°C in 20 mm. Presumably, however, the intensities drop much more rapidly to less than 50 percent in the same distance. At least part of this decrease in intensity is due to the smaller

luminous region. Measurements are now being made to determine quantitatively this effect of flame width.

It can be seen that the intensity of CH drops very rapidly near the tip of the inner cone and as nearly as can be found (to within 0.1 mm), there is no observable CH emission beyond the tip of the luminous cone. That CH intensity is plotted beyond the tip is an experimental effect due to the slit being 1 mm high. From this lack of CH being observed beyond the tip, an order of magnitude for the upper limit can be set on the lifetime of the excited CH. The velocity of the gas just above the tip is given approximately by

$$v_g = \frac{\text{Volume flow (NTP)}}{\text{Cross-section of flame}} \times \frac{T_f}{T_g} = \frac{(200)(3000)}{\pi(.075)\quad 300} = (1.2)10^6 \text{ mm/sec}$$

No CH is observed 0.1 mm above the tip; and therefore its lifetime is less than 10^{-7} seconds.

In the inner cone, the rotational temperature decreases away from the base of the cone in each flame at a considerably more rapid rate than is to be expected from the rate of cooling in the outer cone. However, the higher temperatures near the base of the cone still indicate an equilibrium distribution of intensities. This higher temperature of the inner cone indicates that OH is formed chemically in the reaction zone. The excess temperature to that in the outer cone continues for about 2 mm beyond the tip of the luminous cone and this indicates a radiative lifetime of OH of the order of 10^{-6} seconds. This time is in agreement with the calculations of Oldenberg and Rieke (5) who give 4×10^{-6} seconds.

It is difficult to reconcile the abnormally high temperatures of the inner cone with this position of the maximum OH intensity. If OH is produced within the flame region in the excited state, it would seem that the maximum concentration should occur within this region. However, the maximum intensity is at the tip and extends some distance into the outer cone. It may be that the amount of excited OH is less than equilibrium and that it takes the order of 10^{-6} seconds to reach chemical equilibrium at this temperature.

The horizontal scans in the outer cone have the same characteristics for all the flames. Figure 14 is representative. The temperature has decreased only 3.5 percent while the intensity has dropped to less than 1 percent. This shows that the cooler layers outside the hot core are ineffective in contributing to the measured OH rotational temperature.

Table II gives the measured rotational temperatures found in the different flames at the base of the flame, at the tip of the inner cone and 20 mm above the tip. These values are compared to measured Na line

---

(5) O. Oldenberg and F. F. Rieke, "Kinetics of OH radicals as Determined by their Absorption Spectra", J. Chem. Phys. 6, 439-447 (1938).

reversal and calculated equilibrium values found in the literature. It is seen that the OH temperatures in the outer cone of hydrogen-oxygen flames are in reasonable agreement with the reversal temperatures whereas the base of the inner cone is close to the calculated values.

Table II Measured OH Rotational Temperatures

Nozzle throat diameter = 1.5 mm

Fuel	Mixture % stoichiometric Fuel	Flow rate (cm^3/sec)	Inner cone (mm)	Measured Temperatures (°K) base Inner cone	tip Inner cone	20 mm Above tip	Na line reversal [6] (°K)	Calculated Equil. temp. (°K)
H_2	1.0	200	9	3025	2725	2625	2750	3100 [7]
	0.66 lean	200	9	3000	2625	2575	2750	2825
	2.0 rich	200	10	3000	2775	2650	2710	2920
C_2H_2	1.0	200	7.5	4250	3150	3025	3300	3320 [8]
	0.5 lean	200	11.7	4100	2775	2750	3200	
	2.0 rich	200	8	4100	3150	2975	3400	
CH_4	1	100	9	3250	2800	2725		3060 [9]
C_3H_8	1	100	10.5	3400	2850	2775		

6 B. Lewis and G. von Elbe, "Combustion, Flames, and Explosions of Gases". p.399. MacMillan (1938).

7 A. G. Gaydon, "Spectroscopy and Combustion Theory". Chapman Hall, p.179. 2nd edition (1948).

8 K. Shuler, private communication.

9 F. Ruegg, private communication.

Figure Legend

1. Photograph of monochromator, acetylene-oxygen flame, and spectral recording apparatus.

   F-flame, S-entrance slit, M-grating monochromator, L-quartz lens, D-rack and pinion assembly, T-photomultiplier tube, P-power supply for photomultiplier, A-d.c. amplifier, R-pen recorder and C-flowmeters.

2. Schematic diagram of light path.

3. A. Record of peak line intensity for one minute from a flame.

   B. Repeated scanning of same line shows the reproducibility of measured intensities.

4. Tracing of part of R_2 and Q_1 branch of (0,0) band of the $^2\Sigma \longrightarrow {}^2\Pi$ transition of OH.

5. Relative response curve of the Leeds and Northrup monochromator used with a 1P28 photomultiplier.

6. Portion of emission spectrum of (0,0) band of the $^2\Sigma \longrightarrow {}^2\Pi$ transition of OH from a hydrogen-oxygen flame. This shows both high and low K lines of the R_2 branch.

7. Plot of log (I_k/A_k) vs E_k for the R_2 branch of OH at the tip of the inner cone of a stoichiometric acetylene-oxygen flame. The most intense lines are reduced in intensity more than 50% by self-absorption.

8. Iso-intensity temperature graph giving temperatures corresponding to iso-intensity pairs of the R_2 branch of the (0,0) band of OH.

9. Intensity distribution in the R_2 branch. Same data as figure 7.

10. Plot of $E_x' - E_x$ vs log (A_x'/A_x) in the R_2 branch. Same data as figure 7.

11. Hydrogen-oxygen flame, stoichiometric mixture. Rotational temperatures and relative intensities plotted as a function of distance above the burners.

12. Acetylene-oxygen flame, stoichiometric mixture. Rotational temperatures of OH and relative intensities of OH and CH each normalized to the respective maximum intensity, plotted as a function of distance above the burner.

13. Methane - oxygen flame, stoichiometric mixture. Rotational temperatures of OH and relative intensities of OH and CH each normalized to

the respective maximum intensity, plotted as a function of distance above the burner.

14. Propane-oxygen flame, stoichiometric mixture. Rotational temperatures of OH and relative intensities of OH and CH each normalized to the respective maximum intensity, plotted as a function of distance above the burner.

15. Acetylene-oxygen flame, stoichiometric mixture, outer cone. Rotational temperatures and relative intensities of OH plotted as a function of distance through the flame.

16. Acetylene-oxygen flame, stoichiometric mixture, inner cone. Rotational temperatures of OH and relative intensities of OH plotted as a function of distance through the flame.

17. Hydrogen-oxygen flame, stoichiometric mixture, inner cone. Rotational temperatures and relative intensities of OH plotted as a function of distance through the flame.

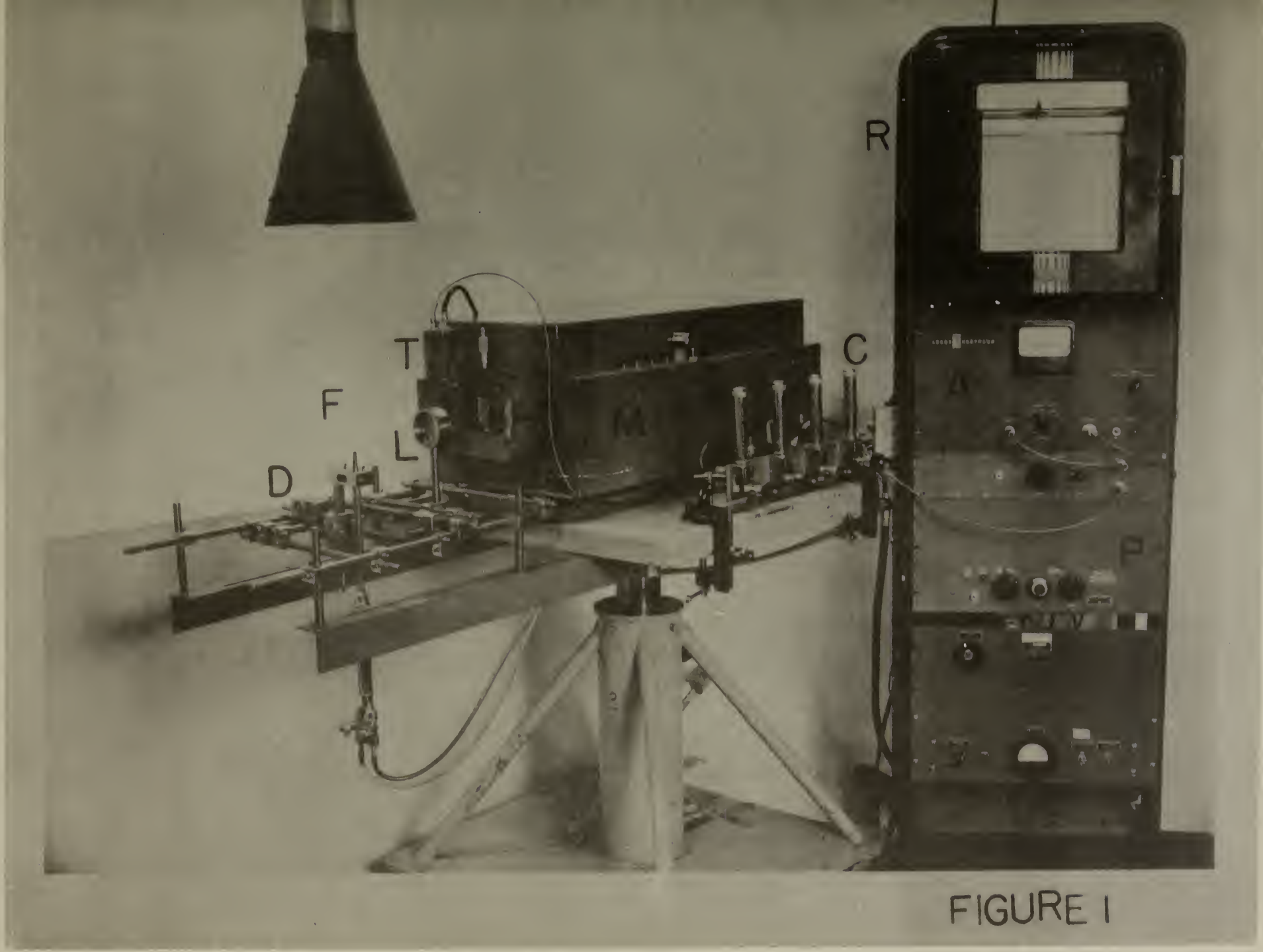

FIGURE 1

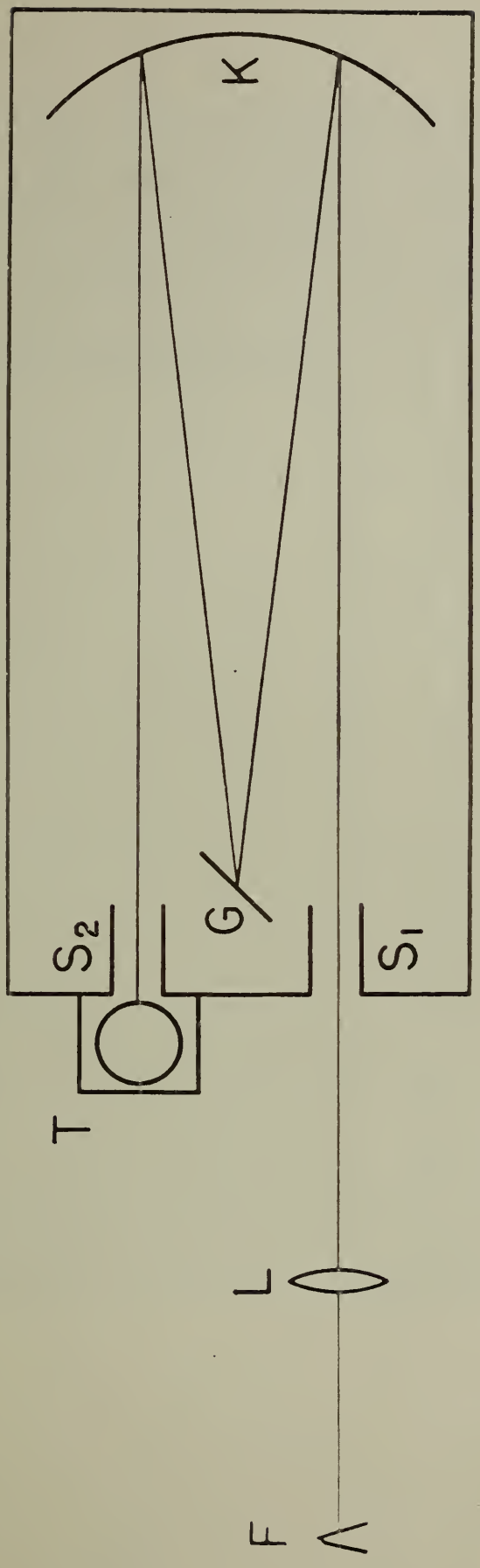

Fig. 2

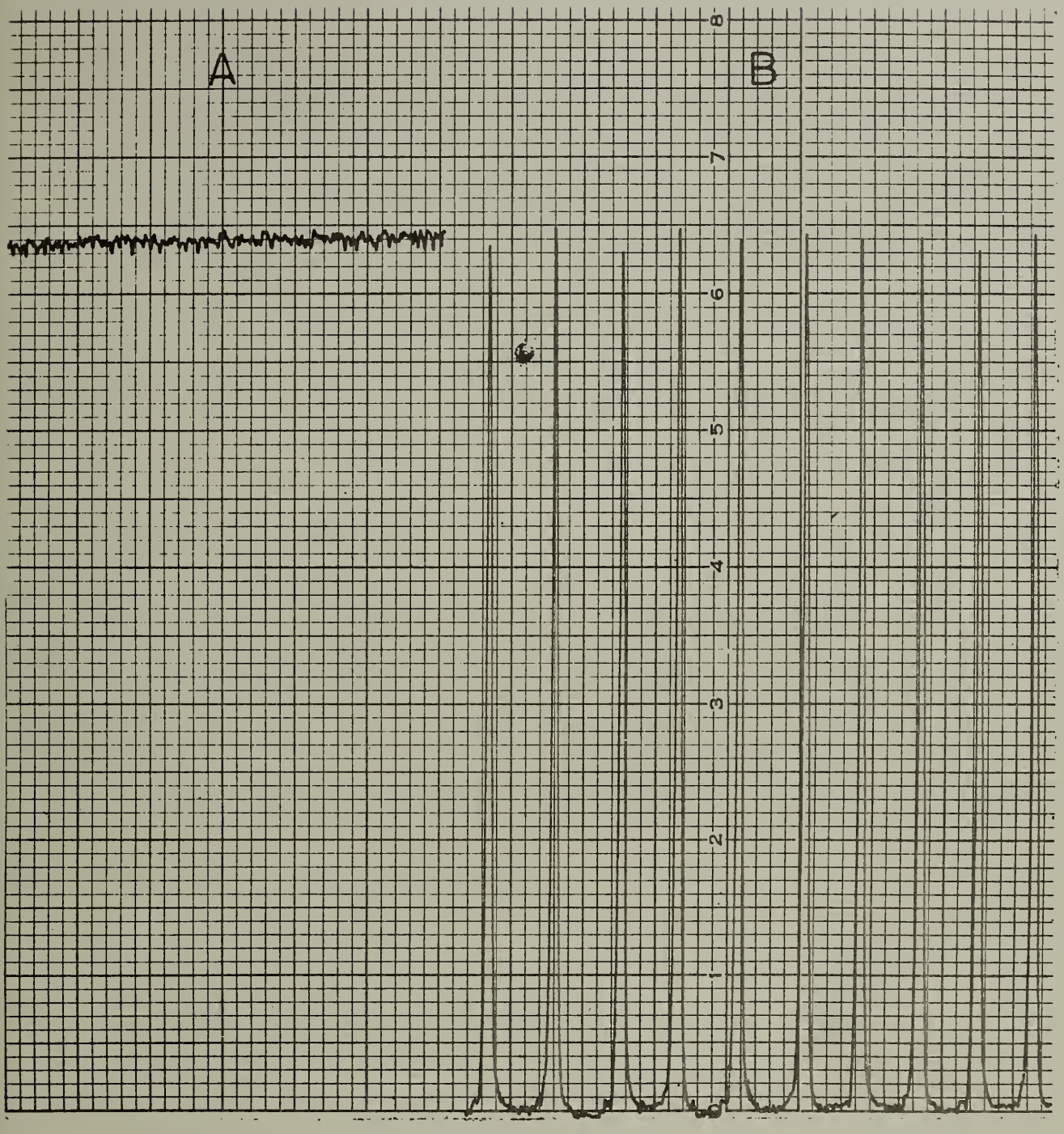

Figure 3

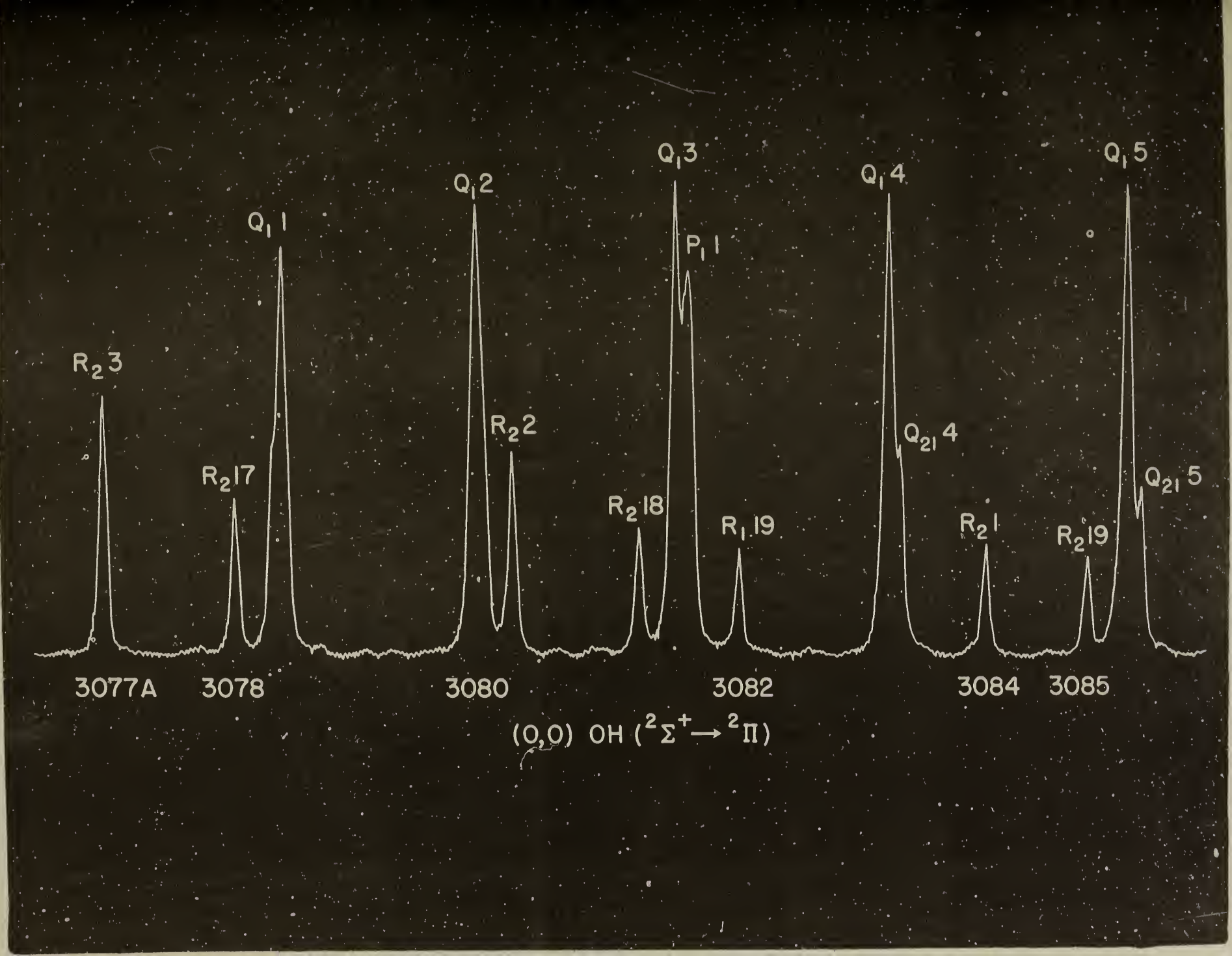

Figure 4
Figure 6
-153-
-155-

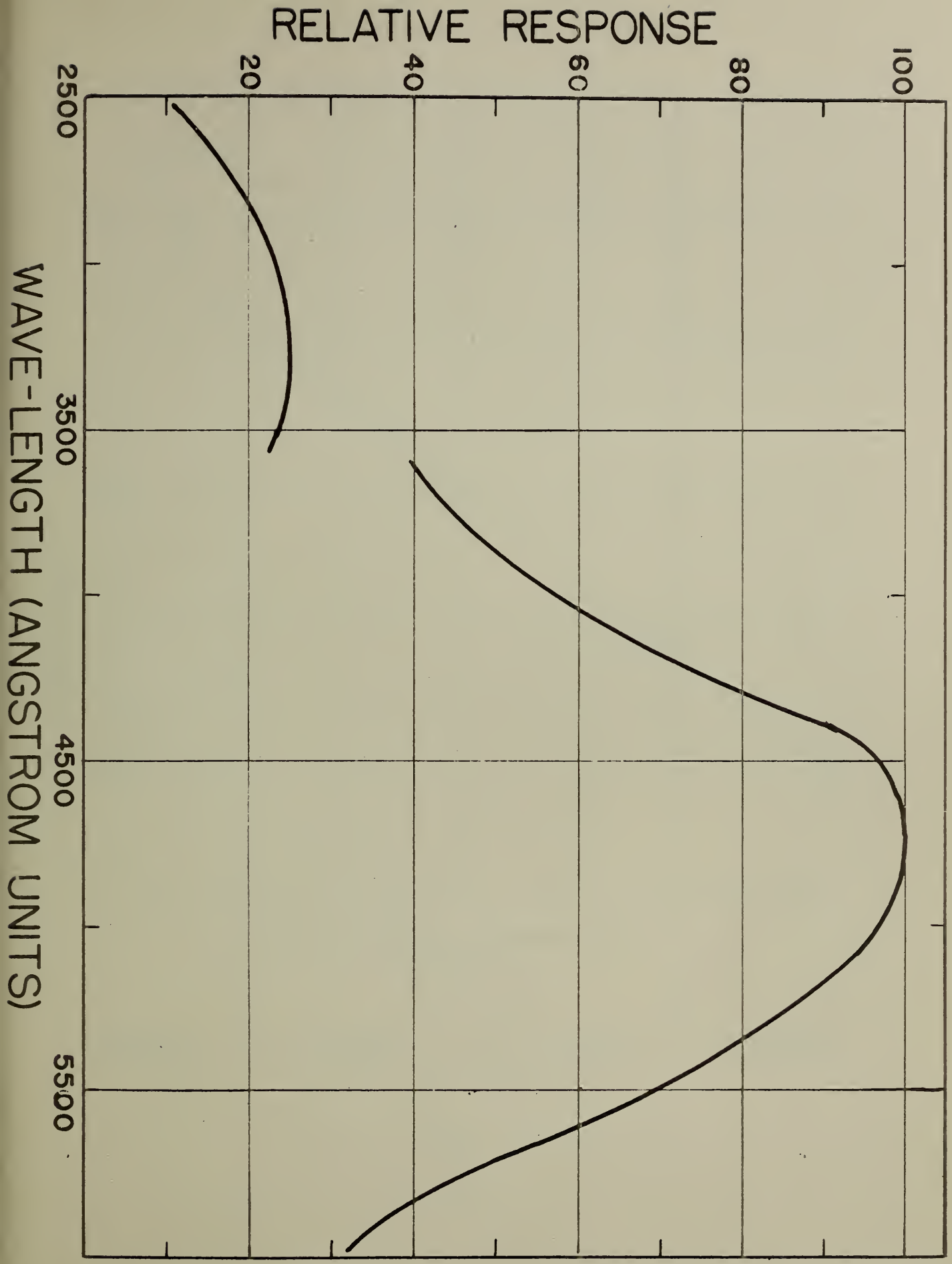
RELATIVE RESPONSE
20
40
60
80
100
WAVE-LENGTH (ANGSTROM UNITS)
2500
3500
4500
5500

Figure 5.

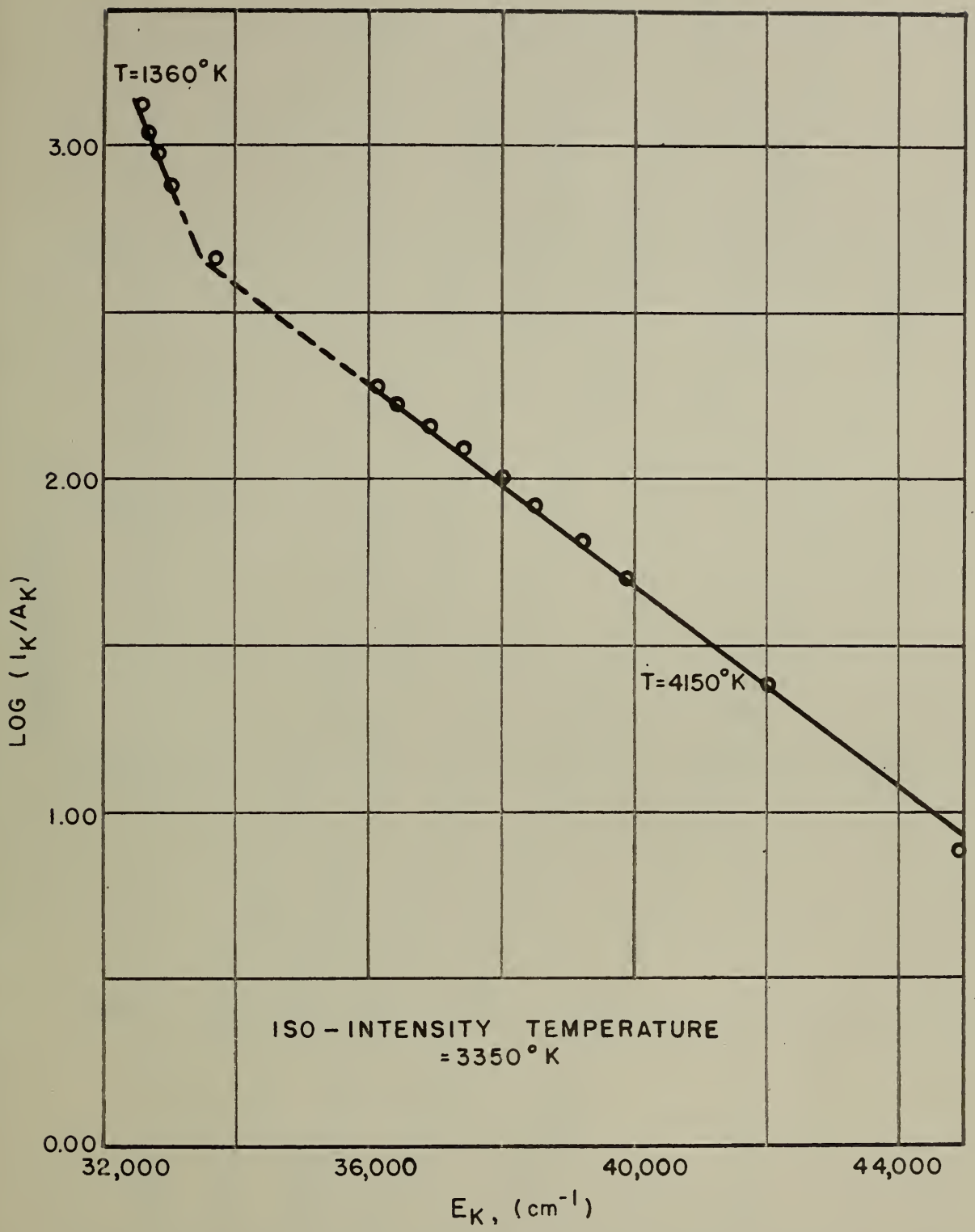
T=1360°K
3.00
2.00
1.00
0.00
LOG (I_K/A_K)
T=4150°K
ISO - INTENSITY TEMPERATURE
= 3350 °K
32,000
36,000
40,000
44,000
E_K, (cm^{-1})

Figure 7

-156-

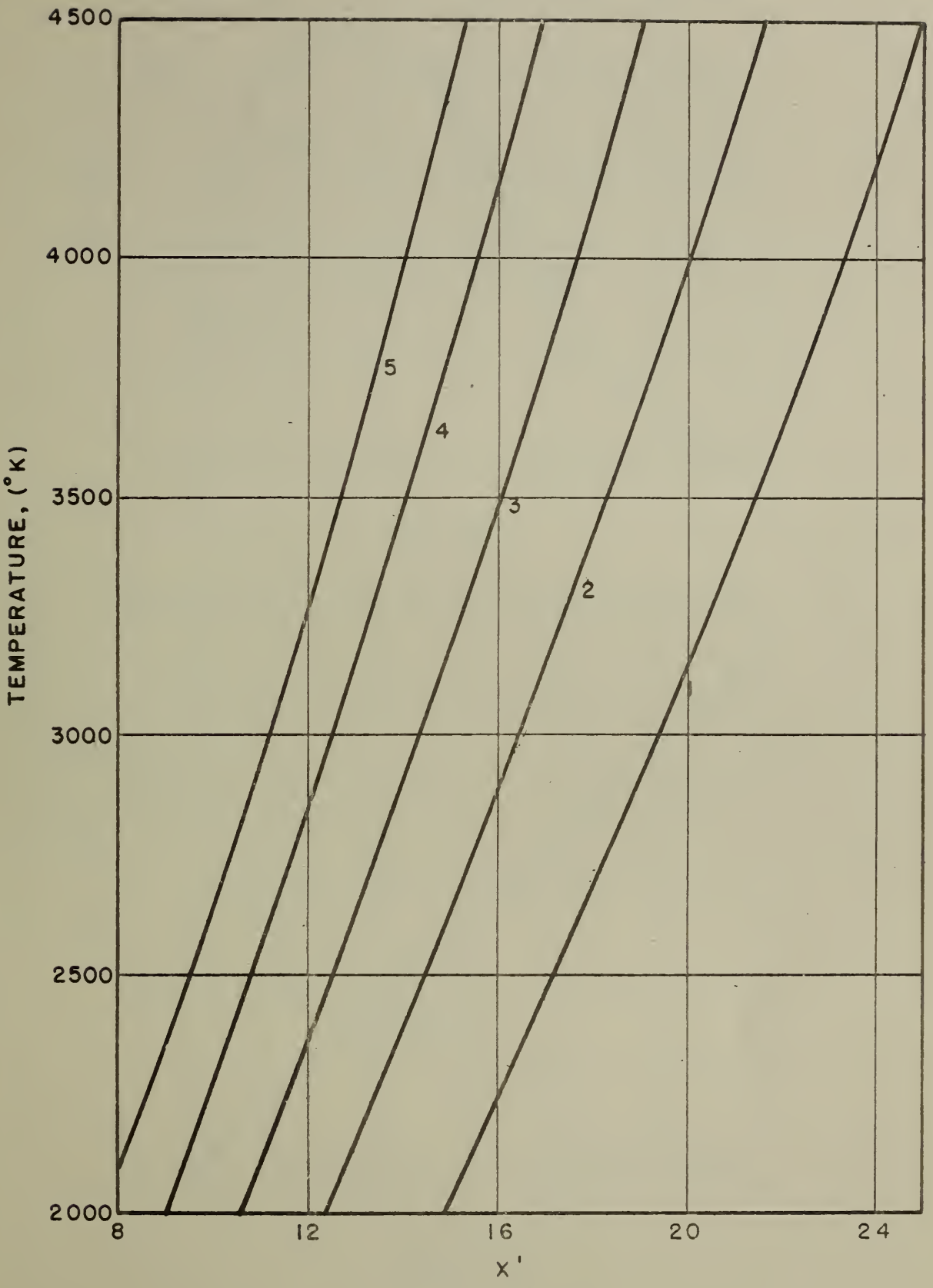
4500
4000
3500
3000
2500
2000
TEMPERATURE, (°K)
8
12
16
20
24
X'
5
4
3
2

Figure 8

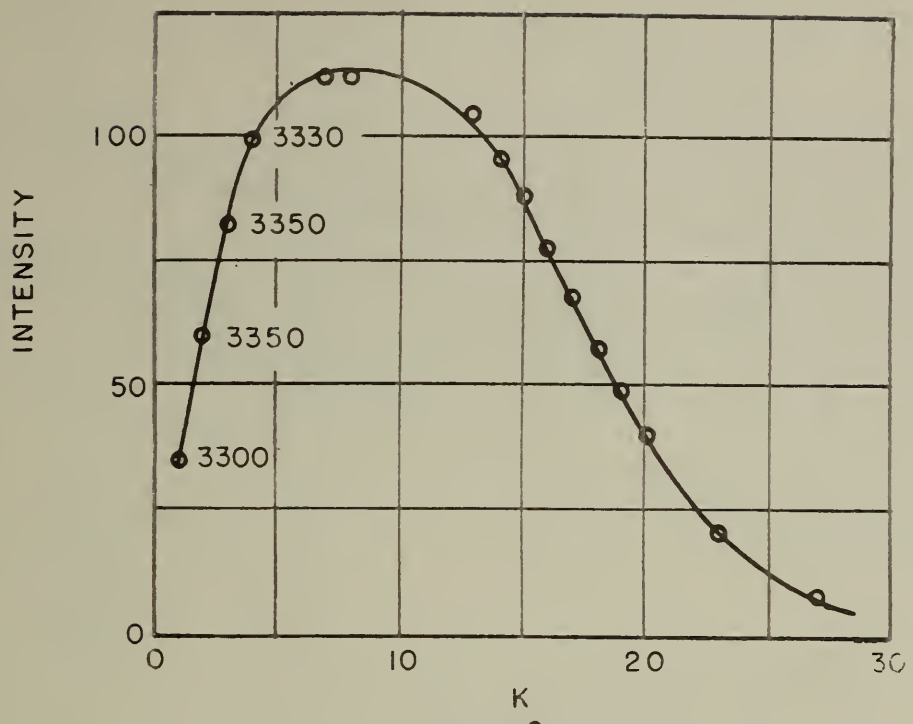

Figure 9

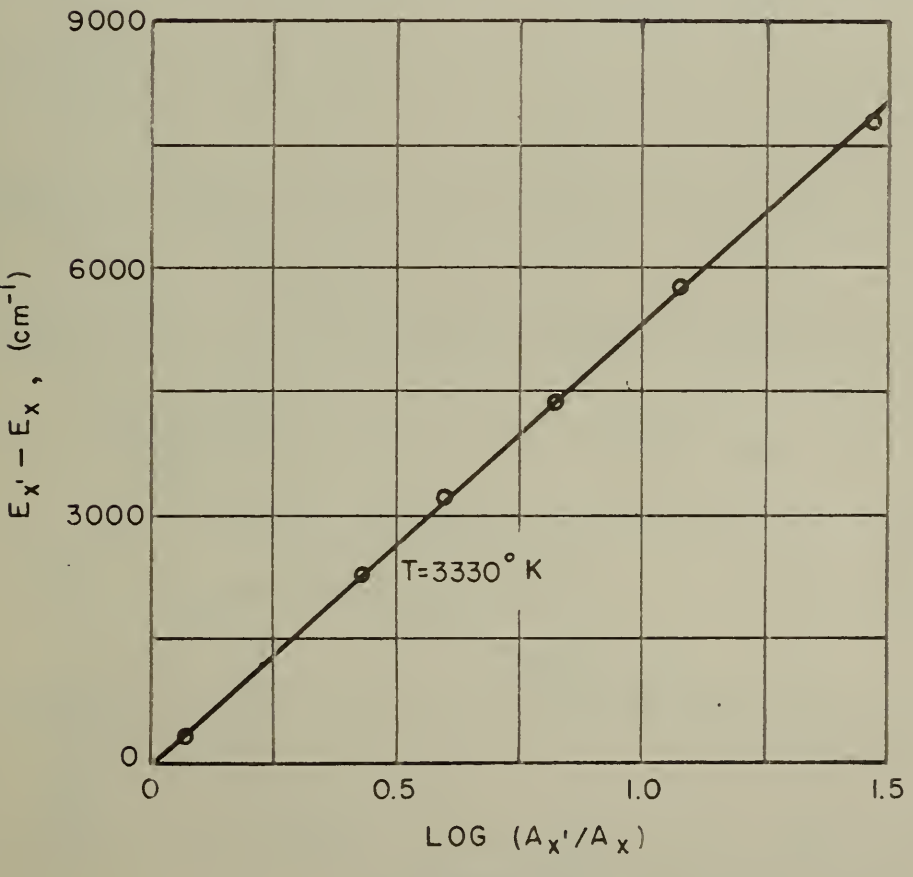

Figure 10

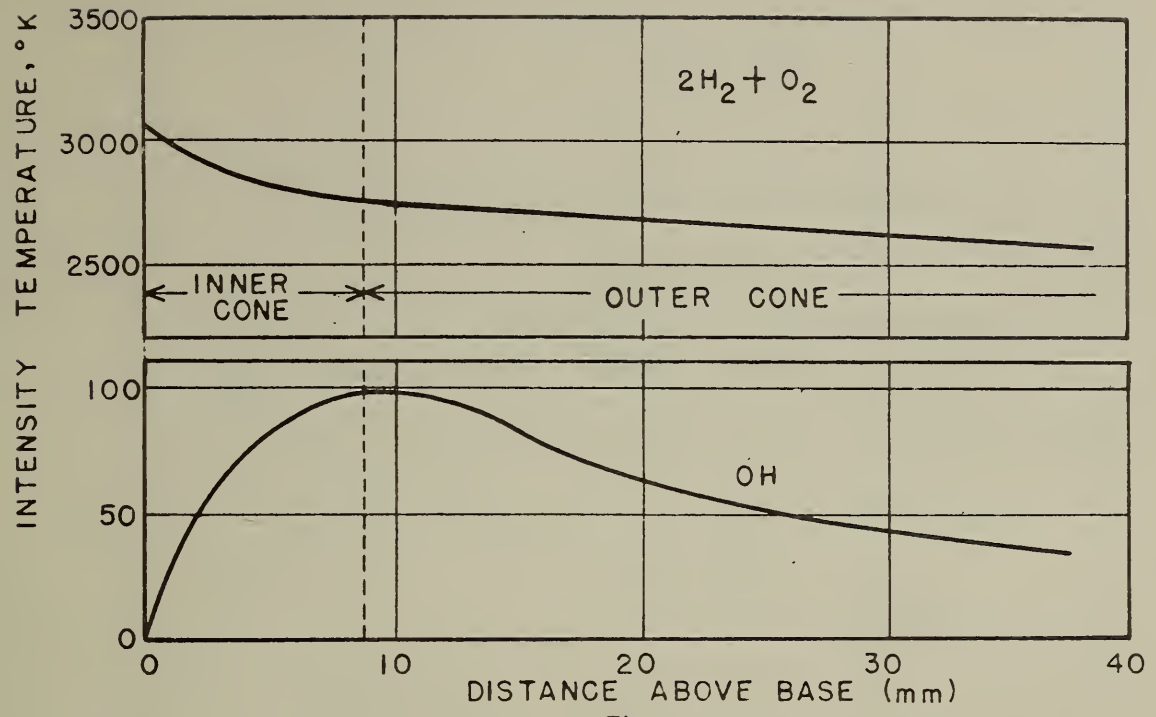

Figure 11

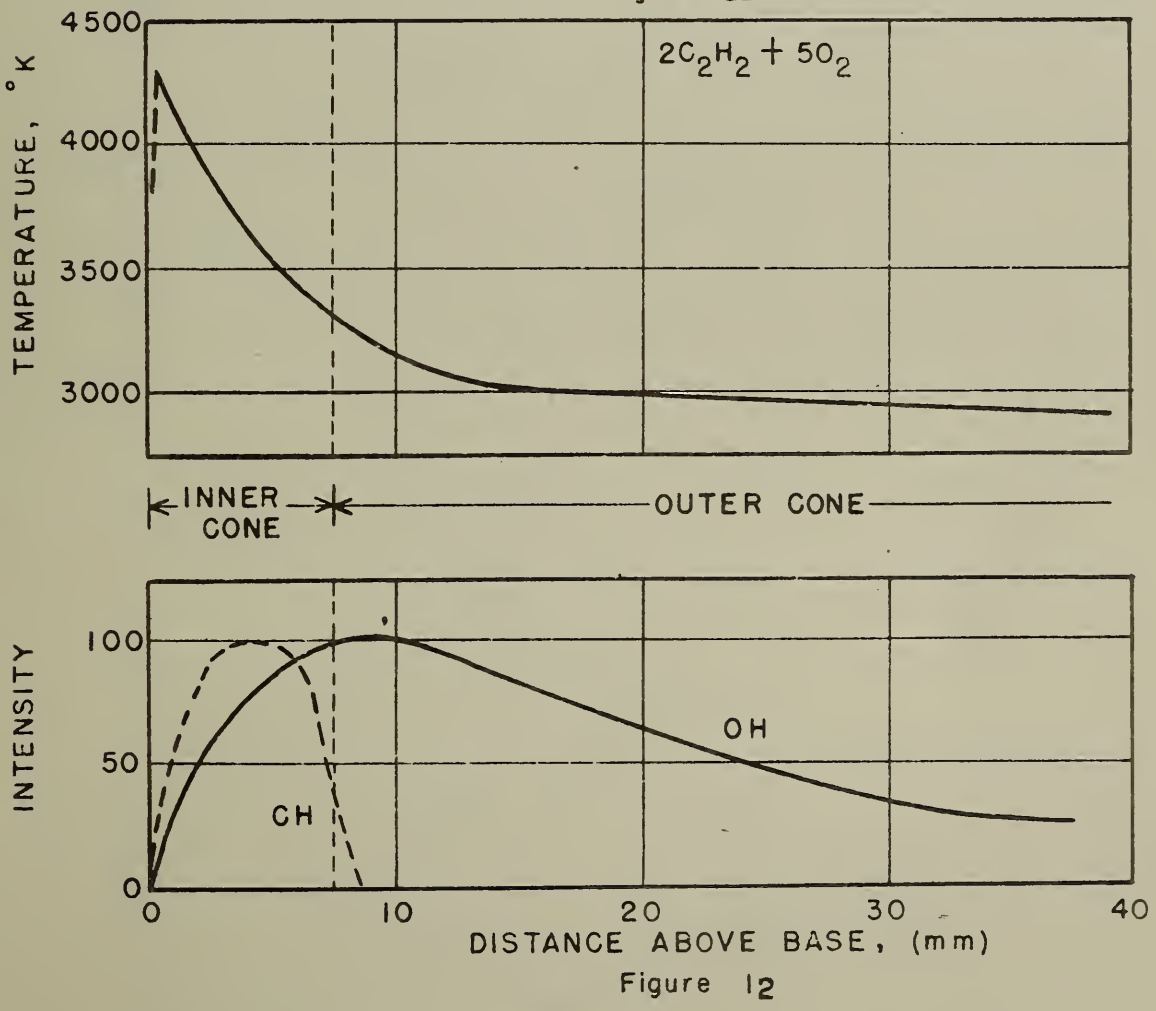

Figure 12

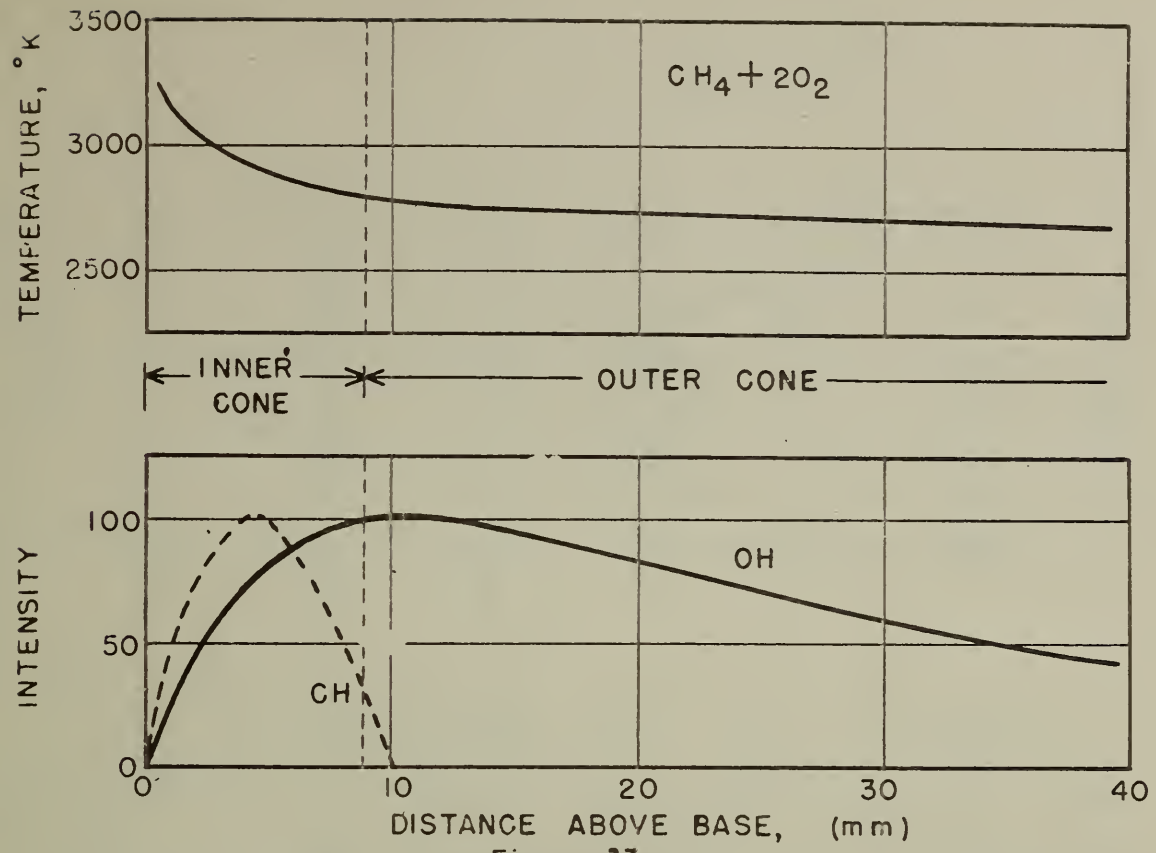

Figure 13

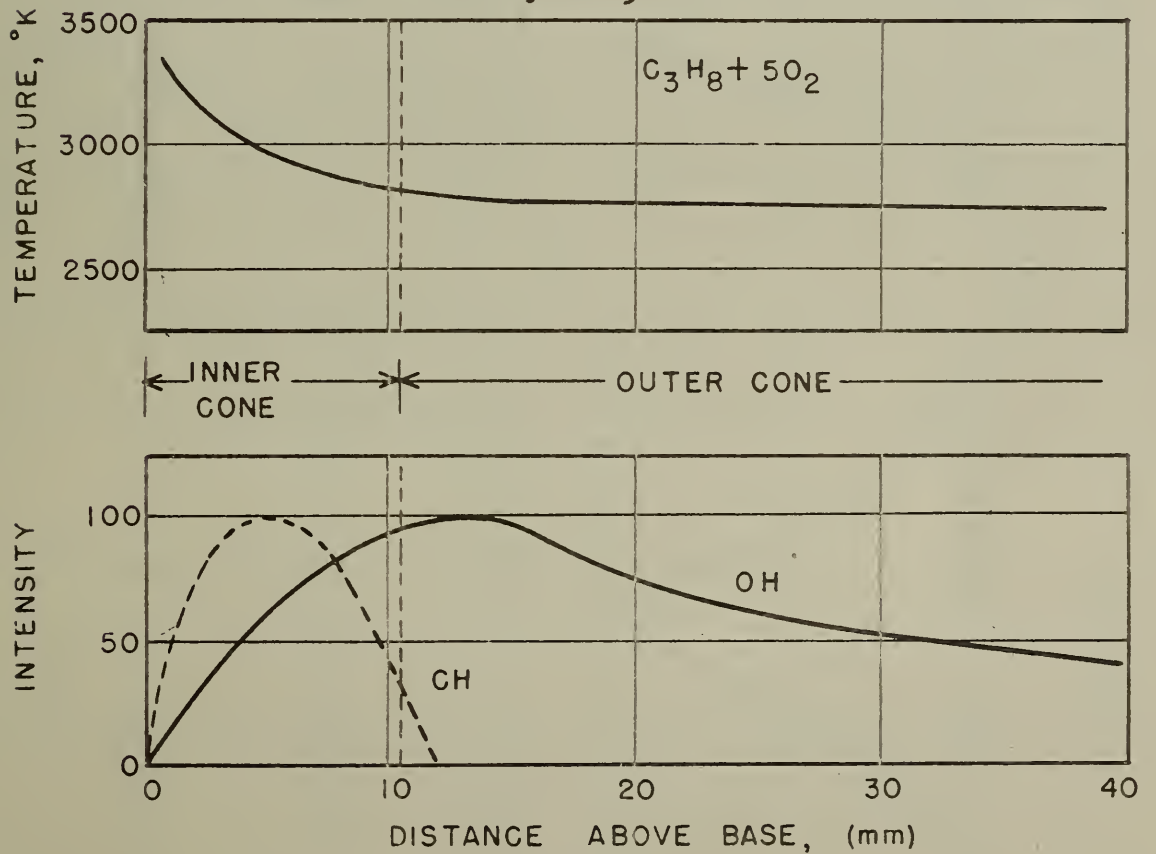

Figure 14

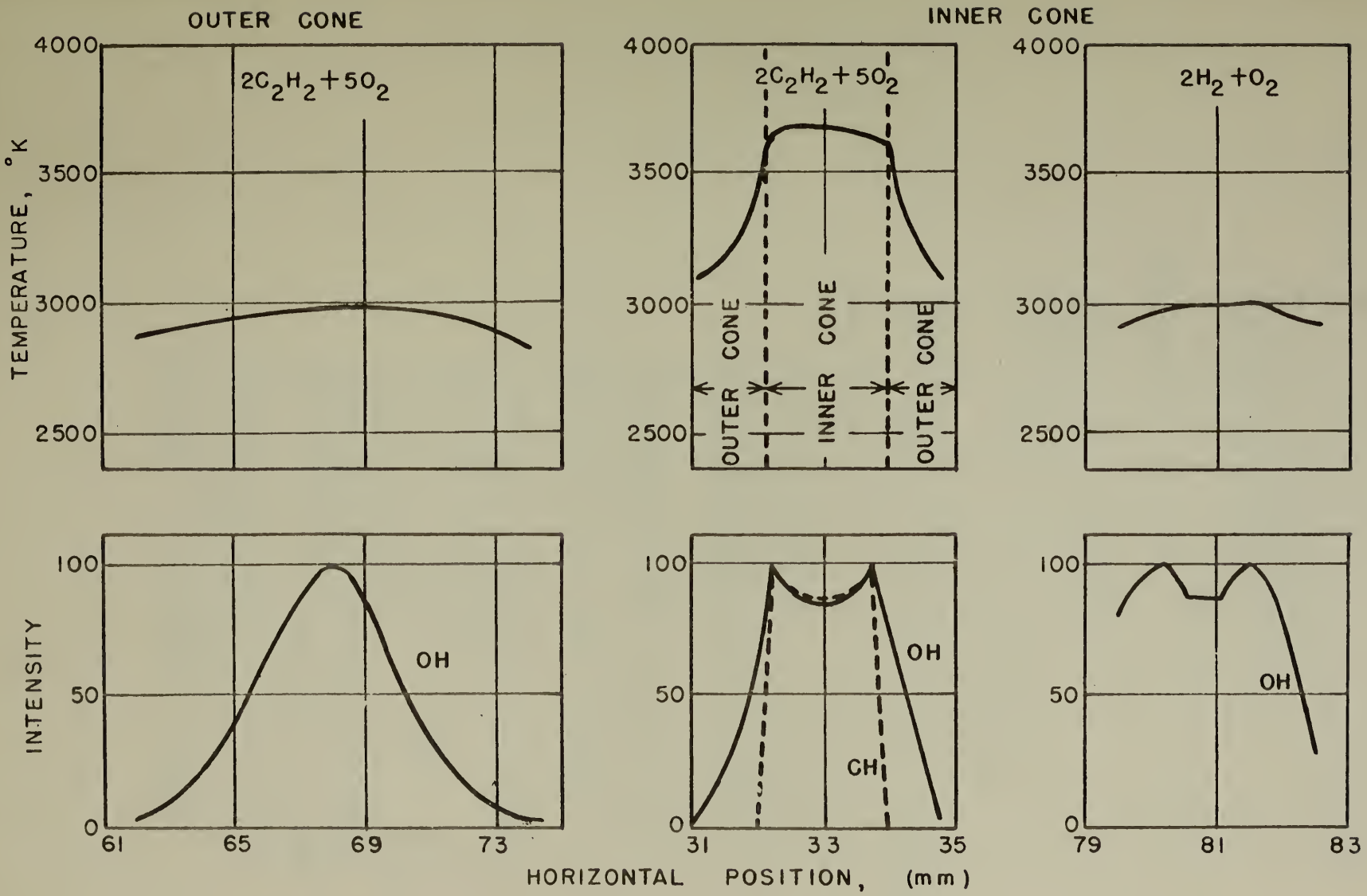

Figure 15

Figure 16

Figure 17

TECHNICAL REPORTS DISTRIBUTION LIST
NATIONAL BUREAU OF STANDARDS
GOVERNMENT ORDER NA-onr-83-49
NR 016 415

A. Government Distribution

Research and Development Board
Committee on Guided Missiles
Pentagon Building
Washington 25, D. C. (2 copies)

Department of the Navy

Chief of Naval Research
Office of Naval Research
Washington 25, D.C.
Attn: Physics Branch (2 copies)

Director, Naval Research Laboratory
Washington 20, D.C.
Attn: Technical Information Office (9 copies)

ONR, Branch Offices

Commanding Officer
U. S. Navy Office of Naval Research
495 Summer Street
Boston 10 Massachusetts (1 copy)

Commanding Officer
U. S. Navy Office of Naval Research
346 Broadway
New York 13, New York (1 copy)

Commanding Officer
U. S. Navy Office of Naval Research
844 North Rush Street
Chicago 11, Illinois (1 copy)

Commanding Officer
U. S. Navy Office of Naval Research
1000 Geary Street
San Francisco 9, California (1 copy)

Commanding Officer
U. S. Navy Office of Naval Research
1030 East Green Street
Pasadena 11, California (1 copy)

Assistant Naval Attache for Research
American Embassy
Navy 100
c/o Fleet Post Office (2 copies)
New York, New York

Chief, Bureau of Ordnance
Department of the Navy
Washington 25, D. C.
Attn: Re 9 (1 copy)

Chief, Bureau of Ships
Department of the Navy
Washington 25, D. C.
Attn: Code 300 (1 copy)
" " 327 (1 copy)

Commander
U. S. Naval Ordnance Test Station
Inyokern, California
P.O. China Lake, California
Attn: Reports Unit (1 copy)

Director
U. S. Naval Research Laboratory
Washington 20, D. C.
Attn: Code 2021 (1 copy)

Commander
Naval Ordnance Laboratory
White Oaks
Silver Spring, Maryland
Attn: Dr. R. J. Seeger (1 copy)

Chief of Naval Operations
Department of the Navy
Washington 25, D. C.
Attn: OP-57 (1 copy)

Naval Aeronautic Rocket Laboratory
Lake Denmark
Dover, New Jersey (1 copy)

Chief, Bureau of Aeronautics
Department of the Navy
Washington 25, D. C.
Attn: TD-4 (1 copy)

Department of the Army

Director, Operations Research Office
Department of the Army
Fort Leslie J. McNair
Washington 25, D.C. (1 copy)

Chief, Guided Missiles Branch
Technical Command
Army Chemical Center, Maryland (1 copy)

Department of the Army
Office, Chief of Ordnance
The Pentagon
Washington 25, D. C.
Attn: ORDTU (1 copy)

Officer-in-Charge
Ordnance R&D Division Sub-Office (Rocket)
Fort Bliss, Texas (1 copy)

Department of the Air Forces

Commanding General
Air Materiel Command
Wright-Patterson Air Force Base
Dayton, Ohio
Attn: MCIDXD (2 copies)

Watson Laboratories
Air Materiel Command
Eatontown, New Jersey (1 copy)

Department of Commerce
Director
National Bureau of Standards
Washington 25, D. C. (1 copy)
Attn: Dr. W. C. Dreichwedde (1 copy)

Director
National Advisory Committee for Aeronautics
1724 "F" Street, N. W.
Washington, D. C.
Attn: Dr. C. H. Helms (1 copy)

National Advisory Committee for Aeronautics
Lewis Flight Propulsion Laboratory
Cleveland Airport
Cleveland 11, Ohio (1 copy)

National Research Council
Division of Physical Sciences
National Academy of Sciences
Washington 25, D. C. (1 copy)

Los Alamos Scientific Laboratory
Los Alamos, New Mexico
Attn: Dr. Calvin Potts (1 copy)

B. Non-Government Distribution

Ohio State University
Department of Physics
Columbus 10, Ohio
Attn: Dr. H. L. Johnston (1 copy)

University of California
Berkeley, California
Attn: Dr. F. R. Parker (1 copy)

Batelle Memorial Institute
Columbus, Ohio
Attn: Dr. H. C. Cross (1 copy)

University of Pennsylvania
Randal Morgan Laboratories of Physics
Philadelphia 4, Pennsylvania
Attn: Dr. F. C. Nix (1 copy)

Rockhurst College
Department of Physics
Kansas City 4, Missouri
Attn: Dr. W. M. Conn (1 copy)

Research Institute
Temple University
Philadelphia 22, Pennsylvania
Attn: A. U. Grosse (1 copy)

Jet Propulsion Laboratory
California Institute of Technology
Pasadena, California
Attn: S. S. Penner (1 copy)

Applied Physics Laboratory
Johns Hopkins University
Silver Spring, Maryland
Attn: Shirleigh Silverman (1 copy)
K. Shuler (1 copy)

Johns Hopkins University
Baltimore, Maryland
Attn: Dr. G. H. Dieke (1 copy)

Mr. C. F. Yost
National Bureau of Standards
Washington, D. C. (2 copies)

U. S. Department of Commerce
National Bureau of Standards

Research Paper RP2110
Volume 45, July 1950

Part of the Journal of Research of the National Bureau of Standards

Heat Capacity of Sodium Between 0° and 900° C, the Triple Point and Heat of Fusion

By Defoe C. Ginnings, Thomas B. Douglas, and Anne F. Ball

Using an improved ice calorimeter and furnace, the enthalpy changes of two samples of pure sodium have been accurately measured by a drop method at a number of temperatures between 0° and 900° C. Equations are derived to fit the data, and values of enthalpy and entropy, based on zero values at 0° C, as well as the heat capacity are tabulated for both the solid and liquid. Sources of significant experimental error are examined critically, and some theoretical implications of the results are discussed qualitatively.

I. Introduction

The advantages of liquid sodium for heat transfer at high temperatures have been known for some time. Not only have experimental values of the heat capacity of sodium been limited to the temperature range below 300° C, but these values have been widely discordant at 200° to 300°. It was the purpose of this investigation to measure the heat capacity of pure liquid sodium with higher accuracy and at higher temperatures than had been done previously.

II. Samples

The measurements were made on two samples of sodium enclosed in stainless steel containers of the type shown in figure 1. The stainless steel used was chosen for its resistance to attack by sodium at high temperatures. The sodium had been distilled once in glass in vacuum at or below 300° C. The weights of the samples were 5.3404 and 6.0297 g, respectively, and each was admitted in vacuum to a stainless steel cylinder weighing 16.840 g and having a capacity of 9.7 cm^3. After admitting helium to a pressure of one-thirtieth atm, each cylinder was sealed by welding and subsequently tested for leakage by noting whether exposure to 850° C for 15 min in an evacuated vessel caused any change in weight. The welding process utilized pulsed inductive heating [1].[1] With this welding technique, it was possible to seal the container without changing its weight by more than a milligram.

[1] Figures in brackets indicate the literature references at the end of this paper.

The sodium sample used for most of the measurements was analyzed spectrochemically at this Bureau after the heat-capacity experiments. Of the 47 elements tested for, including all the common metals, only three were detected. Calcium and lithium were found in amounts estimated at between 0.0001 and 0.001 weight percent, whereas potassium was estimated to be between 0.001 and 0.01 percent. The sample was completely soluble in water.

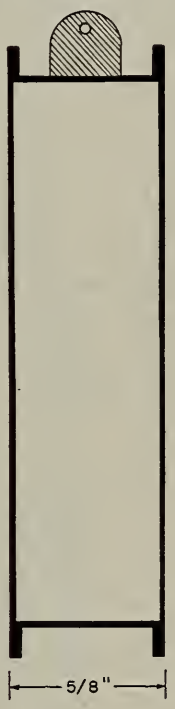

FIGURE 1. *Scale diagram of sample container.*

The spectrochemical analysis did not include a

896958—50——1

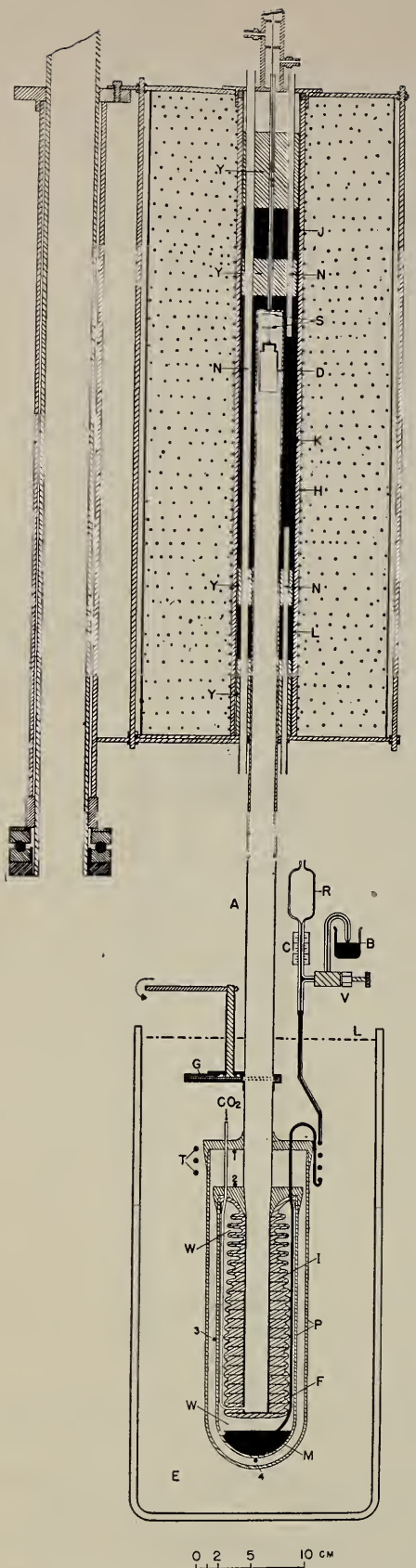

FIGURE 2. *Schematic diagram of furnace and ice calorimeter.*

A, Calorimeter well; *B*, beaker of mercury; *C*, glass capillary; *D*, sample container; *E*, ice bath; *F*, copper vanes: *G*, gate; *H*, platinum heater; *I*, ice mantel; *J*, *K*, *L*, silver cylinders; *M*, mercury; *N*, Inconel tubes; *P*, Pyrex containers; *R*, mercury reservoir; *S*, platinum shields; *T*, mercury "tempering" coil; *V*, needle valve; *W*, water; *Y*, porcelain spacers; 1, 2, 3, 4, thermocouple junctions.

search for the common nonmetals. However, other samples from the same original source and distilled by the same procedure were reported to contain as much as 0.01 percent by weight of oxygen (as Na_2O). The typical content of hydrogen before distillation amounted to 0.006 percent by weight. A melting curve observed by the authors on the principal sample is described in this paper. This indicated that the impurity in solution in the liquid but not in the solid amounted to about 0.0016 mole percent at the triple point.

III. Method and Apparatus

The method as applied to an earlier apparatus has already been described [2, 3, 4]. In brief, the method is as follows. The sample, sealed in its container, is suspended in a furnace until it comes to constant temperature. It is then dropped into a Bunsen ice calorimeter, which measures the heat evolved by the sample plus container in cooling to 0° C. A similar experiment is made with the empty container at the same temperature. The difference of the two values of heat is a measure of the change in enthalpy of the sample between 0° C and the temperature in the furnace. From enthalpy values of the sample so determined for a series of temperatures, the heat capacity can be derived.

1. The Ice Calorimeter

The construction, calibration, and use of an earlier Bunsen ice calorimeter in this Bureau have been described [2]. The present model, shown together with the furnace in figure 2, incorporates several improvements. In the first place, the mercury-water interface is now located in the bottom of the inner glass calorimeter vessel. This has two advantages. First, the area of the interface is much larger than before, so that for a given influx of heat, the level of mercury in the calorimeter changes very little. The calorimeter and its contents are slightly compressible, so that a change in pressure in the calorimeter results in a change in volume that must be distinguished from the change in volume due to heat input. With the earlier calorimeter, the change in volume produced by the change in head of mercury affected the calibration factor by about 0.01 percent, but with the present

calorimeter, the effect of the change in head is only about 0.004 percent. The electrical calibration experiments automatically compensate for this effect in heat measurements. However, reduction of the magnitude of the effect permits determination of the calibration factor of an "ideal" ice calorimeter (one that operates at constant head) with greater accuracy. A second reason for locating the mercury-water interface in the bottom of the calorimeter is to avoid danger of breaking the inner glass vessel. The inlet tube, now being filled with mercury rather than water, is not subject to blocking by freezing, an event that would burst the glass vessel. The present inlet tube includes a coil (T), for bringing the mercury to the temperature of 0° C before it enters the calorimeter.

The present calorimeter has been equipped with a tin-plated system of copper vanes, as pictured in figure 2. This results in more rapid distribution of heat from the well to the ice, so that the lag in reaching thermal equilibrium is now caused almost wholly by the thermal resistance between the heat source (sample in container) and the inner wall of the well. The latter lag has been considerably reduced by using a slow stream of dry helium gas up the well instead of carbon dioxide gas (as shown in fig. 1).

Unlike the earlier calorimeter, the new one has no built-in heater for electrical calibration. Calibrations were made with a removable heater provided with two zones of thermal contact with the calorimeter well for trapping the heat that would otherwise escape through the leads. This heater has a resistance of about 100 ohms instead of the 10 ohms in the earlier calorimeter. This reduces the uncertainty of accounting for the heat developed in the leads between the calorimeter and the jacket to a few thousandths of a percent of the total heat input to the calorimeter.

About one hundred electrical calibration experiments were made with the new calorimeter, with energies varying from 12,000 to 25,000 j. These experiments gave a calibration factor of 270.46 ± 0.03 abs j/g of mercury, which agrees with the value of 270.41 ± 0.06 obtained for the earlier calorimeter within the uncertainty assigned to the latter figure. About a hundred additional calibration experiments were made with low energies (about 100 j) in a search for small absolute errors that might not be detectable in high-energy experiments. These experiments indicated that the calorimeter failed to register about 0.4 j, an amount of heat that is negligible in most measurements.

2. The Furnace

The furnace is shown in position over the ice calorimeter in figure 2. It was mounted on a ball bearing so that it could be swung aside for access to the calorimeter. This furnace incorporated certain improvements that reduced temperature gradients in its central region and permitted more accurate temperature measurements over most of its temperature range.

In order to minimize end effects, the furnace was made 24 in. high, instead of 18 in. as with the earlier one [3]. The furnace was electrically heated by means of No. 26 platinum wire (H) wound on a grooved alundum tube having an inside diameter of 2 in. This heater was made in three separate sections corresponding in elevation to the three silver cylinders, which were located inside the alundum at J, K, and L. Silver was used because of its high thermal conductivity. By maintaining the silver cylinders J and L at the same temperature as the cylinder K, the temperature gradient in K could be made negligible. The silver cylinders were supported by porcelain spacers (Y). The silver and porcelain cylinders were lined with an Inconel tube (14% Cr, 80% Ni, 6% Fe) having an inside diameter of 1 in. in the central and lower parts of the furnace but with a diameter of one-eighth in. in the upper part. This tube served to enclose the sample container and its suspension wire (No. 32 Nichrome V), so that an inert atmosphere could be maintained at high temperatures where the stainless steel container would oxidize in air. Helium was used for the atmosphere in order to minimize the time necessary to hold the capsule in the furnace.

Figure 2 shows some of the vertical holes drilled through the silver and porcelain. These were placed 90 deg apart azimuthally. Three of them (one-fourth-in. in diameter) extended through the length of the furnace while two (three-sixteenth-in. in diameter) extended only to the top and bottom respectively of the center silver cylinder as shown in figure 2. These holes were fitted with thin-walled Inconel tubes, one of which served to hold the platinum-rhodium thermocouple sometimes used for temperature measurement of the central

silver section (K). In the two $\frac{3}{16}$-in tubes were placed differential thermocouples used to keep the end silver sections (J, L) at the same temperature as the central section. All thermocouples were insulated in four-hole porcelain tubes, which fit snugly in the Inconel tubes. A platinum resistance thermometer was encased in a platinum-rhodium tube, which also fit snugly in one of the one-fourth-in. Inconel tubes.

In another one-fourth-in. tube were placed three small auxiliary heaters, located at the elevations of the three silver cylinders. It was possible with these heaters to add heat at a low rate to any silver cylinder for fine-temperature regulation. It was possible to maintain the central silver cylinder constant to 0.01 deg and the end silver cylinders within a few tenths of a degree of the central silver. These auxiliary heaters were very useful in fine-temperature regulation since their heat was mostly delivered to the silver in 30 sec, thus avoiding the larger and troublesome lag that would have been encountered had the fine regulation been dependent on adjusting the currents in the main heaters.

In addition to the thermocouple mentioned, several more were installed just outside the main heaters (H). These thermocouples served to measure the temperature of this region and were used in a safety device to turn off automatically all current in the furnace if its temperature approached 961° C (the melting point of silver).

The suspension of the container in the furnace and its drop into the calorimeter is similar to that described earlier [3]. The braking started after the container entered the calorimeter. The weight of the falling system was kept constant in all experiments. Two platinum shields were used above the container in the same manner as formerly except that the diameters of the shields were increased from five-eighths in. to three-fourths in. since the diameter of the calorimeter well was increased from three-fourths in. to seven-eighths in.

3. Measurement of the Temperature of the Capsule in the Furnace

Up to 600° C, a strain-free platinum resistance thermometer was used to measure the temperature of the central silver cylinder that surrounded the capsule. This thermometer was calibrated at this Bureau on the International Temperature Scale [5] at the ice, steam, and sulfur points, and its resistance was always checked at the ice point after experiments at 600° C. Between 600° and 900°, the resistance thermometer was removed from the furnace, and the platinum-rhodium thermocouple was used. This thermocouple also was calibrated at this Bureau and was checked against a standard thermocouple before and after the measurements. A comparison of the resistance thermometer with the thermocouple showed agreement within 0.2 deg C in the temperature range up to 600° C. Both the resistance thermometer and thermocouple were made to have good thermal contact with the silver, so that their indications would not be affected by heat conduction along their leads. Experimental verification of this was found in tests with varying depths of immersion. The resistance thermometer winding and the principal junction of the thermocouple were both located at approximately the height of the sample container in the furnace.

It has been assumed that the sample container attains the temperature of the central silver, which surrounds it except at the bottom. Although calculations showed this assumption to be justified, experiments were made to test this. These experiments consisted of first making regular drop experiments at 700° C with the end silver pieces (J and L) regulated in the normal manner within a few tenths of a degree of the central silver (K). Then another series of drops was made, regulating both end silver pieces about 50 deg colder than the center. In other words, the temperature difference between the ends and the central silver was exaggerated by a factor of over one hundred. Even under these extreme conditions, the experiments gave a result only 0.1 percent lower. This indicated two main facts. First, with the exaggerated temperature difference, either the temperature gradient in the central silver was small, or the thermocouple was so placed that it represented the temperature of the sample container in spite of the gradient. Actually calculations show that the gradient is negligible in normal use. Second, this also indicated that any lowering of the temperature of the sample container below that of the main silver cylinder K due to radiation loss from the sample container out the bottom of the furnace is negligible. Calculations considering the solid angle had already shown that this should be true.

Since the temperature of the sample container was not directly measured, it was necessary to allow sufficient time for the container to reach the temperature of the silver. Special tests have been made to determine this time, similar to those described in detail in an earlier publication [3]. In the present experiments using helium in the furnace, the container with sodium acquired the temperature of the furnace (within 0.01 deg) within 15 min, whereas the empty container took less time in proportion to its heat capacity. In the experiments with sodium just above its melting point, extra time was taken to allow for absorption of the heat of fusion.

It was also necessary to consider the possibility of azimuthal temperature gradients in the silver due to the periodic addition of small amounts of heat by means of the auxiliary heaters that are located in one of the vertical holes in the silver. Calculations showed that no significant temperature gradients resulted with the relatively small amounts of heat supplied in this way.

4. Errors Due to Cooling of the Sample Container During Its Drop into the Calorimeter

Some users of the "drop" method in the past have simply subtracted the calculated enthalpy of the sample container from the measured enthalpy of the container plus sample. Of course, this procedure does not make allowance for heat lost during the drop. By making drop experiments with the empty container, most of this heat lost is accounted for, since it is approximately the same in both types of experiments. However, for the most accurate measurements, it is desirable to test the validity of this assumption that the heat loss is essentially the same for both empty and filled containers. The heat loss during the drop is dependent on the temperature difference between the container surface and its surroundings. This temperature difference will be slightly greater for the filled container, since its total heat capacity is higher than that of the empty container. This difference between the amounts of heat lost by the empty and the filled containers has been estimated by the authors for a sample assumed to have infinite thermal conductivity and perfect contact with the container. This gives the maximum possible difference. The radiation loss was estimated on the basis of a container with an area of 35 cm^2 with an emissivity of approximately unity. The heat lost by radiation from a container at 900° C dropping through a region near room temperature for one-quarter sec is about 80 j. The convective heat loss is much more difficult to estimate. Using the formula given in the International Critical Tables [6] for horizontal cylinders as being somewhat analogous, the convective loss in helium was calculated as about 80 j. Using these figures with the known heat capacities of the empty and filled containers, it is estimated that there would be a maximum error of about 4 j in the value for the enthalpy of the sample at 900° C. This is equivalent to about 0.06 percent on enthalpy, and a somewhat greater error on heat capacity.

Due to the approximate nature of the calculations of this error, some experiments were made to test if the heat losses calculated in this way were reasonable. Eight experiments were made at 300° C, dropping another container having about the same emissivity. In these experiments, the time of fall of the container was varied by factors of two and four greater than the normal time of fall (almost free fall). Assuming that the heat loss is directly proportional to the time of fall, it was estimated that the total heat lost in a normal fall at 300° C was about 6 j. This figure is considerably less than the value of about 16 j calculated in the manner described above (12 j by convection and 4 j by radiation). This would indicate that the heat loss is less than the calculations indicate and that at 900° C, the error due to this loss may be 0.02 to 0.03 percent. Since this error is small and is not known accurately, no attempt was made to apply a correction.

IV. Results of Enthalpy Measurements

A total of 129 measurements of enthalpy was made, 67 with the two empty containers and 62 with the two containers containing sodium. The average deviation from the mean was ± 0.02 percent with a given sample, and the difference between the values of enthalpy for the two samples did not exceed 0.3 j/g or 0.03 percent, whichever is larger. The detailed results of individual runs are given in table 1. Measurements were often repeated at lower temperatures after experiments at higher temperatures without disclosing any evidence that significant permanent changes had occurred in the samples meanwhile.

896958—50——2

TABLE 1. *Corrected enthalpy values of individual experiments*

Temperature, t [a]	Measured heat		$(H_t-H_{0°C})$		
	Blank experiments	Experiments with sample	Observed	Calculated	Observed—Calculated
°C	*Abs j*	*Abs j*	*Abs j g*$^{-1}$	*Abs j g*$^{-1}$	
30.60	244.1	441.2	37.08	37.10	−0.02
	242.6	441.0			
	242.7	441.0			
	243.6	442.0			
59.00	474.1	862.4	72.64	72.61	+.03
	474.4	862.1			
	474.6	862.6			
	474.3	---			
77.00	622.7	1,135.4	95.86	95.87	−.01
	623.3	1,135.2			
	623.7	1,134.9			
94.00	764.5	1,398.1	118.52	118.52	.00
	765.9	1,399.0			
	765.3	1,399.0			
	---	[d] 1,479.2			
	---	[d] 1,479.8			
	---	[d] 1,479.1			
100.00	815.3	2,096.1	239.90	239.90	.00
	815.1	2,096.3			
	815.2	2,095.5			
	814.1	2,095.2			
	814.8	2,097.5			
	815.3	[d] 2,260.9			
	813.7	[d] 2,260.6			
	814.3	[d] 2,260.9			
	815.2	---			
	[b] 814.0	---			
	[b] 814.8	---			
	[b] 814.6	---			
150.00	1,241.2	2,889.0	308.48	308.47	+.01
	1,241.2	2,889.1			
	[c] 1,242.2	2,888.3			
200.00	1,676.8	3,682.2	375.84	375.95	−.11
	1,676.7	3,686.1			
	1,677.0	3,684.3			
	---	3,683.1			
300.00	2,570.7	5,284.6	508.41	508.03	+.38
	2,570.2	5,285.5			
	2,571.7	5,285.2			
	---	[d] 5,639.6			
	---	[d] 5,636.7			
	---	[d] 5,635.7			
	---	[d] 5,636.3			
400.00	3,498.7	6,904.1	636.87	637.09	−.22
	3,496.1	6,897.2			
	[b] 3,496.9	6,901.3			
	[b] 3,507.4	6,900.0			
	[b] 3,499.0	---			
	[b] 3,499.0	---			
500.00	4,449.1	8,529.3	764.02	764.05	−.03
	4,449.1	8,529.2			
	4,448.3	8,528.4			
600.00	5,422.3	10,175.7	889.97	889.82	+.15
	5,423.3	10,173.3			
	5,422.2	[d] 10,791 6			
	---	[d] 10,788.3			
	---	[d] 10,788.8			
699.5	6,421	11,840	1,014.5	1,014.7	−.2
	6,418	11,836			
	6,420	11,837			
	---	11,836			

See footnotes at end of table.

TABLE 1. *Corrected enthalpy values of individual experiments*—Continued

Temperature, t [a]	Measured heat		$(H_t-H_{0°C})$		
	Blank experiments	Experiments with sample	Observed	Calculated	Observed—Calculated
°C	*Abs j*	*Abs j*	*Abs j g*$^{-1}$	*Abs j g*$^{-1}$	
796.8	7,417	13,496	1,137.2	1,137.5	−.3
	7,420	13,492			
	7,417	13.491			
	[b] 7,423	---			
	[b] 7,420	---			
	[b] 7,422	---			
	[b] 7,420	---			
896.6	8,455	15,211	1,265.2	1.264.9	+.3
	8,458	15,211			
	8,454	15,210			
	[b] 8,458	[d] 16,083			
	[b] 8,453	[d] 16,080			
	[b] 8,453	---			
	[b] 8,448	---			
	[b] 8,449	---			
	[b] 8,449	---			
	[b] 8,452	---			

[a] International Temperature Scale of 1948 [5].
[b] On alternate container of same mass.
[c] Weighted less because of unsteady heat leak.
[d] On alternate container, containing 6.0297 g of sodium. The other container had the same mass but contained 5.3404 g of sodium.

No corrections for impurities were made, since these were believed to be much smaller than the accidental error. All weights were reduced to an in-vacuum basis. Small corrections were made to bring the results to a common basis at the listed temperatures. The values of enthalpy (H_t-H_0) given in table 1 are at the vapor pressure (saturation pressure). Small corrections were made for the thin oxide coatings that the containers acquired in the furnace, using published heat capacities of Fe and Fe_3O_4 [7]. In addition, in order to evaluate the heat capacity of the liquid alone, it was necessary to make small corrections at the highest temperatures for the heat given up in condensing the sodium vapor. These corrections, based on published vapor pressure data and the volumes of the vapor, amounted to about 0.03 percent of the enthalpy at the highest temperature. The total corrections of all kinds did not amount to more than 0.1 percent of the enthalpy.

The experimental values found for the enthalpy of sodium (at saturation pressure) in absolute joules per gram, are represented by the following empirical equations. H_0 is the enthalpy of the solid at 0°C, and t represents degrees C.

$$H_t \text{ (solid)} - H_0 \text{ (solid)} = 1.19926t + (3.247)\ (10^{-4})t^2 + (3.510)(10^{-6})t^3 \qquad (0° \text{ to } 97.80° \text{ C})$$

$$H_t \text{ (liquid)} - H_0 \text{ (solid)} = 98.973 + 1.436744t - 2.90244)\ (10^{-4})t^2 + (1.54097)\ (10^{-7})t^3 + 24000e^{-\frac{13600}{t+273}} \qquad (97.80° \text{ to } 900° \text{ C})$$

The last term of the latter equation (liquid) accounts for the difference between $H_t - H_0$ and the net heat measured. As shown by Osborne [10], this difference is equal to PV/m, where P is the vapor pressure of the sodium, V is the volume of the container, and m is the mass of sodium. In the temperature range investigated, this term reaches a maximum value of 0.02 percent at 900° C and is entirely negligible for the solid. These equations give 113.2 abs j/g as the heat of fusion at the triple point, 97.80° C.

After dropping the last term in the equation for the enthalpy of the liquid, the two preceding equations then give the measured heat differences along the saturation curve. Therefore their direct differentiation gives the heat capacities (C_s) under saturation temperature and pressure, as follows:

$$C_s \text{ (solid)} = 1.19926 + (6.494)\ (10^{-4})t + (1.0531)\ (10^{-5})t^2 \qquad (0° \text{ to } 97.80° \text{ C})$$

$$C_s \text{ (liquid)} = 1.43674 - (5.8049)\ (10^{-4})t + (4.6229)\ (10^{-7})t^2 \qquad (97.80° \text{ to } 900° \text{ C})$$

From these equations directly result the following equations for the entropy (also at saturation pressure), absolute joules g^{-1} deg K^{-1}, in excess of that at 0° C. T represents degrees Kelvin (taking 0° C=273.16° K).

$$S_T \text{ (solid)} - S_{273.16°K} \text{ (solid)} = 4.16241 \log_{10} T - (5.1036)\ (10^{-3})\ T + (5.2656)\ (10^{-6})\ T^2 - 9.14016 \qquad (0° \text{ to } 97.80° \text{ C})$$

$$S_T \text{ (liquid)} - S_{273.16°K} \text{ (solid)} = 3.75276 \log_{10} T - (8.3303)\ (10^{-4})\ T + (2.3112)\ (10^{-7})\ T^2 - 8.67398 \qquad (97.80° \text{ to } 900° \text{ C})$$

Values of enthalpy, heat capacity, and entropy calculated from these equations for rounded temperatures are listed in table 2.

TABLE 2. *Enthalpy, specific heat, and entropy of sodium*

Temperature, t	$H_t - H_{0°C}$	C_s	$S_T - S_{273.16°K}$
°C	abs j g^{-1}	abs j g^{-1} deg^{-1}	abs j g^{-1} deg^{-1}
0	0	1.1991	0
25	30.25	1.2221	.10590
50	61.21	1.2555	.20569
75	93.26	1.3071	.30116
97.80 (solid)	123.68	1.3636	.38581
[Melting	113.2	------	*.30510*]
97.80 (liquid)	236.86	1.3845	.69090
100	239.90	1.3832	.69906
200	375.95	1.3393	1.0222
300	508.03	1.3042	1.2757
400	637.09	1.2786	1.4832
500	764.05	1.2619	1.6590
600	889.82	1.2548	1.8121
700	1,015.3	1.2569	1.9481
800	1,141.6	1.2682	2.0715
900	1,269.4	1.2887	2.1853

V. Determination of the Triple Point and the Temperature Change During Melting

In order to measure the triple point and the amount of impurities (liquid-soluble, solid-insoluble) in the sodium, a resistance thermometer (60 ohms of No. 40 enameled copper wire) was wound directly around the lower half of the sample container used in most of the enthalpy measurements. This container was raised into the furnace, and the copper resistance thermometer was then calibrated at 94° and 100° C against the platinum resistance thermometer located in the silver cylinder (K). Starting with this container and the furnace at equilibrium at 94° C, the container was heated adiabatically using the copper resistance thermometer as an electric heater and raising the temperature of the furnace at about the same rate. After an appropriate time interval the electric power was turned off, and

the container was allowed to come to a constant temperature, which was observed by the copper resistance thermometer. This cycle was repeated about 20 times, using electric power of one-fourth watt over a total heating period of 90 min. It was therefore possible to observe the relation between the temperature of the sodium and the fraction that had melted.

The temperature and fraction of the sample melted were consistent with Raoult's law within the precision of the measurements, and indicated the triple point of the sample to be 97.792° C and that of pure sodium to be 97.80°. This triple-point lowering corresponds to a liquid-soluble, solid-insoluble impurity of 0.000016 mole/gram-atom of sodium. The freezing point of pure sodium at 1-atm pressure is calculated to be 97.81° C.

VI. Effect of Mechanical State of the Solid

E. Griffiths [9] claimed that he found reproducible changes in the heat capacity of crystalline sodium amounting to as much as 1.5 percent, depending on whether in its previous heat treatment, the sample had been "quenched" or "annealed". Similar tests were made by the authors on the two sodium samples reported here, and with conditions of quenching and annealing somewhat more extreme than employed by Griffiths. The furnace temperatures used were chosen to cover the temperature range where he found the greatest difference. The results are summarized in chronological order in table 3.

The first set of experiments (Set 1) was made after freezing slowly over an interval of 1 hr and then cooling at the rate of about 5 deg/hr. Preceding the experiments in Set 2 and on the same day, the molten sample was quenched by putting its container into a tube immersed in ice. The treatments before Sets 3 and 4 were respectively similar, except that the annealing carried out on the day preceding Set 3 involved freezing the sample over a period of 3 hr and then cooling the solid to room temperature at a rate varying from 3 to 5 deg/hr. Before observing Set 5, the sample was remelted and requenched by immersing its container directly into a dry ice-acetone bath (−78° C). It was then kept at this temperature overnight until just before the experiments.

Table 3. *Experiments to determine the reproducibility of the mechanical state of solid sodium*

Set No.	Temperature t	Mass of Na in sample	Prior heat treatment	Measured heat (Na and container)	
				Individual experiment	Mean of set
	°C	g		abs j	abs j
1	59.00	5.3404	Annealed	860.7 861.7 863.4 862.2	862.0
2	59.00	5.3404	Quenched	864.5 862.7 863.2	863.5
3	39.90	6.0297	Annealed	619.2 615.8 616.0 616.7 617.9	617.1
4	39.90	6.0297	Quenched	616.3 616.8 616.0	616.4
5	39.90	6.0297	Requenched rapidly by dry ice	614.4 616.2 615.2 616.5	615.6

The results tabulated in table 3 indicate that the quenching and annealing treatments did not change the heat capacity of the sodium by more than 0.2 percent and that these changes seem to be accidental and within the precision of the measurements.

VII. Reliability

An index to the reproducibility, or "precision", of the enthalpy measurements is afforded by the deviations from the mean, as shown by the results of the individual measurements shown in table 1. Another index is provided by the deviations (also listed in table 1) from the smoothed values given by the empirical equations adopted. All the results for liquid sodium lead to a probable error of the mean of from 0.01 to 0.03 percent on enthalpy (depending on the temperature), and as much as 0.3 percent on the derived heat capacity values, with a somewhat increased uncertainty below 200° and above 800° C because of the difficulty of determining the derivative of an empirical function accurately near its ends. For solid sodium, the relative uncertainties become considerably greater at the low temperatures, owing to the inability to determine heats by the ice calorimeter with a precision of better than 0.4 j.

In addition, all factors suspected of contributing appreciable systematic errors were analyzed to determine their likely contributions. Direct comparisons between the platinum resistance thermometer and the platinum-rhodium thermocouple up to 600° indicated differences in temperature of from 0.0 to 0.2 deg. Calculations indicated that errors due to the very small temperature gradients inside the silver cylinder in the furnace were entirely negligible. As far as uncertainties in measuring the temperatures on the International Temperature Scale are involved, the resulting probable error [2] in the enthalpy is thought to be only about 0.02 percent between 100° and 600°, and perhaps three times this much at 900°, where it was necessary to resort to measurement using a thermocouple. As a consequence, the probable error in the heat capacity due to uncertainty in temperature measurement may be considered to lie within 0.03 percent from 100° to 600°, but may reach 0.2 percent at 900° C.

In case the sample contained 0.01 percent by weight of oxygen as sodium oxide, as discussed earlier in this report, the error in enthalpy or heat capacity due to its gradual deposition from solution as the temperature fell might be as much as 0.05 percent. A similar error would be present if the liquid sodium dissolved appreciable amounts of the steel container; but recent measurements on the solubility of iron in liquid sodium by L. F. Epstein [8], of the Knolls Atomic Power Laboratory, indicate a solubility at 900° C of 22 parts per million, which would lead to negligible error in the present measurements. The analysis of the difference between the heat lost, during the drop into the calorimeter, by the sample container and by the empty container, showed that this effect, greatest at the highest temperatures, might lead to errors of 0.03 percent on enthalpy and 0.1 percent on heat capacity at 900°. Taking due consideration of the sources of error mentioned and other less significant ones, the authors believe that the probable error of the enthalpy values of sodium reported here may be considered to be between 0.1 and 0.2 percent (except below 100°, as mentioned above), whereas the probable error of the heat capacity was similarly estimated to be between 0.3 and 0.4 percent.

One experimental check on the over-all accuracy of the apparatus in measuring enthalpy was made by measuring the heat delivered to the ice calorimeter by a Monel capsule containing water and dropping from 250° C. By thus determining in several measurements the difference in heats for two amounts of water differing by about 6 g, a value of 1042.05 abs j/g for $\alpha]_0^{250°}$ of water, defined elsewhere [10], was obtained. This figure differs by only 0.02 percent from the value of 1041.85 published in the latest report [11] on the thermal properties of water as accurately measured earlier in this laboratory with an adiabatic calorimeter.

The value found for the triple point is considered to have a probable error of 0.03 deg, dependent mostly on the uncertainty in the calibration of the copper resistance thermometer used for the measurements. A probable error of 0.3 percent is assigned to the heat of fusion. This figure is based on the estimated reliability of the enthalpy values in the neighborhood of the triple point. If all the impurity indicated by the measured melting curve were actually in liquid solution at 94°, then 0.25 percent of the sample was liquid at this temperature. In that case, the value of the enthalpy of the solid given in table 1 would be 0.2 j/g too high due to this effect, making the calculated heat of fusion 0.3 j/g too low.

VIII. Comparison with Results of Other Investigations

A number of other investigators [9, 12, 13, 14, 15, 16, 17] have made measurements of the heat capacity of solid and liquid sodium above 0° C, and most of these are shown for comparison in figure 3, where the full-line curves represent the values of the present investigation as given by the equations presented earlier in this paper. Each experimental point (NBS) given for the liquid in figure 3 was calculated from two adjacent observed enthalpies given in table 1. Rengade's [12] measurements, which made use of an ice calorimeter, extended from 15° to 100°, and although he stated that his sample was not very pure, his precision amounted to about 0.2 percent. Griffiths [9] employed a dynamic method and covered the range 0° to 140°, claiming a

[2] "Probable error" as used in the remainder of this paper includes the authors' estimate of certain systematic errors. To each factor subject to error, there was assigned a figure such that it was believed that the actual error was as likely greater as smaller than this figure. These figures were then combined statistically to yield an over-all probable error in the given experimental quantity.

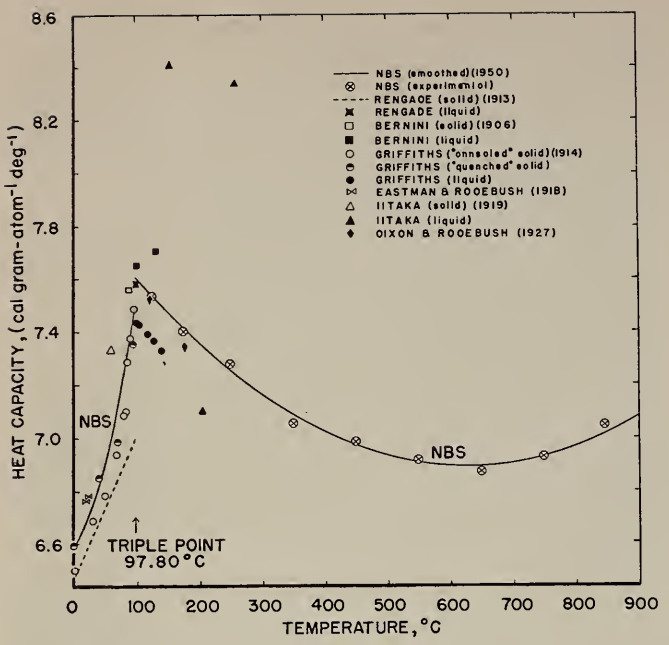

FIGURE 3. *Comparison of heat-capacity values.*

reproducibility of better than 0.1 percent, except for the variation of about 1.5 percent on the solid caused by varying the heat treatment, as mentioned above. Eastman and Rodebush's [13] measurements were mostly at low temperatures, but afford a comparison at 20° C. Iitaka [14] made determinations of the heat capacity of the liquid between 125° and 290°, the latter being the highest temperature attained prior to the present investigation. He dropped his samples from a furnace into his calorimeter and took due precaution to avoid certain systematic errors, but his precision was not better than several percent, and it will be noted from the graph that his values for heat capacity are considerably higher

TABLE 4. *Values for the melting point and heat of fusion of sodium*

Source	Melting point	Heat of fusion
	°C	*abs j g⁻¹*
This investigation	97.81±0.03	113.2
Ladenburg and Thiele [18]	97.8 ±0.1	----------
Edmondson and Egerton [19].	97.7	----------
Tammann [18]	97.8	----------
Griffiths [9]	97.61	115.35 (113.4, less accurate)
Bridgman [20]	97.63	125.5
Rengade [12]	97.90	----------
Bernini [11]	97.63	74.5
Iitaka [14]	----------	108.8
Joannis [16]	----------	132.6

than those of the other investigators. Dixon and Rodebush [15] made measurements with a precision of about 1 percent, from 121° to 178°. Their method consisted in measuring the adiabatic temperature-pressure coefficient, and seems to have been subject to experimental difficulties due to the high thermal conductivity of the sodium.

The values reported for the melting point and heat of fusion of sodium are given in table 4. These melting point values in themselves are not, of course, a reliable criterion of the relative purity of the various samples used.

IX. Discussion of Results

The values of the heat capacity of sodium reported herein have practical importance, inasmuch as they cover the temperature range between 0° and 300° C with greater accuracy and precision than has been the case heretofore, and in addition extend the measurements to much higher temperatures, where experimental values for sodium have been entirely lacking until now. At the same time these values should be of considerable theoretical interest, since the extensive interest in the structure and properties of the liquid state in recent years has led to the theoretical calculation of the heat capacity of certain liquids, including sodium, whereas accurate experimental measurements on liquid metals have been relatively very meager.

The accuracy of the results given in this report is sufficient to show clearly the trends of the heat capacity curves of sodium with temperature, both below and above the triple point. The fall of the liquid curve to a minimum, a phenomenon in contrast to the steady rise with temperature for the great majority of liquids, is by no means unique in the case of metals, being paralleled by the heat capacity of mercury [21]. The entropy of fusion of sodium, 7.03 j deg^{-1} gram-atom^{-1}, is one of the lowest values for metals. According to current theories, the metal does not acquire complete randomness on melting, and the increased heat capacity of the liquid over what it displays at much higher temperatures is to be attributed to a further absorption of "communal" entropy above the melting point. Taking the values of the present investigation and extrapolating linearly to the melting point that part of the curve (fig. 3) above 700°, it was calculated

that the excess heat capacity between the triple point and 600° is equivalent to an entropy increase of 1.3 j deg^{-1} gram-$atom^{-1}$, a figure of the right order of magnitude to be explained in this way.

It has been pointed out further that the increase of heat capacity of the solid alkali metals with increasing temperature is enhanced in the regions of temperature just below the respective melting points, and this has been attributed to an acquisition of a part of the randomness, most of which occurs in fusion. The equation which Rengade [12] gave for the heat capacity of solid sodium from 15° to the melting point, being linear with temperature, does not of course show this feature. The equation found for the solid in this investigation, however, does have the sign of curvature just referred to, and so in this respect is at variance with an unmodified Debye function above the characteristic temperature.

Aside from any theoretical explanation of its approximate values, the heat capacity of liquid sodium is, as is well known, one of the determinants of the curvature of the vapor-pressure curve. Ladenburg and Thiele [18], in a critical evaluation of numerous vapor-pressure data of sodium, were forced to assume an average heat capacity of the liquid. Although their calculations are based on an approximate partition function for the vapor which is not accurate at these temperatures, the effect of this on the vapor pressures is probably relatively small, and they were able to show that for the range 100° to 500° C an average heat capacity of liquid sodium of 1.326 j g^{-1}, deg^{-1}, based on the measurements of Dixon and Rodebush [15], have better agreement with the vapor-pressure data and theoretically calculated "chemical constant" than a value of 1.452, the latter being Iitaka's [14] mean value. The results of the present investigation lead to an average heat capacity of 1.310 in this temperature interval.

X. Summary

The enthalpy of sodium has been measured in the range 0° to 900° C and with an accuracy of 0.1 to 0.2 percent over most of the range. Values of heat capacity are derived from the enthalpy values with an accuracy of 0.3 to 0.4 percent over most of the range. The triple point of sodium was shown to be 97.80°±0.03° C, whereas the heat of fusion is 113.2±0.4 abs j/g.

This investigation was made possible by the splendid cooperation of the Knolls Atomic Power Laboratory, Schenectady, N. Y., in preparing the samples and developing techniques of handling and sealing the samples without changing the mass of the containers. For this assistance, the authors are particularly indebted to Clifford Mannal and William D. Davis, who planned and supervised the work; and to William A. Ruggles, who was responsible for filling, sealing, and testing the sample containers.

XI. References

[1] R. J. Bondley, G. E. Research Laboratory Report No. RL–269.
[2] D. C. Ginnings and R. J. Corruccini, J. Research NBS **38,** 583 (1947) RP 1796.
[3] D. C. Ginnings and R. J. Corruccini, J. Research NBS **38,** 593 (1947) RP 1797.
[4] D. C. Ginnings and R. J. Corruccini, J. Research NBS **39,** 309 (1947) RP 1831.
[5] H. F. Stimson, J. Research NBS **42,** 209 (1949) RP 1962.
[6] International Critical Tables **5,** 234 (McGraw-Hill Book Co., New York, N. Y., 1929).
[7] K. K. Kelley, Contributions to the data on theoretical metallurgy. II. High-temperature specific-heat equations for inorganic substances. Bureau of Mines Bulletin 371. (U. S. Government Printing Office, Washington 25, D. C., 1934).
[8] Private communication.
[9] Ezer Griffiths, Proc. Roy. Soc. (London) **A89,** 561 (1914).
[10] N. S. Osborne, BS J. Research **4,** 609 (1930) RP168.
[11] N. S. Osborne, H. F. Stimson, and D. C. Ginnings, J. Research NBS **23,** 261 (1939) RP 1229.
[12] E. Rengade, Compt. Rend. **156,** 1897 (1913).
[13] E. D. Eastman and W. H. Rodebush, J. Am. Chem. Soc. **40,** 489 (1918).
[14] I. Iitaka, Sci. Reports Tohoku Imp. Univ. (Sendai) **8,** 99 (1919).
[15] A. L. Dixon and W. H. Rodebush, J. Am. Chem. Soc. **49,** 1162 (1927).
[16] A. Joannis, Ann. Chim. Phys. [7] **12,** 358 (1887).
[17] A. Bernini, Physik. Z. **7,** 168 (1906).
[18] R. Ladenburg and E. Thiele, Z. physik. Chem. **B7,** 161 (1930).
[19] W. Edmondson and A. Egerton, Proc. Roy. Soc. (London) **A113,** 521, 533 (1927).
[20] P W Bridgman, Phys. Rev. **3,** 153 (1914).
[21] T. B. Douglas, Anne F. Ball, and D. C. Ginnings, J. Research NBS (publication pending).

Washington, July 8, 1949.

U. S. GOVERNMENT PRINTING OFFICE: 1950

For sale by the Superintendent of Documents, U. S. Government Printing Office
Washington 25, D. C. - Price 10 cents

Journal of Research of the National Bureau of Standards Vol. 46, No. 3, March 1951 Research Paper 2191

Calorimetric Properties of Diphenyl Ether From 0° to 570°K

George T. Furukawa, Defoe C. Ginnings, Robert E. McCoskey, and Raymond A. Nelson

The heat capacity, enthalpy, and entropy of diphenyl ether from 0° to 570° K are calculated from experimental heat capacities obtained by using an adiabatic vacuum calorimeter and a Bunsen ice calorimeter. The heat of fusion and the triple-point temperature are given as 17,216 ±17 absolute joules mole^{-1} and 300.03 ±0.01° K, respectively. Heat of combustion experiments in a bomb calorimeter gave the value −6,135.64 ±0.88 absolute kilojoules mole^{-1} for the standard heat of combustion of the liquid at 30° C. The standard heats of combustion and formation are computed for both liquid and solid at 25° C. The standard entropy and Gibbs free energy of formation for the solid at 25° C are given as −590.1 ±0.5 absolute joules deg^{-1} mole^{-1} and 143.8 ±0.9 absolute kilojoules mole^{-1}, respectively.

I. Introduction

Frequently in calorimetry it is desirable to have access to standard substances whose thermal properties are accurately known to calibrate and test calorimeters under conditions of actual use. Water has been used quite extensively as a standard substance in heat capacity and latent heat of vaporization calorimeters, but it has a relatively limited temperature range of application due to its rather rapid vapor pressure increase above 100° C and its large change in volume on freezing. Often the choice of a standard is dictated by the calorimeter design, consequently there should be a number of standards from which to select the most suited. In heat-capacity calorimetry, as well as in other types of calorimetry, the basic requirements for any standard substance are high chemical stability; high purity, which can be attained and retained easily; reproducibility of physical state; and easy manipulation in the calorimetric apparatus. It is advisable to test heat capacity calorimeters under conditions such that the heat capacity of the calorimetric system is closely the same whether it contains the standard material or the test material. If a standard of high heat capacity per unit volume is available, this condition can be met easily by adjusting its quantity in the calorimeter.

Diphenyl ether has been known to be relatively stable and to be obtainable in a high state of purity by fractional distillation followed by crystallization. As this material melts close to room temperature, it is being developed at this Bureau for use in triple-point cells, as a thermostatic medium at its melting point and in a modified Bunsen calorimeter. The accurate measurement of the thermal properties of diphenyl ether is desirable for these applications as well as for improvement in design of high-temperature heat-transfer equipment in which diphenyl ether is being used in the form of diphenyl-diphenyl ether eutectic mixture.

The heat capacity of diphenyl ether was measured between 18° and 573° K, using two calorimeters widely different in design. An adiabatic vacuum calorimeter was used from 18° to 360° K, and a "drop" method was used from 273° to 573° K with an accurately thermostated furnace and an improved Bunsen ice calorimeter. The two methods overlap in the temperature range between 273° to 360° K, where they serve to check each other. The triple point and heat of fusion were measured in the adiabatic vacuum calorimeter. An isothermal jacket water calorimeter was used for the determination of heat of combustion.

II. Low-Temperature Calorimetry

1. Apparatus

The melting-point studies and heat-capacity measurements from 18° to 360° K were made with an adiabatic vacuum-type calorimeter essentially the same as that described in the paper on 1,3-butadiene by Scott, et al [1].[1] Briefly, the apparatus and procedure were as follows. The diphenyl ether, freed of air and water, was sealed in a copper container, which in turn was suspended inside an evacuated adiabatic shield system. The copper sample container had a volume of about 60 ml and was provided with a central well for a thermometer and heater. For rapid dissipation of heat to the sample, copper vanes radiated out from this well. No part of the sample was more than 2 mm from the copper vanes. A thin coating of pure tin was applied to the inner surfaces of the container to provide an inert surface to the sample and to solder the vanes in place. The outer surface of the container, as well as the adjacent surface of the adiabatic shield, were polished to cut down the effect of heat transfer by radiation. The heat transfer by convection was made negligible by pumping the vacuum space to 10^{-5} mm Hg or better. During an experiment the shield temperature was kept, at all times, equal to that of the sample container surface by controlling the shield heaters, using constantan-chromel *P* thermels to integrate surface temperatures. One set of three-junction thermels and another of two-junction thermels were used. In the melting-point studies and heat-capacity experiments, the electrical energy introduced into the sample and container was determined by means of a precision potentiometer in conjunction with a volt box and a

[1] Figures in brackets indicate the literature references at the end of this paper.

standard resistor. The time was measured by using a precision interval timer operated on standard 60 cycles furnished by the Radio Section of this Bureau. This timer was compared periodically with time signals from the Time Section and found not to vary by more than 0.02 sec for any heating period, which was never less than 2 min. The initial and final temperatures of a heating interval were measured by means of a platinum resistance thermometer and a G–2 Mueller bridge. The platinum resistance thermometer was calibrated at this Bureau above 90° K on the International Temperature Scale [2] and between 10° to 90° K on a provisional scale [3], which consists of a set of platinum resistance thermometers calibrated against a gas thermometer. The resistance of the thermometer was frequently checked at the ice point, and the small fluctuations observed were too insignificant to affect the results of the measurements. The volt box, standard resistor, potentiometer, and bridge were calibrated recently at this Bureau.

2. Purity and Triple-Point Temperature

The diphenyl ether used in this investigation was purified by F. L. Howard of this Bureau by means of a fractional distillation followed by 25 fractional crystallizations. A portion of this diphenyl ether was treated by the following procedure in order to remove the dissolved air and water. The material was slowly frozen in a glass bulb during evacuation; then after melting, this process was repeated. After distilling the sample completely into a second bulb, the process of slow freezing while evacuating was repeated again. A portion (36.7724 g in vacuum) of this sample was transferred to the copper container by gravity, and the container was sealed with solder.

The purity of this air-free diphenyl ether was determined calorimetrically from the melting-point studies. In this method the equilibrium temperatures are measured at various increasing liquid-solid ratios as determined from the electric energy input, heat of fusion, and heat capacity of the system. The experimental data are treated on the assumption that Raoult's law is obeyed and no solid solution is formed in the concentration range under investigation. The simplified equation, $N_2=A\Delta T$, is used to represent the relation between mole fraction impurity, N_2, and the depression, ΔT, of the triple point. The cryoscopic constant, A, is calculated from $A=L_f/RT_t^2$, where L_f is the heat of fusion, R the gas constant and T_t the triple-point temperature. The observed equilibrium temperatures are plotted against $1/F$, the reciprocal of the fraction of material in the liquid state. This curve is extrapolated to $1/F=0$ to obtain the triple point of the pure substance, and the slope of this curve is multiplied by the cryoscopic constant to obtain mole fraction impurity.

The purity of diphenyl ether was determined before and after the heat-capacity measurements to ascertain whether any chemical change had taken place under the conditions inside the calorimeter

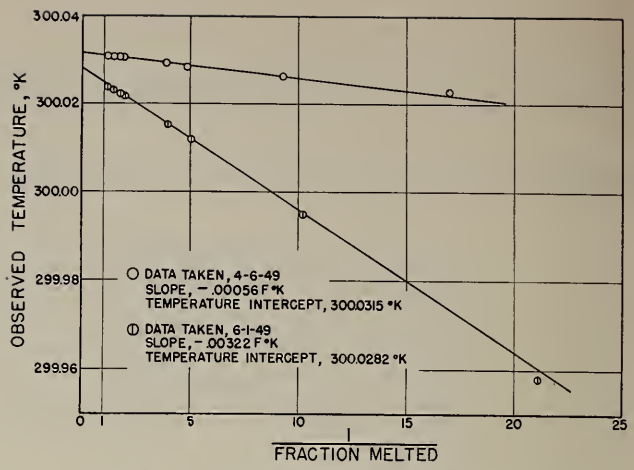

FIGURE 1. *Melting curves of diphenyl ether.*

sample container. Table 1 and figure 1 show the results of these measurements. Although the inside of the container is completely covered with pure tin, which is considered to be inert, the results show that the liquid soluble-solid insoluble impurity has increased from 0.000013 to 0.000074 mole fraction. This is rather surprising compared to only 0.00002 mole fraction increase indicated in the high-temperature measurements mentioned in a later section. Perhaps the inner surface of the sample container used with the adiabatic calorimeter has a catalytic effect on the decomposition of diphenyl ether even as low as 360° K. As the absolute purity is still high, the impurities would have only a negligible influence on the heat capacities.

TABLE 1. *Melting points of diphenyl ether*

$N_2=0.0230\ \Delta T$

Before the heat-capacity measurements		
$1/F$	$T_{obs.}$	$T_{calc.}$
17.01	300.0231	300.0219
9.33	300.0264	300.0262
4.90	300.0285	300.0287
3.93	300.0292	300.0293
2.01	300.0308	300.0304
1.79	300.0306	300.0305
1.50	300.0306	300.0307
1.26	300.0308	300.0308
1.00	--------	300.0309
Temperature intercept, 300.0315°K. Impurity, 0.000013 mole fraction.		
After the heat-capacity measurements		
$1/F$	$T_{obs.}$	$T_{calc.}$
21.11	299.9581	299.9603
10.25	299.9951	299.9952
5.08	300.0122	300.0118
4.02	300.0154	300.0153
2.00	300.0219	300.0217
1.79	300.0223	300.0229
1.50	300.0231	300.0234
1.27	300.0240	300.0241
1.00	--------	300.0250
Temperature intercept, 300.0282°K. Impurity, 0.000074 mole fraction.		

The difference in the two temperature intercepts, 300.0315° and 300.0282° K,[2] amounting to 3.3 mdeg is believed to have been caused by small changes in the resistance thermometer and bridge between periods of the measurements. This change, however, does not affect the slope of the melting curve, as it only causes a parallel displacement in temperature. For a given set of measurements the temperatures agreed to within a few tenths of a millidegree. Considering the calibration uncertainties in the bridge and platinum resistance thermometer and uncertainty in the absolute temperature scale, the triple point of diphenyl ether is taken to be 300.03±0.01° K.

The third column of table 1 gives temperatures obtained from the equation $T_t - T_{\text{calc}} = N_2/AF$. Here N_2 is the mole fraction impurity calculated from the experimental data. The relation between the results in the second and third columns shows that Raoult's law was followed quite closely. The value of the cryoscopic constant A used in all the calculations is 0.0230 deg^{-1}.

3. Heat of Fusion

The latent heat of fusion of diphenyl ether was determined by adding electric energy continuously from a temperature a few degrees below the triple point to a temperature above the triple point. The quantity of energy was corrected for the heat capacity of the material plus the container on both sides of the triple point and for a small amount of premelting caused by the presence of impurities. The heat of fusion was determined soon after the first purity measurements, thus the premelting corrections have been calculated on the basis of 0.000013 mole fraction impurity. The results and corrections are tabulated in table 2. $\int CdT$ is the sum of the heat capacity corrections above and below the triple point. The mean value obtained for three determinations is 17,216 abs j mole^{-1}, and the mean deviation is ±2 abs j mole^{-1}. Considering the arbitrariness involved in the heat-capacity correction a probable error[3] of ±0.1 percent is assigned. The value for the heat of fusion is taken as 17,216 ±17 abs j mole^{-1}.

TABLE 2. *Heat of fusion of diphenyl ether*

Mole weight, 170.20 g; mass of sample, 36.7724 g

Defined calorie=4.1840 abs j.

Temperature interval	Total energy	$\int CdT$	Premelting correction	L_f
°K	*abs j*	*abs j*	*abs j*	*abs j*
298.4668 to 305.2408	4357.49	639.47	1.34	3719.36
296.1288 to 303.6634	4404.12	685.48	0.54	3719.18
295.5214 to 303.0956	4401.96	682.00	.30	3720.26
Mean				3719.60
Mean deviation				±0.44
Heat of fusion	101.152±0.012[a] abs j g^{-1}			
	17,216 ±2[a] abs j mole^{-1}			

[a] These values are mean deviations.

4. Heat Capacity

The heat capacity of the diphenyl ether sample (36.7724 g mass) plus the container was measured from 18° to 360° K in the adiabatic vacuum calorimeter. Between 18° and 80° K solid and liquid hydrogen were used to cool the material and above 80° K liquid air, solid carbon dioxide, and ice were used. During heat-capacity experiments in the temperature range 18° to 30° K, where the heat-capacity curve changes rapidly in slope, the temperature change per heating interval was about 2 deg. The interval was increased to 4 or 5 deg up to 100° K, and above this temperature intervals of 6 to 10 degrees were used.

Nine series of experiments were made on the full container in the solid range, and the temperature ranges covered were 20° to 98° K, 15° to 29° K, 13° to 100° K, 88° to 234° K, 215° to 295° K, 125° to 295° K, 105° to 216° K, 90° to 105° K, and 101° to 205° K. Five series of experiments in the liquid range consisted of the following temperature ranges: 302° to 367° K, 304° to 370° K, 305° to 367° K, 303° to 320° K, and 321° to 348° K. Six series of experiments were made on the empty container, and the temperature ranges were 13° to 35° K, 15° to 31° K, 28° to 60° K, 90° to 370° K, 50° to 119° K, and 279° to 342° K. Curvature corrections were applied to these measurements wherever significant, using the relation given by Osborne, et al. [4]:

$$Z_{T_m} = Q/\Delta T - \left(\frac{\partial^2 Z}{\partial T^2}\right)_{T_m} \frac{\Delta T^2}{24} \cdots \qquad (1)$$

Z_{T_m} is the corrected heat capacity at the mean temperature, T_m, of the interval ΔT; Q is the electrical energy added; and $(\partial^2 Z/\partial T^2)_{T_m}$ is the second derivative of the heat capacity with respect to temperature at T_m. The observed results (corrected for curvature) were plotted on a large scale as deviations from an approximate empirical equation and a smooth curve was drawn through the deviation points. The smooth deviation curve and the empirical equation were then used to obtain smoothed heat capacities at equally spaced integral temperatures. Similar heat-capacity experiments were made with the empty container, and the results were treated in the same manner. The weight of the container was different for the experiments with and without the sample. This arose from small differences in the weights of the copper filling tube and solder for the two experiments. Corrections for these differences in weights were applied to the smoothed heat capacities for the empty container from known heat capacities of copper and solder. The deviations of experimental

[2] All temperatures expressed in degrees Kelvin were obtained from the relation °K=°C+273.1600.

[3] For these experiments a true probable error cannot be statistically computed. The values given are estimates arrived at by examining contributions to the inaccuracy from all known sources, and they are to be considered (unless stated otherwise) as the authors' best estimate of the error, which is just as likely to be exceeded as not.

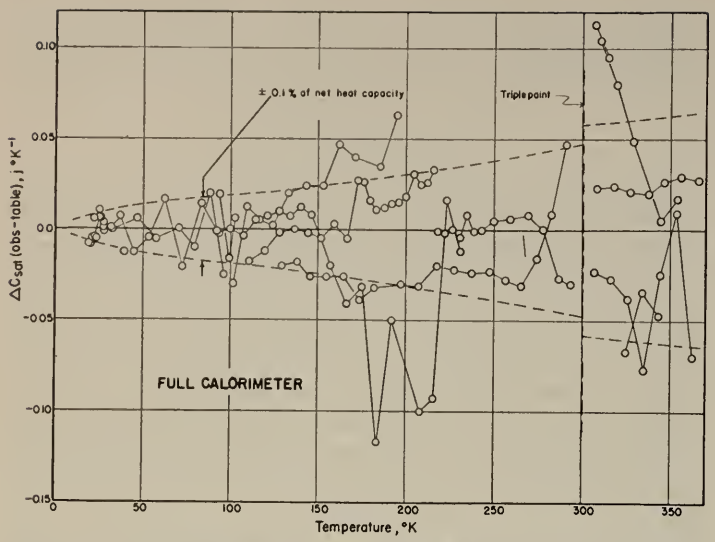

FIGURE 2. *Deviations of experimental heat capacities (corrected for curvature) from smoothed values for the container plus diphenyl ether.*

The experiments in a single series of measurements are connected by lines.

heat capacities from the smoothed values for the full and empty container are shown in figures 2 and 3. Most of the points lie within 0.1 percent of the net heat capacity. The net heat capacities were calculated, using the equation given by Hoge [5],

$$C_{\text{sat.}}=\frac{Z_2-Z_1-T\frac{d}{dT}\left[\frac{dp}{dT}(V-mv_c)\right]}{m/M}, \qquad (2)$$

where Z_2 and Z_1 are the tabulated heat capacities for the full and empty container, respectively, at the same temperature T; p is the vapor pressure; m is the mass of sample; M is the molecular weight of diphenyl ether; V is the volume of the container; and v_c is the specific volume of the condensed phase. The term involving the vapor correction was not actually used, for it does not contribute significantly to the results obtained with the low-temperature adiabatic calorimeter. At 360° K this vapor correction amounts to only 0.002 percent. The values of heat capacity listed in table 4 from 18° to 300° K are those obtained from these calculations. The heat-capacity values below 18° K in this table were obtained by extrapolation, using the Debye equation,

$$C_{\text{sat.}}=59.91D\left(\frac{112}{T}\right), \qquad (3)$$

fitted to the heat capacity at 18°, 20°, and 22° K. The values tabulated between 300° and 360° K were obtained by adjusting the slight differences between the results with the low-temperature adiabatic calorimeter and the ice calorimeter. The method of adjustment is discussed in a later section.

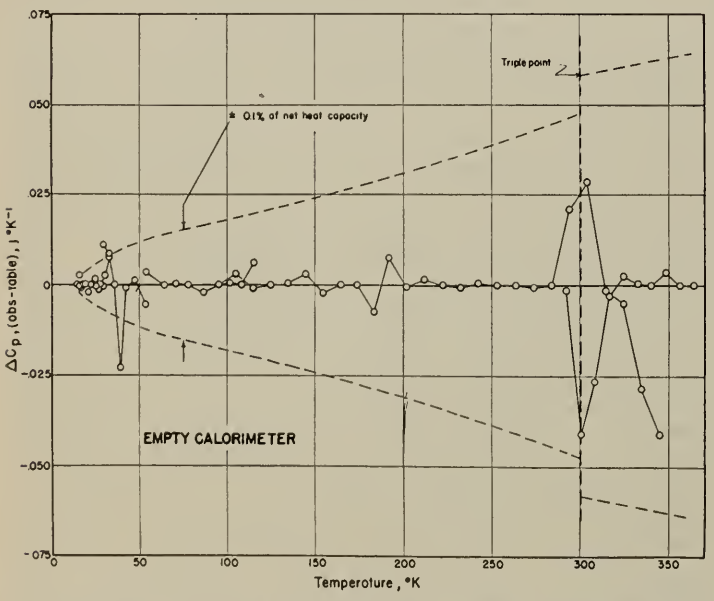

FIGURE 3. *Deviations of experimental heat capacities (corrected for curvature) from smoothed values for the empty container.*

The experiments in a single series of measurements are connected by lines.

5. Reliability of Heat-Capacity Results Obtained With the Low-Temperature Adiabatic Calorimeter

The precision of the heat-capacity experiments is shown in figures 2 and 3 of the previous section, in which the results (corrected for curvature) of the individual measurements are plotted as deviations from smoothed heat-capacity values for sample plus container and for container alone. As the experiments were made over a wide temperature range instead of a series of experiments over the same temperature interval, it is believed that a statement of average deviation is misleading in this situation. The conditions, particularly the heating rate, in the calorimeter were made as close as possible in the two series of experiments, so that certain systematic additive errors would cancel out. As a further check, the heat-capacity experiments were made at heating rates of 0.9 and 1.5 deg/min. Under these conditions large heat leaks dependent upon heating rate should be detectable, but the results obtained with the two heating rates showed no obvious differences on the large-scale deviation plot. In the two sets of measurements, although precaution was taken to install the sample container in the same position within the adiabatic shield system, it is possible that there were some differences in the positioning of the thermels and leads. Any error from this source is indeterminate, but it is believed that the probable error is not greater than ±0.05 percent.

The effect of impurities on the heat-capacity results is considered to be negligible.

Upon consideration of the above uncertainties the probable error of ±0.2 percent is assigned to the heat-capacity values above 50° K in table 4. Below 50° K the accuracy is less, increasing to about 1 percent at 18° K.

III. High-Temperature Calorimetry

1. Method and Apparatus

The enthalpy measurements at higher temperatures, which supplement the heat-capacity measurements made from 18° to 360° K, covered the range 273° to 573° K (0° to 300° C). These were carried out by essentially the same method and apparatus as used previously in measurements on sodium up to 900° C [6]. In brief, the method is as follows. The sample, sealed in its container, is suspended in a furnace until it comes to the chosen constant temperature, as measured by a platinum resistance thermometer. It is then dropped into a Bunsen ice calorimeter, which measures the heat evolved by the sample plus container in cooling to 0° C. A similar experiment is made with the empty container at the same temperature. The change in enthalpy of the sample between 0° C and the temperature in the furnace is computed from the difference in the two values of heat. The heat capacity can be derived from enthalpy values of the sample so determined for a series of temperatures.

The sample was taken from the same supply as that used in the low-temperature measurements. A sample of about 8 g of the solid was melted and transferred to a monel container (volume, about 11 ml), which was similar to the container used in earlier measurements on *p*-xylene [7]. In order to remove most of the air and water in the sample, the container was heated to about 100° C while evacuating the space above the sample. The method of sealing the container while still evacuating is shown in figure 4. One end of the container is made with a threaded projection, which can be temporarily sealed to a connecting fitting by means of a tin gasket, *C*. The container can be evacuated and filled through the filling tube, *B*. The actual sealing of the container is at the gold gasket, *D*, which is attached to the bottom end of the monel screw insert. Rotation of the screw insert for sealing is accomplished by the screw driver, *A*, which is sealed from the atmosphere by a packing not shown. In this way, it is possible to retain all the advantages of a valve with a packing, but reduce the mass and thereby the heat capacity, of the sealed container to a minimum. Also, the mass of the metal container is definite and not dependent on a soldered seal, as in the low temperature adiabatic calorimeter.

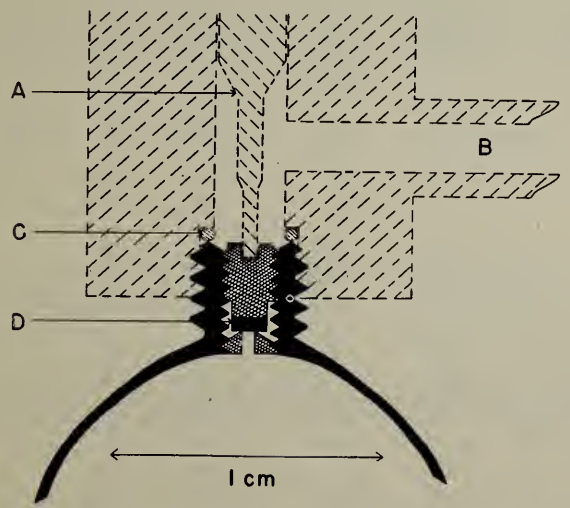

FIGURE 4. *Filling device and the seal for the capsule.*

A, Screw driver; B, filling tube; C, tin gasket; D, gold gasket.

2. Results

The results of the individual experiments are given in columns 2 and 3 of table 3. The measured heats listed are obtained from the mass of mercury drawn into the ice calorimeter, using the calorimeter calibration factor [6] of 270.46 abs j/g of mercury.

About 100 measurements were made, of which 56 were made with 7.8152 g (in vacuum) of sample in the container and the remainder with the empty container. The diphenyl ether was found to be solidified at 0° C in all experiments. Hence, every enthalpy calculated from a drop experiment starting with the liquid includes the heat of fusion. The sample was initially in the liquid state in all experiments except a few at furnace temperatures of 25.00° and 26.60° C (just below the triple point). In these experiments, the sample was solidified by dropping into the ice calorimeter prior to holding the solid sample in the furnace. By also making experiments with the supercooled liquid at the same temperatures as with the solid, there was obtained by differences the heats of fusion of 17,059 and 17,071 abs j mole^{-1} at 25.00° and 26.60° C, respectively. Upon extrapolation to the triple point, 26.87° C, using the heat capacities of solid and liquid found with the low-temperature adiabatic vacuum calorimeter, these values yield respectively 17,154 and 17,085 for the heat of fusion at the triple point. These values are lower by 0.3 and 0.7 percent, respectively, than the corresponding value of 17,216 abs j mole^{-1} found with the adiabatic calorimeter, and are considered much less reliable than the latter value. This is partly because of the small absolute uncertainty inherent in all measurements of heat by the ice calorimeter and partly because the sample used in the ice-calorimeter measurements was much smaller, so that a trace of impurity soluble in the diphenyl ether may have caused enough premelting at these temperatures to explain part of the discrepancy.

The difference between the measured heats for the empty container and the container with sample (columns 2 and 3 in table 3) gives essentially the enthalpy change in the sample between 0° C and the temperature involved. Actually, to get the true enthalpy change, this difference was corrected by an equation given by Osborne [8],

$$[Q]_1^2=[q-pV+mH+(V-mv)L/(v'-v)]_1^2, \qquad (4)$$

where $[Q]_1^2$ is the heat evolved in cooling a closed container in which there is a liquid in equilibrium with its vapor from temperature 2 to temperature 1;

937997—51——2

TABLE 3. *Experimental results with the furnace and ice calorimeter*

Furnace temperature	Measured heat		[a] Enthalpy change of the $(C_6H_5)_2O$		
	Empty container	With $(C_6H_5)_2O$	Observed	Calculated from equation 5	Observed minus calculated
°C	abs j	abs j	abs j mole^{-1}	abs j mole^{-1}	abs j mole^{-1}
		[b] 366.8			
		[b] 367.4			
		[b] 367.9			
		370.1			
		368.9			
		368.4	5,146		
		366.7			
		368.3			
	132.8	368.1			
	132.5	368.2			
	131.8	368.2			
	131.9	368.6			
[c] 25.00 (solid)	131.6	1150.3			
	129.9	1151.0			
	132.1	1148.2			
	132.0	1150.1			
		1154.4			
		1150.0	22,206	22,209	−3
		1152.7			
		1149.9			
		1151.8			
[c] 25.00 (liquid)		1153.2			
		1153.5			
		1152.0			
		395.9			
		394.5			
		394.9			
[c] 26.60 (solid)		[d] 397.1			
		[d] 397.7			
		[d] 397.2			
		[d] 397.2			
[c] 26.60 (liquid)		1181.1			
		1179.4			
	[c](258.2)				
	262.3				
	264.2	1600.4			
	263.8	1597.5			
	264.1	1598.9			
50.00	263.5	1598.5	29,078	29,042	+36
	264.2				
	262.6				
	263.4				
	264.6				
	400.5				
	397.5				
75.00	398.1				
	[c](410.4)				
	399.2				
	535.2				
	535.0	2531.2			
	534.9	2531.0			
100.00	534.0	2536.0	43,484	43,548	−64
	536.8	2528.6			
	534.2				
	534.6				
	809.1	3528.7			
	809.1	3528.2			
150.00	810.1	3527.0	59,203	59,176	+27
	809.1	[c](3521.0)			
	1089.8	4578.6			
	1084.9	4574.5			
200.00	1092.3	4575.6	75,922	75,927	−5
	1089.2	4574.6			
	1089.7				
	1372.1	5687.6			
250.00	1374.0	5685.5	93,856	93,799	+57
	1373.4	5681.2			
		5679.8			
	1660.4	6837.4			
300.00	1660.3	6837.2	112,754	112,794	−40
	1658.9	6837.8			

[a] The contribution from vaporization has been eliminated.
[b] Not included in the mean because for these experiments the diphenyl ether was frozen rapidly, using dry ice.
[c] State of the sample at the furnace temperature.
[d] Experiment made after the higher-temperature experiments. The preceding three experiments of this set were made before the diphenyl ether had been heated above 150° C.
[e] Rejected by Chauvenet's criterion.

q is the contribution to Q made by the empty container, shields, and suspension wire; p is the vapor pressure of the liquid; V is the volume of the container; m is the total mass of liquid and vapor; H is the enthalpy per unit mass of the "saturated" liquid (i. e., at pressure p); v' and v are the specific volumes of saturated vapor and liquid, respectively; and L is the enthalpy of vaporization per unit mass. The maximum value of each of the two correction terms that convert measured heats ($[Q-q]_1^2$) to get true enthalpy $[H]_1^2$ amounted to only 0.05 percent at the highest temperature, 300° C. The mean values of enthalpy listed in column 4 of table 3 have been corrected in this way and converted to molal basis.

The mean values of enthalpy of the liquid diphenyl ether at each temperature (26.87° to 300° C) were fitted by an equation whose constants were determined by least squares:

$$H_t(\text{liquid})-H_0(\text{solid})=15657.2+256.4649t+0.224409t^2, \quad (5)$$

where $H_t(\text{liquid})-H_0(\text{solid})$ is the enthalpy difference in abs j mole^{-1} (mole wt=170.20) between the liquid at t° and the solid at 0° C. In evaluating the constants, equal weight was given to values of enthalpy, and at each temperature a weighting factor was used to correspond to the number of determinations made at that temperature.[4] The values calculated from eq 5 are given in column 5 of table 3.

Values of $C_{\text{sat.}}$ the heat capacity of the "saturated" liquid (in equilibrium with its vapor), were calculated from the thermodynamic relation

$$C_{\text{sat.}}=\left(\frac{\partial H}{\partial T}\right)_{\text{sat.}}-V_{\text{sat.}}\left(\frac{dp}{dT}\right)_{\text{sat.}}, \quad (6)$$

where $V_{\text{sat.}}$ is the molal volume of the liquid and p the vapor pressure. The values of $(\partial H/\partial T)_{\text{sat.}}$ were determined by differentiating eq 5. The maximum contribution of the last term in the temperature range studied is at 300° C, and amounts to 0.15 percent of the heat capacity. The values of heat capacity so calculated may be represented by the equation

$$C_{\text{sat.}}=0.448818(T-273.16)+256.4649-V_{\text{sat.}}\left(\frac{dp}{dT}\right)_{\text{sat.}}. \quad (7)$$

The values of heat capacity listed in table 4 at temperatures of 370° K and above are those calculated from this equation.

[4] Actually, the weighting factor used was $(1/a+1/b)^{-1}$, where a and b are the number of runs on the empty and the filled container, respectively, as it is the difference between the enthalpies of these two, which determines the net enthalpy of the sample.

TABLE 4. *Heat capacity, enthalpy, and entropy of solid and liquid diphenyl ether at saturation pressures*

T	$C_{sat.}$	$(H_{sat.}-E_0^*)$	$(S_{sat.}-S_0)$
	SOLID		
° K	*abs j deg* $^{-1}$ *mole* $^{-1}$	*abs j mole* $^{-1}$	*abs j deg* $^{-1}$ *mole* $^{-1}$
2	0.027	0.014	0.009
4	.213	.213	.068
6	.718	1.077	.240
8	1.699	3.401	.567
10	3.283	8.272	1.105
12	5.497	16.952	1.889
14	8.272	30.670	2.941
16	11.52	50.413	4.255
18	14.91	76.845	5.807
20	18.06	109.83	7.542
22	21.17	149.08	9.409
24	24.29	194.54	11.386
26	27.33	246.11	13.451
28	30.30	303.81	15.585
30	33.16	367.29	17.769
32	35.88	436.39	19.998
34	38.48	510.77	22.262
36	40.95	590.25	24.526
38	43.28	674.50	26.806
40	45.44	763.18	29.087
42	47.45	856.11	31.351
44	49.34	952.95	33.597
46	51.13	1053.4	35.827
48	52.85	1157.4	38.040
50	54.53	1264.8	40.235
55	58.41	1547.3	45.614
60	61.92	1848.2	50.856
65	65.14	2166.0	55.928
70	68.11	2499.2	60.881
75	70.97	2846.9	65.663
80	73.77	3208.8	70.344
85	76.52	3584.6	74.888
90	79.19	3973.8	79.347
95	81.80	4376.4	83.704
100	84.35	4791.8	87.959
105	86.90	5219.9	92.129
110	89.49	5661.0	96.231
115	92.15	6115.0	100.28
120	94.82	6582.5	104.25
125	97.53	7063.3	108.18
130	100.26	7557.7	112.06
135	103.04	8066.0	115.89
140	105.88	8588.3	119.68
145	108.77	9124.9	123.46
150	111.72	9676.2	127.19
155	114.68	10243	130.90
160	117.64	10823	134.59
165	120.64	11419	138.25
170	123.70	12030	141.91
175	126.80	12656	145.54
180	129.98	13298	149.15
185	133.20	13956	152.75
190	136.45	14632	156.35
195	139.75	15321	159.94
200	143.09	16028	163.53
205	146.47	16751	167.10
210	149.88	17493	170.68
215	153.35	18251	174.23
220	156.86	19027	177.81
225	160.41	19820	181.37
230	164.00	20630	184.94
235	167.65	21459	188.50
240	171.32	22306	192.07
245	175.05	23173	195.65
250	178.83	24058	199.22
255	182.64	24962	202.79
260	186.49	25884	206.37
265	190.37	26825	209.96
270	194.25	27787	213.55
275	198.15	28769	217.16
280	202.04	29770	220.77
285	205.98	30789	224.38
290	209.94	31829	227.98
295	213.98	32888	231.61
298.16	216.56	33569	233.91
300	218.06	33969	235.25
300.032	218.25	33975	235.27

TABLE 4. *Heat capacity, enthalpy, and entropy of solid and liquid diphenyl ether at saturation pressures*—Continued

T	$C_{sat.}$	$(H_{sat.}-E_0^*)$	$(S_{sat.}-S_0)$
	LIQUID		
° K	*abs j deg* $^{-1}$ *mole* $^{-1}$	*abs j mole* $^{-1}$	*abs j deg* $^{-1}$ *mole* $^{-1}$
300.032	268.42	51188	292.61
310	272.71	53884	301.45
320	277.17	56634	310.18
330	281.71	59428	318.78
340	286.25	62268	327.25
350	290.79	65153	335.62
360	295.35	68084	343.87
370	299.90	71060	352.03
380	304.39	74082	360.08
390	308.86	77148	368.05
400	313.33	80259	375.93
410	317.89	83415	383.72
420	322.36	86617	391.43
430	326.84	89863	399.07
440	331.30	93155	406.64
450	335.77	96491	414.13
460	340.32	99872	421.56
470	344.71	103298	428.93
480	349.16	106769	436.23
490	353.60	110284	443.48
500	358.04	113845	450.66
510	362.48	117450	457.80
520	366.92	121100	464.88
530	371.35	124794	471.91
540	375.78	128534	478.89
550	380.19	132318	485.83
560	384.63	136148	492.72
570	389.05	140022	499.57

3. Reliability of Results With Ice Calorimeter

In order to check the over-all accuracy of operation of the apparatus, heat-capacity experiments were made at temperatures of 25° and 250° C with water sealed in the container. In these tests, it was convenient for comparison of the results to make two series of measurements similar to those described in the measurements with water [9]. One series was made with the container mostly full of water, while the other series was made with a small amount of water. The results of the experiments compare very favorably with the results of the earlier work [9] with an adiabatic calorimeter. The average heat capacity from 0° to 250° C, as measured with the present apparatus, is about 0.02 percent lower than that measured with the earlier apparatus, with a reproducibility of about ±0.02 percent. This is well within the accuracy of the earlier work. At 25° C the reproducibility of the present apparatus was relatively poor, giving a value of about ±0.14 percent for the average deviation of the mean. In spite of this, the measured average heat capacity from 0° to 25° C was only about 0.05 percent lower than the accepted accurate value [9].

The reliability of the results may be considered in two ways. First, there is the reproducibility or precision of the experiments. The average deviation of a single experiment from the mean at a given temperature was ±0.19 percent in the case of the empty containers and ±0.09 percent in the case of the containers with the sample. As the enthalpy of the sample was about two to three times as great

as that of the empty container, the larger deviations with the empty container are not so important. At a given temperature the calculated probable error of the mean of the net enthalpy of liquid diphenyl ether, referred to that of the solid at 0° C, is about 0.04 percent. This error is about the same at all furnace temperatures.

In addition to the reproducibility of the results, there must be considered the sources of systematic errors. Many such errors have already been considered in other measurements with this apparatus [10] and will not be reviewed here. The ice-point reading of the platinum resistance thermometer was frequently redetermined during the measurements. On the basis of the small changes thereby noted, small corrections were applied to the heat measurements for deviations from the nominal temperatures. As these corrections were always less than 0.01 percent of the heat measured, it is believed that errors in the temperature scale did not appreciably affect the values of heat capacity.

Another source of systematic error is the effect of impurity in the sample. The measurements with the low-temperature adiabatic calorimeter indicated that the impurities in the sample amounted to only about 0.000013 mole fraction. However, in these measurements, considerable effort was made to remove both air and water. In the measurements with the ice calorimeter, some solid sample was melted and quickly transferred to the sample container, which was heated while pumping before sealing the capsule. Under these conditions, it seems improbable that the impurities amounted to more than 0.00005 mole fraction, a value that may be neglected insofar as effect on the heat-capacity values reported. However, small impurities affect greatly the measurements on the heat of fusion where the enthalpy of the solid is measured at temperatures close to the triple point. For example, in the measurements at 26.60° C (triple point=26.87° C), the measurements with the ice calorimeter gave a value of the enthalpy of the solid that corresponded to a heat of fusion value about 0.7 percent lower than that obtained with the adiabatic calorimeter. This difference could be explained by an impurity of about 0.00005 mole fraction in the sample. It is believed that the heat of fusion value obtained with the adiabatic calorimeter is the more accurate value.

Another factor affecting the reliability of the results is the question of the chemical stability of the diphenyl ether at the higher temperatures. The rate of spontaneous decomposition of diphenyl ether at 300° C does not seem to have been estimated previously. As this is the highest temperature to which the sample was subjected, a number of enthalpy determinations were made on the solid at 26.60° C (0.27 deg below the triple point) before and after several hours of heating to the higher temperatures.

Considering only the mean results of these two sets, it appears that the apparent relative enthalpy was greater in the second set of experiments by 47 abs j $mole^{-1}$. This corresponds to 0.3 percent more of the sample melted. It can readily be shown that this would be caused by an increase in impurity of only 0.00002 mole fraction. Here again, this impurity would not affect the reliability of the heat-capacity results, although it would have some significance in the heat of fusion value calculated from the measurements on the solid at 26.60° C.

Another source of systematic error lies in the uncertainty in the mass of the sample. The mass of the empty container was 0.0033 g less during the experiments with the empty container than it was before introducing the sample. The mass of the sample was taken to be the difference in weight of the full container and the container after removing the sample. It is possible that some material other than the sample was removed in this process, in which case, an uncertainty of as large as 0.04 percent might exist in the mass of the sample. The other sources of error, such as temperature measurement, calorimeter calibration factor, variation in heat loss on dropping the sample from the furnace, and possible slightly inaccurate correction for condensation of vapor inside the container, are estimated each to contribute an uncertainty to the enthalpy and heat capacity of from 0.01 to 0.02 percent.

Considering these various sources of error, it is believed that the values of relative enthalpy represented by eq 5 have the probable error of ± 0.15 percent, except below 100° C, where the probable error must be considered greater. Similarly, it was estimated that the values of heat capacity of the liquid as determined by the ice calorimeter (eq 7) have the probable error of ± 0.25 percent, except near 25° and 300° C, where the course of the enthalpy curve is more uncertain.

IV. Tabulated Heat Capacities

In the temperature range 300° to 360° K, values of heat capacity are obtained with both the low-temperature adiabatic calorimeter and the ice calorimeter. The values, except between 300° and 320° K, are displaced almost parallel from each other, the displacement being about 0.45 abs j deg^{-1} $mole^{-1}$. This difference between the two sets of values, however, is smaller than the estimates of absolute error claimed with the two methods. The results with the two methods were adjusted so that continuity exists in the heat capacity curve between the overlap range and the range above 360° K. The problem of continuity at 300° K does not arise because the heat-capacity curve is discontinuous at the triple-point temperature (300.03° K). The results from the two methods were adjusted with the following considerations. The enthalpy experiments with the ice-calorimeter method decrease in sensitivity with approach to the ice point; furthermore, derivatives of the enthalpy equation become less accurate toward the end of the experimental temperature range. The shield control in the adiabatic vacuum calorimeter becomes a little unwieldy at higher temperatures, and at the same time heat transfer by radiation can be significant if any unknown thermal gradients exist in the calorimeter.

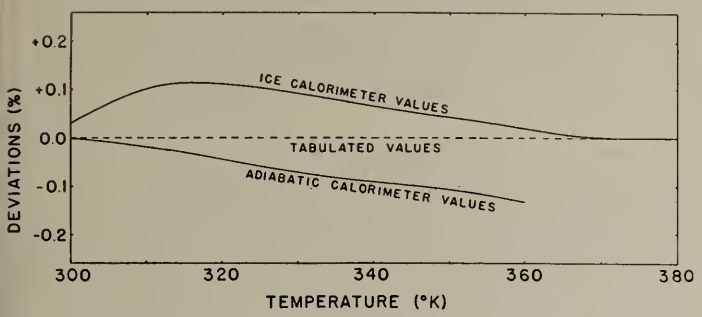

FIGURE 5. *Comparison of smoothed heat capacities obtained by the two experimental methods with the final values in table 4.*

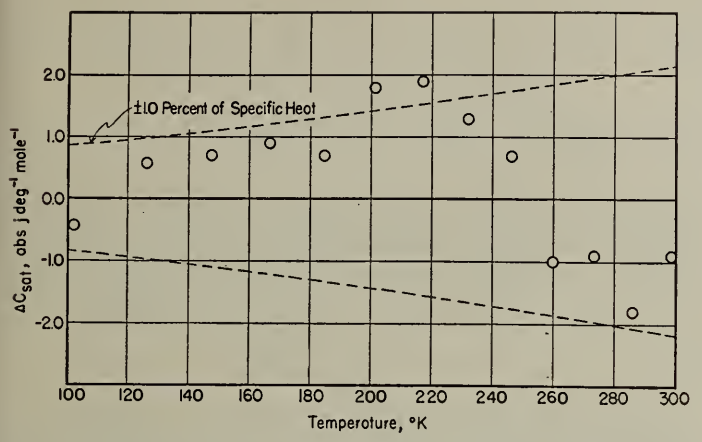

FIGURE 6. *Comparison of the values of heat capacity given in table 4 with the results of Smith and Andrews.*

The base line represents the values from the table.

The results from the ice calorimeter were given progressively greater weight toward 360° K and the results from the adiabatic vacuum calorimeter greater weight toward 300° K. A comparison of the results from these two calorimeters with the adjusted tabulated values from table 4 is given in figure 5, which shows that the maximum difference is about 0.13 percent.

The survey of literature revealed only one publication on the heat capacity of diphenyl ether. Smith and Andrews [11] measured the heat capacity from 100° to 300° K, using a heat conduction calorimeter. In figure 6 these results are compared with the tabulated values of table 4. In general, the values given by these authors are higher below 246° K and lower above this temperature. The over-all discrepancy amounts to about ±1 percent; the maximum discrepancy amounts to 1.2 percent. These authors claimed an accuracy of 1 percent for their apparatus.

V. Combustion Calorimetry

1. Apparatus and Procedure

The apparatus and procedure used in measuring the heat of combustion, with the exception of the Wheatstone bridge used in measurement of temperature, have been described in several previous publications [12, 13, 14]. The bridge used is a special Mueller type instrument with gold-chromium alloy resistance coils, which have negligible temperature coefficient of resistance so that the bridge does not need to be thermostated. The energy equivalent of the calorimetric system was determined by six experiments with NBS Standard Sample 39f, benzoic acid, using the value 26,433.8 abs j/g mass (weight in vacuum), previously obtained in this laboratory [15, 16, 17], for the heat of combustion of this substance under the standard conditions of the bomb process. The mean value obtained for the energy equivalent is 13,976.42 abs j deg^{-1}, and the standard deviation of the mean is ±0.64 abs j deg^{-1}. (See footnote a, table 5 for the definition of standard deviation.)

The observed heat of combustion in each experiment was corrected for the heat of stirring and the heat transfer between the jacket and calorimeter, for the energy used in firing the charge and for the energy of formation of nitric acid in the bomb. The observed values of the heat of combustion of diphenyl ether were reduced to $-\Delta U_C^\circ$ [18], the decrease in intrinsic energy accompanying the combustion reaction

$$C_{12}H_{10}O_{(l)} + 14O_{2(g)} = 12CO_{2(g)} + 5H_2O_{(l)}$$

with the components in their thermodynamic standard states at 30° C. In the above reaction the standard state for diphenyl ether was taken as that of the liquid at 1-atm pressure.

Three combustion experiments were made with the samples of diphenyl ether in an open platinum crucible, and three with the samples enclosed in thin-walled glass bulbs [19, 20] flattened on opposite sides. The method for filling the bulbs is described in the references given. The weight of the glass in each bulb was about 0.05 g. There was no significant difference in the results obtained by the two methods.

The carbon dioxide formed in the combustion was absorbed in Ascarite and weighed, following the procedure described by Prosen and Rossini [21]. The absorption train, however, did not contain any provision to oxidize and absorb products of incomplete combustion. When the escaping bomb gases in each experiment were tested for carbon monoxide, using a NBS colorimeter method [22], only negligible traces of carbon monoxide were found.

2. Results

Table 5 gives the results of the heat of combustion measurements, where $-\Delta U_B$ is the observed heat of combustion under the conditions specified by the volume of the bomb (381 ml), the mass of water (1 g) placed in the bomb and the data given in columns 1 and 3; and $-\Delta U_C^\circ$ represents the decrease in intrinsic energy accompanying the combustion reaction when the components of the reaction are in their appropriate thermodynamic standard states at 30° C.

Except for the first experiment, in which the weight of the sample was apparently in error, the values obtained for the masses of carbon dioxide formed in the combustion are lower than the corresponding values calculated stoichiometrically from

Table 5. *Heat of combustion of diphenyl ether*

Defined calorie=4.1840 abs j

Mass of sample	Initial O_2 pressure at 30° C	Mass of CO_2	Heat of combustion at 30° C	
			$-\Delta U_B$	$-\Delta U_c^\circ$
Burned in platinum crucible				
g	*atm*	*g*	*abs j/g* CO_2	*abs j/g* CO_2
1.13560	31.1	3.52667	11613.33	11606.00
1.08319	30.4	3.35893	11616.98	11609.84
1.09104	30.4	3.38367	11620.74	11613.59
Burned in glass bulb				
1.12596	31.4	3.49271	11613.26	11605.87
1.10658	30.3	3.43144	11616.85	11609.68
0.99321	30.2	3.08082	11612.05	11605.06
Mean				11608.06
Standard deviation of the mean [a]				±1.34

	kj/mole	*kcal/mole*
$-\Delta U_c^\circ$ (*l*, 30° C)	[b] 6130.60 ±0.88	[b] 1465.25 ±0.21
$-\Delta H_c^\circ$ (*l*, 30° C)	[b] 6135.64 ±0.88	[b] 1466.45 ±0.21
$-\Delta H_c^\circ$ (*l*, 25° C)	[b] 6136.36 ±0.88	[b] 1466.63 ±0.21
$-\Delta H_c^\circ$ (*c*, 25° C)	[b] 6119.24 ±0.88	[b] 1462.53 ±0.21

[a] Standard deviation of the mean as used above is defined as $[\Sigma d^2/n(n-1)]^{1/2}$; where d is the difference between a single observation and the mean, and n is the number of observations.

[b] The value following the ± sign is a measure of the precision of the result, which is defined as follows [23]:

$$s=Q\sqrt{(s_E/E)^2+(s_Q/Q)^2+(s_B/B)^2+(s_R/R)^2}.$$

In this expression, s_E is the standard deviation of the mean of the results of the series of experiments with benzoic acid to determine E, the energy equivalent of the calorimetric system; s_Q is the standard deviation of the mean of the results of the series of experiments to determine the heat of combustion, Q, of the diphenyl ether; s_B/B is an allowance of 5×10^{-5} for the standard deviation of the value used for the heat of combustion of benzoic acid; s_R/R is an allowance of 5×10^{-5} for the standard deviation associated with the determination of the amount of the combustion reaction from the mass of carbon dioxide formed.

the masses of the sample burned. Excluding the first experiment, the average difference between the observed and calculated masses of carbon dioxide is 0.05 percent. The masses of carbon dioxide formed in the combustion of NBS Standard Sample 39f, benzoic acid, before and after the work with diphenyl ether agreed with the calculated values on the average within 0.010 percent. The low experimental value for the carbon dioxide formed in the combustion of diphenyl ether is probably due to air and water absorbed by the sample before the combustion experiment was made. These impurities have practically no effect on the value obtained for the heat of combustion per gram of carbon dioxide formed.

In table 5 are listed the values obtained for the heat of combustion per mole of liquid diphenyl ether at 30° C and of both liquid and solid at 25° C. The calculations were based on the mass of carbon dioxide formed in the combustion reaction, using the mean $-\Delta U_c^\circ$ per gram of carbon dioxide given in the same table and the value 44.010 g for the molecular weight of carbon dioxide. The results at 25° C were obtained, using the values of heat capacity and heat of fusion of diphenyl ether obtained in this work, together with the values of the heat capacity of gaseous carbon dioxide and oxygen and liquid water given in references [9, 24].

VI. Derived Thermal Properties

1. Enthalpy and Entropy

In table 4, columns 3 and 4, the values of enthalpy and entropy, respectively, are tabulated at integral temperatures for intervals of 2 deg from 0° to 50° K, 5 deg from 50° to 300° K, and 10 deg from 300° to 570° K. For most purposes any intermediate values can be obtained by linear interpolation or more accurately by quadratic interpolation. These properties were obtained by evaluating the thermodynamic relations

$$H_{sat.}-E_0^s=\int_0^T C_{sat.}dT+L_f+\int_0^T V_{sat.}\left(\frac{dp}{dT}\right)_{sat.}dT, \quad (8)$$

$$S_{sat.}-S_0=\int_0^T \frac{C_{sat.}dT}{T}+\frac{L_f}{T_t}, \quad (9)$$

where E_0^s is the internal energy of the solid diphenyl ether at absolute zero to which the enthalpy values are referred. S_0 is the entropy of the solid at absolute zero, which is considered to be zero for diphenyl ether. The other symbols have the same significance as previously indicated. The term $\int_0^T V_{sat.}(dp/dT)_{sat.}dT$ in the enthalpy equation was not applied up to 360° K; even at 570° K, the contribution from this term is only 0.03 percent. The term L_f (heat of fusion) in both expressions obviously is not applicable below the triple point. Below 18° K eq 8 and 9 were evaluated analytically, using the Debye heat capacity function given in eq 3. Between 18° and 570°K these equations were evaluated by tabular integration, using Lagrangian four-point integration coefficients. When the enthalpy values from tabular integration were checked in the interval from 370° to 570° K by evaluating the enthalpy eq 5, the discrepancy was found to be only 3 abs j mole^{-1}. No attempt was made to fit the tabulated values of heat capacity, enthalpy, or entropy between 18° and 370° K to an equation. The internal consistency of tabular integration in this lower temperature range, however, was checked by evaluating the thermodynamic identity:

$$\int_0^T (S_{sat.}-S_0)dT=T(S_{sat.}-S_0)-\int_0^T C_{sat.}dT-L_f. \quad (10)$$

Considering the accuracy claimed for the heat-capacity values and the uncertainty involved in the Debye extrapolation, a probable error of ±0.2 percent is assigned to the tabulated values of enthalpy above 50° K and a probable error of ±0.4 abs j deg^{-1} mole^{-1} to entropy in the whole temperature range.

2. Standard Heat of Formation

The standard heat of formation for both liquid and solid diphenyl ether at 298.16° K was calculated from the values of standard heat of combustion for this

material listed in table 5 and from the accepted standard heat of formation for liquid water ($-285{,}840\pm42$ abs j $mole^{-1}$) and carbon dioxide ($-393{,}513\pm45$ abs j $mole^{-1}$) [24] by evaluating the relation:

$$\Delta H_f^\circ = \Sigma \Delta H_f^\circ \text{ (products)} - \Delta H_c^\circ, \qquad (11)$$

where ΔH_f° is the standard heat of formation; and $\Sigma\Delta H_f^\circ$ (products) is the sum of the standard heats of formation for the products of the combustion reaction. The results so obtained are given by

Solid, $\Delta H_{f_{298.16°K}}^\circ = -32.11\pm0.93$ abs kj $mole^{-1}$ [5]

Liquid, $\Delta H_{f_{298.16°K}}^\circ = -14.99\pm0.93$ abs kj $mole^{-1}$ [5]

3. Standard Entropy of Formation

The standard entropy of formation for solid diphenyl ether at 298.16°K was computed from the standard entropies of diphenyl ether (table 4), graphite (5.720 ± 0.050 abs j deg^{-1} $mole^{-1}$), gaseous hydrogen (130.574 ± 0.010 abs j deg^{-1} $mole^{-1}$), gaseous oxygen (205.073 abs j deg^{-1} $mole^{-1}$) [25] by evaluating the expression:

$$\Delta S_f^\circ = S_C^\circ - \Sigma S_E^\circ, \qquad (12)$$

in which ΔS_f° is the standard entropy of formation; and the subscripts C and E indicate the compound and the element, respectively. The standard entropy of formation for diphenyl ether so obtained is

$$\Delta S_{f_{298.16°\ K}}^\circ = -590.1\pm0.5 \text{ abs j deg}^{-1} \text{ mole}^{-1}.$$

The assigned probable error was estimated from the probable errors in the standard entropy for diphenyl ether and the elements.

Actually, in carrying out the above calculation the tabulated entropy (table 4) was used directly without correcting to standard state. The amount of this correction can be obtained using the following thermodynamic expression:

$$\left(\frac{\partial S}{\partial P}\right)_T = -\left(\frac{\partial V}{\partial T}\right)_P. \qquad (13)$$

There are no data for the temperature coefficient of expansion for solid diphenyl ether around 298° K, consequently the densities of solid diphenyl ether at 20° C and the liquid at 30° C [26] were used to calculate the maximum possible correction. This correction amounts to 0.02 abs j deg^{-1} $mole^{-1}$, which does not significantly affect the value of standard entropy of formation.

[5] The precision was determined by evaluating the expression:

$$s = \sqrt{(12s_1)^2+(5s_2)^2+(s_3)^2}$$

where s_1 and s_2 are the standard deviations of the mean of the heat of combustion values for carbon dioxide and water, respectively. s_3 is the precision s given in footnote b, table 5.

4. Standard Gibbs Free Energy of Formation

The standard Gibbs free energy of formation for solid diphenyl ether at 298.16° K was obtained from the values of standard heat and entropy of formation given in previous sections by evaluating the relation:

$$\Delta F_f^\circ = \Delta H_f^\circ - T\Delta S_f^\circ. \qquad (14)$$

The value so obtained is

$$\Delta F_{f_{298.16°K}}^\circ = 143.8\pm0.9 \text{ abs kj mole}^{-1}.$$

The probable error of ±0.9 abs kj $mole^{-1}$ was obtained from statistical combination of the probable errors assigned to the various data used in the calculation.

VII. Discussion

The results of the purity determination indicate that diphenyl ether can be prepared in a state of extremely high purity. This material can be purified quite easily by slow fractional crystallization at room temperature. There is the question of chemical stability with the adiabatic vacuum calorimeter, but the heat of fusion results with the ice calorimeter indicate that even after several hours at 570° K in contact with monel the impurity increased by only 0.00002 mole fraction. No conclusion can be drawn without additional data in regard to the chemical reactivity of diphenyl ether with different metals.

There is implied in one set of enthalpy experiments (table 3) with the ice calorimeter that perhaps conditioning of the diphenyl ether crystal might affect the results of the experiments. The results indicate that the enthalpy is slightly lower for the material when cooled in dry ice. This difference is, however, so small that it is difficult to ascertain whether the effect is real or not. The experiments in the solid range with the adiabatic vacuum calorimeter do not indicate any unusual discrepancy in the results, although the material was subjected to extreme treatments such as freezing rapidly with liquid air and freezing slowly across a vacuum with ice. In the melting-point studies the diphenyl ether required relatively long periods for temperature equilibrium. This, however, is not uncommon with compounds of high molecular weight.

The results of the heat capacity experiments indicate that diphenyl ether is a suitable standard to be used in heat capacity calorimeters below 600° K. It might be possible to use this material above this temperature, but the increase in vapor correction would be undesirable. The material should be provided freed of air and water in ampoules of suitable volume.

As indicated by the 0.05-percent discrepancies in the weighed carbon dioxide from the stoichiometric value, the solubility of air and water in diphenyl ether is relatively high, for there is incomplete

combustion. Considering the difficulties involved in preventing the test material from being exposed to the atmosphere in combusiton calorimetry, diphenyl ether is undesirable as a combustion standard.

The authors express their indebtedness to several members of the Bureau—to F. L. Howard for purifying the diphenyl ether, to R. B. Scott for many helpful suggestions in the use of the adiabatic vacuum calorimeter, to T. B. Douglas and Anne F. Ball for help in taking the measurements and calculating the results with the ice calorimeter, and to R. S. Jessup for many suggestions and help with the combustion bomb calorimeter.

VIII. References

[1] R. B. Scott, C. H. Meyers, R. D. Rands, Jr., F. G. Brickwedde, and N. Bekkedahl, J. Research NBS **35,** 39 (1945) RP1661.
[2] H. F. Stimson, J. Research NBS **42,** 209 (1949) RP1962.
[3] H. J. Hoge and F. G. Brickwedde, J. Research NBS **22,** 351 (1939) RP1188.
[4] N. S. Osborne, H. F. Stimson, T. S. Sligh, and C. S. Cragoe, BS Sci. Pap. **20,** 65 (1925) S501.
[5] H. J. Hoge, J. Research NBS **36,** 111 (1946) RP1693.
[6] D. C. Ginnings, T. B. Douglas, and Anne F. Ball, J. Research NBS **45,** 23 (1950) RP2110.
[7] R. J. Corruccini and D. C. Ginnings, J. Am Chem. Soc. **69,** 2291 (1947).
[8] N. S. Osborne, BS J. Research **4,** 609 (1930) RP168.
[9] N. S. Osborne, H. F. Stimson, and D. C. Ginnings, J. Research NBS **23,** 197 (1939) RP1228.
[10] D. C. Ginnings and R. J. Corruccini, J. Research NBS **38,** 593 (1947) RP1797.
[11] R. H. Smith and D. H. Andrews, J. Am. Chem. Soc. **53,** 3661 (1931).
[12] H. C. Dickinson, Bul. BS **11,** 189 (1914) S230.
[13] R. S. Jessup and C. B. Green, J. Research NBS **13,** 469 (1934) RP721.
[14] D. E. Roberts, W. W. Walton, and R. S. Jessup, J. Research NBS **38,** 627 (1947) RP1801.
[15] R. S. Jessup, J. Research NBS **29,** 247 (1942) RP1499.
[16] R. S. Jessup, J. Research NBS **36,** 421 (1946) RP1711.
[17] NBS Circular 475, p. 22 (1949).
[18] E. W. Washburn, BS J. Research **10,** 525 (1933) RP546.
[19] T. W. Richards and F. Barry, J. Am. Chem. Soc. **37,** 993 (1915).
[20] R. S. Jessup, J. Research NBS **18,** 115 (1937) RP966.
[21] E. J. R. Prosen and F. D. Rossini, J. Research NBS **27,** 289 (1941) RP1420.
[22] M. Shepherd, Anal. Chem. **19,** 77 (1947).
[23] F. D. Rossini and W. E. Deming, J. Wash. Acad. Sci. **29,** 416 (1939).
[24] Selected values of chemical thermodynamic properties NBS Circular 500 (Dec. 31, 1947).
[25] F. G. Brickwedde, M. Moskow, and J. G. Aston, J. Research NBS **37,** 263 (1946) RP1747; H. W. Woolley, R. B. Scott, and F. G. Brickwedde, J. Research NBS **41,** 379 (1948) RP1932; H. W. Woolley, J. Research NBS **40,** 163 (1948) RP1864; The NBS–NACA Tables of thermal properties of gases, Tables 7.10 and 9.10.
[26] D. I. Zhuravlev, J. Phys. Chem. (USSR) **9,** 876 (1937).

Washington, September 6, 1950.

U. S. GOVERNMENT PRINTING OFFICE: 1951

For sale by the Superintendent of Documents, U. S. Government Printing Office
Washington 25, D. C. - Price 10 cents

Journal of Research of the National Bureau of Standards Vol. 46, No. 4, April 1951 Research Paper 2204

Heat Capacity of Liquid Mercury Between 0° and 450° C; Calculation of Certain Thermodynamic Properties of the Saturated Liquid and Vapor

Thomas B. Douglas, Anne F. Ball, and Defoe C. Ginnings

The enthalpy of liquid mercury was measured from 0° to 450° C by the "drop" method. These and other precise published data were used to calculate a number of thermodynamic properties of liquid and gaseous mercury at the vapor pressures from the triple point, −38.88°, to +500° C. The entropy calculated from data on the vapor and liquid was compared with that derived from published low-temperature heat-capacity data for the solid. The calculated values of vapor pressure, also using data on the vapor and liquid, were found to agree over a wide temperature range with certain published experimental values when independently derived gas-imperfection and published temperature-scale corrections were applied.

I. Introduction

It is of considerable practical and theoretical importance that the physical properties of mercury be known accurately. The element has found an important use as the fluid in certain heat engines operating at high temperatures. Furthermore, it can be highly purified, perhaps more easily than almost any other commonly available substance. Because of their reproducibility, the physical properties of mercury have often been used as standards.

The accuracy of the values of many thermodynamic properties, over a temperature range, often depends on how accurately the heat capacity is known. As various past observers have shown considerable disagreement above room temperature in their values for the heat capacity of mercury, the measurements reported in this paper were undertaken primarily to furnish accurate values of this property up to a vapor pressure of 4 atm. This investigation is the second in a current series of measurements at this Bureau of the heat capacities of liquid metals.

II. Experimental Procedure

1. Method and Apparatus

The method and apparatus have been described previously [1, 2, 3].[1]

In brief, the method consists in heating the sample in a furnace to a known temperature and dropping it into an ice calorimeter, thereby measuring the heat evolved in cooling the sample to 0° C. The calibration factor of the calorimeter was determined electrically to be 270.46 ±0.03 absolute joules per gram of mercury. The samples were sealed in cylindrical containers of stainless steel. The heat capacities of the empty containers were accounted for by "blank" experiments employing them, these experiments being carried out at the same temperatures as with the filled containers. The temperature of the sample in the furnace was measured by a platinum resistance thermometer that had been calibrated at this Bureau.

2. Samples

Two samples of mercury of about 130 g each were sealed in the containers made of stainless steel No. 347, each having about 10-cm³ capacity. The capsules had the same mass (17 g) and composition as those used in the sodium investigation [3]. The samples, purified and sealed, were furnished by the Knolls Atomic Power Laboratory, of Schenectady, N. Y. Commercially pure mercury that was believed to have been triply distilled was redistilled four more times in vacuum. The samples were sealed in the containers under a pressure of helium of about 1/30 atm. The sealing process [4] was completed by a pulse of high-frequency current induced locally at the top of the container. It was found possible to seal the containers in this manner without changing their weight by more than a milligram. The "empty" containers were sealed in the same manner with the same pressure of helium. The containers filled with mercury were tested for tightness at 450° C and were found to have a leakage rate of about 0.1 microgram of mercury per hour at this temperature, an amount that is without significant effect on the enthalpy measurements.

The mercury sample actually used for most of the thermal measurements was examined spectrochemically at this Bureau. Of 34 elements looked for as possible impurities, only copper and nickel were detected by this means, and these were found to be present only in traces amounting to less than 0.01 percent of the mass of the sample. The stock supply of mercury from which the sample for the thermal measurements had been taken was analyzed by the Knolls Atomic Power Laboratory. The total nonvolatile impurity found, mostly silver, amounted to 0.00001 percent. A mass-spectrographic examination by them for "volatile" impurities indicated the possible presence of traces of aluminum, manganese,

[1] Figures in brackets indicate the literature references at the end of this paper.

iron, cobalt, nickel, zinc, and rhodium; the total amount of these, however, was shown not to exceed 0.001 percent.

III. Experimental Results

A total of 111 measurements of enthalpy was made, from 0° to 450° C (to about 4 atm pressure). Of these, 66 were made with the two empty capsules and 45 with the two capsules containing mercury. The average deviation of a single measurement from the mean at a given temperature was 0.03 percent. One of the mercury samples, measured at only 250° C (to ensure that no systematic error in mass was present), gave a mean value for the enthalpy of mercury that differed from that obtained when using the other sample by only 0.01 percent. The detailed results of individual runs are given in table 1.

No corrections for impurities were made, as these were undoubtedly so small as to lie well within the accidental error. All weights were corrected for buoyancy. No corrections for temperature were made, as the thermometer reading was held to within ± 0.01 deg of the stated temperature in each case. The ice point of the resistance thermometer changed so slightly during the course of the measurements as to indicate a negligible error in computing the temperatures. Corrections were applied to account for small differences in masses of capsule and exterior oxide coatings. In addition, corrections were made at the higher temperatures for the small heats evolved in condensing some mercury vapor inside the container, in order that the results would refer to the liquid alone.

This last-mentioned correction, and that needed to evaluate the enthalpy change that would have resulted under maintenance of saturation from the heat measurements made on the system maintained at constant volume, were conveniently calculated by an equation given by Osborne [5],

$$[Q]_1^2=[q-PV+mH_{(l)}+(V-mv)L/(v'-v)]_1^2, \quad (1)$$

where $[Q]_1^2$ is the heat evolved in cooling a closed container in which there is a liquid in equilibrium with its vapor from temperature 2 to temperature 1; $[q]_1^2$ is the contribution to $[Q]_1^2$ made by the empty container, shields, and suspension wire; P is the vapor pressure of the liquid; V is the internal volume of the container; m is the total mass of liquid and vapor; $H_{(l)}$ is the enthalpy, per unit mass, of the "saturated" liquid (i. e., at pressure P); v' and v are the specific volumes of saturated vapor and liquid, respectively; and L is the enthalpy of vaporization per unit mass.

The total of the various corrections did not exceed 0.03 percent of the enthalpy, except in the case of some of the first runs, where a correction of approximately 0.2 percent was necessitated by the use of a shield system that was later broken and so had to be replaced by one of different heat capacity.

TABLE 1. *Corrected heat and enthalpy values of individual experiments*

Furnace temperature	Measured heat		[a] Enthalpy change of mercury, H_t-H_0		
	Blank	With mercury	Observed	Calculated	Difference
°C	*abs j*	*abs j*	*abs-j g⁻¹*	*abs-j g⁻¹*	*abs-j g⁻¹*
	400.5				
	403.4				
	401.6	[b](1269.3)			
	397.1	1298.7			
50.00	401.1	1298.7	6.942	6.946	−0.004
	400.8	1298.1			
	[c] 401.0				
	[c] 401.0				
	[c] 399.2				
	814.3				
	814.0				
	815.6				
	[c] 816.5	2605.0			
100.00	[c] 815.9	2603.8	13.835	13.831	+0.004
	[c] 816.2	2604.8			
	813.2				
	814.4				
	814.6				
	1238.6	3913.6			
	1242.0	3914.9	20.672	20.669	+0.003
150.00	1239.9	3914.8			
	1241.9				
	1676.6				
	1673.5	5223.9			
	1678.8	5228.9			
	1678.1	5226.4			
200.00	1674.9	5223.0	[d] 27.461	27.470	−0.009
	1676.3	5230.2			
	1677.5	5227.4			
	[c]1674.1	5228.6			
	[c]1674.2	5228.1			
	[c]1675.6				
		6548.5			
	2117.5	6548.0			
250.00	2121.5	6549.3	34.250	34.250	0.000
	2120.2	[e] 6484.0			
	2119.4	[e] 6481.9			
		[e] 6482.8			
	2571.3				
	2567.0				
	2572.2	[b](7868.3)			
	2570.0	7875.9			
300.00	2570.0	7874.8	41.027	41.019	+0.008
	2568.8	7877.9			
	[c]2571.6	7875.3			
	[c]2569.6				
	[c]2569.1				
	3030.5	9205.5			
	3028.0	9209.5	47.791	47.790	+0.001
350.00	3028.2	9211.0			
	3029.1	9207.8			
	3496.6				
	3493.5				
	3494.3	10548.9			
	3490.6	10544.6			
	3493.4	10550.8	[d] 54.569	54.577	−0.008
400.00	3493.7	10553.0			
	3492.8	10548.2			
	[c]3489.5	10547.5			
	[c]3489.4				
	[c]3491.2				
	[b](3957.4)	11900.7			
	3964.1	11902.0			
	3965.6	11900.9			
450.00	3964.1	11902.8	[d] 61.396	61.392	+0.004
	[c]3965.0	11897.3			
	[c]3965.9	11900.7			
	[c]3964.3				

[a] Values apply to saturation (i. e., at the vapor pressure).
[b] Rejected by Chauvenet's criterion.
[c] On alternate capsule of same mass.
[d] This mean obtained by weighting each set proportionately to the number of measurements in the set and inversely proportionately to the average deviation from the mean of the set.
[e] On alternate capsule, containing 127.411 g Hg. The other capsule had the same mass of container but contained 129.344 g Hg.

Within the accidental error the heats of the empty containers ("blank" experiments) were found to vary perfectly smoothly with temperature up to 450° C. By plotting against t(°C) the function

$$\frac{H_t - H_0}{1.86t + 0.0025t^{1.73}}, \quad (2)$$

which varied only 1 percent between 50° and 450°, these blank values were thereby smoothed. The net enthalpies of mercury given in table 1 have been calculated by using the smoothed values for the empty container, although the heat values listed for the empty containers in the table are those actually obtained.

The experimental values of the enthalpy of liquid mercury (at saturation pressure), less the enthalpy at 0° C, are represented by the following equation, whose constants were fitted by least squares:

$$\left.\begin{aligned} H_t - H_0 = 0.139612t - 1.4673\,(10^{-5})\,t^2 \\ +1.6874\,(10^{-8})\,t^3 \qquad (0° \text{ to } 450°\text{C}) \end{aligned}\right\}, \quad (3)$$

where H is in absolute joules per gram and t in deg C (International Temperature Scale). The values in the fifth column of table 1 were calculated from this equation.

IV. Calculation of Thermodynamic Properties

1. General Procedure

The more common thermodynamic properties of liquid and gaseous mercury, at the existing vapor pressures, were accurately calculated as a function of temperature over the range from the triple point, —38.88°, to 500° C. Except for what may be considered as minor but unavoidable correction terms, the calculated values of most of these properties rest on three sets of precise experimental data, namely, (1) the enthalpy measurements of the liquid reported in this paper, (2) a previously published series of vapor pressure measurements covering a 13-deg temperature range in the vicinity of the normal boiling point, and (3) the experimental values of the fundamental physical constants that made possible the statistical evaluation of the entropy of the ideal vapor. The additional experimental data employed, whose accuracy is of secondary effect on the accuracy of the calculated properties, are (1) those giving certain fundamental constants of the Hg_2 molecule (used to arrive at data of state for mercury vapor), (2) accurate gas-thermometer measurements of one laboratory (used to make corrections from the International to the thermodynamic temperature scale), and (3) PVT data for the liquid (necessary in an accurate evaluation of the heat capacities from the measured enthalpy).

The procedure of calculation followed will now be outlined. The heat capacities of liquid mercury were calculated from the enthalpy data by the usual thermodynamic relations. The changes with temperature of the entropy of the saturated liquid were next calculated from the values of heat capacity, and were combined with the statistically calculated value of the entropy of the vapor (at the vapor pressure) to give the absolute entropy of the liquid. The heat capacity (C_p) of the vapor was calculated by first assuming it to be an ideal monatomic gas and then making small corrections for imperfections of the gas. By integration of the resulting heat capacity equation and evaluation of the integration constant by using the value of the heat of vaporization at the normal boiling point calculated from the vapor-pressure data and the Clapeyron equation, values of enthalpy of the vapor (relative to the liquid at a fixed temperature) were obtained. The free energies of the liquid and vapor followed from the calculated entropy and enthalpy values. By equating the expressions for these free energies of "saturated" liquid and vapor, a vapor-pressure relation was obtained that is applicable over a much larger temperature range than the supporting vapor-pressure data.

At the present time, the uncertainty in the corrections for gas imperfection and temperature scale, referred to above, limit slightly the accuracy of the calculated properties. Because of these uncertainties it was considered advisable merely to indicate these two corrections in the equations derived. The values of the properties tabulated (in tables 3, 4, and 5) were arrived at, however, by assigning to the corresponding correction terms, on the basis of what are judged to be the best existing data, specific values that are separately listed (in tables 6 and 7 and in the text preceding them). This procedure facilitates an estimation of the uncertainties introduced into the present values and also should simplify any future desired revision of the values, should more accurate corrections become available.

2. Nomenclature and General Assumptions

In what follows, energy will be expressed in calories (1 cal=4.1840 abs j); all extensive properties, per gram-atom of mercury (atomic weight=200.61); and temperature (T), in degrees absolute (0° C=273.16° K), unless otherwise stated. Each value calculated from the equations applies at the existing vapor pressure, except in those cases where pressure is an explicit variable in the equations given. In addition, the subscripts in the heat capacities C_p, C_v, and C_s signify that the respective heat changes are those occurring under the maintenance of constant pressure, constant volume, and liquid-vapor equilibrium, respectively. The equations for relative enthalpy and relative free energy contain the term $H_{TP(l)}$, the enthalpy of the liquid at the triple point, —38.88° C. Liquid and vapor are distinguished by the subscripts l and g, respectively. In the numerical equations (i. e., those in which some or all of the numerical constants have dimensions), P, the pressure, is to be expressed in millimeters of mercury (760 mm=1 standard atm); and V, the volume, in cm^3 $g\text{-}atom^{-1}$.

Log and *ln* indicate logarithms to the bases 10 and e, respectively.

Saturated mercury vapor at pressures not exceeding 2 atm has been found experimentally to have densities that differ from those calculated for an ideal gas by less than 2 percent (the uncertainty of the measurements). It is therefore permissible to assume that practically all of the gas imperfection arises from binary collisions only. Statistical mechanics shows that under this circumstance the correct form for the equation of state of the vapor is

$$PV_{(g)}=RT\left[1+\frac{B}{V}\right], \tag{4}$$

where B, the so-called "second" virial coefficient, is a function of temperature only. However, for convenience it will be used here in the approximately equivalent form

$$PV_{(g)}=RT+PB. \tag{5}$$

In the numerical equations of this paper, B is to be expressed in cm^3 g-atom^{-1}. The values of dB/dT and d^2B/dT^2 at the temperature at which the equation is applied will be designated by B' and B'', respectively, and the corresponding values at the normal boiling point, 629.74° K, will be designated by B_0, B_0', and B_0''.

θ and T will be used to designate the values of a given temperature on the International and thermodynamic absolute temperature scales, respectively.

3. Enthalpy and Heat Capacity of the Liquid

By extrapolating the experimental enthalpy values (represented by eq 3) to the triple point, −38.88° C (234.28° K), and changing to the units as indicated above (to cal, g-atom, deg K), the enthalpy of the liquid $H_{(l)}$ at any temperature θ, relative to the enthalpy $H_{TP(l)}$ at the triple point, becomes

$$H_{(l)}-H_{TP(l)}=7.25939\theta-1.36651\ (10^{-3})\theta^2 +8.0906(10^{-7})\theta^3-1636.13. \tag{6}$$

The heat capacity equations that are derived from eq 6 must be multiplied by $d\theta/dT$ to account for the difference between thermodynamic (T) and International (θ) temperature scales. However, in the temperature range in which the equations are applicable, the heat capacity varies by only 3 percent. Since $d\theta/dT$ is, at all these temperatures, very close to unity, an error negligible in comparison with the experimental errors of the supporting data is introduced by the more convenient procedure of multiplying by $d\theta/dT$ only the average value of $(\partial H_{(l)}/\partial\theta)s$, taken to be 6.55. This is equivalent to adding as a correction term $6.55[(d\theta/dT)-1]$.

The "saturation" heat capacity ($C_{s(l)}$) can be found from the thermodynamic equation

$$C_{s(l)}=\left(\frac{\partial H_{(l)}}{\partial\theta}\right)_s\frac{d\theta}{dT}-V_{(l)}\left(\frac{\partial P}{\partial\theta}\right)_s\frac{d\theta}{dT}. \tag{7}$$

For mercury below 500° C the last term is small and therefore may be approximated with sufficient accuracy by replacing $d\theta/dT$ by 1 and by substituting for $V_{(l)}$ the constant value 15.9 cm^3 g-atom^{-1}, equal to the volume of the saturated liquid at 400° C [6]. A simple vapor pressure equation, sufficiently accurate for the present purpose, is

$$P=6.345(10^7)e^{-7136.5/\theta}. \tag{8}$$

(This was derived from the values of P and $dP/d\theta$ given at the normal boiling point by eq 19, and provides on differentiation an equivalent of $(\partial P/\partial\theta)_s$). With these substitutions, together with the equivalent of $(\partial H/\partial\theta)_s$ obtained by differentiating eq 6, eq 7 becomes

$$\left.\begin{aligned}C_{s(l)}=7.25939-2.73302(10^{-3})\theta+2.42718(10^{-6})\theta^2\\ -\frac{2.294(10^8)}{\theta^2}e^{-\frac{7136.5}{\theta}}+6.55(d\theta/dT-1).\end{aligned}\right\} \tag{9}$$

The heat capacity at constant pressure may be found from the thermodynamic relation

$$C_p=C_s+T(\partial V/\partial T)_p(\partial P/\partial T)_s. \tag{10}$$

The last term is small in this case and need not be highly accurate. In fact, it will be used with T replaced by θ. Deriving $(\partial P/\partial\theta)_s$ from eq 8 as before, and substituting as a constant value for the slowly changing $(\partial V_{(l)}/\partial\theta)_p$ the value at 400° C [6], $3.09(10^{-3})$ cm^3 g-atom^{-1} deg^{-1}, eq 10 becomes

$$C_{p(l)}=C_{s(l)}+\frac{44585}{\theta}e^{-\frac{7136.5}{\theta}} \tag{11}$$

The heat capacity at constant volume may in turn be calculated from the thermodynamic relation

$$C_v=C_p-\frac{\alpha^2VT}{\beta}, \tag{12}$$

where α and β are the coefficients of isobaric thermal expansion and isothermal compressibility, respectively.

In the use of eq 12 to calculate C_v, use was made of the following equation for the liquid (t being in deg. C):

$$V_{(l)}=14.756+2.678(10^{-3})\,t+1.36(10^{-7})\,t^2 +9.8(10^{-11})t^3+9.93(10^{-13})t^4. \tag{13}$$

This equation was derived from the equation of Sears [6,7] for the relative volume and from the mean experimental value of the density of the liquid at 0° C. Sears' equation seems to be based on data covering the range 0° to 300° C only. However, it fits well the available data for temperatures below 0° C. Its use in this paper between 300° and 500° does not introduce an appreciably increased uncertainty to any of the thermal properties calculated, as

the affected terms in the equations are relatively small.

For the isothermal compressibility, the values of Smith and Keyes [8], extrapolated to zero pressure (the approximate vapor pressure up to 200° C), were used. The values of C_v tabulated in this paper extend only up to 200° C, because reliable values of the compressibility above this temperature are not now available.

4. Entropies of Liquid and Vapor

The entropy of the saturated liquid is

$$S_{(l)}=\int_{T_0}^{T}\frac{C_{s(l)}}{T}dT+S_{0(l)}, \tag{14}$$

where T_0 is the thermodynamic temperature of the normal boiling point (θ=629.74), $S_{0(l)}$ is the absolute entropy of the saturated liquid at that temperature, and C_s is the heat capacity given by eq 9. Of the terms in the second member of eq 9, the sum of all except 6.55000 $d\theta/dT$ is always relatively small, as discussed in the preceding section and may thus, without appreciable error, be conveniently divided by and integrated with respect to θ instead of T. The remaining term must be divided by and integrated with respect to T, giving

$$6.55000\int_{629.74}^{\theta}\frac{d\theta}{T},$$

and this will be replaced by

$$6.55000\ln\frac{\theta}{629.74}+6.55\int_{629.74}^{\theta}\left(\frac{1}{T}-\frac{1}{\theta}\right)d\theta,$$

in order that again the term including the correction will be small. Upon integrating, it is found that

$$\left.\begin{aligned}S_{(l)}=&16.71536\ \log\ \theta-2.73302(10^{-3})\theta\\&+1.21359(10^{-6})\theta^2\\&-4.511\left(\frac{7136.5}{\theta}+1\right)e^{-\frac{7136.5}{\theta}}\\&+6.55\int_{629.74}^{\theta}\left(\frac{1}{T}-\frac{1}{\theta}\right)d\theta\\&-45.548507+S_{0(l)}.\end{aligned}\right\} \tag{15}$$

The value of the entropy of the liquid at the normal boiling point, $S_{0(l)}$, will now be evaluated as a function of the corrections for gas imperfection and temperature-scale divergence. The result is eq 24.

The entropy of the ideal vapor (S^0), with ideality assumed to imply monatomicity as well, is given by the well-known statistical mechanical (so-called Sackur-Tetrode) equation. (The ground state of the mercury atom is singlet. As for all values of entropy in this paper, nuclear-spin and isotopic contributions are omitted.) The equation is as follows:

$$S^0=R\ln\left(\frac{2\pi m}{h^2}\right)^{3/2}\frac{(kT)^{5/2}}{P}+\frac{5}{2}R, \tag{16}$$

where R is the gas constant, m is the mass of the atom, h is Planck's constant, k is Boltzmann's constant, and P is the pressure. The entropy of the real gas at the same pressure can be shown thermodynamically to be less by PB' (see eq 5). Subtracting this and adding the temperature-scale correction lead to

$$S_{(g)}=R\ln\left(\frac{2\pi m}{h^2}\right)^{3/2}\frac{(k\theta)^{5/2}}{P}+\frac{5}{2}R+\frac{5}{2}R\ln\frac{T}{\theta}-PB'. \tag{17}$$

Making the substitutions R=1.98719 cal g-atom^{-1}, m=3.3308(10^{-22})^2 g-molecule^{-1}, h=6.624(10^{-27}) erg-sec, k=1.38047(10^{-16}) erg molecule^{-1} deg^{-1}, and 1 cm^3-mm (of mercury)=3.186484(10^{-5}) cal, eq 17 becomes, for any pressure P,

$$\left.\begin{aligned}S_{(g)}=&11.439185\log\theta-4.575674\log P+26.6702\\&+11.44\log\frac{T}{\theta}-3.186(10^{-5})PB'.\end{aligned}\right\} \tag{18}$$

Beattie, Blaisdell, and Kaminsky [9] have accurately measured the vapor pressure of mercury from 349° to 362° C. They have given the normal boiling point (P=760) as 356.58° C, and in this temperature range the vapor pressure equation (t=deg C International),

$$\left.\begin{aligned}t=&356.580+7.30951(10^{-2})(P-760)\\&-3.9866(10^{-5})(P-760)^2\\&+3.191(10^{-8})(P-760)^3\end{aligned}\right\}, \tag{19}$$

from which their individual determinations vary by only 0.001 deg on the average. Equation 19, which will be adopted in what follows, gives a value of 13.6808 (mm deg^{-1}) for $dP/d\theta$ at the normal boiling point. This value will be substituted into the Clapeyron equation to obtain a value for the entropy of vaporization at this temperature. Substituting for the vapor volume its equivalent from eq 5, the Clapeyron equation may be written

$$S_{(g)}-S_{(l)}=\frac{RT}{P}\left(\frac{\partial P}{\partial T}\right)_s+(B-V_{(l)})\left(\frac{\partial P}{\partial T}\right)_s. \tag{20}$$

If T be replaced by θ, only the first term of the second member is large enough at the boiling point to require the addition of a correction term, which is obviously

$$\frac{R}{P}\left(\frac{\partial P}{\partial\theta}\right)_s\left(T\frac{d\theta}{dT}-\theta\right).$$

[2] Mean molecular mass for the naturally occurring isotopic mixture. The strictly correct procedure of using in eq 17 the weighted mean of the logarithms of the isotopic masses would have resulted, in the case of mercury, in a value of the entropy of the vapor that is only 0.00005 cal g-atom deg^{-1} different.

Equation 20 then becomes

$$S_{(g)}-S_{(l)}=\left(\frac{R\theta}{P}+B-V_{(l)}\right)\left(\frac{\partial P}{\partial\theta}\right)_s + \frac{R}{P}\left(\frac{\partial P}{\partial\theta}\right)_s\left(T\frac{d\theta}{dT}-\theta\right). \quad (21)$$

Letting $\theta=629.74$, at which temperature $V_{(l)}=15.748$ [6], applying the subscript "0" to designate this temperature, and substituting the above value 13.6808 mm deg^{-1} for $(\partial P/\partial\theta)_s$, eq 21 gives

$$\left.\begin{aligned} S_{0(g)}-S_{0(l)}&=22.519887+4.359(10^{-4})B_0\\ &+0.03577(T-\theta)_0\left(\frac{d\theta}{dT}\right)_0\\ &+22.53\left(\frac{d\theta}{dT}-1\right)_0. \end{aligned}\right\} \quad (22)$$

At $\theta=629.74$, eq 18 gives

$$S_{0(g)}=45.508660+11.44\log\left(\frac{T}{\theta}\right)_0-0.02422\,B_0'. \quad (23)$$

Substituting for $S_{0(g)}$ from eq 23 into 22 gives

$$\left.\begin{aligned} S_{0(l)}&=22.988773-0.02422\,B_0'-4.359(10^{-4})\,B_0\\ &+11.44\log\left(\frac{T}{\theta}\right)_0-0.03577\,(T-\theta)_0\left(\frac{d\theta}{dT}\right)_0\\ &-22.53\left(\frac{d\theta}{dT}-1\right)_0. \end{aligned}\right\} \quad (24)$$

And finally, the value of $S_{0(l)}$ may be substituted into eq 15 to give an equation for the absolute entropy of the "saturated" liquid at any temperature in the range covered:

$$\left.\begin{aligned} S_{(l)}&=16.71536\log\theta-2.73302(10^{-3})\theta\\ &+1.21359(10^{-6})\theta^2-4.511\left(\frac{7136.5}{\theta}+1\right)e^{-\frac{7136.5}{\theta}}\\ &-22.559734-0.02422B_0'-4.359(10^{-4})B_0\\ &+6.55\int_{629.74}^{\theta}\left(\frac{1}{T}-\frac{1}{\theta}\right)d\theta+11.44\log\left(\frac{T}{\theta}\right)_0\\ &-0.03577(T-\theta)_0\left(\frac{d\theta}{dT}\right)_0-22.53\left(\frac{d\theta}{dT}-1\right)_0. \end{aligned}\right\} \quad (25)$$

5. Enthalpy of the Vapor; Free Energy; General Vapor Pressure Equation

The relative Gibbs free energy of the liquid may next be found from the entropy and the relative enthalpy, by using the thermodynamic definition

$$F=H-TS. \quad (26)$$

For this purpose eq 26 may be written in the form

$$-(F_{(l)}-H_{TP(l)})=\theta S_{(l)}-(H_{(l)}-H_{TP(l)})+(T-\theta)S_{(l)} \quad (27)$$

From the thermodynamic relation

$$C_P=T\left(\frac{\partial S}{\partial T}\right)_p \quad (28)$$

and eq 18, there is obtained for the heat capacity of the gas at constant pressure

$$C_{p(g)}=4.96797-3.186(10^{-5})P\theta B''. \quad (29)$$

Integration of eq 29 with respect to T at constant pressure yields the enthalpy of the gas at pressure P,

$$H_{(g)}=4.96797\theta+3.186(10^{-5})[B-\theta B']P +4.97(T-\theta)+A. \quad (30)$$

The integration constant A may be expressed in terms of $H_{TP(l)}$ the constant used in the case of the liquid, by utilizing the value obtained from eq 22 for the enthalpy of vaporization at the boiling point. Multiplying eq 22 by the temperature $T_0(=629.74+(T-\theta)_0)$ and neglecting the very small terms as before, there results:

$$\left.\begin{aligned} H_{0(g)}-H_{0(l)}&=14181.674+0.2745B_0\\ &+22.53(T-\theta)_0\left(\frac{d\theta}{dT}+1\right)_0\\ &+1.419(10^4)\left(\frac{d\theta}{dT}-1\right)_0. \end{aligned}\right\} \quad (31)$$

Evaluating eq 6 at $\theta=629.74$ gives

$$H_{0(l)}-H_{TP(l)}=2595.531. \quad (32)$$

By evaluating eq 30 at $\theta=629.74$ and substituting the resulting equivalent of $H_{0(g)}$ into the sum of eq 31 and eq 32, an equivalent of the constant A in terms of $H_{TP(l)}$ is provided that when substituted for A into eq 30 gives

$$\left.\begin{aligned} H_{(g)}-H_{TP(l)}&=13648.676+4.96797\theta\\ &+2022e^{-7136.5/\theta}[B-\theta B']+0.2503B_0\\ &+15.25B_0'+22.53(T-\theta)_0\left(\frac{d\theta}{dT}+1\right)_0\\ &+1.419(10^4)\left(\frac{d\theta}{dT}-1\right)_0\\ &+4.97[(T-\theta)-(T-\theta)_0]. \end{aligned}\right\} \quad (33)$$

In this equation, the vapor pressure has been evaluated (with sufficient accuracy, for the correction

term, from eq 8) and has been substituted for P. Subtraction of eq 6 from eq 33 will give the heat of vaporization at any temperature in the range studied.

The relative Gibbs free energy of the gas, as does that for the liquid, now follows by the use of eq 26, which may now be written in the form

$$-(F_{(g)}-H_{TP(l)})=\theta S_{(g)}-(H_{(g)}-H_{TP(l)})+(T-\theta)S_{(g)}. \tag{34}$$

By equating the free energies of saturated liquid and gas from eq 27 and 34; substituting for the enthalpy and entropy of vapor and liquid from eq 33, 18, 6, and 25; and solving for log P contained in S_g, the following vapor pressure equation is obtained:

$$\left.\begin{aligned}\log P=&11.259839-\frac{3340.449}{\theta}-1.153092\log\theta\\&+2.98647(10^{-4})\theta-8.8409(10^{-8})\theta^2\\&+9.526(10^{-5})\left(\frac{\theta-629.74}{\theta}\right)(B_0+55.56B_0')\\&-\frac{6.963(10^{-6})}{\theta}(PB-760B_0)\\&+0.9860\left(\frac{7136.5}{\theta}+1\right)e^{-\frac{7136.5}{\theta}}\\&+2.500\log\frac{T/\theta}{(T/\theta)_0}-1.431\int_{629.74}^{\theta}\left(\frac{1}{T}-\frac{1}{\theta}\right)d\theta\\&+7.817(10^{-3})\left(\frac{\theta-629.74}{\theta}\right)\\&\left[629.74\left(\frac{d\theta}{dT}-1\right)_0+(T-\theta)_0\left(\frac{d\theta}{dT}\right)_0\right]\\&+\frac{1}{\theta}\left[\left\{1.8705-1.1531\log\theta+\frac{3099.3}{\theta}\right.\right.\\&+5.973(10^{-4})\theta\\&\left.\left.-2.652(10^{-7})\theta^2\right\}(T-\theta)-3.838(T-\theta)_0\right].\end{aligned}\right\}\tag{35}$$

(In the part of the last bracketed term which represents the entropy of vaporization, all minor terms have been omitted, since they would be multiplied by the very small factor $(T-\theta)$. In this bracketed term, P (contained in the equivalent of $S_{(g)}$) has been replaced by its equivalent in terms of θ, by using eq 8.)

If the specific corrections for gas imperfection and temperature-scale differences described in the next two sections be adopted, eq 35 may be approximated by the following more readily applicable vapor pressure equation:

$$\left.\begin{aligned}\log P=&11.257555-\frac{3339.202}{\theta}-1.153092\log\theta\\&+2.95697(10^{-4})\theta-7.4588(10^{-8})\theta^2\\&-1.5605(10^{-11})\theta^3+3.600e^{-5360/\theta}.\end{aligned}\right\}\tag{36}$$

Between 100° and 500° C, this equation reproduces the vapor pressures of eq 35 to within 0.01 percent. Below 100°, however, it gives lower values, the discrepancy amounting to 0.1 percent at 25° and 0.6 percent at −39°, the triple point.

6. Calculation of the Second Virial Coefficient; Corrections for Gas Imperfection

Smith and Menzies [10] found the density of mercury vapor to be ideal between 360° and 400° C to within their probable experimental error, about 2 percent. Apparently no one has measured such densities with much greater accuracy.

Approximate values for the degrees of gas imperfection at various temperatures have been calculated for many gases by the use of some equation of state, such as Berthelot's. To employ the last equation, the critical constants must be known. In the case of mercury, however, the values that have been reported for the critical temperature (around 1,500° C) and critical pressure (from 1,000 to 3,500 atm) show such wide variations that this method is hardly applicable.

There is abundant spectroscopic evidence that mercury vapor contains appreciable amounts of the dimer Hg_2, which is known to possess a singlet ground state. Adopting suitable constants for this molecule as described below, values of the second virial coefficient B of mercury vapor, treated as an imperfect monatomic gas in which only binary collisions are important below 500° C, were calculated from the following statistical mechanical equation [11]:

$$B(T)=-2\pi N\int_0^{\infty}(e^{-U(r)/RT}-1)r^2dr, \tag{37}$$

where N is Avogadro's number, and $U(r)$ is the potential energy of a mole of Hg_2 molecules, all at an interatomic separation of r. $U(r)$ was calculated from a Morse potential function in which it was assumed that the equilibrium separation is $3.2(10^{-8})$ cm, and that the first vibrational constant ω_e is 36 cm^{-1}. The former figure, derived from data on liquid mercury, has been generally accepted as approximately correct. The latter figure, considered by Kuhn [12] to be the most likely choice among alternative multiples for which there is spectroscopic evidence, is supported by the theoretical calculation of a value of 35 cm^{-1} by Heller [13], whose values for a number of other diatomic molecules are in good agreement with well-established experimental values.

The third parameter needed in the use of the Morse function is the molar dissociation energy of the Hg_2 molecule in its ground state. Evidence for various values has been described in the literature. London [14] made a theoretical calculation of the polarization

force and arrived at 2.0 kcal mole^{-1}; however, Kuhn [12] points out that this is undoubtedly too high because of the neglect of repulsion forces. Kuhn measured the total absorption in the discrete band system (2,540 A) at 175° C and calculated a value for the concentration of Hg_2. He claims that the extrapolation to 0° K (giving a dissociation energy of 2.1 kcal) yields too high a value because of the neglect of vibrational anharmonicity. If this be true, then, as he claims, the values obtained by measuring the decrease in absorption with rising temperature are too low. By the latter method and with the assumption of vibrational harmonicity, Koernicke [15] found a dissociation energy of 1.4 kcal, Kuhn and Freudenberg [16] found 1.6 kcal, and Winans and Heitz [17] found 1.38 ±0.07 kcal. Gaydon [18] recommends the latter value for the dissociation energy, whereas Herzberg [19] lists 1.84 kcal.

Equation 37 was solved graphically by the authors for values of B at the temperatures T=430, 530, 630, and 730, by using for each temperature values of 1.4, 1.5, 1.6, and 1.7 kcal for the molar dissociation energy of Hg_2. In these ranges the calculated value of B for a given temperature varies almost linearly with the value of the dissociation energy used. The thermodynamic properties of mercury listed in this paper were calculated assuming a value of 1.5 kcal as a reasonable weighted mean of the above values of the dissociation energy. This particular value was adopted partly because of the support it receives in figure 4, where calculated and experimental vapor pressures are compared. The following empirical equation represents the corresponding values of the second virial coefficient B, in cm^3 g-atom^{-1}, in this temperature range:

$$B=56.4-43.82e^{\frac{655}{\theta}}, \tag{38}$$

which agrees with the directly calculated values to within 0.5 percent from θ=430 to θ=730. On differentiation with respect to temperature, eq. 38 gives:

$$B'=\frac{655}{\theta^2}(56.4-B). \tag{39}$$

Values calculated from eq 38 and 39 are listed in table 2.

TABLE 2. *Second virial coefficient (B) and its temperature derivative (B') for mercury vapor*

Temperature	B	B'	Temperature	B	B'
°C	cm^3 g-atom^{-1}	cm^3 g-atom^{-1} deg^{-1}	°C	cm^3 g-atom^{-1}	cm^3 g-atom^{-1} deg^{-1}
100	−197	+1.19	320	−76	+0.25
120	−175	0.98	340	−71	.22
140	−158	.82	356.58(bp)	−68	.20
160	−142	.69	360	−67	.20
180	−130	.59	380	−63	.18
200	−118	.51	400	−60	.17
220	−109	.45	420	−56	.15
240	−101	.39	440	−53	.14
260	−93	.34	460	−51	.13
280	−87	.31	480	−48	.12
300	−81	.27	500	−46	.11

7. Corrections to Basis of Thermodynamic Temperature Scale

The results of recent investigations [20] of the differences between the thermodynamic and International temperature scales have been formulated by an equation [21] equivalent to the following:

$$T-\theta=0.6381-4.809(10^{-3})\theta+1.1096(10^{-5})\theta^2 -7.481(10^{-9})\theta^3 \tag{40}$$

(The value of $(T-\theta)$ is so small and changes so slowly with temperature that when desirable, θ may be replaced by T in the second member of eq 40 without appreciably changing the corrections calculated.)

It is believed that the differences given by eq 40 are the most probable values in the light of the evidence now available, and that their uncertainties may be considered to correspond to probable errors of about half their respective values. All thermodynamic properties given in this paper have been corrected by this equation to units involving deg K thermodynamic, though for convenience of usage the tabulated values of these properties have been calculated for rounded temperatures on the International scale of 1948.

By use of eq 40 it may be shown that the integral appearing in eq 25 and 35 is approximately as follows

$$\left.\begin{aligned}\int_{629.74}^{\theta}\left(\frac{1}{T}-\frac{1}{\theta}\right)d\theta=0.01107\ \log\ \theta+\frac{0.6381}{\theta}\\ -1.1096(10^{-5})\theta\\ +3.7405(10^{-9})\theta^2-0.0264958\end{aligned}\right\} \tag{41}$$

V. Tables

1. Thermodynamic Properties

In tables 3, 4, and 5, values calculated from preceding equations are given for saturated liquid and gaseous mercury at temperatures from the triple point, −38.88° C [22], to 500° C. The numbers in parentheses given under the symbols heading the various columns indicate the particular equations from which the values were calculated.

Though the tabulated values of the heat capacities of the liquid were calculated to apply at the vapor pressures, the corresponding values of $C_{p(l)}$ at any small fixed pressure are practically identical. For it may be readily shown by using eq 13 that $C_{p(l)}$ varies by not more than 0.001 percent in this temperature range when the pressure varies by 1 atm.

It will be noted that the free-energy values calculated from eq 27 and listed in table 5 apply to either the saturated liquid or vapor.

TABLE 3. *Relative enthalpy; heat of vaporization; compressibility factor*

Temperature	Relative enthalpy		Heat of vaporization, $H_{(g)}-H_{(l)}$	Compressibility factor of vapor, $pV_{(g)}/RT$
	Liquid, $H_{(l)}-H_{TP\,(l)}$ (6)	Vapor, $H_{(g)}-H_{TP\,(l)}$ (33)	(6, 33)	(5)
°C Int	cal g-atom^{-1}	cal g-atom^{-1}	cal g-atom^{-1}	
−38.88[a] (tp)	0.00	14800.8	14800.8	1.0000
−20	127.20	14894.5	14767.3	1.0000
0	261.37	14993.8	14732.4	1.0000
20	394.98	15093.1	14698.1	1.0000
25	428.29	15118.0	14689.7	1.0000
40	528.06	15192.5	14664.4	1.0000
60	660.65	15291.8	14631.2	1.0000
80	792.80	15391.2	14598.4	1.0000
100	924.54	15490.6	14566.1	1.0000
120	1055.91	15590.0	14534.1	1.0000
140	1186.96	15689.4	14502.4	1.0000
160	1317.71	15788.8	14471.1	1.0000
180	1448.21	15888.1	14439.9	1.0000
200	1578.49	15987.5	14409.0	0.9999
220	1708.60	16086.8	14378.2	.9999
240	1838.58	16186.0	14347.4	.9998
260	1968.46	16285.1	14316.6	.9997
280	2098.28	16384.1	14285.8	.9996
300	2228.08	16482.9	14254.8	.9994
320	2357.90	16581.6	14223.7	.9992
340	2487.78	16679.9	14192.1	.9990
356.58 (bp)	2595.53	16761.2	14165.7	.9987
360	2617.76	16778.0	14160.2	.9986
380	2747.88	16875.7	14127.8	.9982
400	2878.17	16973.1	14094.9	.9978
420	3008.67	17070.0	14061.3	.9972
440	3139.42	17166.4	14027.0	.9966
460	3270.47	17262.3	13991.8	.9959
480	3401.85	17357.7	13955.8	.9950
500	3533.59	17452.4	13918.8	.9942

TABLE 4. *Heat capacity*

Temperature	Heat capacity			
	Liquid			Vapor
	$C_{s\,(l)}$ (9)	$C_{p\,(l)}$ (11)	$C_{v\,(l)}$ (12)	$C_{p\,(g)}$ (29)
°C Int	cal g-atom^{-1} deg^{-1}	cal g-atom^{-1} deg^{-1}	cal g-atom^{-1} deg^{-1}	cal g-atom^{-1} deg^{-1}
−38.88[a] (tp)	6.7578	6.7578	5.969	4.968
−20	6.7272	6.7272	5.900	4.968
0	6.6967	6.6967	5.831	4.968
20	6.6683	6.6683	5.769	4.968
25	6.6615	6.6615	5.752	4.968
40	6.6419	6.6419	5.708	4.968
60	6.6176	6.6176	5.650	4.968
80	6.5954	6.5954	5.594	4.968
100	6.5752	6.5752	5.544	4.968
120	6.5571	6.5571	5.494	4.968
140	6.5410	6.5410	5.449	4.968
160	6.5270	6.5270	5.403	4.968
180	6.5150	6.5150	5.364	4.969
200	6.5050	6.5050	5.335	4.969
220	6.4970	6.4970	----------	4.970
240	6.4909	6.4910	----------	4.970
260	6.4867	6.4869	----------	4.971
280	6.4845	6.4847	----------	4.973
300	6.4840	6.4843	----------	4.975
320	6.4853	6.4858	----------	4.977
340	6.4884	6.4890	----------	4.980
356.58 (bp)	6.4922	6.4930	----------	4.983
360	6.4931	6.4940	----------	4.984
380	6.4993	6.5005	----------	4.988
400	6.5071	6.5087	----------	4.993
420	6.5164	6.5186	----------	4.999
440	6.5270	6.5298	----------	5.005
460	6.5390	6.5426	----------	5.013
480	6.5522	6.5567	----------	5.021
500	6.5666	6.5723	----------	5.030

[a] Triple point.

TABLE 5. *Entropy; relative free energy; vapor pressure*

Temperature	Absolute entropy		Relative free energy (liquid or vapor), $-(F-H_{TP\,(l)})$	Vapor pressure, P
	Liquid, $S(l)$ (25)	Vapor, $S(g)$ (18)	(27)	(35)
°C Int.	cal g-atom^{-1} deg^{-1}	cal g-atom^{-1} deg^{-1}	cal g-atom^{-1}	mm Hg
−38.88 [a] (tp)	16.5045	79.6736	3867.1	$2.191(10^{-6})$
−20	17.0267	75.3563	4183.4	$2.336(10^{-5})$
0	17.5367	71.4701	4529.0	$1.996(10^{-4})$
20	18.0088	68.1470	4884.4	$1.268(10^{-3})$
25	18.1215	67.3906	4974.7	$1.935(10^{-3})$
40	18.4480	65.2766	5248.9	$6.340(10^{-3})$
60	18.8584	62.7760	5622.0	0.026048
80	19.2436	60.5809	6003.2	.090954
100	19.6065	58.6409	6391.8	.27710
120	19.9494	56.9161	6787.6	.75213
140	20.2745	55.3742	7190.0	1.8499
160	20.5836	53.9894	7598.9	4.1795
180	20.8781	52.7401	8013.8	8.7734
200	21.1594	51.6086	8434.4	17.273
220	21.4286	50.5798	8860.6	32.147
240	21.6870	49.6414	9292.1	56.931
260	21.9351	48.7828	9728.6	96.481
280	22.1741	47.9949	10169.9	157.234
300	22.4045	47.2699	10615.9	247.413
320	22.6270	46.6013	11066.4	377.27
340	22.8421	45.9828	11521.2	559.22
356.58 (bp)	23.0153	45.5047	11901.4	760.00
360	23.0505	45.4098	11980.2	808.00
380	23.2525	44.8776	12443.1	1140.65
400	23.4486	44.3824	12909.9	1576.64
420	23.6391	43.9207	13380.4	2137.76
440	23.8246	43.4895	13854.6	2848.09
460	24.0051	43.0861	14332.2	3733.8
480	24.1812	42.7080	14813.2	4822.9
500	24.3529	42.3531	15297.5	6145.4

[a] Triple point.

2. Effects of Gas Imperfection and Temperature Scale

The values listed in tables 3, 4, and 5 contain contributions from the small terms (in the equations) that contain B, or its derivatives, or T and that thus correct for gas imperfection of mercury vapor and for the deviations between the thermodynamic and International temperature scales. When these contributions for a given property vary appreciably with temperature, they are listed separately in tables 6 and 7 for a number of temperatures. (Except for vapor pressure these are listed in the same units as the values in tables 3, 4, and 5.) The magnitudes of these contributions depend in most cases on the particular way in which the properties have been calculated in this paper, as well as on what basic data have been used. Consequently, they are not intrinsically characteristic of the properties themselves.

Table 3. There are no contributions to the relative enthalpy of the liquid, as the values used are those measured essentially directly. The contributions are hence identical for the relative enthalpy of the vapor and for the heat of vaporization. These are listed in tables 6 and 7.

Table 4. The three calculated heat capacities of the liquid have no contribution from gas imperfection. At a given temperature they have identical contributions from the temperature-scale correction, as listed in table 7. The contribution to $C_{p\,(g)}$ from gas imperfection is the deviation from 5/2 R (i. e., from 4.968 cal g-atom^{-1}deg^{-1}).

TABLE 6. *Contributions to thermodynamic properties from gas imperfection of mercury vapor*

Temperature	To $H_{(g)}-H_{TP(l)}$ and $H_{(g)}-H_{(l)}$	To $S_{(g)}$	To $-(F-H_{TP(l)})$	To vapor pressure
°C	*Cal g-atom*$^{-1}$	*cal g-atom*$^{-1}$ *deg*$^{-1}$	*cal g-atom*$^{-1}$	*Percent*
−38.88	−13.8	0.0000	+5.7	+1.73
0	−13.8	.0000	+6.7	+1.31
40	−13.8	.0000	+7.7	+0.98
80	−13.8	.0000	+8.6	+.73
120	−13.8	.0000	+9.6	+.53
160	−13.9	−.0001	+10.6	+.37
200	−14.0	−.0003	+11.6	+.24
240	−14.3	−.0007	+12.6	+.14
280	−15.1	−.0015	+13.5	+.061
320	−16.5	−.0030	+14.5	+.015
356.58	−18.6	−.0049	+15.4	.000
360	−18.8	−.0052	+15.5	.000
400	−22.4	−.0085	+16.5	+.021
440	−27.8	−.0129	+17.4	+.082
480	−35.1	−.0186	+18.4	+.18
500	−39.7	−.0218	+18.9	+.25

TABLE 7. *Contributions to thermodynamic properties from correction to thermodynamic temperature scale*

Temperature	To $H_{(g)}-H_{TP(l)}$ and $H_{(g)}-H_{(l)}$	To $C_{s(l)}$, $C_{p(l)}$, $C_{v(l)}$	To $-(F-H_{TP(l)})$	To vapor pressure
°C	*cal g-atom*$^{-1}$	*cal g-atom*$^{-1}$ *deg*$^{-1}$	*cal g-atom*$^{-1}$	*Percent*
−38.88	+2.0	+0.0055	+1.0	−0.20
0	+1.9	+.0028	+0.7	−.47
40	+1.8	+.0004	+0.6	−.49
80	+1.8	−.0015	+0.8	−.43
120	+1.9	−.0029	+1.1	−.33
160	+2.0	−.0039	+1.7	−.23
200	+2.2	−.0044	+2.3	−.14
240	+2.3	−.0044	+3.0	−.077
280	+2.4	−.0039	+3.6	−.031
320	+2.5	−.0030	+4.2	−.006
356.58	+2.6	−.0017	+4.6	.000
360	+2.6	−.0016	+4.6	+.002
400	+2.6	+.0003	+4.8	−.009
440	+2.6	+.0026	+4.6	−.035
480	+2.4	+.0054	+4.1	−.075
500	+2.4	+.0070	+3.7	−.100

Table 5. To the entropy of the liquid the contribution from gas imperfection is the same at all temperatures, +0.0245 cal g-atom^{-1}deg^{-1}. The contribution to the entropy from the temperature-scale correction is practically constant, being equal to +0.002 cal g-atom^{-1}deg^{-1} at all temperatures in the case of the liquid and not lying outside the range 0.000 to +0.001 in the case of the vapor. The other contributions to the entropy of the vapor, the free energy, and the vapor pressure are listed in tables 6 and 7.

VI. Discussion of Results

1. Reliability

An index to the reproducibility, or "precision", of the enthalpy measurements on liquid mercury is afforded by the deviations from the means, as shown by the results of the individual measurements, which are recorded in table 1. Another index is provided by the deviations (also listed in table 1) from the smoothed values as represented by the empirical equation adopted. All the results lead to an average probable error of the mean of about 0.02 percent on enthalpy, and a corresponding magnitude of about 0.1 percent on the derived heat capacity values ($C_{s(l)}$ or $C_{p(l)}$).

One check on the over-all accuracy of the apparatus in measuring enthalpy was made by measuring the heat delivered to the ice calorimeter by a Monel capsule containing water and dropping from 250° C. By thus determining in several measurements the difference in heats for two amounts of water differing by about 6 g, a mean value of 1042.05 abs j g^{-1} for α_0^{250} of water, an enthalpy function defined elsewhere [23], was obtained. This figure differs by only 0.02 percent from the value of 1041.85 published in the latest report [24] on the thermal properties of water as accurately measured earlier in this laboratory by an adiabatic calorimeter.

The various sources of appreciable systematic error were examined in order to estimate their likely contributions. As measurements by the General Electric Co. [24a] of Nitralloy and of Swedish iron in mercury at various temperatures indicate a solubility of less than 1 part in 100,000,000 at 500° C, no error in the enthalpy should be caused by the dissolving of the container. Considering the uncertainty in each possible error, the authors believe that the values of the enthalpy of the liquid given in table 3 are accurate to 0.1 percent, except below 100° C, where small errors in measurement become relatively more important as 0° C is approached. As a consequence, it is believed that the corresponding uncertainties in the heat capacity values $C_{s(l)}$ and $C_{p(l)}$ (table 4) may be as large as 0.3 percent between 25° and 425° C. Outside this temperature range the values given should be considered much more uncertain, as they resulted from the extrapolation of an empirical function beyond the range of experimental measurements.

The calculated properties other than the enthalpy and heat capacity of the liquid are, as pointed out earlier in this paper, subject to varying uncertainties caused by uncertainties in the corrections for gas imperfection and temperature scale. The values in tables 6 and 7 should aid in estimating such uncertainties in specific cases. In many cases the difference between the values at two temperatures for a given property will be much more accurate than the listed absolute magnitude of the property itself.

The value of the absolute entropy as calculated here may be compared with that arrived at through use of low-temperature heat-capacity data for solid mercury. For liquid mercury at the triple point, for example, table 5 gives a value of 16.50 cal g-atom^{-1}deg^{-1}, based principally on vaporization data. If eq 19, representing the vapor pressure data of Beattie, Blaisdell, and Kaminsky [9], can be accepted as having an accuracy comparable to that which they claim, the entropy value just quoted should not be uncertain beyond a very few hundredths of a cal g-atom^{-1}deg^{-1}. This estimate includes the consideration of the aforementioned uncertainty in the extrapolated heat capacity of the liquid between 0° C and the triple point.

Pickard and Simon [25] have recently measured the heat capacity of solid mercury down to 3° K.

By using their data and those of others, the authors have computed a value of 14.34 cal g-atom^{-1}deg^{-1} for the entropy of solid mercury at the triple point. Addition of the entropy of fusion, 2.38 cal g-atom^{-1}-deg^{-1} [26, 27], gives a value of 16.72 for the liquid at the same temperature. This is 0.2 cal g-atom^{-1}-deg^{-1} higher than the value in table 5. The discrepancy seems to the authors as more likely due to errors in the low-temperature heat-capacity data than to any other source.

The effect of certain possible errors on the accuracy of vapor pressures as calculated by eq 35 will now be examined. As stated earlier, this equation has been adjusted to agree with the empirical eq 19 at, and in the immediate vicinity of, the normal boiling point, which both equations give as 356.58° C. (However, according to the experimental results on which eq 19 is based, there may be an absolute error of 0.01 deg in this temperature, corresponding to an error of 0.02 percent in the vapor pressure at any neighboring temperature.) Equation 19 gives values of vapor pressure at 350° and 362° C (temperatures near the extremes of the range of claimed validity of the equation) that are higher by 0.004 and 0.001 percent, respectively, than those given by eq 35. These divergences are within the precision of the data on which eq 19 is based.

The small uncertainty in the temperature assumed for the normal boiling point will affect all vapor pressures calculated from eq 35 by the same percentage. There are four other factors contributing significant uncertainty to these calculated pressures, and as the temperature becomes increasingly higher or lower than the boiling point, the effect of each of these four factors becomes acceleratingly greater. These factors are (1) degree of gas imperfection, (2) thermodynamic temperature scale, (3) heat of vaporization at the normal boiling point, and (4) average heat capacity of the liquid between the boiling point and the temperature in question. Taking the uncertainty in the last factor to be 0.3 percent, as estimated above, it was computed that the resulting uncertainties in the calculated vapor pressures would be as follows: At −39° C, 0.7 percent; at 100°, 0.15 percent; and at 250° or 500°, 0.02 percent. The assumption of these and reasonable uncertainties in each of the other factors has led to the assignment of the following uncertainties in individual values of vapor pressure calculated from eq 35 and listed in table 5: At −39° C, 1.5 percent; at 100°, 0.5 percent; at 250° or 500°, 0.2 percent; and at 357° (the boiling point), 0.03 percent. These figures were arrived at without consideration of agreement of the calculated vapor pressures with any direct measurements, except those represented by eq 19.

A number of investigators [28 to 33] have directly measured the vapor pressure of mercury in this temperature range. The deviations of most of the more precise of these experimental values from those given by eq 35 are shown in figure 1. In most of these measurements there was an average variation of several times the uncertainties just stated.

2. Comparison of Liquid Heat Capacity Values With Those of Other Experimental Investigations

A number of other investigators [34 to 47] have measured the heat capacity of mercury above 0° C. Most of these results are shown in figure 2 for comparison with the results reported in this paper. The experimental points labeled NBS were calculated by dividing by the temperature interval the differences in the mean unsmoothed experimental heats for pairs of successive furnace temperatures. A very small correction for curvature was applied.

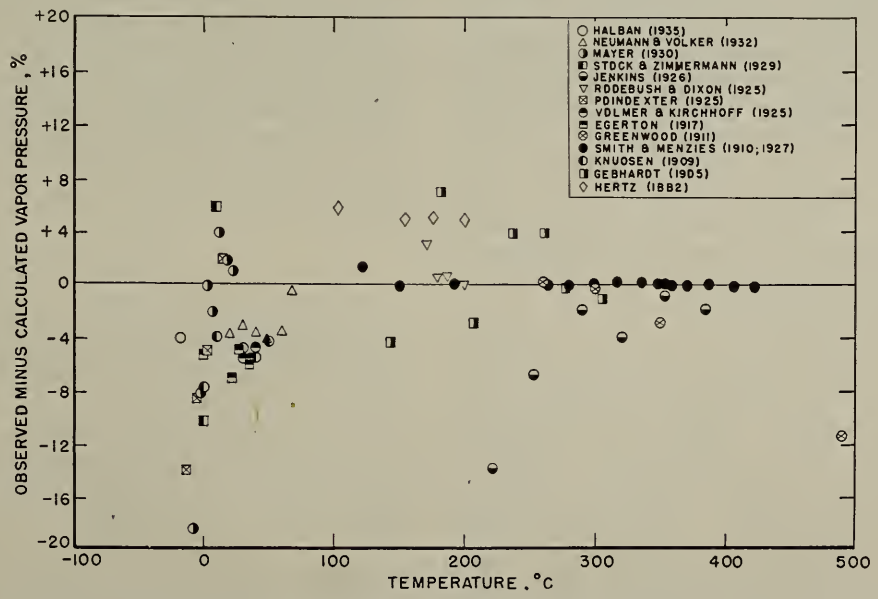

FIGURE 1. *Comparison between values of vapor pressure of mercury observed by various workers and values calculated from eq. 35.*

To avoid confusion, only representative data of each worker are shown. The temperatures of Smith and Menzies have been corrected by table 8.

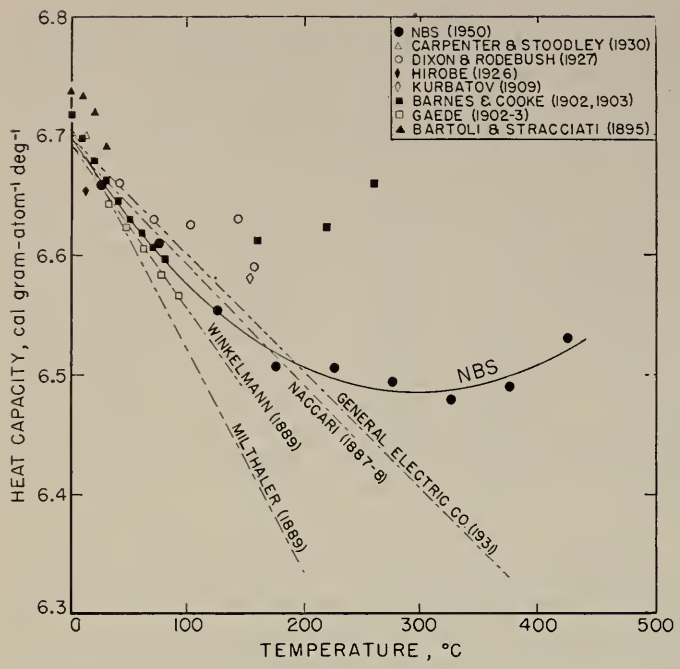

FIGURE 2. *Saturation heat capacity (C_s) of liquid mercury, as found by various investigators.*

Most observers are in substantial agreement below 100° C, but those who extended their measurements to higher temperatures show considerable disagreement. Gaede [42] employed an essentially adiabatic calorimeter; Hirobe [46] used an isothermal one; and Dixon and Rodebush [41], claiming an accuracy of approximately 1 percent, resorted to adiabatic compression. The observations of Milthaler [39], Naccari [37], and Winkelmann [38], all of whom employed the method of mixtures, agree approximately, as to a value of the negative temperature coefficient, with the later measurements of the General Electric Co. [45]. The measurements of Barnes and of Barnes and Cooke [34] were made, apparently, with considerable care by using a continuous flow method previously employed in measuring the specific heat of water. They considered their measurements below 100° to be accurate to 0.1 percent. However, above 150° their values differ markedly from those of all other observers, including the present authors. In spite of this difference, their values have often been considered by some in the past to have a reliability superior to the heat-capacity values of mercury of the other observers.

Recently Kleppa [48] has used an electronic pulse-circuit technique to measure ultrasonic velocities in mercury at 50° and 150° C, obtaining a precision of about 1 percent. When these velocities were combined with the coefficients of thermal expansion given by eq 13 and with the values of $C_{p\,(l)}$ interpolated from table 4, they gave values of $C_{v\,(l)}$ of 5.72 $\pm$0.01 and 5.49 $\pm$0.01 cal g-atom^{-1}-deg^{-1}, respectively, at these two temperatures. The corresponding values of $C_{v\,(l)}$ interpolated from table 4, based on the directly measured compressibilities of Smith and Keyes [8], are 5.68 and 5.43, respectively.

3. Isobaric and Isochoric Heat Capacities of the Liquid

The values of the heat capacities of the liquid C_p and C_v that are given in table 4 are represented graphically in figure 3 as multiples of the gas constant R. It is of interest that the curve for C_p shows a minimum at a temperature somewhat below the boiling point. This is analogous to the results obtained by the authors for two other liquid metals, sodium [3] and potassium [49], whose values of C_p were found to exhibit even deeper minima than mercury, and at temperatures somewhat below their respective normal boiling points.

It is well known that the theoretical interpretation of C_v is simpler than that of C_p. The curve for C_v of liquid mercury in figure 3, in contrast to that for C_p, shows no definite evidence of extrapolating to a minimum below the critical temperature, indicating that the distinct minimum in C_p is caused by the increasing difference between C_p and C_v as the temperature rises. (Though Smith and Keyes [8] measured the compressibility of mercury up to 300° C, their values above 200° show a very rapid and unexpected increase, which would lead to a minimum in the calculated curve for C_v above this temperature. However, they discredited their results above 200° because of invalidating experimental circumstances.)

It is of interest that the value of C_v calculated in this paper (table 4) for liquid mercury at its triple point is only 0.1 percent different from $3R$, which is the value predicted at this temperature by a recent fairly successful theoretical treatment of liquid mercury [50]. According to some recently published theories [51], a liquid exhibits a fairly continuous transition from the crystalline to the gaseous state as the temperature rises. The heat capacity C_v of a monatomic liquid, taken at small pressures, may be expected to vary from approximately $3R$ at the triple point and approach $\frac{3}{2}R$ near the critical point. The decrease in C_v as the temperature rises may be interpreted as being due to a decreasing contribution to disorderliness in the liquid. The curve for C_v of mercury shown in figure 3 is consistent with this picture.

4. Vapor Pressure

Near the normal boiling point, 357° C, the terms for gas imperfection have very little influence on the values calculated for the vapor pressure from eq 35. However, as pointed out in an earlier section, the effect is many times as great at much higher or lower temperatures. If the calculated vapor pressures at such temperatures agree with corresponding measured values, there is thus afforded an independent experimental check on the adopted value of the principal parameter determining the gas-imperfection corrections in the various equations for thermodynamic properties. This assumes, of course, that the experimental values of vapor pressure have sufficient accuracy and precision.

The vapor pressure of mercury has been measured by various workers [52] from the triple point to 1400° C. Though at very low and very high temperatures in this range the percentage accuracy of the vapor pressure measurements need not be very great, the precision of most of these results is so relatively poor as to exclude their use for this test.

In 1910 Smith and Menzies [53] carefully measured the vapor pressure of mercury from about 250° to 435° C with a precision of about ±0.1 percent. The temperatures were recalculated by Menzies [52] in 1927 on the basis of the new value for the sulfur boiling point. Menzies added three more experimental points between 120° and 200° C and derived the following equation to represent the data:

$$\log P = 9.957094 - \frac{3283.92}{\theta'} - 0.665240 \log \theta', \quad (42)$$

where

$$\theta' = t' + 273.1, \quad (43)$$

t' being deg C Int as measured by the platinum thermometer of Smith and Menzies.

The authors have recalculated Menzies' centigrade temperatures, as given by eq 43, in accordance with the present knowledge of the platinum-thermometer scale. Smith and Menzies [54] had reported for their thermometer a δ value of 1.6147, on the basis of their assumed sulfur boiling point of 445° C. Correcting this to the basis of the temperature assumed by Menzies in 1927, 444.6°, yields a value of δ of 1.5919. Equation 42 gives a mercury normal boiling point of 356.711° C, which is 0.13 deg higher than reported by Beattie, Blaisdell, and Kaminsky [9]. Waidner and Burgess [55] and Beattie, Blaisdell, and Kaye [56] have found independent evidence that a platinum thermometer accurately calibrated at the ice, steam, and sulfur points indicates for the mercury boiling point a temperature depending fairly systematically on the δ value of the thermometer. In fact, Beattie et al. have argued that by adding the mercury boiling point as a fourth calibration point and using a cubic temperature-resistance relation, the platinum-thermometer scale will be approximately independent of the thermometer constants.

This recommendation has been followed here. A cubic temperature-resistance equation has been derived that gives the same temperatures for the ice, steam, and sulfur points but a value of 356.58° C. for the mercury boiling point when there are substituted the resistances given for these four temperatures by a Callendar equation with $\delta = 1.5919$, and with the mercury boiling point taken as 356.711° C. Equating the resistances given by the two equations indicates that the Centigrade temperatures given by eq 42 should be changed by the amounts shown in table 8 to accord with a four-point calibration. Though a fourth calibration point is obviously, in itself, an asset toward greater accuracy, it is believed that considerably more uncertainty should be attached to the interpolations of temperature provided by a thermometer with such a high δ value than to those by thermometers meeting present-day standards.

After correcting the Centigrade temperatures of eq 42 by the values of table 8, figure 4 was obtained for the differences between the experimental vapor pressures of Smith and Menzies and those calculated from eq 35. The four curves represent the differences obtained depending on what dissociation energy is made the basis of calculating the gas-imperfection terms in the latter equation. This equation has been derived to give the experimentally measured normal boiling point regardless of the magnitudes of the gas imperfections assumed. For a range of 200 deg below the boiling point, the best agreement between experimental and calculated vapor pressures is seen to correspond to a gas imperfection equivalent to a dissociation energy of 1.5 kcal mole^{-1} of Hg_2. This value was claimed earlier in this paper to be a reasonable weighted mean of those indicated by independent spectroscopic evidence. However, in view of the smallness of the

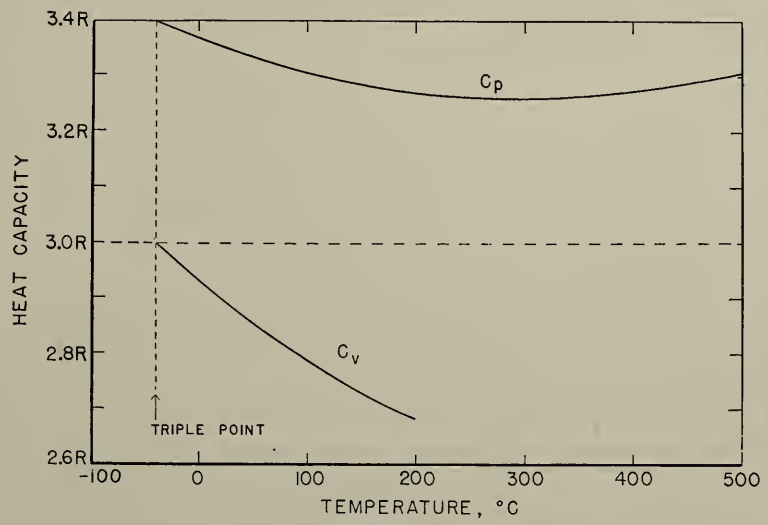

FIGURE 3. *Heat capacities of liquid mercury at constant pressure and constant volume.*

deviations of figure 4 and the uncertainties in some of the small corrections applied to both experimental and calculated vapor pressures, the agreement may be somewhat fortuitous.

TABLE 8. *Correction of temperature values of a platinum thermometer with $\delta = 1.5919$ to accord with a four-point calibration in which the mercury boiling point is changed from 356.711° to 356.58° C*

Temperature	Correction
°C Int.	*°C Int.*
100	0.000
150	−.033
200	−.076
250	−.115
300	−.138
330	−.140
356.58	−.131
400	−.089
430	−.034
444.6	.000

It will be noted that above the boiling point all four curves indicate lower experimental than calculated vapor pressures. This may be attributed quantitatively, in large part, to the fact that as the temperature rises the saturated vapor becomes denser, and as a result the empirical eq 42, derived to fit the data well near the boiling point and at lower temperatures, is too simple to represent the increasing importance of gas imperfection and liquid volume.

The ordinate differences in figure 4 are of the same order of magnitude as the absolute uncertainties assigned in an earlier section to the vapor pressures calculated from eq 35. However, the several factors named there as affecting the accuracy of this equation have effects that vary in roughly comparable ways with temperature. Therefore, errors in the adopted magnitudes of their effects on the calculated vapor pressures at various temperatures would be capable of being compensated considerably by the choice of a single somewhat erroneous value for the dissociation energy of Hg_2 for calculating the effects of gas imperfection. It is thus possible that the choice of 1.5 kcal per mole (made partly on the basis of the apparent agreement in fig. 4 between observed and calculated vapor pressures when this value is selected) is of this nature.

Nevertheless, it is believed that the comparison afforded by figure 4 provides confirmatory evidence that the values of dissociation energy and second virial coefficient of mercury that were selected in this paper are not far from the correct ones. That this comparison between observed and calculated vapor pressures has such significance is due in no small degree to the accuracy of the experimental values of liquid heat capacity recently measured and reported in this paper. For a given temperature, an error in the heat capacity produces an approximately proportional error in the vapor pressure calculated in this manner. The previously available heat capacity values, because of their disagreement in the region above and below the boiling point, would no doubt have been considered up to 10 times as uncertain. Therefore had it been necessary to rely on these previous values, the relatively small differences of such a comparison graph as figure 4 would have had very much less significance.

The heat-capacity measurements were greatly expedited by the commendable cooperation of Leo F. Epstein and his associates, of the Knolls Atomic Power Laboratory, Schenectady, N. Y. Under his direction the mercury samples were painstakingly prepared and supplied in a state of very high purity and ready for the thermal measurements. Collaborating with him in this work were L. W. Hibbs, Jr., who purified the mercury, filled and sealed the containers, and tested them; George Strichman, who tested the containers for tightness; and R. E. Schofield, who performed the mass-spectrometer analyses.

The authors express their special indebtedness also to certain members of this Bureau. B. F. Scribner and his associates performed a spectrochemical

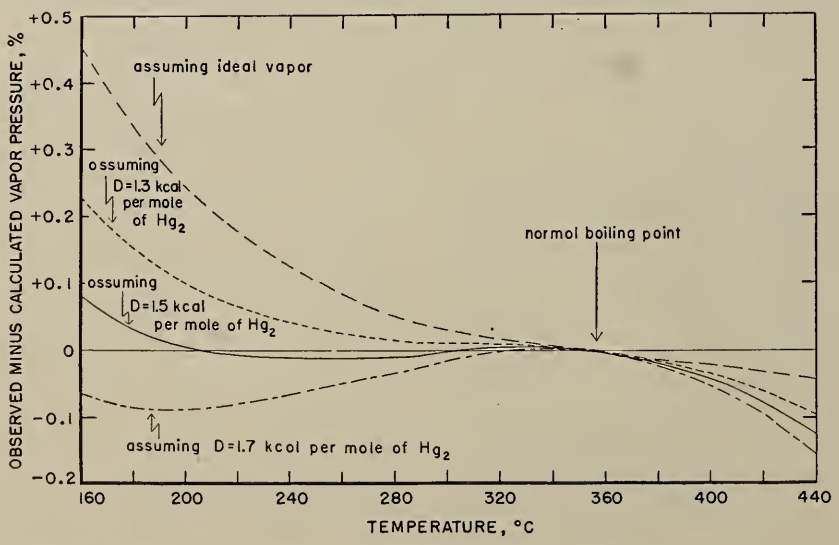

FIGURE 4. *Comparison between observed vapor-pressure values of Smith and Menzies (corrected to present temperature scale) and values calculated from eq 35, taking as a parameter several degrees of gas imperfection.*

examination of the mercury sample used, and in the course of the calculations of thermodynamic properties there were very helpful discussions with W. S. Benedict and H. F. Stimson.

VII. References

[1] D. C. Ginnings and R. J. Corruccini, J. Research NBS **38,** 583 (1947) RP1796.
[2] D. C. Ginnings and R. J. Corruccini, J. Research NBS **38,** 593 (1947) RP1797.
[3] D. C. Ginnings, T. B. Douglas, and Anne F. Ball, J. Research NBS **45,** 23 (1950) RP2110.
[4] R. J. Bondley, GE Research Laboratory Report No. RL–269 (1949).
[5] N. S. Osborne, BS J. Research **4,** 609 (1930) RP168.
[6] International Critical Tables **II** 457 (McGraw-Hill Book Co., Inc., New York, N. Y., 1927).
[7] F. W. Sears, Proc. Phys. Soc. London **26,** 95 (1913).
[8] L. B. Smith and F. G. Keyes, Proc. Am. Acad. Adv. Sci. **69,** 313 (1933–34).
[9] J. A. Beattie, B. E. Blaisdell, and J. Kaminsky, Proc. Am. Acad. Arts Sci. **71,** 361, 375 (1937).
[10] A. Smith and A. W. C. Menzies, J. Am. Chem. Soc. **32,** 1541 (1910).
[11] S. Glasstone, Theoretical chemistry, p. 441 (D. Van Nostrand Co., Inc., New York, N. Y., 1944).
[12] H. Kuhn, Proc. Royal Soc. London **A158,** 230 (1937).
[13] R. Heller, J. Chem. Phys. **9,** 154 (1941).
[14] F. London, Z. physik. Chem. **B11,** 222 (1930).
[15] E. Koernicke, Z. Physik **33,** 219 (1925).
[16] H. Kuhn and K. Freudenberg, Z. Physik **76,** 38 (1932).
[17] J. G. Winans and M. P. Heitz, Phys. Rev. **65,** 65 (1944).
[18] A. G. Gaydon, Dissociation energies, p. 209 (Chapman and Hall, Ltd., London, 1947).
[19] G. Herzberg, Molecular spectra and molecular structure: I. Diatomic molecules, p. 488 (Prentice-Hall, Inc., New York, N. Y., 1939).
[20] J. A. Beattie, M. Benedict, B. E. Blaisdell, and J. Kaye, Proc. Am. Acad. Arts Sci. **77,** 255 (1949).
[21] H. F. Stimson, J. Research NBS **42,** 209 (1949) RP1962.
[22] Temperature, p. 1322 (Reinhold Publishing Corp., New York, N. Y., 1941).
[23] N. S. Osborne, Trans. Am. Soc. Mech. Eng. **52,** 221 (1930).
[24] N. S. Osborne, H. F. Stimson, and D. C. Ginnings, J. Research NBS **23,** 261 (1939) RP1229.
[24a] A. L. Marshall, L. F. Epstein, and F. J. Norton, J. Am. Chem. Soc. **72,** 3514 (1950).
[25] G. L. Pickard and F. E. Simon, Proc. Phys. Soc. **61,** 7 (1948).
[26] F. Pollitzer, Z. Elektrochem. **17,** 5 (1911); **19,** 513 (1913).
[27] P. W. Bridgman, Proc. Am. Acad. Sci. **47,** 347 (1911).
[28] R. W. Ditchburn and J. C. Gilmour, Rev. Mod. Phys. **13** (No. 4), 310 (1941).
[29] H. Hertz, Ann. Physik [3] **17,** 193 (1882).
[30] A. Gebhardt, Ber. physik. Ges. **7,** 184 (1905).
[31] M. Knudsen, Ann. Physik **29,** 179 (1909).
[32] H. C. Greenwood, Z. physik. Chem. **76,** 484 (1911).
[33] A. C. Egerton, Phil. Mag. **33,** 33 (1917).
[34] H. T. Barnes, Rep. Brit. Assoc. Winnipeg **1909,** 403; H. T. Barnes and H. L. Cooke, Rep. Brit. Assoc. Adv. Sci. **1902,** 530; Phys. Rev. **16,** 65 (1903).
[35] Bartoli and Stracciati, Rend. reale estit. Lombardo sci. e lettere **28,** 469 (1895).
[36] J. N. Brönsted, Z. Elektrochem. **18,** 714 (1912).
[37] A. Naccari, J. phys. radium **8,** 612 (1889); Atti. Torini **23,** 107, 594 (1887–88).
[38] Winkelmann, Ann. Physik **149,** 1 (1873).
[39] J. Milthaler, Wied. Ann. **36,** 897 (1889).
[40] L. G. Carpenter and L. G. Stoodley, Phil. Mag. [7], **10,** 249 (1930).
[41] A. L. Dixon and W. H. Rodebush, J. Am. Chem. Soc. **49,** 1162 (1927).
[42] W. Gaede, Phys. Z. **4,** 105 (1902–03).
[43] S. Lussana, Nuovo cimento **4,** 207 (1912).
[44] V. Kurbatov, Russ. Phys.-Chem. Soc. **40,** 811 (1909).
[45] Research Laboratory, General Electric Company, private communication (1931).
[46] H. Hirobe, J. Fac. Sci. Imp. Univ. Tokyo **1** (Part 4), 155 (1926).
[47] O. Pettersson and E. Hedelius, J. prakt. Chem., N. F. **24,** 135 (1881).
[48] O. J. Kleppa, J. Chem. Phys. **17,** 668 (1949).
[49] T. B. Douglas, Anne F. Ball, and D. C. Ginnings (publication pending).
[50] J. F. Kincaid and H. Eyring, J. Chem. Phys. **5,** 587 (1937).
[51] J. Walter and H. Eyring, J. Chem. Phys. **9,** 393 (1941).
[52] A. W. C. Menzies, Z. physik. Chem. **130,** 90 (1927).
[53] A. Smith and A. W. C. Menzies, J. Am. Chem. Soc. **32,** 1434 (1910).
[54] A. Smith and A. W. C. Menzies, J. Am. Chem. Soc. **32,** 1412 (1910).
[55] C. W. Waidner and G. K. Burgess, Bul. BS **6,** 149 (1909) S124.
[56] Temperature, p. 127 (Reinhold Publishing Corp., New York, N. Y., 1941).

Washington, August 9, 1950.

U. S. GOVERNMENT PRINTING OFFICE: 1951

For sale by the Superintendent of Documents, U. S. Government Printing Office
Washington 25, D. C. - Price 10 cents

THE NATIONAL BUREAU OF STANDARDS

Functions and Activities

The National Bureau of Standards is the principal agency of the Federal Government for fundamental and applied research in physics, mathematics, chemistry, and engineering. Its activities range from the determination of physical constants and properties of materials, the development and maintenance of the national standards of measurement in the physical sciences, and the development of methods and instruments of measurement, to the development of special devices for the military and civilian agencies of the Government. The work includes basic and applied research, development, engineering, instrumentation, testing, evaluation, calibration services, and various scientific and technical advisory services. A major portion of the NBS work is performed for other government agencies, particularly the Department of Defense and the Atomic Energy Commission. The functions of the National Bureau of Standards are set forth in the Act of Congress, March 3, 1901, as amended by Congress in Public Law 619, 1950. The scope of activities is suggested in the listing of divisions and sections on the inside of the front cover.

Reports and Publications

The results of the Bureau's work take the form of either actual equipment and devices or published papers and reports. Reports are issued to the sponsoring agency of a particular project or program. Published papers appear either in the Bureau's own series of publications or in the journals of professional and scientific societies. The Bureau itself publishes three monthly periodicals, available from the Government Printing Office: the Journal of Research, which presents complete papers reporting technical investigations; the Technical News Bulletin, which presents summary and preliminary reports on work in progress; and Basic Radio Propagation Predictions, which provides data for determining the best frequencies to use for radio communications throughout the world. There are also five series of nonperiodical publications: the Applied Mathematics Series, Circulars, Handbooks, Building Materials and Structures Reports, and Miscellaneous Publications.

Information on the Bureau's publications can be found in NBS Circular 460, Publications of the National Bureau of Standards ($1.00). Information on calibration services and fees can be found in NBS Circular 483, Testing by the National Bureau of Standards (25 cents). Both are available from the Government Printing Office. Inquiries regarding the Bureau's reports and publications should be addressed to the Office of Scientific Publications, National Bureau of Standards, Washington 25, D. C.


NBS